# Virtual Antenna Arrays

by
Mischa Dohler

November 2003

A thesis submitted to the University of London
for the degree of Doctor of Philosophy

Department of Electrical and Electronic Engineering
King's College London, University of London
Strand, London WC2R 2LS

*The reasonable man adapts himself to the world.*
*The unreasonable man persists in trying to adapt the world to himself.*
*Therefore all progress depends on the unreasonable man.*
George Bernard Shaw

# Acknowledgements

It's this city, London. The spectrum of people one meets in London is just unbelievable. There are some, I wouldn't have liked to meet, but I did (mostly landlords and traffic wardens). There are some, I would have liked to meet, but I didn't. There are many, however, I would have loved to meet and I did. This acknowledgement is dedicated to those. Their beautiful, creative and unpretentious mind has made my journey worthwhile calling an experience.

The first line, I feel, belongs to those who, among their heavy problems, cared most in the past years: Gemma (finalment et cases amb mi), my mom and Hamid. Simply saying 'thank-you' is far too little, however, dwelling on their virtues is something they wouldn't have liked.

A big kiss to my little brother Edd, my big sister Anitchen, and my father for their patience and support throughout the years! Also, a big kiss to my granny who, with 92, is still happily digging somewhere in a cosy garden in a remote village by Moscow.

My office hours I have spent with the craziest guys in London! There is no other department like CTR on this globe. I cannot name you all, guys, but I want to thank a couple of very special people: Vasilitis, Monica, Nikuli, Bilal, Nikolas, Thanuli, Andreitschik, Robert, Ali, Paul, Adil, Piyush, Estephane and, our valuable newcomer, Ben. Thanks also to Fatin, Mohammad, Reza, Nooshin, Jonathan, Mike and all the smiling faces in the EE division.

There are many things I have learned during the past years being involved with Mobile VCE. I want to thank all industrial and academic members of M-VCE for their steady moral and financial support during the development of the concept presented in this thesis. I am particularly grateful to Walter, Mike, Dean, Mark, Lajos, Steve, Kari and Sunil.

There was not much time outside office life; but what left, I had spent with people who know what enjoying life is all about. Eva, Alberto, Marco, Matrixel, Elizzabeta, Unix, Paula, Terrible, Giorita, Laurita, Moriella, Rubina and many many more, thanks for simply being there when I actually wanted to rest (just kidding!). Life without you would be extremely pale.

Kisses to Nastia, Roman, Vanja, Nin and Andrej in Moscow; Ilia, Fridie, Anja, Andrei, Steffen, Jana, Plamen and Denise in Germany; Zina, Georgio and Nomiki in Greece, Gianni in Pisa, Warrick in NZ, Shi-Chwei in NY, Kwadja in Sri-Lanka; the 'mafia' in Brussels, Paris and Italy; Victor and Marta in Barcelona.

Being half German, half Russian, it is not easy to adopt another nationality, but I have decided to become one-third Catalan. This is due to the sweetest family on earth: the Guileras. Merce, Jordi, Gemma, Totti and Dau, you have given to me what I have never really had. Thanks so much.

And then ... there is this small village in the mountains of Catalunia, defying the powers of nature and politics, living their own life, but welcoming every stranger with incredible love: Sant Llorenç de Morunys. Their main inhabitants, Totti & Lluis (import), Ramon, Miquel, Marc, Monica & Lluis, Alex and Sergi, have seen more sunrises than sunsets, most of them in a swimming pool surrounded by the beautiful pre-Pyrenees. This is where I found the true meaning of life!

# Abstract

The ubiquitous trend to "go wireless" is a symbol of our need for independence and flexibility. To allow for such an "all-wireless" world, large amounts of information with widely varying content have to be exchanged, utilising a limited wireless spectrum. Wireless capacity is thus the keyword and research concentrates on an efficient utilisation of the available frequency spectrum.

Recently, it has been proven that the link capacity in the Shannon sense of a Multiple-Input-Multiple-Output (MIMO) system can be substantially higher than that of a single link system. The promised limits, however, can only be reached if appropriate coding schemes are applied to spatially decorrelated propagation channels. Naturally, physical limitations within the mobile terminal will lead to mutual correlation among the antenna elements, jeopardising MIMO capacity bounds.

In this thesis, a novel implementation of a MIMO wireless system is presented that allows the application of MIMO capacity enhancement techniques to mobile terminals with a limited number of antenna elements. Such a system can be realised by permitting adjacent mobile terminals to cooperate among each other and thus form a Virtual Antenna Array (VAA).

The analysis presented here relates to a generalised deployment of VAAs, where an information source communicates with an information target via a given number of relaying VAAs. Each relaying VAA consists of distributed and possibly cooperating mobile terminals, thereby realising a distributed-MIMO multi-stage communication system. Such a system is shown in this thesis to yield a drastic increase in data throughput, where analysis is composed of three stages.

First, novel information theoretical results are presented which characterise the capacity for ergodic channels and rate outage probability for non-ergodic channels at each relaying stage. For example, the capacity integral is introduced, and solved, which enables the derivation of closed form capacity expressions for Rayleigh flat fading MIMO channels, as well as space-time block encoded fading channels with arbitrary statistics and channel gains.

Second, the previously derived capacity and rate outage probabilities are utilised to derive communication protocols which allocate resources in terms of power, bandwidth, and frame duration to each relaying stage such as to achieve maximum end-to-end data throughput from source to sink. The strategies are derived for general MIMO and space-time block encoded communication scenarios with transceivers of infinite complexity, where resources may or may not be reused among the relaying stages. The applicability of the protocols is assessed by means of numerous example scenarios.

Third, fractional resource allocation strategies are derived which are near-optimum for finite-complexity transceivers. The analysis is performed for space-time block encoded transceivers only, which is easily extended to any form of channel and space-time coding schemes if required. The exposure of the allocation strategies is preceded by the derivation of the error rates of distributed space-time block encoded communication systems. Again, numerous simulation results corroborate the applicability of the derived protocols.

# Contents

# List of Acronyms

| | |
|---|---|
| 3G | Third Generation |
| AWGN | Additive White Gaussian Noise |
| BER | Bit Error Rate |
| BLAST | Bell Labs Layered Space Time |
| BPSK | Binary Phase Shift Keying |
| BS | Base Station |
| cdf | Cumulative Density Function |
| CDMA | Code Division Multiple Access |
| CRC | Cyclic Redundancy Check |
| CSI | Channel State Information |
| dB | Decibel |
| EGC | Equal Gain Combining |
| FDMA | Frequency Division Multiple Access |
| FER | Frame Error Rate |
| GHz | Giga Hertz |
| GSM | Global System for Mobile Communications |
| HiperLAN2 | High Performance LAN type 2 |
| IEEE | Institute of Electrical and Electronics Engineers |
| LAN | Local Area Network |
| LOS | Line of Sight |
| ISI | Inter Symbol Interference |
| M-PSK | M-ary Phase Shift Keying |
| M-QAM | M-ary Quadrature Shift Keying |
| M-VCE | Mobile Virtual Centre of Excellence |
| MAC | Medium Access Control |
| MC-CDMA | Multi-Carrier CDMA |
| MGF | Moment Generating Function |
| MHz | Mega Hertz |
| MIMO | Multiple-Input-Multiple-Output |
| MISO | Multiple-Input-Single-Output |
| MMSEC | Minimum Mean Square Error Combining |
| MRC | Maximum Ratio Combining |
| MT | Mobile Terminal |
| nLOS | non-Line of Sight |
| O-MIMO | Orthogonalised MIMO |
| ODMA | Opportunity Driven Multiple Access |
| OFDM | Orthogonal Frequency Division Multiplexing |
| OFDMA | Orthogonal Frequency Division Multiple Access |
| ORC | Orthogonality Restoring Combining |

| | |
|---|---|
| pdf | Probability Density Function |
| PAN | Personal Area Network |
| PHY | Physical Layer |
| r-MT | Relaying Mobile Terminal |
| RRM | Radio Resource Management |
| Rx | Receiver |
| s-MT | Source Mobile Terminal |
| SER | Symbol Error Rate |
| SISO | Single-Input-Single-Output |
| SIMO | Single-Input-Multiple-Output |
| SINR | Signal-to-Interference and Noise Ratio |
| SNR | Signal-to-Noise Ratio |
| STBC | Space-Time Block Code |
| STC | Space-Time Code |
| STTC | Space-Time Trellis Code |
| t-MT | Target Mobile Terminal |
| TDD | Time Division Duplex |
| TDMA | Time Division Multiple Access |
| THz | Tera ($10^{12}$) Hertz |
| Tx | Transmitter |
| UK | United Kingdom |
| UMTS | Universal Mobile Telecommunications System |
| UTRA | UMTS Terrestrial Radio Access |
| UWB | Ultra-Wide Band |
| VAA | Virtual Antenna Array |
| W-CDMA | Wideband CDMA |
| W-LAN | Wireless LAN |

# List of Symbols

| | |
|---|---|
| $\partial$ | Partial Differentiation |
| $A^{\mathrm{H}}$ | Hermitian Transpose of $A$ |
| $a * b$ | Convolution of $a$ and $b$ |
| $\|\mathbf{H}\|$ | Frobenius Norm of $\mathbf{H}$ |
| arg max | Maximum among Arguments |
| det | Determinant |
| diag | Diagonal of Matrix |
| $\mathrm{E}_x\{\cdot\}$ | Expectation with respect to $x$ |
| inf | Infimum of Argument |
| lim | Limit |
| max | Maximum of Argument |
| min | Minimum of Argument |
| Pr | Probability |
| sup | Supremum of Argument |
| tr | Trace of Matrix |
| vect | Vectorised Matrix |
| | |
| ${}_2F_1$ | Gauss Hypergeometric Function |
| $(a)_n$ | Pochhammer Symbol |
| $\mathrm{Ei}(x)$ | Exponential Integral |
| $F_1$ | Appell Hypergeometric Function |
| $\Gamma(x)$ | Complete Gamma Function |
| $\gamma(a, x)$ | Lower Incomplete Gamma Function |
| $\hat{C}_\zeta(a)$ | Capacity Integral |
| $L_k(x)$ | Laguerre Polynomial of order $k$ |
| $\mathcal{W}$ | Wishart Matrix |
| ${}_xF_y$ | Generalised Hypergeometric Function |
| | |
| $\mathbb{C}$ | Complex Numbers |
| $\mathbb{N}$ | Natural Numbers |
| $\mathcal{N}$ | Normal/Gaussian Distribution |
| $\mathcal{N}_c$ | Complex Gaussian Distribution |

| | |
|---|---|
| $\alpha$ | Fractional Frame Duration / Bandwidth |
| $\beta$ | Fractional Transmission Power |
| $\gamma$ | Average Channel Gain |
| $\epsilon$ | Fractional Transmit Power per Antenna in Array |
| $\lambda$ | Eigenvalue |
| $\lambda$ | Instantaneous Channel Power |
| $\lambda$ | Wave-Length |
| $\mu$ | Mean |
| $\nu$ | Repetition of Roots |
| $\sigma^2$ | Variance |
| $\varsigma$ | Shadowing Power |
| $\tau$ | Number of Transmit Antennas |
| $\phi_\lambda(s)$ | Moment Generating Function |
| $\chi^2$ | $\chi^2$ Distribution |
| $\Theta$ | Normalised Throughput |
| $\Lambda(t,r)$ | Approximate MIMO Gain |
| $\Phi$ | Communication Rate |
| | |
| $a, b$ | Fitting Parameters |
| $d$ | Number of STBC Symbols |
| $d$ | Distance |
| $e$ | Natural Constant |
| $e$ | Error |
| $f$ | Radio Frequency |
| $f$ | Nakagami Fading Factor |
| $g_{\text{QAM,PSK}}$ | Modulation-dependent Constants |
| $h$ | Channel Coefficient |
| $m$ | $\min(t,r)$ |
| $n$ | $\max(t,r)$ |
| $n$ | Pathloss Coefficient |
| $p$ | Relative Channel Gains |
| $q$ | Number of adjacent MTs |
| $r$ | Number of Receive Antennas |
| $s$ | Number of Information Symbols |
| $t$ | Number of Transmit Antennas |
| $u$ | $t \cdot r$ |

| | |
|---|---|
| $B$ | Number of Bits per Packet |
| $C$ | Capacity |
| $D$ | Number of Symbols per Frame |
| $E$ | Energy |
| $E_b$ | Bit Energy |
| $E_s$ | Symbol Energy |
| $\mathcal{G}$ | STBC Generator Matrix |
| $H$ | Entropy |
| $I(x, y)$ | Mutual Information |
| $K$ | Number of Relaying Stages |
| $K$ | Ricean Fading Factor |
| $K_i$ | Expansion Coefficient |
| $M$ | Modulation Order |
| $N$ | Noise Power |
| $N_0$ | Noise Power Spectral Density |
| $O$ | Number of Modulation Orders |
| $P_{\mathrm{f,e2e}}$ | End-to-End Frame Error Rate |
| $P_s(e)$ | Symbol Error Rate |
| $P_{out}(\Phi)$ | Outage Probability |
| $Q$ | Number of Clusters |
| $R$ | STBC Rate |
| $S$ | Signal Power |
| $S_{Rx}$ | Receive Power |
| $S_{Tx}$ | Transmit Power |
| $T$ | Frame Duration |
| $W$ | Bandwidth |
| $Z$ | Interference Zones |
| | |
| $\mathbf{H}$ | Channel Matrix |
| $\mathbf{I}_r$ | Identity Matrix of Size $r \times r$ |
| $\mathbf{0}_r$ | All-Zero Matrix of Size $r \times r$ |
| $\mathbf{S}$ | Signal Covariance Matrix |

# List of Figures

# List of Tables

# Chapter 1

# Overview

## 1.1 Introduction

It would be foolish to believe that the capacity offered by the wireless medium is limited. With Thousands of THz of electromagnetic spectrum known, auctioning 140MHz of bandwidth for about £21bn on the grounds of scarce spectrum seems to be beyond ridicule. It could be compared to somebody sitting in a small shelter in London and claiming there is not enough space in the universe.

Unfortunately, such an auction has happened in the UK. It marked the beginning of an era which is generally referred to as 3G. It also marked the beginning of an era where we have only just begun to understand what freedom of information means, where we have grasped the idea of having access to any information anywhere anyhow at any cost, but where we have only started to explore ways of delivering this information. We are, to my belief, only in the cradle of an information society.

There is a long path to pace until we are entitled to call the development of transmission technologies to be mature. There is little we can predict at this stage, except that the way the electromagnetic spectrum is handled has to change. Hopefully, in a couple of decades it will be understood that the wireless medium is not the data bottleneck as frequently claimed. It will then be the time when research can move on to more important things than designing transceivers which operate as close as possible to the predicted capacity limits.

Until this will happen, however, the existence of researchers like me is justified and the work which I expose within this thesis will be read. Indeed, this thesis is about increasing the capacity of wireless systems under the constraints of limited bandwidth and limited transmission power.

In its original formulation, the capacity of a communications channel characterises the maximum amount of error-free information (in bits) which can be transmitted over that channel in a given time (in seconds) over a given bandwidth (in Hertz). Shannon was the first to associate the entropy of a random signal with its information contents, which allowed him to analytically derive the capacity for an additive Gaussian noise channel [1].

This capacity bound evolved over the consecutive years to encompass wireless single-input-single-output (SISO) and later wireless multiple-input-multiple-output (MIMO) channels. The latter can be accomplished by systems where several antenna elements are available at the transmitter and receiver side. The landmark contributions by Telatar [2] and Foschini & Gans [3] have demonstrated that the capacity of a MIMO system exceeds the capacity of a SISO system.

For example, a single wireless link can be shown to offer a capacity of approximately 3 bits/s/Hz at a signal-to-noise ratio (SNR) of 10dB. Such a spectral efficiency is rather poor for high data rate services, which could hence only be delivered by opening up the frequency spectrum; however, this is not a viable solution for many years to come.

However, recently explored MIMO channels promise to meet the required spectral efficiency of up to several tens of bits/s/Hz in dependency of the communication scenario [2, 3]. The immediate price to pay is an increased transceiver complexity. However, these costs fall short in comparison to the potential capacity gained.

The capacity for MIMO channels derived in [2] and [3] are known to depend on the correlation between the transmitting and receiving antenna elements [4]. The reason is that the extra capacity is provided through spatially uncorrelated sub-channels. A high correlation among the antenna elements reduces the MIMO wireless channel towards that of a single link channel. Therefore, failing to provide uncorrelated antenna elements prevents the deployment of high capacity MIMO systems. The main challenge a MIMO communications engineer thus faces in practice is to design an antenna array with mutually decorrelated antenna elements. Correlation among the antenna elements is firstly influenced by the surrounding environment and secondly by the transceiver hardware design.

A dominant plane wave arriving at the receiving array is seen to be highly correlated between array elements, whereas a field resulting from impinging waves from all directions tends to be uncorrelated at a distance $d \approx \lambda/2$ between antenna elements, where $\lambda$ is the wavelength [4]. In conjunction with this behaviour another dilemma occurs in practice: for line-of-sight communication, the field tends to be highly correlated thus counteracting the capacity improvement promised by MIMO channels.

As for the hardware design, correlation among the antenna elements is caused if their mutual spacing is too small causing electromagnetic coupling [5].

MIMO channels hence promise an increase in capacity only if decorrelated signals are present at the antenna elements. Naturally, physical limitations within the mobile terminal will lead to mutual correlation among the elements jeopardizing MIMO capacity bounds. A solution to overcome this problem by means of spatially distributed antenna elements, termed Virtual Antenna Arrays, is introduced and analysed in this thesis.

## 1.2 Virtual Antenna Arrays

This thesis presents a novel communications scheme which allows the deployment of MIMO capacity techniques to terminals with only a few closely spaced antenna elements. The system deployment is referred to as **Virtual Antenna Arrays** (VAAs), the concept of which is briefly explained below.

Traditionally, a communications system is designed such that a base station communicates with each mobile terminal individually. Such a system as a whole, however, offers theoretically much more in terms of capacity bounds and data throughput. A more pragmatic approach to system design would allow mutual communication between the mobile terminals to create virtual MIMO channels. Since many single antenna terminals form a mutually communicating entity, the concept was termed Virtual Antenna Array (VAA) [6].

The underlying principle for cellular deployment is depicted in Figure 1.1. A base station array consisting of several antenna elements transmits a space-time encoded data stream to the associated mobile terminals which can form several independent VAA groups. Each mobile terminal within a group receives the entire data stream, extracts its own information and concurrently relays further information to the other mobile terminals. It then receives more of its own information from the surrounding mobile terminals and, finally, processes the entire data stream. The wired links within a traditional receiving antenna array are thus replaced by wireless links. The same principle is applicable to the uplink.

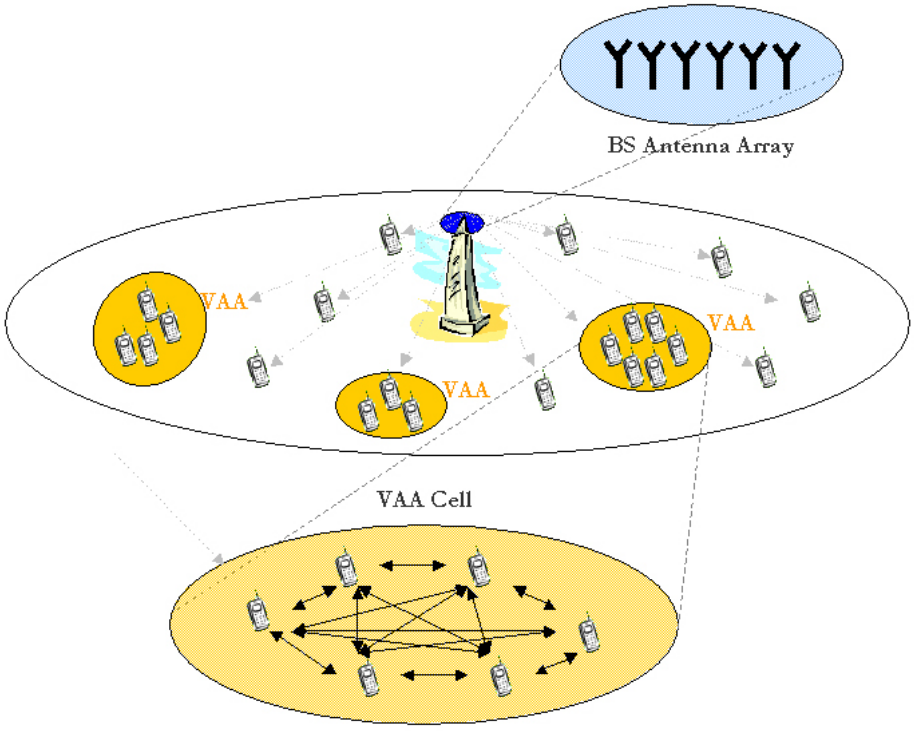


Figure 1.1: Virtual Antenna Arrays in cellular deployment.

In this situation, VAA accomplishes a special type of network which bridges cellular and ad-hoc concepts to establish a heterogenous network with increased capacity. It calls for intelligent synchronisation, relaying and data scheduling algorithms, the exact realisation of which depends on the access scheme, choice of main link technology, choice of relaying technology, technological limits, number of antennas within a given geographical area and other factors, e.g. the ability of the cellular system to synchronise users, etc.

An example shall illustrate the previously mentioned deployment, where a VAA is embedded into a 3G communication system. Here, the direct link between base station (BS) and mobile terminals (MTs) is based on 3G UMTS W-CDMA [7]. For the relaying link a current standard with direct mode communication capabilities is required, which is chosen to be Bluetooth [8]. Therefore, MTs which happen to be in communication range of the Bluetooth transceiver form a VAA in the sense that they start supporting each other via mutual communication. They continue communicating with the BS using the W-CDMA link and, at the same time, relay further captured information to the other MTs within the VAA group utilising Bluetooth, thereby increasing the end-to-end link capacity.

The deployment of VAAs creates various problems which need to be addressed. For instance, the ability of the terminals to transmit and receive simultaneously and thus to operate in full duplex mode. The duplex communication problem can be solved by assuming that the frequency bands for the main link (BS to MT) and the relaying links (MT to MTs) differ. However, such duplex deployment still poses serious constraints on the MT radio frequency (RF) chain. Particularly, if the receiving main link band and the transmitting relaying band are not spaced sufficiently far apart in the frequency domain, the transmitter front-end duplex filter may not be able to protect the receiving branch sufficiently well. However, I believe that problems like these are either already solved (e.g. MEMS) or will be solved in the near future with the ever increasing technological advances.

Of further importance is the actual relaying process. Similar to satellite transponders, the signal can be retransmitted using a transparent or regenerative relay [9]. A transparent relay is generally easier to deploy since only a frequency translation is required. However, additions to the current standards are required. For a simpler adaptation of VAA to current standards, regenerative relays ought to be deployed. This generally requires more computational power, but will be shown in this thesis to increase the capacity of the network.

Finally, the right choice on main link and relaying access technologies has a severe impact on the performance and merit of VAAs. An assessment of the applicability of current standards, such as GSM, UMTS, HiperLAN2, IEEE802.x, is beyond the scope of this thesis. The interested reader is therefore referred to [10]. In contrast to a specific deployment, this thesis deals with a generic realisation of Virtual Antenna Arrays, where the above-given cellular example is only a subset of such a realisation.

Such generic realisation of VAAs has been introduced in [10], which is henceforth referred to as **distributed-MIMO multi-stage relaying network**. An example realisation is depicted in Figure 1.2. Here, a source MT communicates with a target MT via a number of relaying MTs. Spatially adjacent relaying MTs form a VAA, each of which receives data from the previous VAA and relays data to the consecutive VAA until the target MT is reached. Note that each of the involved terminals may have more than one antenna element. Furthermore, an arbitrary number of MTs of the same VAA may cooperate among each other. The suggested topology, as depicted in Figure 1.2, encompasses a variety of communication scenarios.

For instance, a cellular system operating on the downlink is obtained by replacing the source MT by the BS antenna array which communicates directly with the VAA containing the target MT. It may also represent a system where a BS array communicates with a VAA formed somewhere in the cell, which in turn relays the data to another VAA containing the target MT. This allows the coverage area of the BS to be extended. The same topology is applicable to mesh, ad-hoc and sensor networks [11, 12].

Although naturally more complex to deploy, it will be shown in this thesis how such deployment can boost the system capacity. Also, a VAA allows an automatic scaling of a network as depicted by means of Figure 1.2. This is because a higher density of MTs requires more capacity, which is more easily provided if more antenna elements are available to form VAAs.

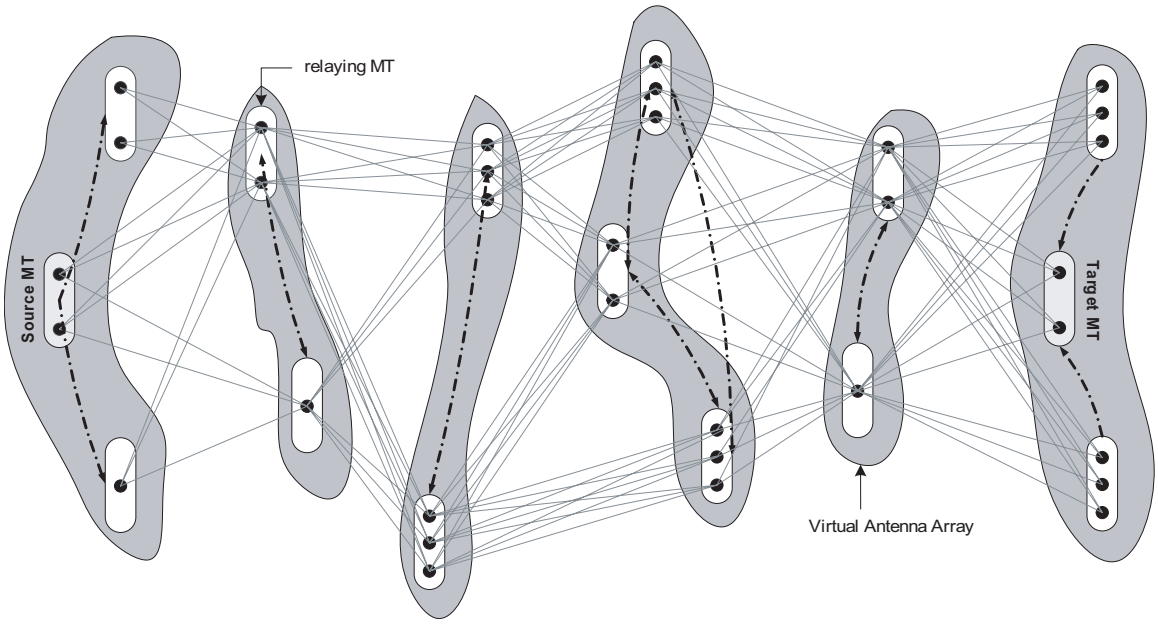


Figure 1.2: Distributed-MIMO multi-stage communication system.

## 1.3 Background & State of the Art

The concept of Virtual Antenna Arrays with application to cellular networks has been introduced in February 2000 [6]. To the best of my knowledge, the generalisation of the concept to distributed-MIMO multi-stage communication networks with application of distributed space-time codes has been introduced shortly after and consequently patented for M-VCE in June 2001 [10]. Other excellent research has been performed in parallel, all of which led to the currently flourishing research area of distributed wireless communication networks.

In its infancy, the concept of VAA evolved from the contributions by [13] and [14] on relaying and by [2] and [15] on MIMO communication aspects.

The work exposed in [13] was undertaken from 1996 until approximately 2000 within the scope of the Universal Mobile Communications System Terrestrial Radio Access (UTRA) Concept Group Epsilon and mainly driven by Vodafone. The system was referred to as Opportunity Drive Multiple Access (ODMA), the main purpose of which was to increase the high data rate coverage within a cell. It is a relaying protocol and not a stand-alone PHY layer technology, which was the reason why it had been rejected as a potential candidate for UTRA. However, due to its capacity benefits, it is now an optional protocol for UTRA TDD/CDMA.

The methodologies suggested in [13] have been studied in [14]. In this study, SISO relaying has enabled an extension of the serving area of a BS by utilising r-MTs at the coverage edge to provide data services to MTs out of reach. It has been demonstrated that, although each r-MT consumes additional power to accommodate the relaying process, all MTs in the network gain on average in performance. Simple relaying protocols have also been suggested which are based on shortest distance relaying. The gains of the relaying process have been attributed to the non-linear pathloss equation, which reduces the aggregate pathloss when breaking a long distance into several shorter communication distances.

As for the MIMO aspects, the elegant analysis exposed by Telatar in [2] has enabled a fundamental understanding of the potential gains offered by ergodic and non-ergodic MIMO channels. Telatar showed that the capacity offered by the wireless channel increases drastically when the number of transmit and receive antennas is increased. With the exposed analysis on uncorrelated flat Rayleigh fading MIMO channels, Telatar has opened the door to evaluating the capacity offered by MIMO channels obeying more general conditions, e.g. different fading statistics, different correlation, flat or frequency selective fading.

The work by Alamouti [15] has triggered a revolution on the way pre-processing at the transmitting side is viewed. It is certainly far from the complex theories exposed in later works by Tarokh [16, 17]; however, it was the first transmission scheme which allowed the deployment of transmit diversity as opposed to the well established receive diversity.

Although these contributions have triggered the invention of Virtual Antenna Arrays and distributed-MIMO multi-stage communication systems, they have not been the first and only contributions in the field of relaying and MIMO systems. For this reason, a short summary on the state of the art related to the work of this thesis is given below. Note that the description given below of prior contributions is not complete; however, more contributions are detailed in the introduction to the respective technical chapters.

**Relaying Communication Systems.** The method of relaying has been introduced in 1971 by van der Meulen in [18] and has also been studied by Sato [19]. A first rigorous information theoretical analysis of the relay channel has been exposed by Cover in [20], a more detailed description to which can be found in his book [21].

In these contributions, a source MT communicates with a target MT directly and via a relaying MT. In [20] the maximum achievable communication rate has been derived in dependency of various communication scenarios, which include the cases with and without feedback to either source MT or relaying MT, or both. The capacity of such a relaying configuration was shown to exceed the capacity of a simple direct link. It should be noted that the analysis was performed for Gaussian communication channels only; therefore, neither the wireless fading channel has been considered, nor have the power gains due to shorter relaying communication distances been explicitly incorporated into the analysis.

Only in the middle of the 90s, research in and around the Concept Group Epsilon revived the idea of utilising relaying to boost the capacity of wireless networks, thereby leading to the concept of ODMA [13]. As already mentioned, the power gains due to the shorter relaying links have been the main incentive to investigate such systems to reach MTs out of BS coverage. However, the emphasis of the study was its applicability to cellular systems, as well as a suitable protocol design. The research did not encompass more theoretical investigations into capacity bounds, transmission rates or outage probabilities.

Interesting milestones into the above-mentioned theoretical studies have been the contributions by Sendonaris, Erkip and Aazhang, which date back to 1998 [22]. In their study, a very simple but effective user cooperation protocol has been suggested to boost the uplink capacity and lower the uplink outage probability for a given rate. The designed protocol stipulates a MT to broadcast its data frame to the BS and to a spatially adjacent MT, which then re-transmits the frame to the BS. Such a protocol certainly yields a higher degree of diversity because the channels from both MTs to the BS can be considered uncorrelated. The simple cooperative protocol has been extended by the same authors to more sophisticated schemes, which can be found in the excellent contributions [23] and [24]. Note that in its original formulation [22], no distributed space-time coding has been considered.

The contributions by Laneman in 2000 [25] are a conceptual and mathematical extension to [22], where energy-efficient multiple access protocols are suggested based on decode-and-forward and amplify-and-forward relaying technologies. It has been shown that significant diversity and outage gains are achieved by deploying the relaying protocols when compared to the direct link. Note again, that no distributed space-time coding has been considered. Also, a short-coming of the developed theory is that the comparison with a direct communication system is not really fair because the relaying system is inherently allocated more resources, either in terms of total communication duration or bandwidth. For instance, given a two-hop relaying system with deployed time division multiple access (TDMA), a frame of 10ms requires a total transmission time of 20ms to reach the target receiver, whereas a direct communication system would require only 10ms.

The case of distributed space-time coding has been analysed by Laneman in his PhD dissertation [26]. In his thesis, information theoretical results for distributed SISO channels with possible feedback have been utilised to design simple communication protocols taking into account systems with and without temporal diversity, as well as various forms of cooperation. He has demonstrated that cooperation yields full spatial diversity, which allows drastic transmit power savings at the same level of outage probability for a given communication rate. A vital asset of his thesis is also a discussion on the applicability of the suggested protocols to cellular and ad-hoc networks. However, [26] does not incorporate an analysis of distributed-MIMO multi-stage communication systems as proposed within this thesis. Nonetheless, the analysis exposed in this thesis can be used to design protocols similar to the ones in [26].

Gupta and Kumar were the first to statistically analyse the information theoretically offered throughput for large scale relaying networks [27]. They showed that under somewhat ideal situations of no interference, hop-by-hop transmission and pre-defined terminal locations, capacity per MT decreases by $1/\sqrt{M}$ with an increasing number of MTs $M$ in a fixed geographic area. They also showed that if the terminal and traffic distributions are random, then the capacity per terminal decreases even in the order of $1/\sqrt{M \log M}$. The analysis in [27] has been extended by the same authors to more general communication topologies, where the interested reader is referred to the landmark paper [28].

Furthermore, Grossglauser and Tse have shown that mobility counteracts the decrease in throughput for an increasing number of users in a fixed area [29]. The protocols suggested therein benefit from the decreased power for a hop-per-hop transmission for decreasing transmission distances. It also benefits from the location variability due to mobility, i.e. a packet is picked up from the source MT by any passing by r-MT and only re-transmitted (and hence delivered) when passing by the target MT.

**MIMO Communication Systems.** Contributions on MIMO systems have flourished ever since the publication of the landmark papers by Telatar [2] and Foschini & Gans [3] on capacity and Foschini [30], Alamouti [15] and Tarokh [16, 17] on the construction of suitable space-time transceivers.

The contributions on the capacity are further detailed in Chapter 2. As for the BLAST system introduced by Foschini in 1996 [30], a transmitter spatially multiplexes signal streams onto different transmit antennas which are then iteratively extracted at the receiving side using the fact that the fades from any transmit to any receive antenna are uncorrelated and of different strength. The BLAST concept has ever since been extended to more sophisticated systems, a good summary of which can be found in [4]. Note that these systems require a quasi-static (or slow-fading) channel as the iterative cancellation process requires a precise knowledge on the channel coefficients.

Alamouti introduced a very appealing transmit diversity scheme by orthogonally encoding two complex signal streams from two transmit antennas, thereby achieving a rate one space-time block code [15]. His work was then mathematically enhanced by the landmark paper of Tarokh [17], who essentially exposed various important properties of space-time block codes. In [16], he also showed how to construct suitable space-time trellis codes which were shown to yield diversity and coding gain. Many other contributions on coherent and differential space-time block and trellis code design followed, a summary of which is beyond the scope of this overview.

**MIMO Relaying Systems.** A landmark contribution on relaying systems deploying multiple antennas at transmitting and receiving side has been made by Gupta and Kumar [28]. The network topology exposed therein is the most generic one can think of, i.e. any MT may communicate with any other MT in the network such as to achieve a maximum system capacity. This is in contrast to the scheme depicted in Figure 1.2, which considers only stage-by-stage relaying. In [28], an information theoretic scheme for obtaining an achievable communication rate region in a network of arbitrary size and topology has been derived. The analysis showed that sophisticated multi-user coding schemes are required to provide the derived capacity gains. Note also that the exposed theory is fairly intricate, which makes the design of realistic communication protocols a difficult task.

Specific distributed space-time coding schemes have also been suggested recently, e.g. [31]. In this publication, two spatially adjacent MTs cooperate to achieve a lower frame error rate to one or more destination(s), where a quasi-static fading channel has been assumed. Distributed space-time trellis codes have been designed which maximise the performance for the direct link from either of the MTs to the destination and the relaying link.

Although contributions on the topic of MIMO relaying have begun to emerge, the amount of work done is scarce in comparison to the vast amount of potential scenarios.

## 1.4 Aim & Organisation of the Thesis

The work during recent years on Virtual Antenna Arrays for the Mobile-VCE originally endeavoured to embed this concept into existing and emerging communication systems. It was understood, however, that a deployment, capacity and performance analysis for generic communication topologies as depicted in Figure 1.2 would be more beneficial in understanding relaying systems.

To simplify analysis and understanding, investigations first concentrated on an end-to-end scenario where a given source MT communicates with target MT separated by various relaying hops. Analysis was then extended to the case where each relaying hop contained more than one relaying MT, henceforth referred to as the relaying stage. In due course it became apparent that enough problems were unsolved for such a communication scenario, some of which are exposed and solved in this thesis.

During the period of my research, the contribution by Gupta and Kumar [28] emerged. Their topology can be seen as a generalisation of the one depicted in Figure 1.2, which is the reason why it is referred to as a 'fairly' generic communication scenario throughout the thesis. With hindsight to [28], this thesis can be seen as a bridge between the intricate information theoretical description of the maximum achievable sum rate of large scale networks and the information and performance theory needed to deploy comparably simple communication protocols as introduced in [26].

With this in mind, it is the aim of this thesis to design communication protocols which yield optimum or near-optimum end-to-end data throughput for an information source communicating with an information sink via a given number of topologically imposed relaying stages. As will be demonstrated, such protocols have to guarantee an optimum assignment of resources to each relaying stage as a function of the channel conditions. These protocols are henceforth referred to as **fractional resource allocation strategies**.

For a potential deployment, these strategies have to be as simple and robust as possible. Their role is to allocate resources in terms of power, bandwidth and frame duration to each relaying stage dependent upon of the prevailing channel conditions.

To derive optimum allocation algorithms, a thorough understanding of the offered end-to-end capacity is needed first. Only after that, allocation strategies can be developed which achieve maximum end-to-end throughput. Since the notion of capacity assumes transceivers of infinite (or very high) complexity, their deployment is only justified in systems which deploy such transceivers. A system operating below the capacity limit, simply because it utilises less complex transceivers, may require different allocation strategies to achieve maximum throughput. A derivation of these fractional allocation strategies is also of great interest.

Once the throughput maximising protocols are derived for a single end-to-end communication link, they can then be enhanced to allow optimum throughput in multiple end-to-end communication links. This can be seen as a further step towards the realisation of generic systems as introduced in [28]; however, with reference to the amount of material presented in this thesis, this has been left open for future research.

To accomplish a logical thread in deriving the fractional allocation strategies, the thesis has been organised as follows. In Chapter 2, the information theoretical foundations are laid where the stage-to-stage capacity and outage probabilities are derived for a vast range of communication scenarios. These are then utilised in Chapter 3 to derive fractional allocation strategies which achieve end-to-end throughput; again, a wide range of scenarios is covered by the analysis. Finally, Chapter 4 deals with the derivation of resource allocation strategies for transceivers utilising distributed space-time block codes only. Note that each chapter is concluded with a thorough summary on the achieved results, the author's contributions to the field, and the future research tailored to each particular chapter. Conclusions to the entire thesis are drawn in Section 5, which are accompanied by suggestions on future research taking the result of the whole thesis into account.

In more details, the major contributions of Chapter 2 can be summarised as follows. First, a closed form expression for the MIMO capacity originally derived by Telatar in integral form has been given. This analysis is then used to derive closed form expressions of the capacity achieved by distributed space-time block encoded communication systems. Also, for these scenarios, the associated outage probabilities are derived assuming non-ergodic MIMO channels. Finally, approximations to the MIMO capacity and outage probability are introduced, which prove useful in the consecutive chapter.

The effort of Chapter 3 concentrates on the derivation of fractional resource allocation strategies assuming transceivers of infinite complexity are available. The capacities and their approximations are hence utilised to develop algorithms for general MIMO systems, as well as space-time block encoded MIMO systems operating over channels of possibly different statistics and gains. Similar throughput-maximising algorithms are then developed for non-ergodic channels which invoke the outage probabilities instead of capacities.

Finally, Chapter 4 derives throughput-maximising resource allocation strategies assuming space-time block encoded systems without an outer Shannon code. The deployed finite-complexity transceivers lead to different optimisation criteria, and hence to different allocation strategies than in the previous chapter. The derivation of the allocation strategies is partially facilitated by the closed form expressions of the symbol error rate of space-time block codes with different channel statistics and gains.

Chapters 2−4 contain almost exclusively novel material with background information kept to a minimum.

# Chapter 2

# Fundamental Capacity Limits

## 2.1 Introduction

Capacity is a concept related to the vast area of Information Theory, a branch of science which really commenced after the publication of Shannon's legendary monogram on "A Mathematical Theory of Communication" in 1948 [1]. More than half a century has passed since, during which major achievements in the field of theoretical and practical communications have been achieved. A brilliant overview on the milestones of Shannon's information theory from its very infancy until the year 1998 can be found in [32], and is briefly summarised below.

Back in 1915, Whittaker discovered how to reconstruct losslessly a bandlimited function from appropriately taken samples. Almost a decade later, Nyquist related the transmission rate to the logarithm of the number of signal levels in a unit duration [33]. In 1928, Hartley recognised the need to introduce a "quantitative measure of information" [34]. He denoted it $H$ and related it in a logarithmic manner to the number of symbols available in the selection process representing the communication from an information source towards an information sink. He further concluded that the communication rate of a system is proportional to the bandwidth of the utilised channel.

None of the aforementioned scientists included the effects of noise or the random nature of signals into their theory, a theory which was majorly influenced by Wiener and Rice [35]. With their developed mathematical foundations, the year 1948 bore seven theories encompassing fundamental trade-offs between bandwidth, signal-to-noise ratio, transmission rate and reliability. It was Shannon's Information Theory which survived.

The Shannon information theory predicts the achievable error-free communication rate for a communication system with given input distribution, transmission power, noise power, and bandwidth. The maximum achievable rate is referred to as the channel capacity. The theory also suggests design rules of how such an error-free transceiver can be constructed at the expense of infinite complexity; however, the theory does not suggest design criteria for transceivers operating at the capacity limits with finite complexity.

Major research effort hence concentrated on the construction of transceivers operating close to the capacity bound. This has been achieved only recently with the aid of Turbo Codes [36]. Nobody, however, has ever managed to communicate beyond the bound, indicating its universal nature.

Information theorists thought that with the discovery of Turbo Codes the research area was almost closed, when Telatar [2] and Foschini & Gans [3] suggested utilising the additional spatial dimension to further boost capacity. Their contributions gave birth to the nowadays well established research branch of multiple-input-multiple-output (MIMO) communication systems. The multiplexing scheme suggested by Foschini & Gans resulted in practical MIMO BLAST-like systems, whereas Telatar's contribution formed a profound mathematical foundation for further developments in MIMO information theory. Both contributions passed almost unnoticed, until Tarokh published minute code design rules which allowed the derived capacity bounds to be approached [16, 17]. His work was inspired by the works of Telatar, Foschini & Gans and Alamouti [15], and so is this thesis.

Although communication at the MIMO capacity limit requires a transceiver of infinite complexity, this limit serves very well as a general characterisation and differentiation of communication systems. An assessment of the applicability of VAA-type systems introduced in Chapter 1 will therefore rely on a characterisation in terms of capacity first. It is hence the aim of this chapter to deal with generic issues related to MIMO capacity, as well as specific issues applicable to VAA-type systems. Although many theorems on the capacity behaviour of MIMO channels have been proven to date, some interesting and novel results can be found herein. The derivation of a closed expression of the Shannon capacity over ergodic flat Rayleigh fading MIMO channels is worth mentioning, as it is so far only given in integral form. Other contributions of this chapter to the research community are summarised in Section 2.6

This chapter is structured as follows. First, some basic concepts related to the Shannon notion of capacity are reiterated. Emphasis is put on the difference between capacity over Gaussian and fading channels, leading to different representations over ergodic and non-ergodic fading channels. This shall aid in understanding the capacity of MIMO channels, which is dealt with second. To this end, a fairly intricate expression of the Shannon capacity over ergodic flat Rayleigh fading MIMO channels is derived in closed form. The analysis is then extended to non-ergodic MIMO channels. Third, various aspects of the capacity of MIMO channels are analysed, which are being orthogonalised with the deployment of orthogonal space-time block codes (STBCs). Fourth, an approximation of the exact capacity and its associated outage probability is introduced, and its accuracy assessed. Finally, chapter specific conclusions are drawn, contributions are listed, and the most important results summarised.

## 2.2 Basics in Understanding Capacity

### 2.2.1 The Gaussian Case

In his landmark development [1], Shannon introduced the entropy $H(x)$ of a continuous random variable $x$ with probability density function (pdf) $pdf_x(x)$ as

$$H(x) \triangleq -\int pdf_x(x) \log_2\big(pdf_x(x)\big)\, dx \tag{2.1}$$

Here, as in its original thermodynamical notion, entropy relates to the uncertainty in $x$. Shannon further showed that if $x$ is limited in its second moment $\sigma^2$ (with any mean $\mu$), then the $pdf_x(x)$ which maximises (2.1) must obey a Gaussian distribution, i.e.

$$x \sim \mathcal{N}(\mu, \sigma^2) \tag{2.2}$$

for which the entropy $H(x)$ is easily calculated as

$$H(x) = \frac{1}{2} \log_2\left(2\pi e \sigma^2\right) \tag{2.3}$$

where $e = 2.718$ is the natural constant. The mutual information between two random variables $x$ and $y$ is defined as

$$I(x, y) \triangleq H(x) - H(x|y) \tag{2.4}$$

which represents the uncertainty inherent to $x$ minus the uncertainty left about $x$ once $y$ is observed. Although (2.4) is very general, $x$ can be associated with the transmitted signal and $y$ with the received signal. Clearly, if after observation of $y$ the uncertainty over $x$ remains, i.e. $H(x|y) = H(x)$, then their mutual information (knowledge) must be equal to zero and the receiver is unable to decide which realisation of $x$ was transmitted. If, however, observing $y$ resolves all uncertainty over $x$, i.e. $H(x|y) = 0$, then the mutual information (knowledge) is equal to the possible realisations of $x$, i.e. the entropy $H(x)$.

Shannon defined the channel capacity $C$ as the maximum mutual information $I(x, y)$ over all possible input distributions $pdf_x(x)$, i.e.

$$C \triangleq \sup_{pdf_x(x)} \big\{I(x, y)\big\} \tag{2.5}$$

where $\sup\{\cdot\}$ denotes the supremum. This allowed him to quantify the capacity per channel use of a channel with additive white Gaussian noise (AWGN). Given a signal $x$ transmitted over an AWGN channel with noise $n$, the received signal $y$ can be represented as $y = x + n$. Because of the Gaussian character of the noise, the capacity as per (2.5) is maximised if $x$ is Gaussian too, leading to the capacity of an AWGN channel as

$$C = \frac{1}{2} \log_2 \left(1 + \frac{S}{N}\right) \tag{2.6}$$

where $S = \sigma^2$ is the average power of signal $x$ and $N$ the average power of noise $n$.

Finally, Shannon showed that a signal essentially limited to a duration $T$ and bandwidth $W$ can be represented by approximately $2WT$ samples (or dimensions). Since the capacity per channel use (or per dimension) is governed by (2.6), the capacity of a bandlimited signal can be found to be

$$C = WT \log_2 \left(1 + \frac{S}{N}\right) \tag{2.7}$$

Shannon then defined as the channel capacity in [bits/s] the capacity of the $2WT$ samples per time $T$, i.e.

$$C \triangleq \lim_{T\to\infty} \frac{WT \log_2 \left(1 + \frac{S}{N}\right)}{T} = W \log_2 \left(1 + \frac{S}{N}\right) \tag{2.8}$$

In this thesis, the normalised channel capacity is used for notational simplicity. It is defined as the channel capacity per unit bandwidth, which simplifies (2.8) to

$$C = \log_2 \left(1 + \frac{S}{N}\right). \tag{2.9}$$

Note that the realised signal $x$ of duration $T \to \infty$ is referred to as the codeword, whereas the ensemble from which $x$ is chosen as the codebook. Finally, Shannon proved that an error-free transmission rate exceeding the channel capacity is impossible.

### 2.2.2 Ergodic versus Non-Ergodic Channels

The concept of ergodicity arises in the context of wireless fading channels. To this end, it is assumed that the transmitter is connected to the receiver via a wireless channel. A wireless channel generally obeys large, medium and small-scale fading. The first is a deterministic effect attributed to pathloss. The second is a random effect observed in the spatial dimension when moved over several tens of wavelengths [37]. Unless otherwise stated, shadowing is incorporated into pathloss assuming low-mobility communication scenarios. The last is a random effect observed in the temporal and spatial dimension, which can be catagorised into slow & fast fading and flat & frequency selective fading. Unless otherwise stated, it is assumed that the channel is flat in frequency.

The channel power gains due to the deterministic effects are unified in one coefficient $\gamma$, whereas the random channel power gains are represented by $\lambda$ with its respective pdf. If the channel power gains are fixed for at least the infinite duration of a codeword transmission, then the capacity of the channel can be expressed as

$$C = \log_2 \left(1 + \lambda\gamma \frac{S}{N}\right) \tag{2.10}$$

Note that this expression is sometimes referred to as the instantaneous capacity, which has obviously no meaning in the Shannon sense where codewords are of infinite duration.

If $\lambda$ varies over the transmitted codeword but all its moments are the same from codeword to codeword, then the channel is referred to as an ergodic channel. In that case, the capacity is given as [2]

$$C = \mathrm{E}_\lambda \left\{ \log_2 \left( 1 + \lambda\gamma \frac{S}{N} \right) \right\} \tag{2.11}$$

where $\mathrm{E}_\lambda\{\cdot\}$ denotes the statistical expectation with respect to $\lambda$. In applicable terms, eq. (2.11) means that if the channel fades fast enough so that over a (possibly finite but very long) codeword the mean of the fading statistics can be observed with almost certain reliability, then such a channel can support any rate not exceeding the above-given capacity $C$. That allows one to plot the capacity versus the signal-to-noise ratio (SNR), as will be extensively made use of in this thesis.

In contrast to an ergodic fading channel, the channel realisations of a non-ergodic channel are randomly fixed at the beginning of the transmission and kept constant over the duration of the codeword transmission. Since the channel realisation is chosen randomly and kept constant over the codeword transmission, there is a non-zero probability that a given transmission rate cannot be supported by the channel [2]. However, the probability that a certain communication rate can be supported by a channel can be gauged, and is referred to as the rate outage probability. That requires the probability of the achievable communication rate to be plotted versus the SNR and rate. Since 3-dimensional plots are difficult to read, a family of outage probability curves are plotted versus the rate for a range of SNR values, or versus the SNR for a range of rates.

## 2.3 Capacity of MIMO Channels

### 2.3.1 System Model

A typical wireless MIMO transceiver model is depicted in Figure 2.1. It is assumed that an information source communicates with an information sink via a channel spanned by $t$ inputs and $r$ outputs. The channel is henceforth referred to as a multiple-input-multiple-output (MIMO) channel.

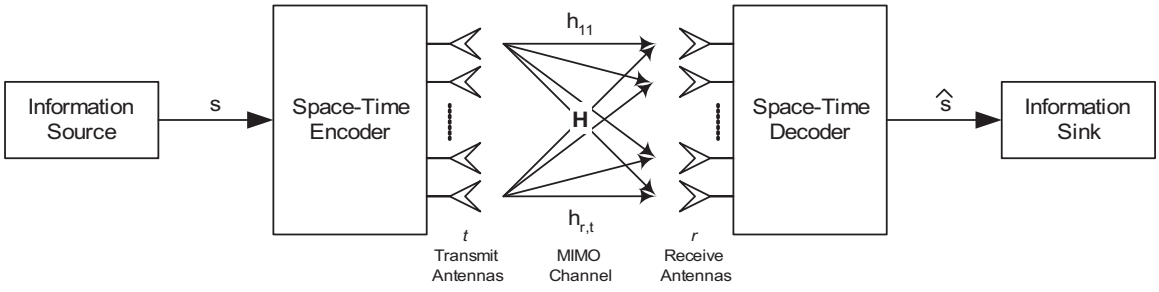


Figure 2.1: Multiple-Input-Multiple-Output Transceiver Model.

Communication is achieved by properly encoding the information $s$ at the transmitter across the temporal and spatial dimensions to produce a given space-time codeword. This codeword is transmitted with average power $S$ and received by the receiver which has an average noise power $N$. The receiver performs appropriate decoding to yield an estimate $\hat{s}$ of the originally transmitted information. It is the aim of this chapter to assess the achievable communication rate (or the probability of supporting such rate) in dependency of the communication scenario.

To produce a neat mathematical representation of the communication system, let $\mathbf{x} \in \mathbb{C}^{t\times 1}$ be the spatial codeword transmitted over the $t$ transmitters at any time instant. With the required constraint on average transmission power, the following holds

$$\mathrm{tr}\Big(\mathrm{E}\big\{\mathbf{x}\mathbf{x}^{\mathrm{H}}\big\}\Big) \leq S \tag{2.12}$$

where $\mathrm{tr}(\cdot)$ denotes the trace operator and $\mathbf{x}^{\mathrm{H}}$ is the Hermitian to $\mathbf{x}$. If all transmission powers $S_{i\in(1,t)}$ are equal, then $S_i = S/t$. The generally complex channel realisation from transmitter $i \in (1,t)$ to receiver $j \in (1,r)$ is denoted as $h_{ij}$. The channel realisations $h_{ij}$ are henceforth referred to as sub-channels. They are conveniently grouped into a channel matrix $\mathbf{H} \in \mathbb{C}^{r\times t}$, where

$$\mathbf{H} = \begin{pmatrix} h_{11} & h_{12} & \cdots & h_{1,t} \\ h_{21} & h_{22} & \cdots & h_{2,t} \\ \vdots & \vdots & \ddots & \vdots \\ h_{r,1} & h_{r,2} & \cdots & h_{r,t} \end{pmatrix} \tag{2.13}$$

Unless mentioned otherwise, it is assumed throughout the thesis that $\mathbf{H}$ is full-rank of rank $\min(t,r)$. That implies that at least $\min(t,r)$ sub-channels are mutually independent. Because of the flat-fading assumption, the received vector $\mathbf{y} \in \mathbb{C}^{r\times 1}$ can now be written as

$$\mathbf{y} = \mathbf{H}\mathbf{x} + \mathbf{n} \tag{2.14}$$

where $\mathbf{n} \in \mathbb{C}^{r\times 1}$ is the noise vector containing the random noise samples from each receiver with average noise power $N$. The noise vector belongs to an $r$-dimensional complex zero-mean circular symmetric Gaussian distribution with variance $N$ per dimension, i.e.

$$\mathbf{n} \sim \mathcal{N}_c(\mathbf{0}_r, N \cdot \mathbf{I}_r) \tag{2.15}$$

where $\mathbf{0}_r$ and $\mathbf{I}_r$ denote respectively an all-zero and identity matrix of dimensions $r \times r$.

### 2.3.2 Fixed Channel Coefficients

The derivation of the MIMO capacity for a fixed channel matrix $\mathbf{H}$ is due to Gallagar [38], Cover & Thomas [21] and more rigorously derived by Telatar [2]. An overabundance of literature on its derivation is now available, see for example the excellent books by [4, 39, 40]. For this reason, only the outcome is summarised here.

For a communication system according to (2.14), where $\mathbf{x} \sim \mathcal{N}_c(\mathbf{0}_t, \mathbf{S})$, $\mathbf{S} = \mathrm{E}\{\mathbf{x}\mathbf{x}^{\mathrm{H}}\}$ and $\mathrm{tr}(\mathbf{S}) = S$, the capacity can be derived to be

$$C = \log_2 \det\left(\mathbf{I}_r + \frac{\mathbf{H}\mathbf{S}\mathbf{H}^{\mathrm{H}}}{N}\right) \tag{2.16}$$

where the codebook covariance matrix $\mathbf{S}$ has to be diagonal [2]. That allows (2.16) to be rewritten as

$$C = \log_2 \det\left(\mathbf{I}_r + \mathbf{H}\mathcal{E}\mathbf{H}^{\mathrm{H}}\frac{S}{N}\right) = \sum_{i=1}^{t} \log_2\left(1 + \epsilon_i \lambda_i \frac{S}{N}\right) \tag{2.17}$$

where $\lambda_{i\in(1,t)}$ are the eigenvalues of $\mathbf{H}^{\mathrm{H}}\mathbf{H}$, and $\epsilon_i$ is the fraction of the total transmit power $S$ allocated to the $i^{th}$ transmit element. The entries of the diagonal matrix $\mathcal{E} = \mathrm{diag}\,(\epsilon_1, \ldots, \epsilon_t)$ are determined with the aid of Lagrangian optimisation, the solution to which yields

$$\epsilon_i = \left(\mu - \left(\lambda_i \frac{S}{N}\right)^{-1}\right)^{+}, \quad i \in (1, t) \tag{2.18}$$

Here, $\mu$ is given implicitly to satisfy $\sum_{i=1}^{t} \epsilon_i = 1$ and $(a)^+$ denotes $\max(a, 0)$. The later operation is required to prevent negative power to be allocated. Such a fractional transmit power allocation strategy is referred to as water-filling. The capacity (2.17) can then be simplified to $C = \sum_{i=1}^{t} \left(\log_2\left(\mu\lambda_i S/N\right)\right)^+$. An approximate but explicit fractional power allocation $\epsilon_{i\in(1,t)}$ is conjectured in Appendix 2.7 (Derivation I). An exact but simple implementation of water-filling can be achieved as follows. It is assumed that the eigenvalues are sorted such that $\lambda_1 \geq \lambda_2 \geq \ldots \geq \lambda_t$. The constraint on $\epsilon_{i\in(1,t)}$ can be rewritten as

$$1 = \sum_{i=1}^{t}\left(\mu - \left(\lambda_i \frac{S}{N}\right)^{-1}\right)^{+} = \sum_{i=1}^{\tau}\left(\mu - \left(\lambda_i \frac{S}{N}\right)^{-1}\right) = \tau\mu - \left(\frac{S}{N}\right)^{-1}\sum_{i=1}^{\tau}\frac{1}{\lambda_i} \tag{2.19}$$

where $\tau$ is chosen such that $\mu - N/S/\lambda_\tau > 0$ and $\mu - N/S/\lambda_{\tau+1} \leq 0$. To determine $\tau \in (1, t)$, the latter inequality can be formulated as

$$\mu = \frac{1 + \left(\frac{S}{N}\right)^{-1}\sum_{i=1}^{\tau}\frac{1}{\lambda_i}}{\tau} \leq \frac{\left(\frac{S}{N}\right)^{-1}}{\lambda_{\tau+1}} \tag{2.20}$$

where $\lambda_{t+1} \triangleq 0$. It can be expressed as

$$\frac{S}{N} + \sum_{i=1}^{\tau}\frac{1}{\lambda_i} \leq \frac{\tau}{\lambda_{\tau+1}} \tag{2.21}$$

In practice, the signal power $S$ and the receiver noise power $N$, as well as the eigenvalues of the channel matrix $\mathbf{H}$, have to be known to the transmitter. A simple iterative summation according to (2.21) is then performed until the inequality holds. Finally, the capacity (2.17) can be rewritten as

$$C = \sum_{i=1}^{\tau}\log_2\lambda_i + \tau\log_2\left(\frac{S}{N} + \sum_{j=1}^{\tau}\frac{1}{\lambda_j}\right) - \tau\log_2\tau \tag{2.22}$$

The water-filling principle is also applicable to channels which vary extremely slowly compared to the data rate, and $\mathbf{H}$ is fed-back to the transmitter via a feed-back channel.

### 2.3.3 Ergodic Fading Channels

In contrast to the previous section, capacity is now obtained by averaging (2.16) over all realisations of $\mathbf{H}$ for a capacity maximising codebook covariance matrix $\mathbf{S}$. The dependency between capacity and codebook covariance $\mathbf{S}$ and channel statistics $\mathbf{H}$ is fairly complicated, which is the reason why capacity expressions for only very few special cases could be determined. The case where each entry in $\mathbf{H}$ obeys uncorrelated Rayleigh fading, has been derived by Telatar [2]. In the opinion of the author, it bears an importance similar to Shannon's information theory itself. The following mathematical developments were available before Telatar's historic contribution:

- The capacity expression (2.16) for a MIMO channel with fixed coefficients [38].
- The pdf of the ordered and unordered eigenvalues of a Wishart matrix [41].

Telatar then showed that if $\mathbf{x} \sim \mathcal{N}_c(\mathbf{0}_t, \mathbf{S})$ then such a codebook maximises capacity and the prior developed capacity expression (2.16) yields

$$C = \mathrm{E}_{\mathbf{H}} \left\{ \log_2 \det \left( \mathbf{I}_r + \frac{\mathbf{H}\mathbf{H}^{\mathrm{H}}}{t} \frac{S}{N} \right) \right\} \tag{2.23}$$

An auxiliary matrix $\mathcal{W}$ is introduced now such that

$$\mathcal{W} \triangleq \begin{cases} \mathbf{H}\mathbf{H}^{\mathrm{H}} & r < t \\ \mathbf{H}^{\mathrm{H}}\mathbf{H} & r \geq t \end{cases} \tag{2.24}$$

where, with defined parameters

$$m \triangleq \min\{t, r\} \tag{2.25}$$

$$n \triangleq \max\{t, r\}, \tag{2.26}$$

$\mathcal{W}$ is referred to as a Wishart matrix with parameters $m, n$. The joint pdf of its ordered eigenvalues $\lambda_{i\in(1,m)}$ is known to be [41]

$$pdf_{\boldsymbol{\lambda}}(\boldsymbol{\lambda}) = \frac{1}{K_{mn}} \prod_i e^{-\lambda_i} \lambda_i^{n-m} \prod_{j>i} (\lambda_i - \lambda_j)^2 \tag{2.27}$$

where $\boldsymbol{\lambda} = (\lambda_1, \ldots, \lambda_m)$ and $K_{mn}$ is a normalisation factor. Therefore, (2.23) turns into

$$C = \mathrm{E}_{\boldsymbol{\lambda}} \left\{ \sum_{i=1}^{m} \log_2 \left( 1 + \frac{\lambda_i}{t} \frac{S}{N} \right) \right\} \tag{2.28}$$

$$= \int_{\boldsymbol{\lambda}} \cdots \int d\boldsymbol{\lambda} \sum_{i=1}^{m} \log_2 \left( 1 + \frac{\lambda_i}{t} \frac{S}{N} \right) \cdot \frac{1}{K_{mn}} \prod_i e^{-\lambda_i} \lambda_i^{n-m} \prod_{j>i} (\lambda_i - \lambda_j)^2 \tag{2.29}$$

After some algebraic manipulations, this finally yields the landmark MIMO capacity theorem derived by Telatar [2]

$$C = \int_0^{\infty} m \log_2 \left( 1 + \frac{\lambda}{t} \frac{S}{N} \right) \cdot \frac{1}{m} \sum_{k=0}^{m-1} \frac{k!}{(k+n-m)!} \left[ L_k^{n-m}(\lambda) \right]^2 \lambda^{n-m} e^{-\lambda} d\lambda \tag{2.30}$$

where $L_k^{n-m}(\lambda)$ is the associated Laguerre polynomial of order $k$. The capacity can also be expressed as

$$C = \mathrm{E}_\lambda \left\{ m \log_2 \left( 1 + \frac{\lambda}{t} \frac{S}{N} \right) \right\} \tag{2.31}$$

with

$$pdf_\lambda(\lambda) = \frac{1}{m} \sum_{k=0}^{m-1} \frac{k!}{(k+n-m)!} \left[ L_k^{n-m}(\lambda) \right]^2 \lambda^{n-m} e^{-\lambda} \tag{2.32}$$

The capacity in (2.30) is given in integral form, to which an iterative and explicit closed form expression are derived below. The advantage of such a development is that long Monte-Carlo simulations are avoided; further, it proves generally useful in a variety of problems relating to the computation of MIMO capacity. Note that in [42] and [43] two independent explicit solutions have been found, which are different from the here-in developed expressions.

The derivation of a closed form expression of (2.30) is performed in two stages: The pdf (2.32) is evaluated first, and then the expectation (2.31) is calculated. To this end, the associated Laguerre polynomial of order $k$ is expressed through the Rodrigues representation [44] (§8.970.1)

$$L_k^{n-m}(\lambda) = \sum_{l=0}^{k} (-1)^l \frac{(k+n-m)!}{(k-l)!(n-m+l)!l!} \lambda^l \tag{2.33}$$

Inserting (2.33) into (2.32) gives

$$pdf_\lambda(\lambda) = \frac{1}{m} \sum_{k=0}^{m-1} \frac{k!}{(k+n-m)!} \left[ \sum_{l=0}^{k} (-1)^l \frac{(k+n-m)!}{(k-l)!(n-m+l)!l!} \lambda^l \right]^2 \lambda^{n-m} e^{-\lambda} \tag{2.34}$$

which is conveniently expressed as

$$\begin{aligned} pdf_\lambda(\lambda) = \frac{1}{m} \sum_{k=0}^{m-1} \frac{k!}{(k+d)!} \Bigg[ & \sum_{l=0}^{k} A_l^2(k,d)\, \lambda^{2l} \\ & + \sum_{l_1=0}^{k} \sum_{\substack{l_2=0, \\ l_2 \neq l_1}}^{k} (-1)^{l_1+l_2} A_{l_1}(k,d)\, A_{l_2}(k,d)\, \lambda^{l_1+l_2} \Bigg] \lambda^d e^{-\lambda} \end{aligned} \tag{2.35}$$

where

$$d \triangleq n-m \tag{2.36}$$

$$A_l(k,d) \triangleq \frac{(k+d)!}{(k-l)!\,(d+l)!\,l!} \tag{2.37}$$

The derived pdf can now be inserted into (2.30), which yields for the capacity in [bits/s/Hz]

$$\begin{aligned} C = \sum_{k=0}^{m-1} \frac{k!}{(k+d)!} \Bigg[ & \sum_{l=0}^{k} A_l^2(k,d)\, \hat{C}_{2l+d}(a) \\ & + \sum_{l_1=0}^{k} \sum_{\substack{l_2=0, \\ l_2 \neq l_1}}^{k} (-1)^{l_1+l_2} A_{l_1}(k,d)\, A_{l_2}(k,d)\, \hat{C}_{l_1+l_2+d}(a) \Bigg] \end{aligned} \tag{2.38}$$

where $a \triangleq \frac{1}{t}\frac{S}{N}$ and $\hat{C}_\zeta(a)$ is defined as

$$\hat{C}_\zeta(a) \triangleq \int_0^\infty \log_2(1+a\lambda)\,\lambda^\zeta\, e^{-\lambda}\, d\lambda \tag{2.39}$$

Due to its frequent occurrence, $\hat{C}_\zeta(a)$ is henceforth referred to as the **Capacity Integral**. Note that according to [44] (§4.337.2)

$$\hat{C}_0(a) = -e^{1/a}\,\mathrm{Ei}\,(-1/a)\,/\log(2) \tag{2.40}$$

where $\mathrm{Ei}(\zeta) \triangleq \int_{-\infty}^{\zeta} \frac{e^t}{t} dt$ is the exponential integral. $\mathrm{Ei}(\zeta)$ is related to $\mathrm{ExpInt}(\zeta)$ typically found in mathematical programmes via $\mathrm{ExpInt}(\zeta) = -\mathrm{Ei}(-\zeta)$. Further, for $\zeta > 0$

$$\begin{aligned}
\hat{C}_\zeta(a) &= -\int_0^\infty \log_2(1+a\lambda)\,\lambda^\zeta\, d\left(e^{-\lambda}\right) && (2.41)\\
&= \zeta\cdot\int_0^\infty \log_2(1+a\lambda)\,\lambda^{\zeta-1}\, e^{-\lambda}\, d\lambda + \frac{1}{\log(2)}\int_0^\infty \frac{a\lambda^\zeta}{1+a\lambda}\, e^{-\lambda}\, d\lambda && (2.42)\\
&= \zeta\cdot\hat{C}_{\zeta-1}(a) + \frac{1}{\log(2)}\int_0^\infty \frac{a\lambda^\zeta}{1+a\lambda}\, e^{-\lambda}\, d\lambda && (2.43)
\end{aligned}$$

The remaining integral can be expressed in closed form, where [44] (§3.353.5)

$$\int_0^\infty \frac{a\lambda^\zeta}{1+a\lambda}\, e^{-\lambda}\, d\lambda = (-1)^{\zeta-1}\,(1/a)^\zeta\, e^{1/a}\,\mathrm{Ei}\,(-1/a) + \sum_{k=1}^{\zeta}(k-1)!\,(-1/a)^{\zeta-k} \tag{2.44}$$

$\hat{C}_\zeta(a)$ can thus be obtained through $\zeta$ iterations in (2.43). $\hat{C}_\zeta(a)$ can also be expressed in an explicit way by consecutively performing the $\zeta$ iterations, which finally yields

$$\begin{aligned}
\hat{C}_\zeta(a) = \frac{1}{\log(2)}\sum_{\mu=0}^{\zeta}\frac{\zeta!}{(\zeta-\mu)!}\Bigg[&(-1)^{\zeta-\mu-1}(1/a)^{\zeta-\mu}e^{1/a}\mathrm{Ei}(-1/a)\\
&+\sum_{k=1}^{\zeta-\mu}(k-1)!(-1/a)^{\zeta-\mu-k}\Bigg]
\end{aligned} \tag{2.45}$$

Hence, (2.38) constitutes a closed solution for the MIMO capacity $C$ with $\hat{C}_\zeta(a)$ given either in iterative form (2.43) or in explicit form (2.45).

The normalised capacities in [bits/s/Hz] versus the SNR in [dB] are shown in Figure 2.2 for various MIMO configurations. The capacities obtained through Monte-Carlo simulations are compared with the capacities obtained through (2.38) and (2.43) or (2.45). Clearly, the three capacities coincide for all of the presented values of $t$ and $r$.

Eq. (2.38) can be simplified considerably if $t = 1$ or $r = 1$, since $m$ will be equal to one. In these cases, the capacities for the respective cases can be expressed as

$$\begin{aligned}
C_{1\times r} &= \hat{C}_{r-1}\left(\frac{S}{N}\right)\Big/\Gamma(r) && (2.46)\\
C_{t\times 1} &= \hat{C}_{t-1}\left(\frac{1}{t}\frac{S}{N}\right)\Big/\Gamma(t) && (2.47)
\end{aligned}$$

where the identity $\Gamma(n) = (n-1)!$ for $n \in \mathbb{N}$ has been used. These capacities are depicted in Figure 2.3 versus the number of antenna elements for an SNR of 10dB. Additionally, the case where the number of transmit elements coincides with the number of receive elements is depicted, which was directly obtained from (2.38). The following observations can be made:

1. **Transmit Diversity:** For a fixed number of receive elements $r$, capacity saturates very fast if the number of transmitters $t$ exceeds the number of receivers. This is corroborated by Figure 2.3, graphs a) & d), where capacity levels off for $t > 1$ & $t > 3$, respectively. This is because the diversity offered by the channel is quickly exhausted with an increasing number of sub-channels created.

2. **Receive Diversity:** For a fixed number of transmit elements $t$, capacity increases logarithmically with the number of receivers $r$, as depicted in Figure 2.3, graph b). Such behaviour is attributed to the additional independent noise sample with each additional receiver element. Recall that the capacity is logarithmically related to the SNR.

3. **Maximum MIMO Capacity:** Capacity increases linearly in the number of elements at either end for $n = t = r$, as shown in Figure 2.3, graph c). This indicates that the offered spatial resources can be utilised in an optimum manner, i.e. capacity does not level off as for transmit diversity and capacity gains are achieved not only due to independent noise samples as for receive diversity. Instead, the uncorrelated spatial signatures of $\mathbf{H} \in \mathbb{C}^{n \times n}$ are used to create $n$ orthogonal sub-channels, to which traditional Shannon coding is applied.

In summary, deploying transmit diversity is a waste of resources if the number of transmit elements does not match the number of receive elements. The deployment of receive diversity yields notable gains due to the additional independent noise samples. A linear increase in capacity is achieved if the number of transmitters equates to the number of receivers. This is an important observation as it dictates the formation requirements of VAA systems.

Note, however, if the increase in complexity due to the deployed MIMO configuration is not negligible, then equating the number of transmit and receive elements may not yield the optimum solution. Transceiver complexity is traditionally caused by the RF front ends and/or the baseband processing unit. With a given cost function, which weighs the achieved capacity gain against the required transceiver complexity, an ultimate answer on an optimum MIMO configuration can be given. A proper analysis of such complexity metrics, however, is beyond the scope of this thesis.

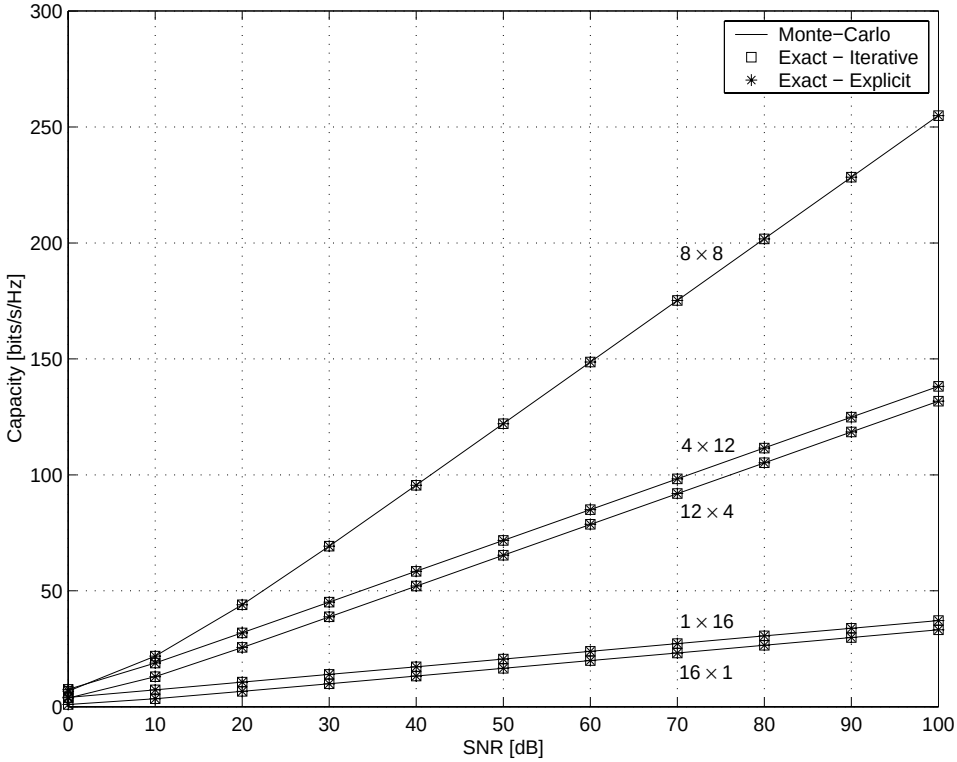


Figure 2.2: Capacity versus SNR for various configurations of $t \times r$.

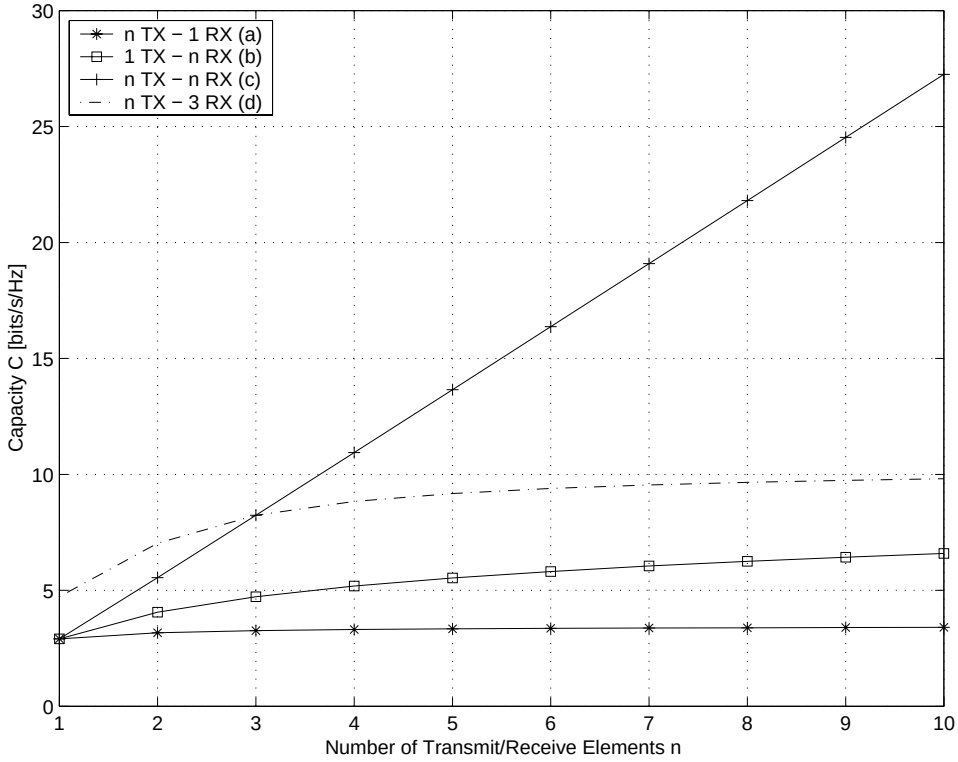


Figure 2.3: Capacity versus the number of transmit and/or receive elements; SNR=10dB.

### 2.3.4 Non-Ergodic Fading Channels

Since for non-ergodic fading channels the channel realisation $\mathbf{H}$ is chosen randomly and kept constant over the codeword transmission, there is a non-zero probability that a given transmission rate $\Phi$ cannot be supported by the channel [2]. As previously mentioned, this probability is called the outage probability and it is denoted here as $P_{out}(\Phi)$. The communication reliability is related to the outage probability, and is defined as $1 - P_{out}(\Phi)$.

It is the aim to minimise the outage probability for a given channel, average codeword power, noise power, and required communication rate. That can be achieved by choosing suitable codewords $\mathbf{x}$ with a given covariance matrix $\mathbf{S} = \mathrm{E}\{\mathbf{x}\mathbf{x}^{\mathrm{H}}\}$ [2]:

$$P_{out}(\Phi) = \inf_{\mathrm{tr}(\mathbf{S}) \leq S} \left\{ \Pr\left( \log_2 \det \left( \mathbf{I}_r + \frac{\mathbf{H}\mathbf{S}\mathbf{H}^{\mathrm{H}}}{N} \right) < \Phi \right) \right\} \tag{2.48}$$

where $\inf\{\cdot\}$ and $\Pr(\cdot)$ denote the infimum and probability, respectively. The choice of codewords $\mathbf{x}$ which minimise the outage probability with given constraint $\mathrm{tr}(\mathbf{S}) \leq S$ is not trivial and has not been solved in a satisfactory form. Telatar, however, provided a conjecture on the optimum form of $\mathbf{S}$ [2]. As outlined there, let's assume that $\tau$ transmit elements and $r$ receive elements are available. The conjecture then states that the covariance $\mathbf{S}$ which minimises the outage probability of (2.48) has to be of the form

$$\mathbf{S} = \frac{S}{t} \begin{pmatrix} \mathbf{I}_t & \mathbf{0}_{\tau - t} \\ \mathbf{0}_{\tau - t} & \mathbf{0}_{\tau - t} \end{pmatrix} \tag{2.49}$$

where $t \in (1, \tau)$ is chosen such that (2.48) is minimised for a given rate $\Phi$ and SNR. That means that out of $\tau$ transmitters only $t$ are utilised. This allows (2.48) to be rewritten as

$$P_{out}(\Phi) = \Pr\left( \log_2 \det \left( \mathbf{I}_t + \frac{\mathbf{H}\mathbf{H}^{\mathrm{H}}}{t} \frac{S}{N} \right) < \Phi \right) \tag{2.50}$$

which, with reference to [2], is equivalently expressed as

$$P_{out}(\Phi) = \Pr\left( \sum_{i=1}^{m} \log_2 \left( 1 + \frac{\lambda_i}{t} \frac{S}{N} \right) < \Phi \right) \tag{2.51}$$

This requires the calculation of an $m$-fold convolution of the pdf of $\log_2 \left( 1 + \frac{\lambda_i}{t} \frac{S}{N} \right)$ generated by the randomness of $\lambda_i$ with $pdf_{\lambda_i}(\lambda_i)$ given by (2.32). For single-input-multiple-output (SIMO) and multiple-input-single-output (MISO) cases with $m = 1$ the solutions are straightforward [2], and are summarised for completeness below. Denoting the single eigenvalue as $\lambda$ and defining $\Psi \triangleq \log_2 \left( 1 + \frac{\lambda}{t} \frac{S}{N} \right)$, eq. (2.51) can be simplified to

$$\Pr\left( \Psi < \Phi \right) = \int_0^{\Phi} pdf_{\Psi}(\Psi)\, d\Psi \tag{2.52}$$

$$= \int_0^{\lambda(\Phi)} pdf_{\lambda}(\lambda)\, d\lambda \tag{2.53}$$

where $\lambda(\Phi)$ can be derived as

$$\lambda(\Phi) = \left( 2^{\Phi} - 1 \right) \frac{t}{S/N} \tag{2.54}$$

### The SIMO Channel

In [2, Example 6] it has been shown that for the SIMO case $\mathbf{S} = S$ is optimal, since $\mathrm{E}\{\mathbf{x}\mathbf{x}^{\mathrm{H}}\} = S$ for $t = 1$. Performing the integration in (2.53) with integrand (2.32) and limit (2.54), yields for the outage probability for the SIMO case

$$P_{out,1\times r}(\Phi) \;=\; \gamma\Big(r, \big(2^{\Phi}-1\big)\Big/\big(S/N\big)\Big)\Big/\Gamma(r) \tag{2.55}$$

where $\gamma(\cdot)$ is the lower incomplete Gamma function defined as

$$\gamma(a,x) \triangleq \int_0^x u^{a-1}e^{-u}\,du \tag{2.56}$$

Figures 2.4 and 2.5 depict the derived dependencies.

In particular, Figure 2.4 displays the outage probability $P_{out,1\times r}(\Phi)$ in [%] versus the SNR in [dB] for a desired rate of $\Phi = 2$ bits/s/Hz. The cases where $r = (1, 2, 4, 8)$ are compared. Clearly, increasing the number of receive antennas drastically decreases the probability that only rates smaller than 2 bits/s/Hz can be supported for a given SNR. For instance, with an SNR of 6dB, a single receive antenna supports only rates smaller than 2 bits/s/Hz in 50% of all cases, whereas eight receive antennas support in virtually 0% of all cases only rates smaller than 2 bits/s/Hz; or, alternatively, eight receivers support at all times rates at least as high as 2 bits/s/Hz. A reliable communication system is traditionally designed to yield an outage probability of less than 10%, which means that for an SNR of 6dB four receive antennas suffice.

Figure 2.5 displays the outage probability $P_{out,1\times r}(\Phi)$ in [%] versus the the desired rate $\Phi$ in [bits/s/Hz] at an SNR of 10dB. Again, the cases where $r = [1, 2, 4, 8]$ are compared. Clearly, increasing the number of receive antennas allows one to communicate at increasing data rates with a constant reliability for a fixed SNR. For instance, a system with $r = (1, 2, 4, 8)$ receive antennas can respectively support $\Phi = (1.0, 2.6, 4.2, 5.5)$ bits/s/Hz at an outage probability of $P_{out,1\times r}(\Phi) = 10\%$; or, alternatively, in 90% of all cases these data rates can be supported.

For the SIMO channel, it can be observed that increasing the number of receive antennas always yields performance benefits. For a fixed rate, increasing the number of receive antennas always decreases the outage, independent of the SNR. For a fixed SNR, increasing the number of receive antennas always decreases the outage, independent of the desired rate. This is in contrast to the MISO channel, as elaborated below.

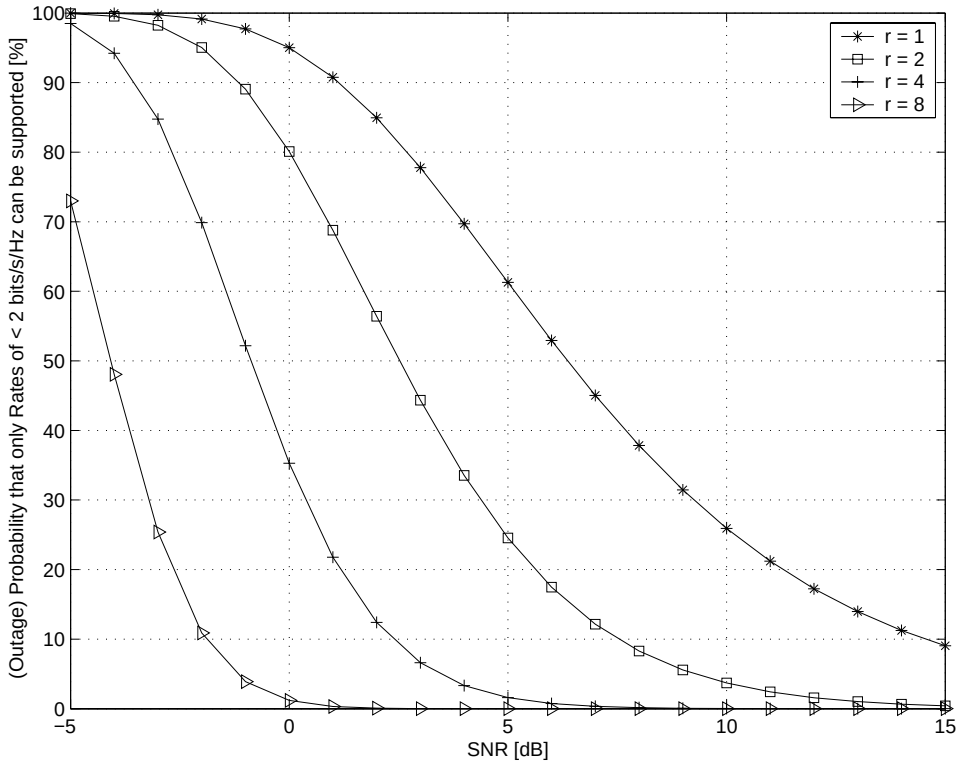


Figure 2.4: Outage probability $P_{out,1\times r}(\Phi)$ versus SNR for a rate of $\Phi = 2$ bits/s/Hz; $t = 1$.

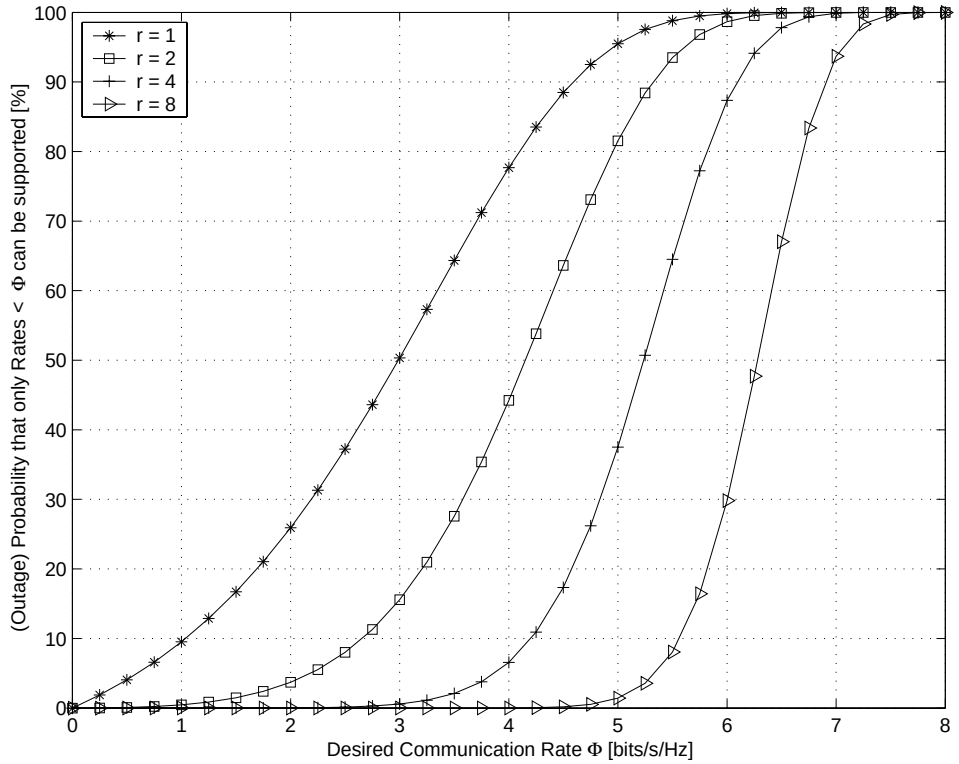


Figure 2.5: Outage probability $P_{out,1\times r}(\Phi)$ versus the rate $\Phi$ at an SNR of 10dB; $t = 1$.

### The MISO Channel

If out of $\tau$ transmit antennas, $t$ antennas are chosen for transmission, then the $\tau \times 1$ MISO channel effectively reduces to a $t \times 1$ MISO channel. With the conjecture (2.51) and the $pdf_\lambda(\lambda)$ of (2.32), the outage probability of the MISO case can be obtained as

$$P_{out,t\times 1}(\Phi) \;=\; \gamma\Big(t, \big(2^\Phi - 1\big)\Big/\big(S/N/t\big)\Big)\Big/\Gamma(t) \tag{2.57}$$

which is depicted for various MISO configurations in Figures 2.6 and 2.7.

Figure 2.6 displays the outage probability $P_{out,t\times 1}(\Phi)$ in [%] versus the SNR in [dB] for a desired rate of $\Phi = 2$ bits/s/Hz. The cases where $t = (1, 2, 4, 8)$ are compared. The curves intersect, in contrast to the SIMO case, indicating that a different number of transmit antennas should be used dependent upon the SNR so as to minimise the outage probability. Since the SNR region of intersection is fairly narrow (which holds for any $\Phi$), the communication system should switch between all available transmit antennas and only one transmit antenna dependent upon the SNR point of operation. If a high SNR is available for communication, then all elements should be utilised to minimise the outage probability, whereas for low SNR only one element should be used. In the current example, where $\Phi = 2$ bits/s/Hz, an available SNR of 10dB yields an outage probability of $(25, 12, 3, 0)\%$ for $t = (1, 2, 4, 8)$. If, however, the available SNR is only 3dB, then the behaviour of the outage probability is reversed and is now $(78, 80, 85, 91)\%$ for $t = (1, 2, 4, 8)$. That means that in 22% of all cases a single transmitter can support a rate of 2 bits/s/Hz, whereas eight transmitters in only 9% of cases.

Figure 2.7 displays the outage probability $P_{out,t\times 1}(\Phi)$ in [%] versus the desired rate $\Phi$ in [bits/s/Hz] at an SNR of 10dB. The cases where $t = [1, 2, 4, 8]$ are compared. Again, the curves intersect at a certain rate, here approximately at $\Phi = 3.5$ bits/s/Hz. The same observations as above can be made. If one built a system operating at 2 bits/s/Hz, then an outage probability of $(25, 12, 4, 0)\%$ for $t = (1, 2, 4, 8)$ would be achieved; a higher number of transmit antennas achieves a lower outage. However, if one built a system operating at 4 bits/s/Hz, then an outage probability of $(77, 80, 85, 91)\%$ for $t = (1, 2, 4, 8)$ would be achieved; a higher number of transmit antennas yields a higher outage.

With reference to Figures 2.6 and 2.7, it can be stated that for a required low outage probability, i.e. high communication reliability, the usage of all transmit elements is always beneficial. If the rate is fixed, then the SNR should be increased, whereas if the SNR is fixed, then the rate should be adjusted. Only if the communication rate and SNR are fixed, then the reliability can be influenced by adjusting the number of utilised transmit antennas.

It can further be observed that for the same system assumptions, the outage probability is much lower for a SIMO system than for a MISO system with the same number of antenna elements. That can clearly be attributed to the additional noise samples of a SIMO system.

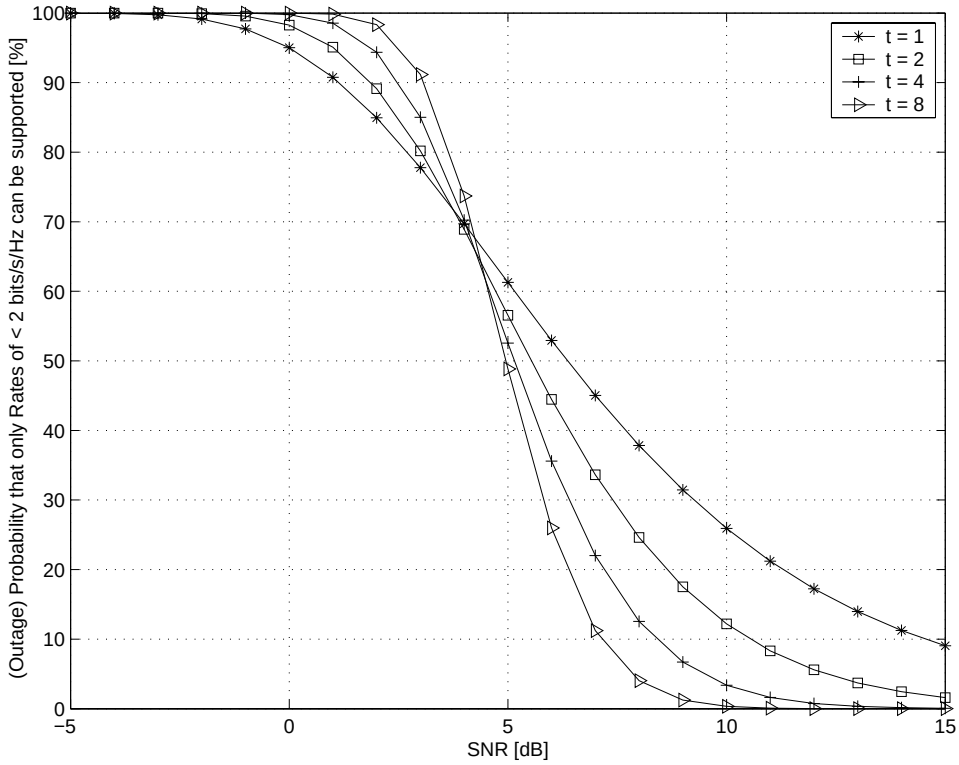


Figure 2.6: Outage probability $P_{out,t\times 1}(\Phi)$ versus SNR for a rate of $\Phi = 2$ bits/s/Hz; $r = 1$.

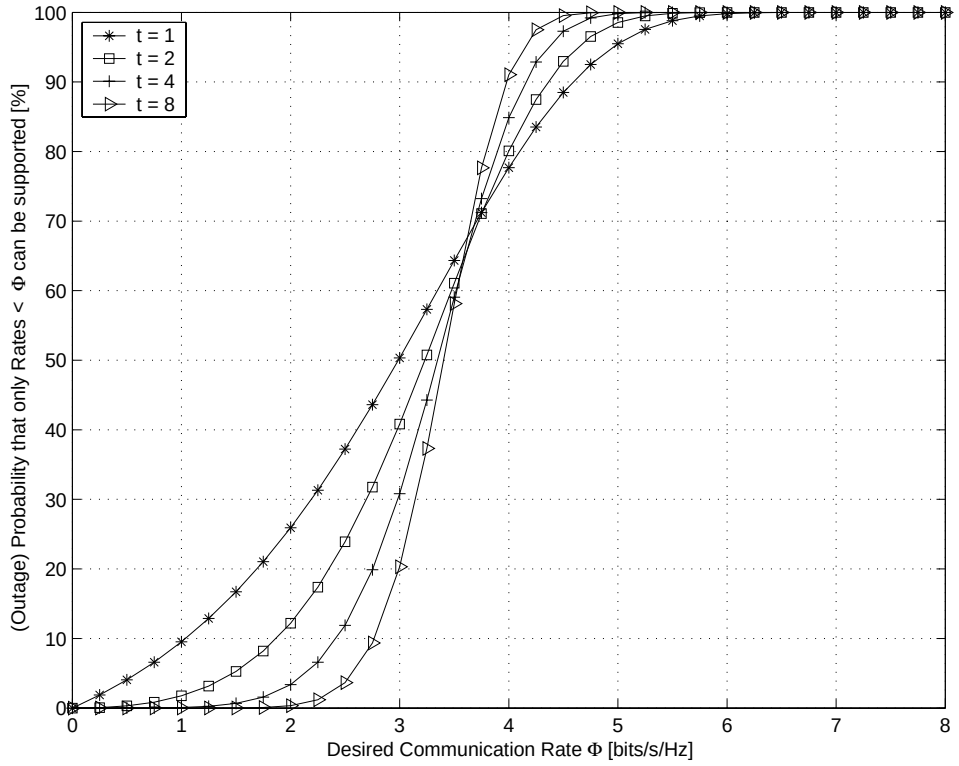


Figure 2.7: Outage probability $P_{out,t\times 1}(\Phi)$ versus the rate $\Phi$ at an SNR of 10dB; $r = 1$.

## 2.4 Capacity of Orthogonalised MIMO Channels

Closed form representations of the capacity of MIMO channels of arbitrary statistics, correlation and attenuation between the transceiver elements have proven to be difficult to derive, mainly because of the difficulty to find the pdf of the eigenvalues involved in representing the power of each uncorrelated sub-channel.

Fortunately, space-time block codes inherently orthogonalise the MIMO channel. They are known to reduce the MIMO channel into parallel SISO channels, which drastically simplifies analysis. The channel is henceforth referred to as the Orthogonal-MIMO (O-MIMO) channel. This section is dedicated to the capacity analysis of O-MIMO channels, where the cases of different statistics and attenuations are dealt with. This will be vital in later chapters for the allocation of optimum resources to MTs belonging to a VAA.

Note that, strictly speaking, Shannon capacity is understood to be the maximum mutual information a given channel can offer between source and sink, independent of the signal processing at either end. In subsequent analysis, however, the maximum mutual information a given channel with applied space-time block coding can accomplish is simply referred to as the capacity of the O-MIMO channel.

### 2.4.1 System Model

According to the communication chain depicted in Figure 2.8, it is assumed that an information source (not depicted) communicates with an information sink (not depicted). The information source sends data to a channel encoder, after which the codeword is space-time block encoded. These space-time encoded codewords are then passed to transmitters which might be spatially distributed, and sent to the receiver elements which might also be spatially distributed. The received signal is then passed to the space-time block decoder to produce the estimated codeword, which is finally passed to the channel decoder. From Figure 2.8 it is clear that the space-time block encoder does not provide any coding gain, which is accomplished by the outer channel code. The space-time block encoder, however, provides a diversity gain which allows the outer channel code to yield better performance.

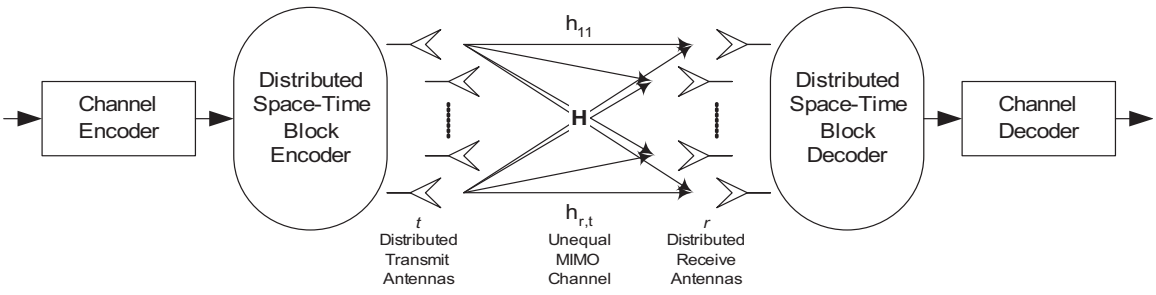


Figure 2.8: Distributed Space-Time Block Code transceiver model.

The theory behind linear orthogonal STBCs is well established, see e.g. the excellent books [4, 39, 40], which is the reason why the theory is only dealt with brevity here.

The space-time block encoder receives $s$ encoded symbols $x_1, x_2, \ldots, x_s$ from the channel encoder, which are part of a longer codeword $\mathbf{x}$. These are encoded with an orthogonal space-time coding matrix $\mathcal{G}$ of size $d \times t$, where $d$ is the number of symbol durations required to transmit the space-time code word, and $t$ is the number of (distributed) transmit elements. At each time instant $1 \leq k \leq d$, the space-time encoded symbol $c_{k,i} \in \mathcal{G}$ is transmitted from the $i^{th}$ distributed transmit element, where $i = 1, \ldots, t$. Such encoding may come at a decrease in transmission rate $R$, defined as $R \triangleq s/d$.

In [16] it was proven that the only full-rate STBC with complex entries exists for $t = 2$, i.e. the Alamouti scheme. Furthermore, half-rate STBCs for $t = 2, \ldots, 8$ and 3/4-rate STBCs for $t = 3, 4$ were given in [16]. To yield orthogonality, the transmission matrix $\mathcal{G}$ has to satisfy

$$\mathcal{G}\mathcal{G}^{\mathrm{H}} \propto \left( \sum_{i=1}^{s} |x_i|^2 \right) \mathbf{I}_s \tag{2.58}$$

Any violation of condition (2.58) will lead to intersymbol interference and thus performance degradation. As an example orthogonal STBC, the complex transmission matrix for the half-rate STBC is given here [16]

$$\mathcal{G} = \begin{pmatrix} x_1 & -x_2 & -x_3 & -x_4 & x_1^* & -x_2^* & -x_3^* & -x_4^* \\ x_2 & x_1 & x_4 & -x_3 & x_2^* & x_1^* & x_4^* & -x_3^* \\ x_3 & -x_4 & x_1 & x_2 & x_3^* & -x_4^* & x_1^* & x_2^* \\ x_4 & x_3 & -x_2 & x_1 & x_4^* & x_3^* & -x_2^* & x_1^* \end{pmatrix} \tag{2.59}$$

For this particular case, $s = 4$ symbols are transmitted during $d = 8$ time instances over $t = 4$ transmit antennas, hence yielding a code rate of $R = 1/2$.

The use of orthogonal space-time block codes is known to reduce the MIMO channel into a single SISO channel with modified channel statistics [39, 45]. For fixed channel realisations $\mathbf{H}$, the normalised capacity in [bits/s/Hz] over such an O-MIMO channel can be expressed as [39]

$$C = R \log_2 \left( 1 + \frac{1}{R} \frac{\|\mathbf{H}\|^2}{t} \frac{S}{N} \right) \tag{2.60}$$

where $S$ is the average transmitted symbol power and $N$ the noise power at the receiver. $\|\mathbf{H}\|$ denotes the Frobenius norm[1] of $\mathbf{H}$, the square of which is given as

$$\|\mathbf{H}\|^2 = \sum_{i=1}^{t} \sum_{j=1}^{r} |h_{ij}|^2 = \mathrm{tr}\left(\mathbf{H}\mathbf{H}^{\mathbf{H}}\right) \tag{2.61}$$

[1]Note that the typically used subscript 'F' denoting the Frobenius norm has been omitted here.

From (2.61), it is clear that $\|\mathbf{H}_{t\times r}\| = \|\mathbf{h}_{1\times t\cdot r}\|$, where $\mathbf{h} \triangleq \text{vect}(\mathbf{H})$. Therefore, the following is adopted

$$\mathbf{h} \triangleq \text{vect}(\mathbf{H}) \tag{2.62a}$$

$$u \triangleq t \cdot r \tag{2.62b}$$

$$\lambda_i \triangleq h_i h_i^* \tag{2.62c}$$

$$\lambda \triangleq \|\mathbf{h}\|^2 = \sum_{i=1}^{u} h_i h_i^* = \sum_{i=1}^{u} \lambda_i \tag{2.62d}$$

$$\gamma_i \triangleq \mathrm{E}\{h_i h_i^*\} \tag{2.62e}$$

to simplify notation.

### 2.4.2 Ergodic O-MIMO Channels

With reference to definitions (2.62), the capacity over an ergodic flat Rayleigh fading O-MIMO channel can be expressed as

$$C = \mathrm{E}_\lambda \left\{ R \log_2 \left( 1 + \frac{1}{R} \frac{\lambda}{t} \frac{S}{N} \right) \right\} \tag{2.63}$$

$$= \int_0^\infty R \log_2 \left( 1 + \frac{1}{R} \frac{\lambda}{t} \frac{S}{N} \right) pdf_\lambda(\lambda) d\lambda \tag{2.64}$$

where the $pdf_\lambda(\lambda)$ of $\lambda = \sum \lambda_i$ solely depends on the statistics of each sub-channel. The aim of this section is to derive a closed solution to (2.64) for various communication conditions.

From (2.62d) it is clear that the $pdf_\lambda(\lambda)$ can be obtained via a $u$-fold convolution in the respective pdfs of $\lambda_i$, i.e.

$$pdf_\lambda(\lambda) = pdf_{\lambda_1}(\lambda_1) * pdf_{\lambda_2}(\lambda_2) * \ldots * pdf_{\lambda_u}(\lambda_u) \tag{2.65}$$

where $*$ denotes the operation of convolution. Although analytically feasible, it has been proven easier to use the moment generating function (MGF) to solve (2.65). The MGF $\phi_\lambda(s)$ of $\lambda$ is defined as

$$\phi_\lambda(s) \triangleq \int_0^\infty pdf_\lambda(\lambda) e^{s\lambda} \, d\lambda \tag{2.66}$$

the application of which is known to transform (2.65) into

$$\phi_\lambda(s) = \prod_{i=1}^{u} \phi_{\lambda_i}(s) \tag{2.67}$$

The pdf of $\lambda$ is now obtained by performing the inverse transformation, obtained as

$$pdf_\lambda(\lambda) = \frac{1}{2\pi j} \int_{\sigma - j\infty}^{\sigma + j\infty} \phi_\lambda(s) e^{-s\lambda} \, ds \tag{2.68}$$

where $j$ denotes the complex number $j = \sqrt{-1}$, and $\sigma$ is chosen in the region of convergence of the integral in the complex $s$ plane. Since the MGF is closely related to the Laplace transform, the operations (2.66) and (2.68) are rarely performed since large tables of either transform are available, see e.g. [44].

To solve (2.64), the only prerequisite is therefore a knowledge of the statistics $pdf_{\lambda_i}(\lambda_i)$ of the instantaneous power $\lambda_i$ of the $i^{th}$ sub-channel. In this thesis, the cases of Rayleigh and Nakagami fading channels are dealt with. Note that the Ricean fading channel is excluded due to the mathematical difficulties associated with its pdf. However, the Ricean distribution with parameter $K$ is very well approximated with a Nakagami distribution with fading parameter $f$, where $f = (1+K)^2/(1+2K)$ [46] [2].

Clearly, the MGF of the instantaneous power $\lambda_i$ is of interest to subsequent analysis. These can be calculated from the respective statistics as [46]

$$\phi_{\lambda_i}(s) = \begin{cases} (1-\gamma_i s)^{-1} & \text{Rayleigh} \\ (1-\gamma_i s)^{-f} & \text{Nakagami} \end{cases} \tag{2.69}$$

which allow one to find closed form expressions for the capacity of channels with the above-given statistics and possibly different channel gains $\gamma_i$, as shown below.

**Rayleigh Fading - Equal Sub-Channel Gains**

If all sub-channel gains are equal then $\gamma_1 = \ldots = \gamma_u$, henceforth simply denoted as $\gamma$. From (2.69) and (2.67), the MGF of the instantaneously experienced power $\lambda$ can then be expressed as

$$\phi_\lambda(s) = \frac{1}{(1-\gamma s)^u} \tag{2.70}$$

the inverse of which yields the desired pdf [47]

$$pdf_\lambda(\lambda) = \frac{1}{\Gamma(u)} \frac{\lambda^{u-1}}{\gamma^u} e^{-\lambda/\gamma} \tag{2.71}$$

which is obviously a central $\chi^2$-distribution with $2u$ degrees of freedom and mean $u\gamma$. With reference to (2.64) and some changes in variables, the capacity of the orthogonalised MIMO channel can be expressed in closed form as

$$C = \frac{R}{\Gamma(u)} \int_0^\infty \log_2 \left(1 + \lambda \frac{1}{R}\frac{\gamma}{t}\frac{S}{N}\right) \lambda^{u-1} e^{-\lambda} \, d\lambda \tag{2.72}$$

$$= \frac{R}{\Gamma(u)} \cdot \hat{C}_{u-1}\left(\frac{1}{R}\frac{\gamma}{t}\frac{S}{N}\right) \tag{2.73}$$

where $\hat{C}_\zeta(a)$ is the Capacity Integral defined in (2.39) and solved in (2.45). The offered capacity is visualised for various MIMO configurations in Figures 2.9−2.12 with $\gamma = 1$.

Explicitly, Figure 2.9 depicts the normalised capacity in [bits/s/Hz] versus the SNR in [dB] for various MIMO system configurations with one receive antenna. Depicted are the following cases: (1) $t = 1$ (SISO), (2) $t = 2$ (Alamouti), (3) $t = 3$ (3/4-Rate), (4) $t = 4$ (3/4-Rate), (5) $t = 3$ (Half-Rate), (6) $t = 4$ (Half-Rate), (7) $t = 3$ (generic MISO), (8) $t = 4$ (generic MISO), and (9) the SISO Gaussian channel with $t = 1$.

[2] Note that traditionally $m$ is used to denote the Nakagami factor; however, it has been used already.

It can be observed that the full-rate Alamouti scheme with $t = 2$ outperforms the SISO scheme with $t = 1$ by approximately 1dB or 0.3 bits/s/Hz. Furthermore, the 3/4-rate and 1/2-rate schemes perform inferior to the full-rate schemes with $t = 1$ and $t = 2$, because of the loss in transmission rate. That means that if a transceiver deploys a channel code operating at the capacity limit, then the use of more than two transmit antennas does not bring any gain for ergodic fading channels. Conspicuously, the differences between the capacities of a 3/4-rate STBC with $t = 3$ and $t = 4$ is very small, which holds as well for the 1/2-rate STBC. Finally, the generic MISO channel without the utilisation of STBCs yields a much higher capacity than with STBCs. Since the STBC reduces the MIMO channel to an equivalent SISO channel, none of the capacities exceeds the capacity of a simple Gaussian SISO link. This is well corroborated by Figure 2.9.

Figure 2.10 is equivalent to Figure 2.9 with the only difference that two receive antennas have been deployed, i.e. $r = 2$. The following observations can be made. First, none of the O-MIMO capacity curves exceed the capacity of the equivalent Gaussian channel. Second, the capacity gap between the cases where $t = 1$ (SIMO) and $t = 2$ (Alamouti MIMO) is reduced compared to Figure 2.9, where only one receive antenna was deployed. This indicates that a major amount of diversity is picked-up by the two receive antennas, which is further corroborated by the fact that the capacities of a 3/4-rate, and also 1/2-rate, STBC with $t = 3$ and $t = 4$ virtually coincide. Therefore, with an increasing number of antennas involved forming the O-MIMO channel, the capacity gap between the O-MIMO channel and the equivalent Gaussian channel will vanish. However, the capacity of a Gaussian channel can not be exceeded; whereas the capacity of a generic MIMO channel drastically increases. The simplicity of STBCs hence limits the ultimate system capacity.

Figure 2.11 depicts the normalised capacity in [bits/s/Hz] versus the number of transmit antennas for the cases of different receive antennas at an SNR of 10dB. For each transmit antenna $1 \leq t \leq 8$, the STBC with highest possible capacity was chosen, i.e. for $t = 2$ the Alamouti scheme, for $t = 3, 4$ the 3/4-rate STBCs, and for $t = 5, \ldots, 8$ the 1/2-rate STBCs. These capacities are compared against the capacities of the equivalent Gaussian channels (dash-dotted lines). Clearly, only the use of two transmit antennas brings any benefit over the SISO case. It can further be observed that the capacity gap between the Gaussian channel and the O-MIMO channel with $t = 2$ and $r = 4$ almost vanishes.

Finally, Figure 2.12 depicts the same schemes as Figure 2.11 with the only difference that now the capacity is compared to the traditional MIMO case. It can again be observed that the capacity of MIMO system of high complexity is higher than for an O-MIMO system with reduced complexity.

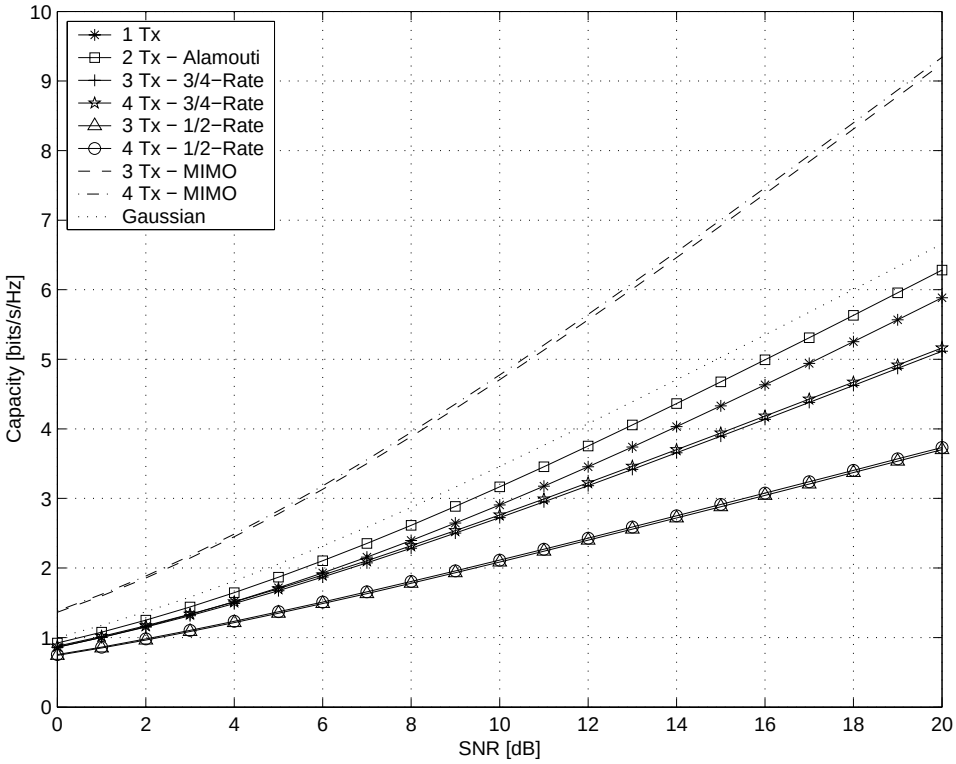


Figure 2.9: Capacity versus SNR for various O-MIMO system configurations; $r = 1$.

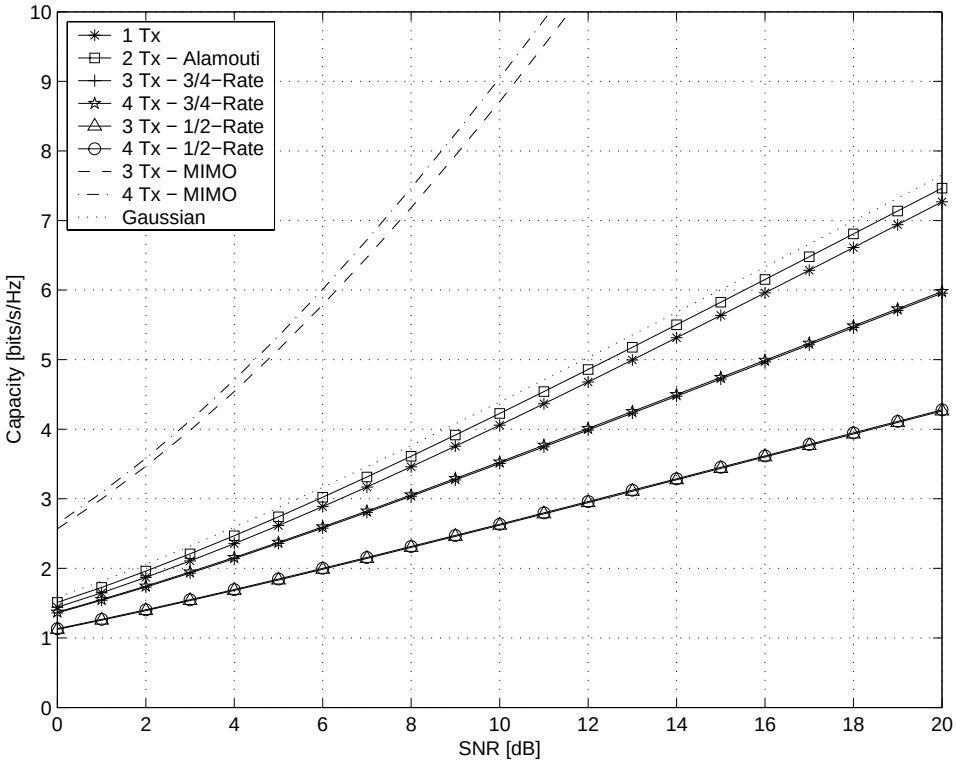


Figure 2.10: Capacity versus SNR for various O-MIMO system configurations; $r = 2$.

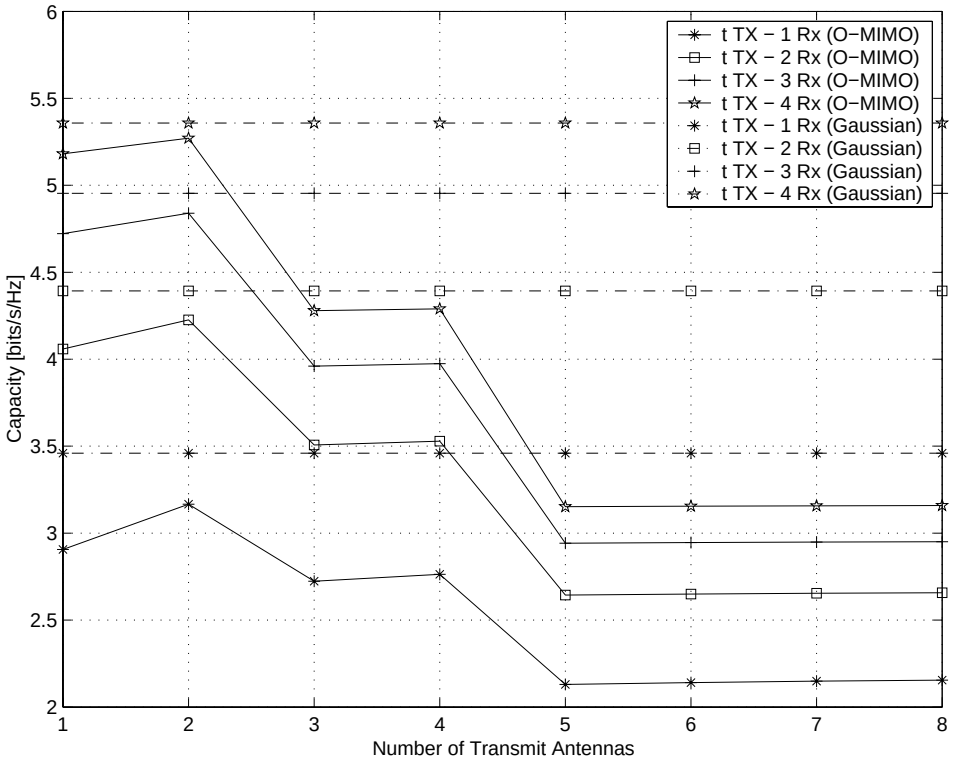


Figure 2.11: Capacity of O-MIMO and Gaussian channels versus the number of transmit antennas labelled on the number of receive antennas; SNR=10dB.

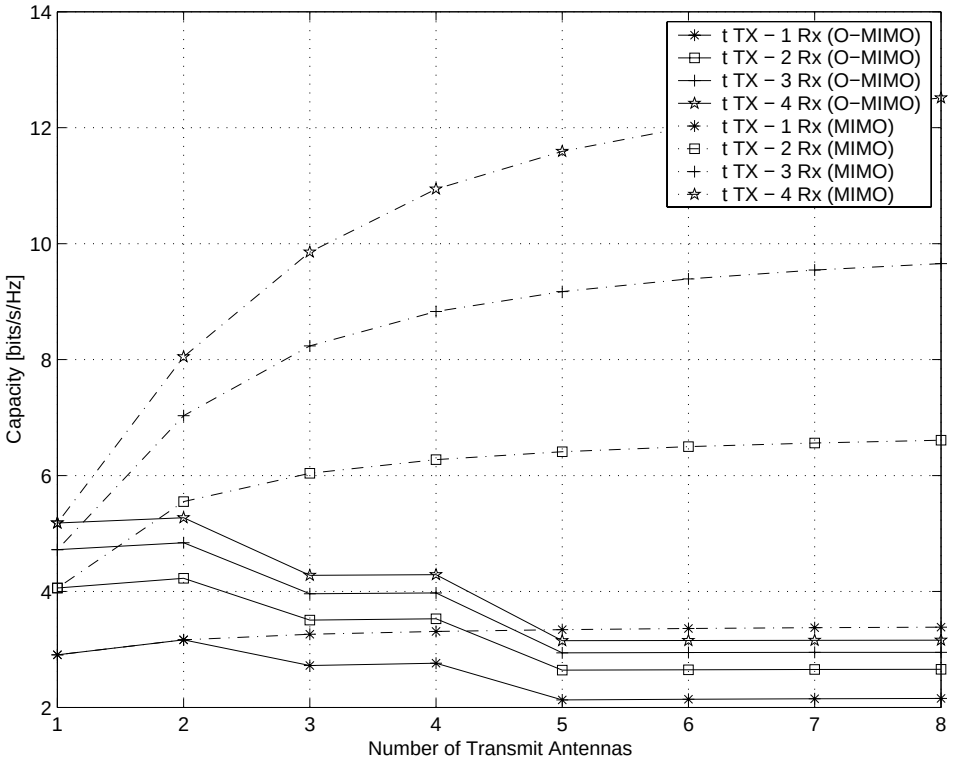


Figure 2.12: Capacity of O-MIMO and traditional MIMO channels versus the number of transmit antennas labelled on the number of receive antennas; SNR=10dB.

**Rayleigh Fading - Unequal Sub-Channel Gains**

From (2.69) and (2.67), the MGF of the instantaneously experienced power $\lambda$ can then be expressed as

$$\phi_\lambda(s) = \prod_{i=1}^{u} \phi_{\lambda_i}(s) = \frac{1}{1-s\gamma_1} \cdot \frac{1}{1-s\gamma_2} \cdots \frac{1}{1-s\gamma_u} \tag{2.74}$$

Resolving (2.74) into its partial fractions, one can write

$$\phi_\lambda(s) = \sum_{i=1}^{u} K_i \phi_{\lambda_i}(s) \tag{2.75}$$

where the constants $K_i$ are obtained by solving the set of linear equations, the solution to which is

$$K_i = \prod_{i'=1, i' \neq i}^{u} \frac{\gamma_i}{\gamma_i - \gamma_{i'}} \tag{2.76}$$

as demonstrated in the Appendix 2.7 (Derivation II) of this chapter. The linearity of the inverse of the MGF allows the pdf of the instantaneous power $\lambda$ to be written as

$$pdf_\lambda(\lambda) = \sum_{i=1}^{u} K_i \cdot \frac{1}{\gamma_i} e^{-\lambda/\gamma_i} \tag{2.77}$$

Evaluating (2.64), the capacity of the O-MIMO channel with unequal channel coefficients can finally be expressed in closed form as

$$C = R \sum_{i=1}^{u} K_i \cdot \hat{C}_0 \left( \frac{1}{R} \frac{\gamma_i}{t} \frac{S}{N} \right) \tag{2.78}$$

Subsequent descriptions relate to Figures 2.14−2.16, which analyse the capacity behaviour when some of the MIMO sub-channels are unequally attenuated, e.g. shadowed.

Figure 2.14 depicts the normalised capacity in [bits/s/Hz] versus the SNR in [dB] for the distributed Alamouti scheme with only one receive antenna. In the case of equal channel coefficients, the expectation of the square of the Frobenius norm of the normalised channel coefficients would yield $t$; here $t = 2$. For this reason, the power of the unequal channel coefficients is chosen such that $\gamma_1 + \gamma_2 \equiv 2$. The particular case where $\gamma_1 : \gamma_2 = 2 : 1$ was chosen, i.e. $\gamma_1 = 4/3$ and $\gamma_2 = 2/3$. The cases are depicted where only the channel with power $\gamma_1$ is utilised, and where only the channel with power $\gamma_2$ is utilised, and where the distributed Alamouti STBC is utilised. The latter is corroborated by numerical simulations.

Clearly, the loss in capacity of the distributed communication scenario is negligible compared to the case where communication happens through the stronger single link. However, a considerable capacity loss can be observed when the weaker single link is utilised. Therefore, when only a single link is deployed then shadowing may severely degrade the link capacity; whereas when a distributed encoding is chosen then the capacity is fairly robust to attenuations in either link. A quantification of the performance gains when independent shadowing dominates the communication system is postponed to Chapter 4.

Figure 2.15 depicts the normalised capacity in [bits/s/Hz] versus the SNR in [dB] for the distributed 3/4-rate STBC scheme. Here, the ratio between the channel coefficients was chosen such that $\gamma_1 : \gamma_2 : \gamma_3 = 4 : 2 : 1$, i.e. $\gamma_1 = 12/7$, $\gamma_2 = 6/7$ and $\gamma_3 = 3/7$. Again, severe capacity losses can be observed when communication happens only over the weaker single links; however, the distributed communication scenario offers a robust capacity. Note, however, that the absolute ergodic capacity of the 3/4-rate STBC is inferior to the ergodic capacity of the full-rate Alamouti scheme.

Figure 2.16 depicts the normalised capacity in [bits/s/Hz] versus the normalised power $\gamma_1$ in the first link for the distributed Alamouti scheme with an SNR of 10dB. Furthermore, depicted are the cases where communication happens only over either of the single links, where $\gamma_2 = 2 - \gamma_1$. The distributed Alamouti scheme outperforms even the strongest link for $0.8 < \gamma_1 < 1.2$. Notably, the capacity of the distributed scheme is much less dependent on the power of the individual links than in the case of the single link schemes. Similar observations can be made for higher order STBCs. This corroborates the advantage of deploying a distributed communication network where channel conditions are not known *a priori* and feedback is limited.

**Rayleigh Fading - Generic Sub-Channel Gains**

Generally, the sub-channel gains $\gamma_{i\in(1,u)}$ can be different where some gains are repeated. There shall be $g \leq u$ distinct sub-channel gains, which are henceforth referred to as $\hat{\gamma}_{i\in(1,g)}$ with each of them being repeated $\nu_{i\in(1,g)}$ times. In this case, the MGF of $\lambda$ is equal to

$$\phi_\lambda(s) = \prod_{i=1}^{g} \phi_{\hat{\lambda}_i}(s) = \frac{1}{(1-s\hat{\gamma}_1)^{\nu_1}} \cdot \frac{1}{(1-s\hat{\gamma}_2)^{\nu_2}} \cdots \frac{1}{(1-s\hat{\gamma}_g)^{\nu_g}} \tag{2.79}$$

where $\sum_{i=1}^{g} \nu_i = u$. Resolving (2.79) into its partial fractions with repeated roots yields

$$\phi_\lambda(s) = \sum_{i=1}^{g} \sum_{j=1}^{\nu_g} K_{i,j} \phi^j_{\hat{\lambda}_i}(s) \tag{2.80}$$

The coefficients $K_{i,j}$ are derived in the Appendix 2.7 (Derivation III) to this chapter as

$$K_{i,j} = \frac{1}{(\nu_i - j)!\,(-\hat{\gamma}_i)^{\nu_i - j}} \frac{\partial^{\nu_i - j}}{\partial s^{\nu_i - j}} \left[ \prod_{\substack{i'=1,\\ i'\neq i}}^{g} \frac{1}{(1-s\hat{\gamma}_{i'})^{\nu_{i'}}} \right]_{s=1/\hat{\gamma}_i} \tag{2.81}$$

This allows one to express the $pdf_\lambda(\lambda)$ in closed form as

$$pdf_\lambda(\lambda) = \sum_{i=1}^{g} \sum_{j=1}^{\nu_g} K_{i,j} \cdot \frac{\lambda^{j-1}}{\Gamma(j) \cdot (\hat{\gamma}_i)^j} e^{-\lambda/\hat{\gamma}_i} \tag{2.82}$$

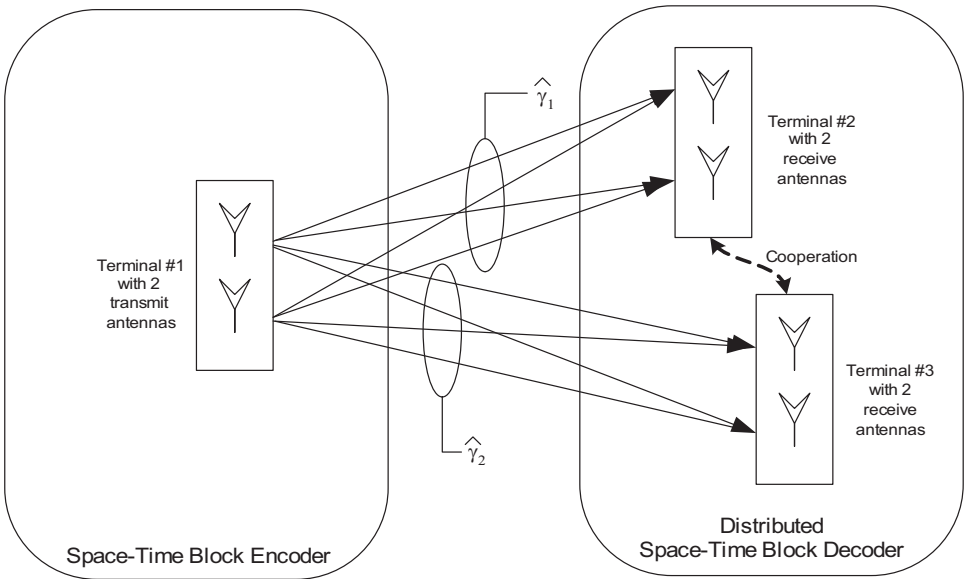


Figure 2.13: Distributed STBC communication scenario with one transmitter and two cooperating receivers, all of which possess two antenna elements.

Finally, evaluating (2.64), the capacity of the O-MIMO channel with unequal but possibly repeated channel coefficients can be expressed as

$$C = R \sum_{i=1}^{g} \sum_{j=1}^{\nu_g} \frac{K_{i,j}}{\Gamma(j)} \cdot \hat{C}_{j-1} \left( \frac{1}{R} \frac{\hat{\gamma}_i}{t} \frac{S}{N} \right) \tag{2.83}$$

The number of different scenarios obeying (2.83) is certainly infinite. To demonstrate its applicability, it is assumed that a terminal with two (uncorrelated) transmit elements communicates with two distributed but cooperating target terminals, each possessing two (uncorrelated) receive antennas. This scenario is depicted in Figure 2.13; it could correspond to the case where an access point in an office communicates with a remote VAA group consisting of two terminals.

The spatial proximity between the elements of the same terminal results in the same channel attenuations from the first terminal to the second terminal, henceforth denoted as $\hat{\gamma}_1$ with repetition $\nu_1 = 4$, and from the first terminal to the third terminal, henceforth denoted as $\hat{\gamma}_2$ with repetition $\nu_2 = 4$. Eq. (2.79) can hence be written as

$$\phi_\lambda(s) = \frac{1}{\left(1 - s\hat{\gamma}_1\right)^4} \cdot \frac{1}{\left(1 - s\hat{\gamma}_2\right)^4} \tag{2.84}$$

The coefficients $K_{i=\{1,2\},j\in(1,4)}$ can be obtained by simply performing the required differentiations to arrive at

$$K_{\{1,2\},j\in(1,4)} = \frac{1}{3!} \frac{(7-j)!}{(4-j)!} \frac{\left(-\hat{\gamma}_{\{2,1\}}/\hat{\gamma}_{\{1,2\}}\right)^{4-j}}{\left(1 - \hat{\gamma}_{\{2,1\}}/\hat{\gamma}_{\{1,2\}}\right)^{8-j}} \tag{2.85}$$

which allows one to calculate (2.83) in closed form for the given scenario.

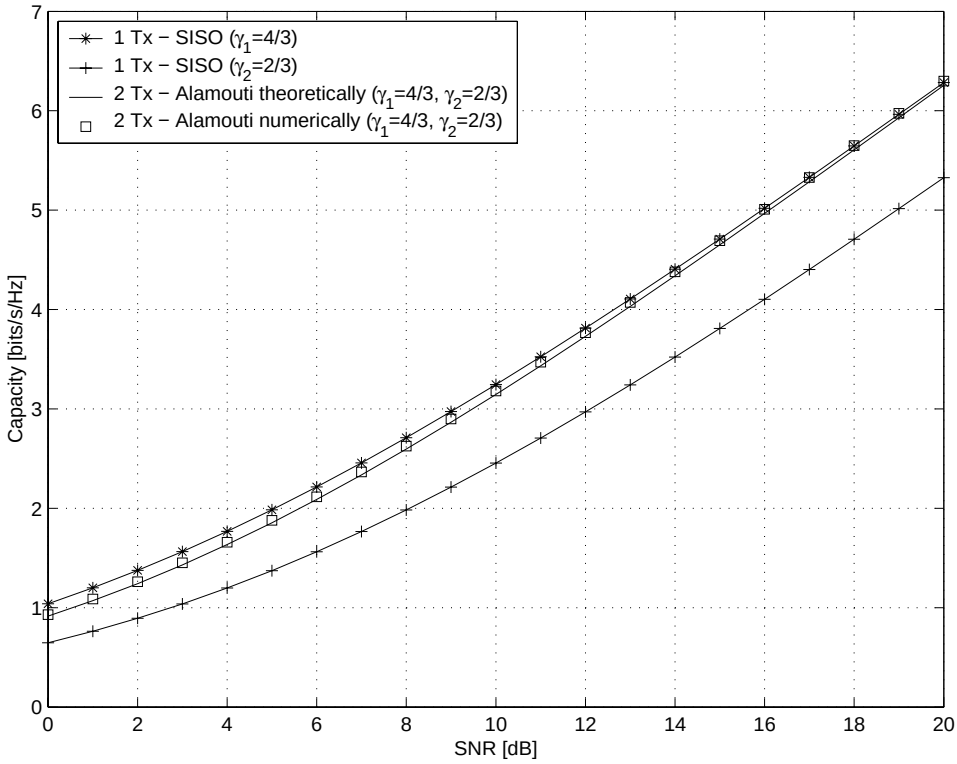


Figure 2.14: Capacity versus SNR for the distributed Alamouti scheme with one receive antenna only; $\gamma_1 + \gamma_2 \equiv 2$ and $\gamma_1 : \gamma_2 = 2 : 1$.

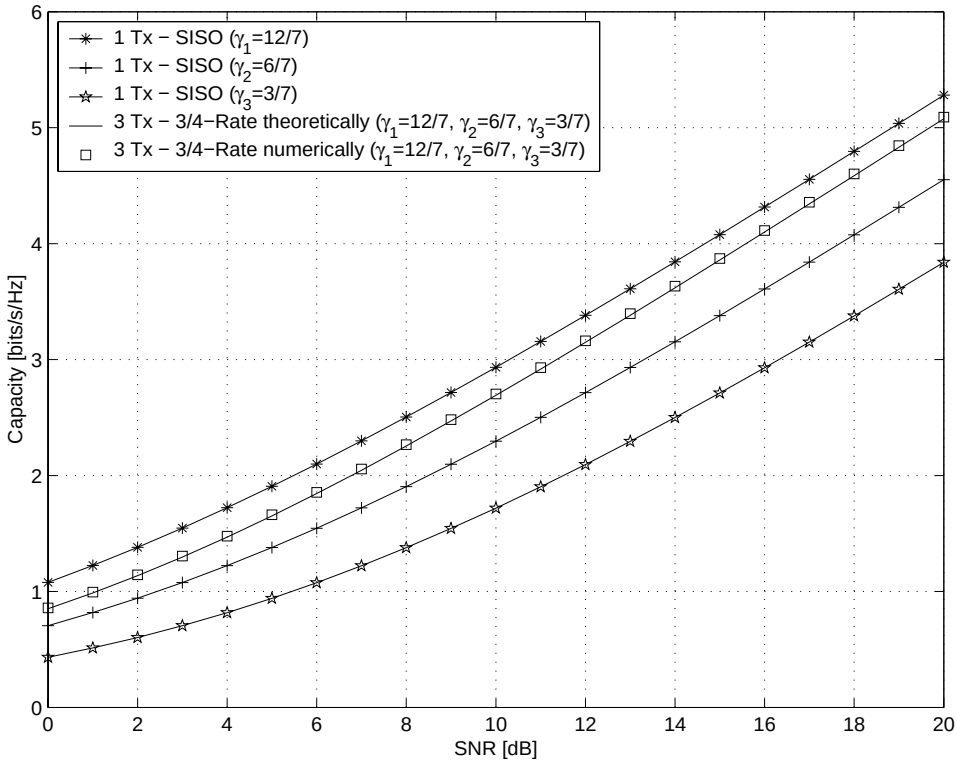


Figure 2.15: Capacity versus SNR for the distributed 3/4-rate STBC scheme with one receive antenna only; $\gamma_1 + \gamma_2 + \gamma_3 \equiv 3$ and $\gamma_1 : \gamma_2 : \gamma_3 = 4 : 2 : 1$.

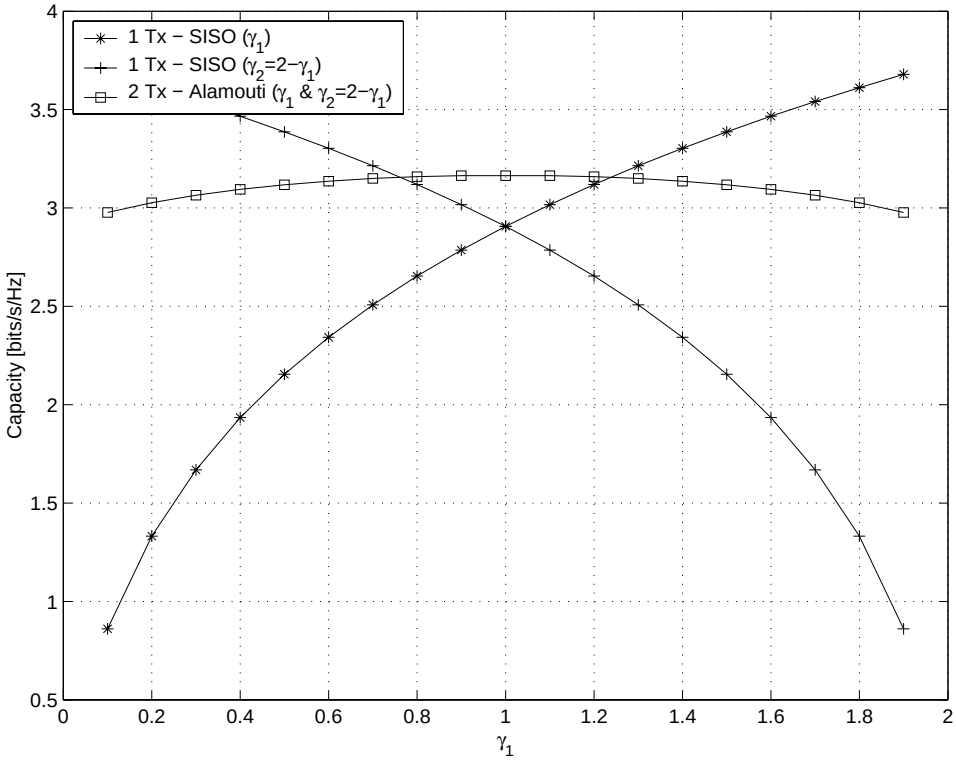


Figure 2.16: Capacity versus the normalised power $\gamma_1$ in the first link for the distributed Alamouti scheme; SNR=10dB and $\gamma_2 = 2 - \gamma_1$.

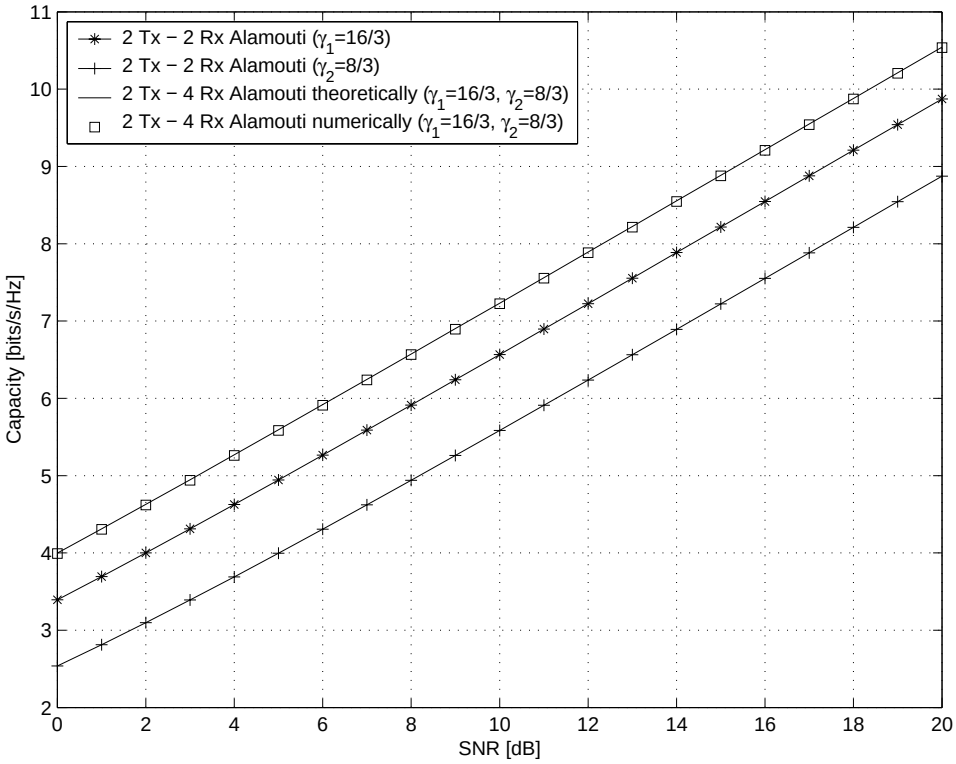


Figure 2.17: Capacity versus SNR for the scheme of Figure 2.13; $\hat{\gamma}_1 + \hat{\gamma}_2 \equiv 8$, $\hat{\gamma}_1 : \hat{\gamma}_2 = 2 : 1$.

Figure 2.17 depicts the normalised Shannon capacity in [bits/s/Hz] versus the SNR in [dB] for the above-given scenario. In the case of equal channel coefficients, the expectation of the square of the Frobenius norm of the normalised channel coefficients would yield $u$; here $u = 2 \cdot 4$. For this reason, the power of the two unequal channel coefficients is chosen such that $\sum_i^8 \gamma_i = \sum_i^2 \hat{\gamma}_i \equiv 8$. The particular case where $\hat{\gamma}_1 : \hat{\gamma}_2 = 2 : 1$ was chosen, i.e. $\hat{\gamma}_1 = 16/3$ and $\hat{\gamma}_2 = 8/3$. The capacities of each individual link are shown, as well as the capacity when both target terminals cooperate and hence realise a $2 \times 4$ O-MIMO system. The latter case yields an expected increase in capacity due to additional receive diversity.

Note that the additional resources in terms of relaying power and bandwidth required to maintain the cooperation are not incorporated into current analysis. It is a fair assumption, however, that the cooperating terminals are spatially sufficiently close as to neglect the relaying power compared to the transmission power at the access point. Furthermore, it can be assumed that with many such VAA groups re-using the relaying bandwidth, the additional bandwidth can also be neglected.

**Nakagami Fading - Equal Sub-Channel Gains**

The MGF of the instantaneously experienced power $\lambda_i$ of the $i^{th}$ Nakagami distributed sub-channel with fading factor $f_i$ can be expressed as [46]

$$\phi_{\lambda_i}(s) = \frac{1}{\left(1 - s\frac{\gamma_i}{f_i}\right)^{f_i}} \tag{2.86}$$

For equal channel gains $\gamma_1 = \ldots = \gamma_u$, henceforth simply denoted as $\gamma$, and equal fading parameters $f_1 = \ldots = f_u$, henceforth denoted as $f$, yields for (2.67) with (2.86)

$$\phi_{\lambda}(s) = \frac{1}{\left(1 - s\frac{\gamma}{f}\right)^{fu}} \tag{2.87}$$

the inverse of which leads to the desired pdf of the instantaneous power [47]

$$pdf_{\lambda}(\lambda) = \frac{f^{fu}\lambda^{fu-1}}{\gamma^{fu}\Gamma(fu)} e^{-f\lambda/\gamma} \tag{2.88}$$

The capacity (2.64) is solvable for $f \in \mathbb{N}$ in closed form as

$$C = \frac{R}{\Gamma(fu)} \cdot \hat{C}_{fu-1}\left(\frac{1}{R}\frac{\gamma}{ft}\frac{S}{N}\right) \tag{2.89}$$

Note that if $f \in \mathbb{R}$ then $f$ should be replaced by $\lfloor f \rfloor$ to obtain a lower bound, i.e. the capacity which is at least achieved by the ergodic Nakagami O-MIMO channel.

Figure 2.18 depicts the normalised capacity in [bits/s/Hz] versus the SNR in [dB] for various O-MIMO system configurations over Nakagami fading channels with $\gamma = 1$ and two receive antennas, i.e. $r = 2$. Depicted are the following cases: (1) $t = 1$ (O-SIMO) with $f = 1$ (Rayleigh), (2) $t = 1$ (O-SIMO) with $f = 10$ (strong LOS), (3) $t = 2$ (Alamouti)

with $f = 1$ (Rayleigh), (4) $t = 2$ (Alamouti) with $f = 10$ (strong LOS), (5) equivalent Gaussian channel for comparison. To observe the small capacity differences between these cases, only a small region for large SNR is depicted. Clearly, for $f = 10$, i.e. a strong LOS communication scenario, capacity reaches Gaussian performance. This is independent from the number of transmit antennas as the fading channel exhibits very little fluctuations for high $f$. Therefore, the deployment of STBCs in environments with a high likelihood of LOS communication is not worthwhile from a capacity point of view.

To gain a better insight on the capacity tendencies in dependency of the Nakagami $f$ fading factor, Figure 2.19 depicts the normalised capacity in [bits/s/Hz] versus the Nakagami $f$ fading factor for various O-MISO system configurations at an SNR of 10dB and one receive antenna only. The Nakagami $f$ fading factor is varied from $f = 1$ (Rayleigh) to $f = 20$ (very strong LOS). Compared are the following scenarios: (1) $t = 1$ (SISO), (2) $t = 2$ (Alamouti), (3) $t = 3$ (3/4-Rate), (4) $t = 4$ (3/4-Rate), (5) $t = 3$ (Half-Rate), (6) $t = 4$ (Half-Rate), (7) Gaussian channel for comparison.

Interestingly, capacity is rather independent of $f$ for the 3/4 and 1/2 rate STBCs; however, generally inferior to the capacity of the full-rate STBCs. Their low dependency is explained with the high diversity already obtained from the 3 and 4 transmit antennas. Their low performance comes from the rate loss due to $R < 1$. Furthermore, the Alamouti STBC converges to the Gaussian capacity faster than the one transmit antenna case does. Finally, increasing the number of receive antennas $r$ lessens the dependency on the Nakagami $f$ fading factor even further. It can hence be stated that the $f$ factor can be traded against the number of transmit elements when deploying STBCs, as corroborated by Figure 2.20 which is an enlargement of Figure 2.19. For example, if one wishes to communicate at a capacity of 3.3 bits/s/Hz, then with $f = 4$ a single transmitter is sufficient, whereas with $f = 2$ one has to deploy Alamouti STBC with two transmit antennas.

**Nakagami Fading - Unequal Sub-Channel Gains**

Here, the same procedure as for the Rayleigh fading case can be repeated. The MGF $\phi_\lambda(s)$ of the O-MIMO Nakagami fading channel can be expressed as

$$\phi_\lambda(s) = \prod_{i=1}^{u} \phi_{\lambda_i}(s) = \frac{1}{\left(1 - s\frac{\gamma_1}{f_1}\right)^{f_1}} \cdot \frac{1}{\left(1 - s\frac{\gamma_2}{f_2}\right)^{f_2}} \cdots \frac{1}{\left(1 - s\frac{\gamma_u}{f_u}\right)^{f_u}} \tag{2.90}$$

where $f_i \in \mathbb{N}$ is the Nakagami fading parameter of the $i^{th}$ link. Repeating the procedure of the O-MIMO Rayleigh fading case, finally yields for the capacity

$$C = R \sum_{i=1}^{u} \sum_{j=1}^{f_i} \frac{K_{i,j}}{\Gamma(j)} \hat{C}_{j-1}\left(\frac{1}{R}\frac{\gamma_i}{jt}\frac{S}{N}\right) \tag{2.91}$$

where the coefficients $K_{i,j}$ are now found by performing partial fractions on (2.90).

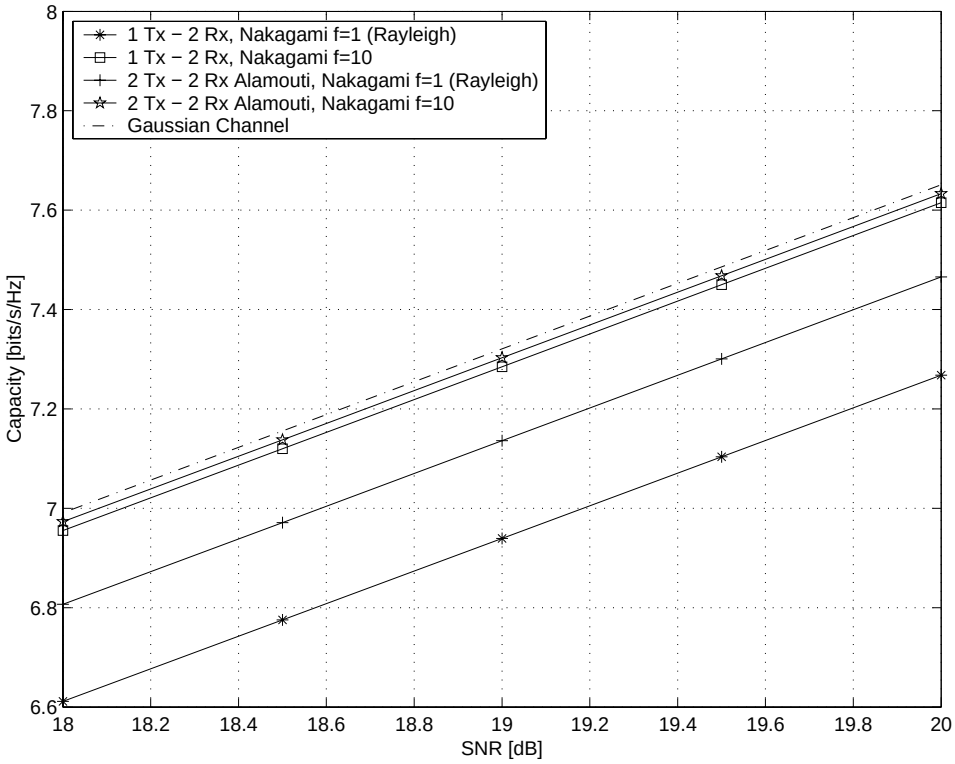


Figure 2.18: Capacity versus SNR for various O-MIMO system configurations with different Nakagami fading parameters; $r = 2$.

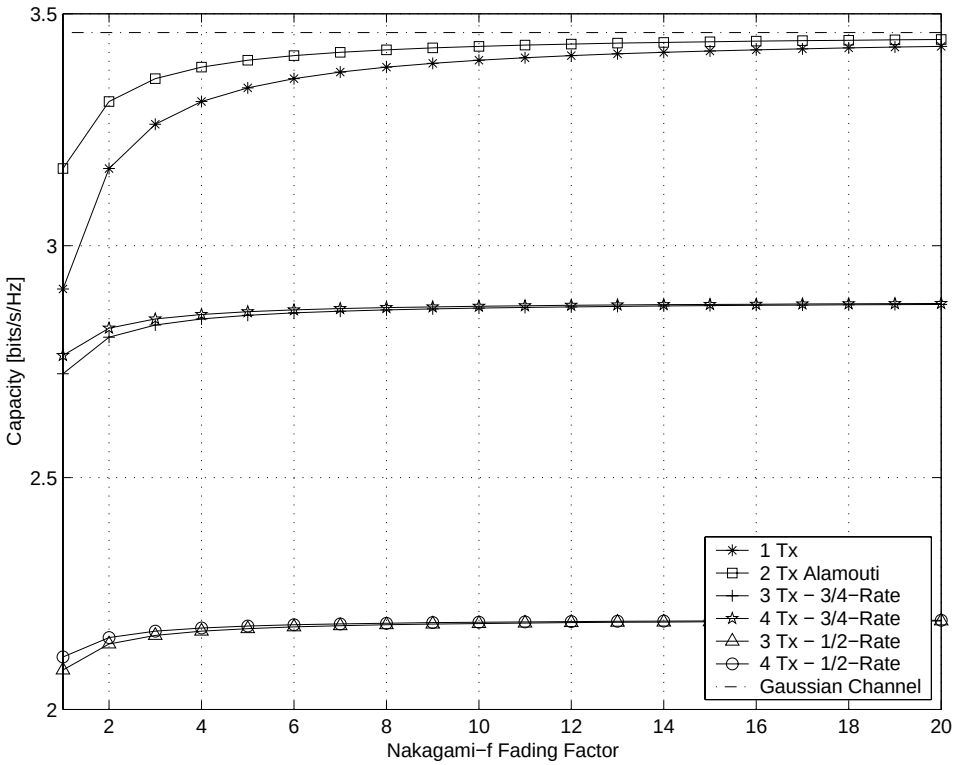


Figure 2.19: Capacity versus the Nakagami $f$ fading factor for various O-MISO system configurations; SNR=10dB, $r = 1$.

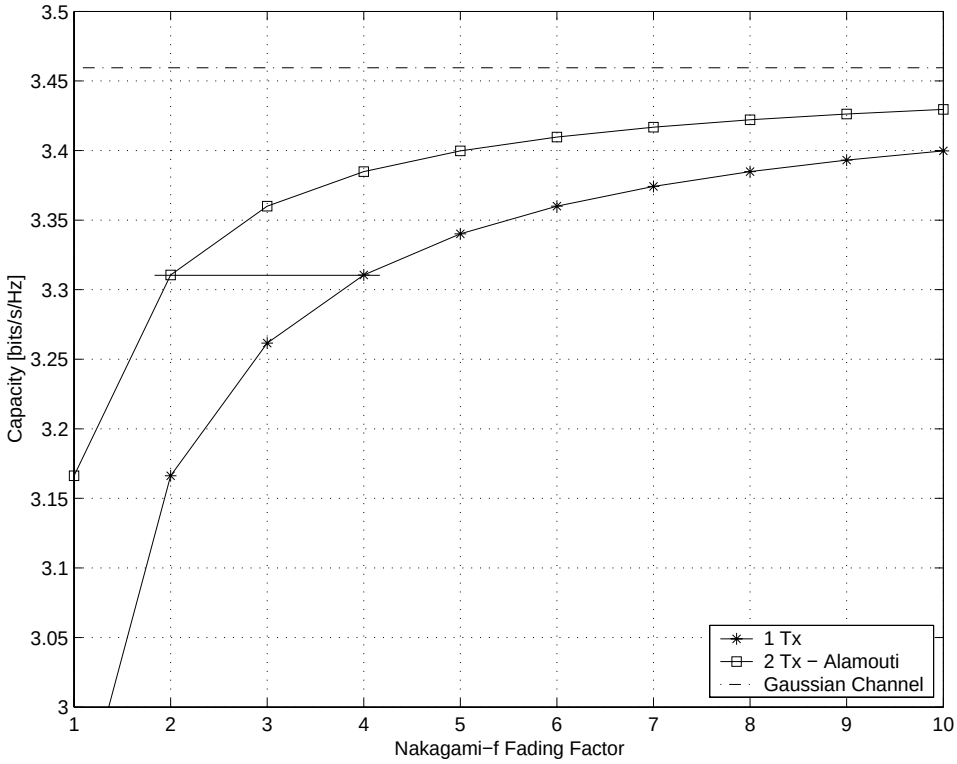


Figure 2.20: Capacity versus the Nakagami $f$ fading factor for the full-rate O-MISO system configurations only; SNR=10dB, $r = 1$.

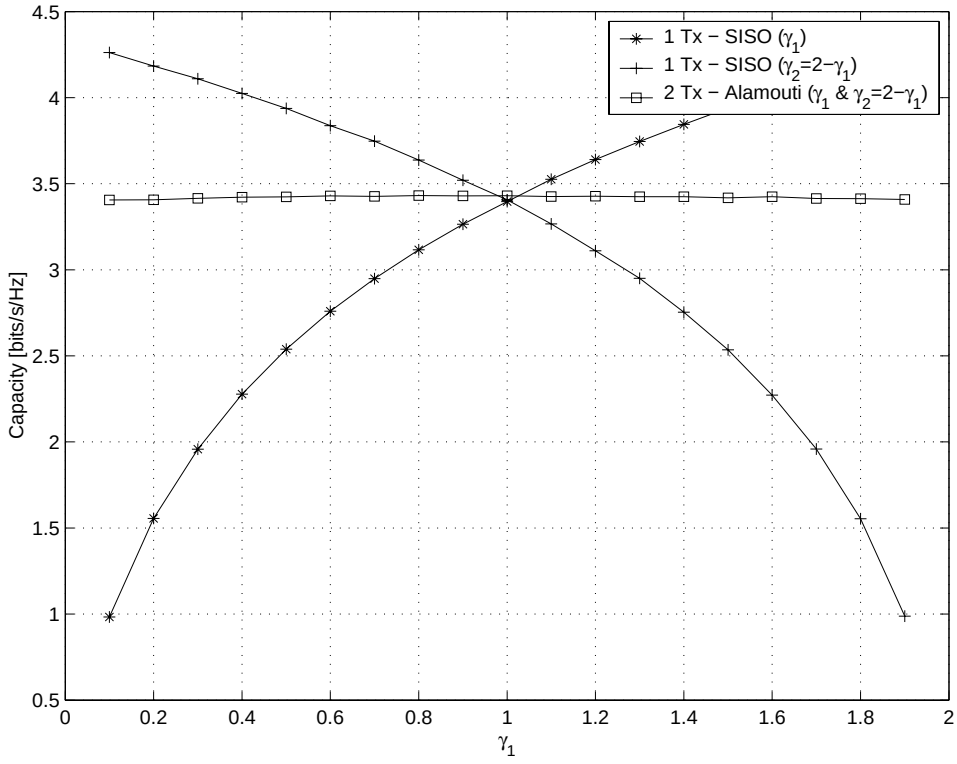


Figure 2.21: Capacity versus the normalised power $\gamma_1$ in the first link for the distributed Alamouti scheme over a Nakagami fading channel; SNR=10dB, $f = 10$ and $\gamma_2 = 2 - \gamma_1$.

Figure 2.21 depicts the normalised capacity in [bits/s/Hz] versus the normalised power in the first link $\gamma_1$ over a Nakagami fading channel with $f = 10$ for the distributed Alamouti scheme at an SNR of 10dB. Again, depicted are the cases where communication happens only over either of the single links, where $\gamma_2 = 2 - \gamma_1$. Clearly, the region where the distributed Alamouti scheme outperforms the stronger link has reduced to a single point for $\gamma_1 = 1$. Furthermore, the capacity of the distributed scenario is up to 15% lower than of the stronger single link case. However, the capacity of the distributed scenario is virtually independent of the fading coefficients. Therefore, if the terminals are potentially shadowed, then the distributed communication scenario offers a significant performance stability.

**Nakagami Fading - Generic Channel Gains**

The case of generic channel coefficients is similarly obtained as for the Rayleigh channel and is thus omitted here.

### 2.4.3 Non-Ergodic O-MIMO Channels

The calculation of the outage capacity for O-MIMO channels with different statistics in each sub-channel is fairly simple. This is because, as demonstrated before, the STBCs are known to reduce MIMO channels into rank one SISO channels, which allows the application of (2.53) and (2.54) with some modifications related to the rate of the STBC. Various communication scenarios are briefly dealt with below.

**Rayleigh Fading - Equal Sub-Channel Gains**

Computing (2.53) for the Rayleigh fading channel with the pdf given by (2.71), one obtains

$$P_{out}(\Phi) = \frac{1}{\Gamma(u)}\gamma\left(u, \left(2^{\Phi/R} - 1\right) \Big/ \left(\frac{1}{R}\frac{\gamma}{t}\frac{S}{N}\right)\right) \tag{2.92}$$

which is visualised in Figures 2.22 & 2.23 for $\gamma = 1$.

Figure 2.22 displays the outage probability $P_{out}(\Phi)$ in [%] versus the the desired rate $\Phi$ in [bits/s/Hz] for one receive antenna at an SNR of 10dB. The following cases are compared: (1) $t = 1$ (SISO), (2) $t = 2$ (Alamouti), (3) $t = 3$ (3/4-Rate), (4) $t = 4$ (3/4-Rate), (5) $t = 3$ (Half-Rate), and finally (6) $t = 4$ (Half-Rate). The curves intersect, indicating that a different number of transmit antennas ought to be used in dependency of the desired rate $\Phi$ at a given SNR such as to minimise the outage probability. In contrast to traditional MISO channels, c.f. Section 2.3, the region of intersection is now fairly wide due to the different rates of the deployed STBCs. However, the general observation of Telatar's conjecture (2.49) holds here as well, i.e. desired high rates with low reliability should be supported by one transmit element, desired low rates with high reliability by four elements with the 3/4-rate STBC. The absolute values of the rate and the outage probability depend on the SNR.

For the chosen SNR of 10dB, a high rate of $\Phi = 4.5$ bits/s/Hz is supported by the single transmitter with 12% reliability, by the Alamouti scheme with 7%, whereas all other schemes with 0%. A lower rate of $\Phi = 1.5$ bits/s/Hz is supported by the single transmitter with 16% outage probability, by the Alamouti scheme with 5%, and by the 3/4-rate STBC with four transmit antennas with only 1% outage probability, i.e. a reliability of 99%.

Only the case for $r = 1$ was shown here; however, similar conclusions can be made for any number of receive antennas, with steeper outage curves with $r$ increasing.

To appreciate the power savings achieved by deploying a higher number of transmit antennas, Figure 2.23 depicts the outage probability $P_{out}(\Phi)$ in [%] versus the SNR in [dB] for a desired rate $\Phi = 2$ bits/s/Hz. For an outage of 10%, the gains with respect to the SISO case are: 1.5dB (1/2-Rate, 3 transmit antennas), 2.0dB (1/2-Rate, 4 transmit antennas), 4.0dB (Alamouti, 2 transmit antennas), 4.0dB (3/4-Rate, 3 transmit antennas), and approximately 5.0dB (3/4-Rate, 4 transmit antennas). It is worth noting that the gains decrease for increasing $\Phi$.

A 5dB gain translates to approximately $(1 - 1/\sqrt{10}) \cdot 100\% = 70\%$ power savings. In contrast to the ergodic channels, it is thus worth deploying O-MIMO systems with more than two distributed transmit element for non-ergodic channel realisations.

**Rayleigh Fading - Unequal Sub-Channel Gains**

Computing (2.53) for the Rayleigh fading channel with unequal channel gains, the pdf of which is given by (2.77), one obtains

$$P_{out}(\Phi) = \sum_{i=1}^{u} K_i \cdot \gamma\left(1, \left(2^{\Phi/R} - 1\right) \Big/ \left(\frac{1}{R}\frac{\gamma_i}{t}\frac{S}{N}\right)\right) \tag{2.93}$$

where the coefficients $K_i$ are given by (2.76). Note that $\gamma(1, x) = 1 - e^{-x}$.

Figure 2.24 depicts the outage probability $P_{out}(\Phi)$ in [%] versus the normalised power in the first link $\gamma_1$ for the distributed Alamouti scheme with a desired communication rate of 2 bits/s/Hz at an SNR of 15dB. Again, the cases where communication happens only over either of the single links are depicted, where $\gamma_2 = 2 - \gamma_1$.

Similar to the ergodic case, the outage probability of the distributed scheme is much less dependent on the power of the individual links than the single link schemes. Furthermore, for the chosen system parameters, the distributed scheme can support a rate of 2 bits/s/Hz with an outage probability of less than 10% for any $\gamma_1$. The single links, however, cannot guarantee this data rate at 10% outage probability as the normalised power in the respective links drops below unity. It can thus be concluded that in the case of independent shadowing between the communication elements, a distributed communication scenario will always bring benefits in terms of power savings or outage probabilities when compared to a single link communication scenario.

Finally, Figure 2.25 depicts the outage probability $P_{out}(\Phi)$ in [%] versus the normalised power in the first link $\gamma_1$ for various distributed communication scenarios with a desired communication rate of 2 bits/s/Hz at an SNR of 15dB. With a varying $\gamma_1$, the remaining channel power was equally distributed between the other sub-channels, i.e. for the Alamouti scheme we have $\gamma_2 = 2-\gamma_1$, for the 3/4-rate STBC scheme with three transmit elements we have $\gamma_2 = \gamma_3 = (3-\gamma_1)/2$, and for the 3/4-rate STBC scheme with four transmit elements we have $\gamma_2 = \gamma_3 = \gamma_4 = (4-\gamma_1)/3$. Note that the sub-channel power distribution has to guarantee that $\sum_{i=1}^{t} \gamma_i \equiv t$ to allow for a fair comparison between the schemes. The given scenario could correspond to the case where one distributed transmit element is subject to severe shadowing, whereas the remaining distributed elements are not.

From Figure 2.25 it is clear again that, at 10% outage probability, the SISO case can only support the rate of 2 bits/s/Hz for a sufficiently high $\gamma_1$, whereas all the distributed cases support such rate for any $\gamma_1$. Furthermore, the 3/4-rate STBC with four distributed transmit elements exhibits the most robust link with a reliability of more than 99%.

Note finally that the case of generic channel gains with repeated $\gamma_{i\in(1,u)}$ is similarly obtained by utilising the appropriate pdf previously derived, and is thus omitted here.

**Nakagami Fading - Equal Sub-Channel Gains**

Computing (2.53) for the Nakagami fading channel with $u$ equal sub-channel gains, the pdf of which is given by (2.88), one obtains for the outage probability

$$P_{out}(\Phi) = \frac{1}{\Gamma(uf)}\gamma\left(uf, \left(2^{\Phi/R}-1\right)\Big/\left(\frac{1}{R}\frac{\gamma}{ft}\frac{S}{N}\right)\right) \tag{2.94}$$

which is not further visualised. Numerical results, however, indicate that for a scenario with $\gamma = 1$, $\Phi = 2$ bits/s/Hz, $t = 4$ and $r = 1$, power savings of approximately 2.6 dB can be achieved by increasing $f$ from 1 to 10 at an outage probability of 10%. Compared to the ergodic capacity, where capacity saturates very fast for increasing $f$, this is a notable power gain.

**Nakagami Fading - Unequal Sub-Channel Gains**

Finally, the outage probability over differently distributed Nakagami fading channels can be obtained as

$$P_{out}(\Phi) = \sum_{i=1}^{u}\sum_{j=1}^{f_i}\frac{K_{i,j}}{\Gamma(j)}\gamma\left(j, \left(2^{\Phi/R}-1\right)\Big/\left(\frac{1}{R}\frac{\gamma}{f_i t}\frac{S}{N}\right)\right) \tag{2.95}$$

which is not further analysed here.

Note again that the case of generic sub-channel gains with repeated $\gamma_{i\in(1,u)}$ and arbitrary $f_{i\in(1,u)}$ is similarly obtained by utilising the appropriate pdf previously derived, and is thus omitted here.

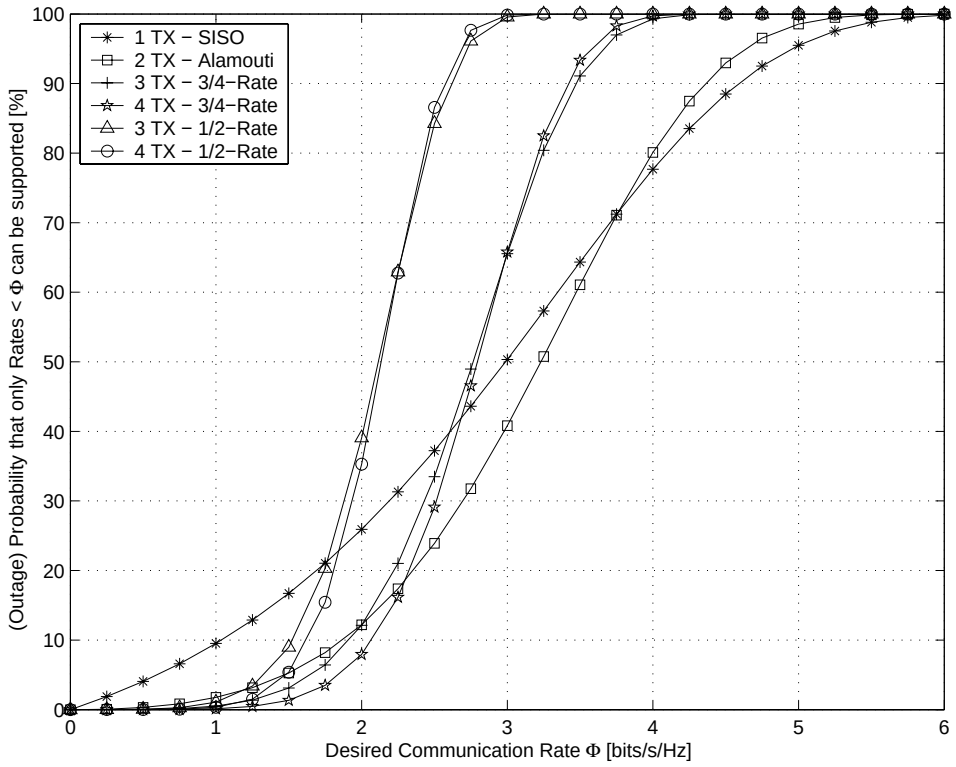


Figure 2.22: Outage probability $P_{out}(\Phi)$ versus the desired rate $\Phi$ for various STBC system configurations; SNR=10dB, $r = 1$.

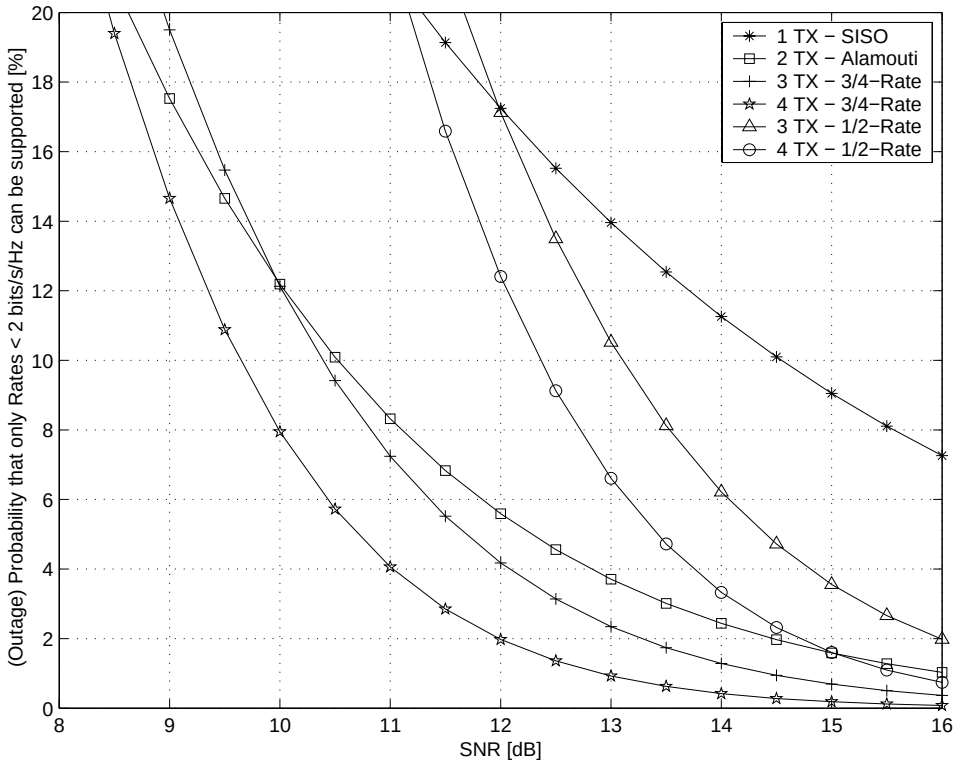


Figure 2.23: Outage probability $P_{out}(\Phi)$ versus SNR for various STBC system configurations at a desired rate of $\Phi = 2$ bits/s/Hz; $r = 1$.

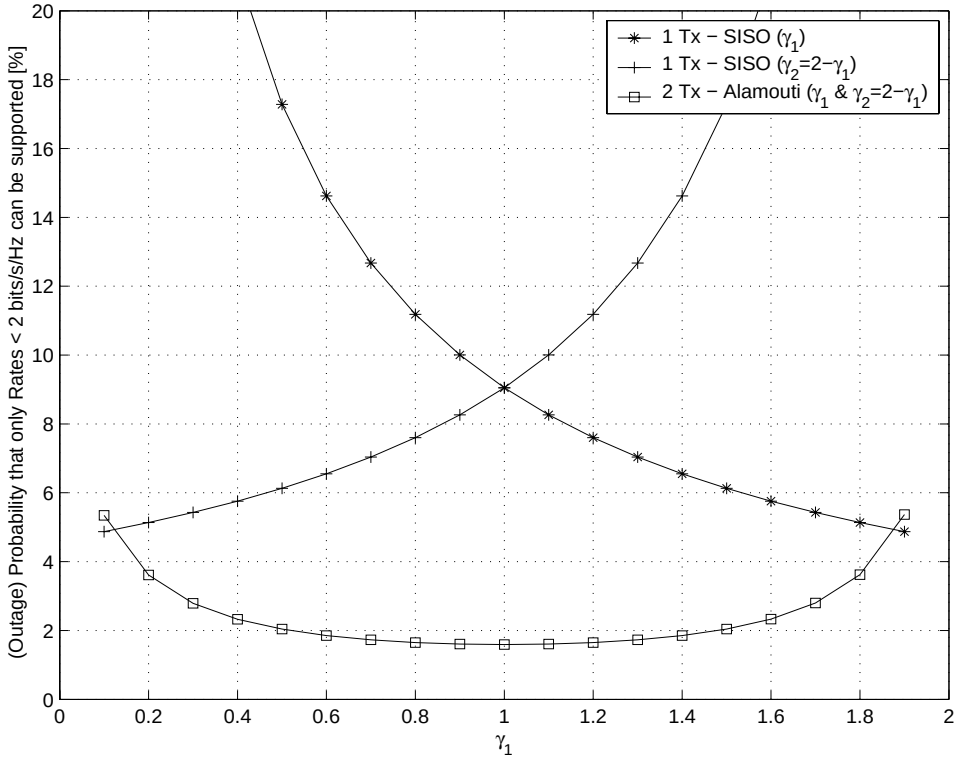


Figure 2.24: Outage probability $P_{out}(\Phi)$ versus the normalised power $\gamma_1$ in the first link for the distributed Alamouti scheme at a desired rate of $\Phi = 2$ bits/s/Hz; SNR=15dB and $\gamma_2 = 2 - \gamma_1$.

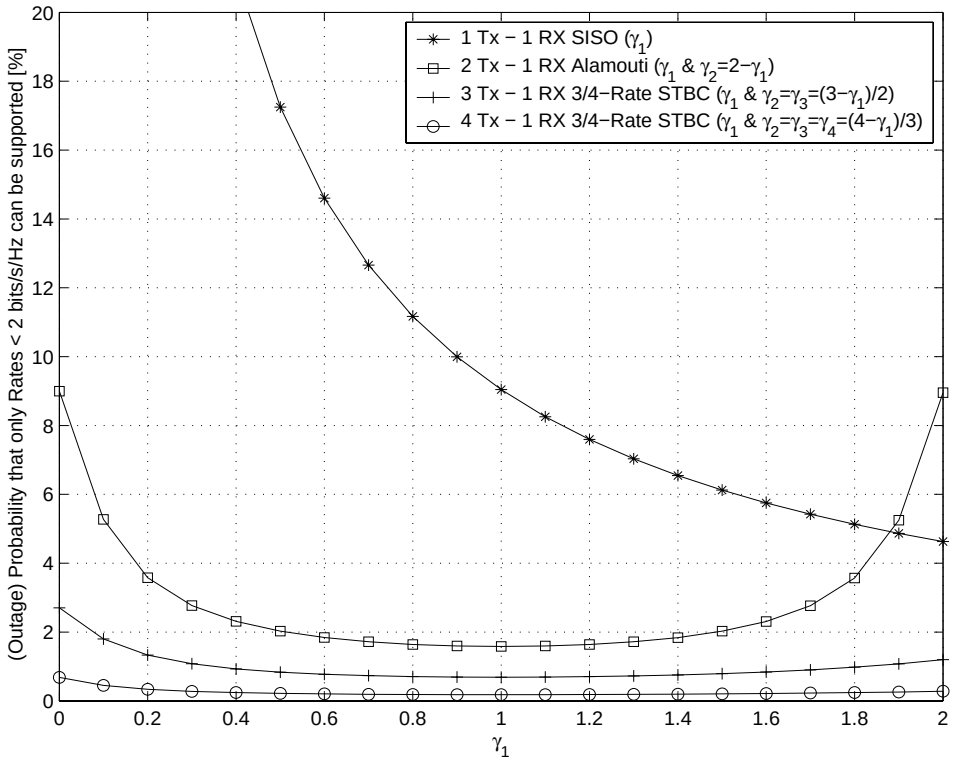


Figure 2.25: Outage probability $P_{out}(\Phi)$ versus the normalised power $\gamma_1$ in the first link for distributed STBC schemes at a desired rate of $\Phi = 2$ bits/s/Hz; SNR=15dB.

## 2.5 Approximations to Capacity and Outage Probability

Distributed-MIMO multi-stage communication systems require optimum resource allocation algorithms which, in the case of FDMA-based relaying, assign each relaying terminal within a relaying stage a fractional bandwidth $\alpha W$ and a fractional power $\beta S$, such as to maximise the end-to-end capacity. In Chapter 3, it will be shown that the normalised capacity of a MIMO link with given fractional bandwidth and power allocations can be expressed as

$$C = \alpha \cdot \mathrm{E}_\lambda \left\{ m \log_2 \left( 1 + \lambda \frac{\beta}{\alpha} \frac{\gamma}{t} \frac{S}{N} \right) \right\} \tag{2.96}$$

where $m = \min\{t, r\}$, $\gamma$ is associated with the pathloss and the expectation is generally calculated with the aid of (2.32). The optimisation process clearly involves some form of differentiation with respect to the fractional resources $\alpha$ and $\beta$, after which a large set of equations has to be solved. If the solution to (2.96) was given in the fairly intricate form of (2.38), no analytical optimisation of the entire multi-stage network is possible.

It is the aim of this section to introduce a sufficiently precise approximation to the MIMO capacity, thereby decoupling the fractional resource allocations from the complicated term associated with the MIMO capacity gain. This will enable closed form resource allocation algorithms for networks of any size, as will be demonstrated in Chapter 3. Note that other approximations were suggested in the literature, see e.g. [48]; however, none of these are sufficiently simple to decouple the fractional resources from the MIMO capacity gain.

In a similar manner, sufficiently precise approximations to the outage probability are introduced which are needed in Chapter 3 to maximise the end-to-end throughput over non-ergodic fading channels.

### 2.5.1 Functional Approximation to the MIMO Capacity

The term $\log_2(1 + x)$ in (2.96) clearly complicates the analysis. To this end, a simple functional approximation is suggested in form of

$$\log_2(1 + x) \approx \sqrt{x} \tag{2.97}$$

the precision and applicability of which is assessed below. The suggested approximation simplifies (2.96) to

$$C \approx \alpha \sqrt{\frac{\beta}{\alpha}} \sqrt{\gamma \frac{S}{N}} \cdot \mathrm{E}_\lambda \left\{ m \sqrt{\lambda / t} \right\} \tag{2.98}$$

The above expression decouples the fractional resources $\alpha$ and $\beta$ from $\mathrm{E}_\lambda \left\{ m \sqrt{\lambda/t} \right\}$, which is associated with the MIMO capacity gain. The expectation with respect to the unordered eigenvalue $\lambda$ is evaluated following exactly the same approach as exposed by (2.32)−(2.39),

to arrive at

$$\mathrm{E}_\lambda\left\{m\sqrt{\lambda/t}\right\} = \frac{1}{\sqrt{t}}\sum_{k=0}^{m-1}\frac{k!}{(k+d)!}\left[\sum_{l=0}^{k} A_l^2(k,d)\,\hat{L}_{2l+d} + \sum_{l_1=0}^{k}\sum_{\substack{l_2=0,\\ l_2\neq l_1}}^{k}(-1)^{l_1+l_2}A_{l_1}(k,d)\,A_{l_2}(k,d)\,\hat{L}_{l_1+l_2+d}\right] \tag{2.99}$$

where, to remind the reader, $d = n - m$, $A_l(k,d) = [(k+d)!]/[(k-l)!\,(d+l)!\,l!]$, and $m = \min(t,r)$, $n = \max(t,r)$. Furthermore, with reference to (2.38), the capacity integral $\hat{C}_\zeta(a)$ is replaced by the capacity approximation integral $\hat{L}_\zeta$, which is defined and solved [44] (§3.381.4) as

$$\hat{L}_\zeta \triangleq \int_0^\infty \sqrt{x}\,x^\zeta\,e^{-x}\,dx \tag{2.100}$$

$$= \Gamma(\zeta + 3/2) \tag{2.101}$$

Interestingly, the expectation in (2.98) with the pdf of (2.32) can be calculated in a more compact form as [44] (§ 7.414.4.1)

$$\mathrm{E}_\lambda\left\{m\sqrt{\lambda/t}\right\} \approx \frac{1}{\sqrt{t}}\sum_{k=0}^{m-1}\frac{k!}{(k+d)!}\int_0^\infty \sqrt{\lambda}\left[L_k^d(\lambda)\right]^2\lambda^d e^{-\lambda}d\lambda \tag{2.102}$$

$$= \frac{1}{\sqrt{t}}\sum_{k=0}^{m-1}\frac{k!}{(k+d)!}\frac{\Gamma^3(d+k+1)\Gamma(d+\frac{3}{2})\Gamma(k-\frac{1}{2})}{(k!)^2\Gamma(d+1)\Gamma(-\frac{1}{2})}\times {}_3F_2(-k, d+\frac{3}{2}, \frac{3}{2}; d+1, \frac{3}{2}-k; 1) \tag{2.103}$$

where ${}_3F_2(\cdot)$ is the generalised hypergeometric function with three parameters of type 1 and two parameters of type 2. For the sake of clarity, $\mathrm{E}_\lambda\left\{m\sqrt{\lambda/t}\right\}$ is henceforth denoted as $\Lambda(t,r)$, which allows simplification of the MIMO capacity expression to

$$C \approx \alpha\sqrt{\frac{\beta}{\alpha}}\sqrt{\gamma\frac{S}{N}}\cdot\Lambda(t,r) \tag{2.104}$$

The same approach is taken to calculate the approximated capacity for various O-MIMO channels, some of which are summarised below as

$$\Lambda(t,r) = \begin{cases} \frac{1}{\sqrt{t}}\sum_{k=0}^{m-1}\frac{k!}{(k+d)!}\left[\ldots\right] & \text{MIMO Rayleigh} \\ \frac{\sqrt{R}}{\sqrt{t}}\frac{\Gamma(u+1/2)}{\Gamma(u)} & \text{O-MIMO Rayleigh - Equal Channel Gains} \\ \frac{\sqrt{R}}{\sqrt{ft}}\frac{\Gamma(fu+1/2)}{\Gamma(fu)} & \text{O-MIMO Nakgami - Equal Channel Gains} \\ \frac{\sqrt{R\pi}}{\sqrt{t}}\sum_{i=1}^{u}K_i\sqrt{\gamma_i} & \text{O-MIMO Rayleigh - Unequal Channel Gains} \end{cases} \tag{2.105}$$

Rounded values of $\Lambda(t,r)$ for the traditional MIMO Rayleigh fading case are tabled in Table 2.1 for $1 \le t \le 10$ and $1 \le r \le 10$. For instance, a $4 \times 1$ MIMO configuration achieves approximately twice the capacity of a SISO communication system. A $10 \times 10$ MIMO configuration yields approximately a nine-fold capacity increase, which is well inline with the observed linear increase of capacity when $t = r$.

Furthermore, in Figure 2.26, the exact and approximated capacities for various example configurations of transmit and receive arrays are depicted. The following MIMO configurations have been chosen: $t = 1$ & $r = 1$, $t = 8$ & $r = 2$, $t = 2$ & $r = 8$ and $t = 8$ & $r = 8$. For the first case, the absolute difference between the exact and approximated capacities is very low. For an increasing number of transmit and/or receive antennae, the approximation error clearly increases. The mean approximation error in [%] is summarised in Table 2.2 for $1 \leq t \leq 10$ and $1 \leq r \leq 10$ calculated for an SNR ranging from 0 to 10. Table 2.2 shows that only MIMO configurations with $t = 1$ and $r \geq 6$ yield an approximation error exceeding 10%. If a higher precision is vital, then a tighter approximation should be used which is introduced in [49]. However, the tighter approximation is not directly applicable to the analysis exposed in the subsequent chapter, which is the reason why it has been omitted here.

### 2.5.2 Functional Approximation to the Outage Probability

If a fractional bandwidth $\alpha$ and a fractional power $\beta$ is allocated to a SIMO link operating over non-ergodic channels, then, with reference to (2.55), the derived outage probability can be expressed as

$$P_{out}(\Phi) = \frac{1}{\Gamma(r)}\gamma\left(r, \left(2^{\Phi/\alpha} - 1\right) \Big/ \left(\frac{\beta}{\alpha}\frac{S}{N}\right)\right) \tag{2.106}$$

where $\gamma(\cdot,\cdot)$ is the lower incomplete and $\Gamma(\cdot)$ the complete Gamma function. Again, an optimisation of the allocated fractional resources is not possible in closed form. Therefore, the following tractable approximation is suggested and briefly assessed below:

$$P_{out}(x) = \frac{\gamma(r,x)}{\Gamma(r)} \approx ax^b \tag{2.107}$$

where the constants $a$ and $b$ are obtained numerically such as to minimise the mean error between approximation and exact values in the outage region below 50%. For instance, with reference to Figure 2.27, the optimisation has been performed over the region $0 \leq x \leq 2.6$ for $r = 3$.

The constants $a$ and $b$ are a function of the parameter $r$, i.e. $a = a(r)$ and $b = b(r)$, and are tabled for $1 \leq r \leq 4$ in Table 2.3 together with the occurring mean error $e$ in [%]. Figure 2.27 depicts the exact outage probability and its approximation (2.107) for various configurations of parameter $r$. Clearly, the suggested approximation fits very well the exact outage probability, which is also corroborated with the low error $e$.

Note that the outage probability fitting parameters $a$ and $b$ can be determined for $r > 4$ in a similar fashion. It has been omitted here, because they will not be required in later chapters. Note finally that the MISO case yields approximately the same coefficients $a$ and $b$, which is the reason why they have not been tabled separately.

Table 2.1: Approximate capacity gain of MIMO systems over a SISO system for various transmit and receive array configurations assuming Rayleigh fading.

| $t\backslash r$ | 1 | 2 | 3 | 4 | 5 | 6 | 7 | 8 | 9 | 10 |
|---|---|---|---|---|---|---|---|---|---|---|
| 1 | 1 | 1 | 2 | 2 | 2 | 2 | 3 | 3 | 3 | 3 |
| 2 | 1 | 2 | 2 | 3 | 3 | 3 | 4 | 4 | 4 | 4 |
| 3 | 1 | 2 | 3 | 3 | 4 | 4 | 4 | 5 | 5 | 5 |
| 4 | 1 | 2 | 3 | 3 | 4 | 5 | 5 | 5 | 6 | 6 |
| 5 | 1 | 2 | 3 | 4 | 4 | 5 | 5 | 6 | 6 | 7 |
| 6 | 1 | 2 | 3 | 4 | 4 | 5 | 6 | 6 | 7 | 7 |
| 7 | 1 | 2 | 3 | 4 | 5 | 5 | 6 | 7 | 7 | 8 |
| 8 | 1 | 2 | 3 | 4 | 5 | 5 | 6 | 7 | 7 | 8 |
| 9 | 1 | 2 | 3 | 4 | 5 | 5 | 6 | 7 | 8 | 8 |
| 10 | 1 | 2 | 3 | 4 | 5 | 6 | 6 | 7 | 8 | 9 |

Table 2.2: Mean capacity approximation error $e$ [%] for various transmit and receive array configurations.

| $t\backslash r$ | 1 | 2 | 3 | 4 | 5 | 6 | 7 | 8 | 9 | 10 |
|---|---|---|---|---|---|---|---|---|---|---|
| 1 | 6% | 8% | 8% | 9% | 10% | **12%** | **13%** | **15%** | **16%** | **18%** |
| 2 | 9% | 5% | 6% | 8% | 8% | 8% | 8% | 9% | 9% | 10% |
| 3 | 8% | 7% | 5% | 6% | 6% | 7% | 7% | 8% | 8% | 8% |
| 4 | 9% | 7% | 5% | 5% | 5% | 6% | 7% | 7% | 7% | 8% |
| 5 | 10% | 8% | 7% | 6% | 5% | 5% | 6% | 6% | 6% | 7% |
| 6 | 9% | 8% | 7% | 6% | 5% | 5% | 6% | 6% | 6% | 7% |
| 7 | 10% | 9% | 7% | 7% | 6% | 5% | 5% | 5% | 6% | 6% |
| 8 | 10% | 9% | 8% | 7% | 6% | 6% | 6% | 5% | 5% | 6% |
| 9 | 10% | 8% | 8% | 7% | 7% | 7% | 6% | 5% | 5% | 5% |
| 10 | 10% | 9% | 9% | 8% | 7% | 7% | 6% | 6% | 5% | 5% |

Table 2.3: Outage probability fitting parameters **a** and **b** for a varying parameter $r$, together with the mean error $e$ caused.

| | $r = 1$ | $r = 2$ | $r = 3$ | $r = 4$ |
|---|---|---|---|---|
| **a** | 0.82 | 1.34 | 1.83 | 2.19 |
| **b** | 6.7e-1 | 2.6e-1 | 8.9e-2 | 3.1e-2 |
| $e$ | 5 % | 3 % | 4% | 4% |

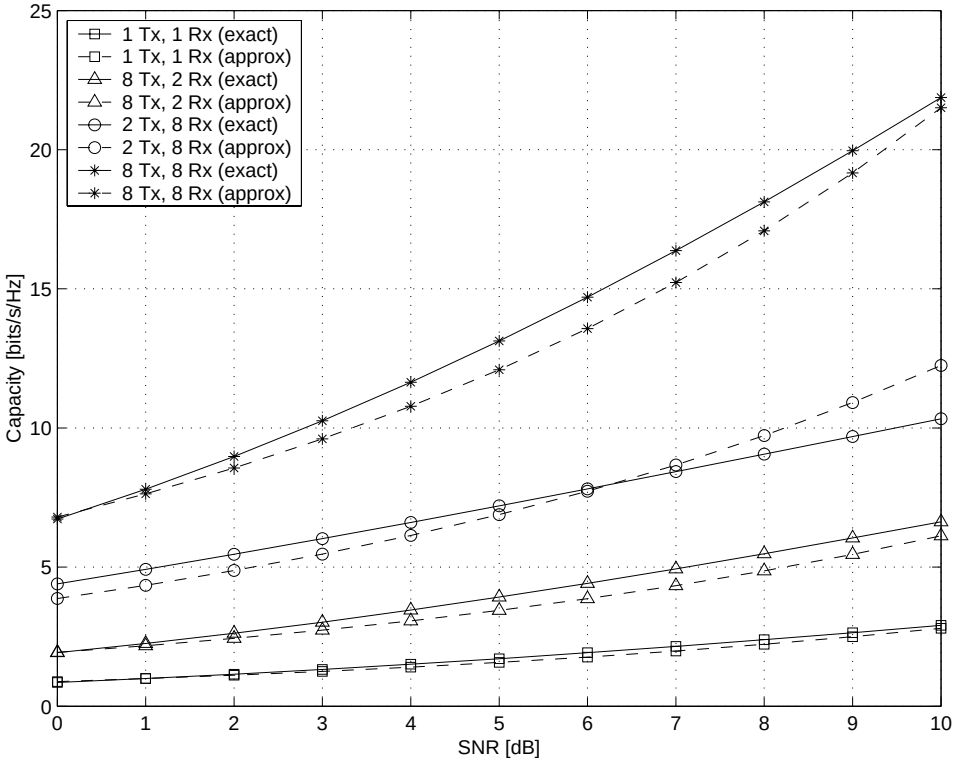


Figure 2.26: Exact and approximate capacities versus SNR for various transmit and receive array configurations; $\log_2(1+x) \approx \sqrt{x}$.

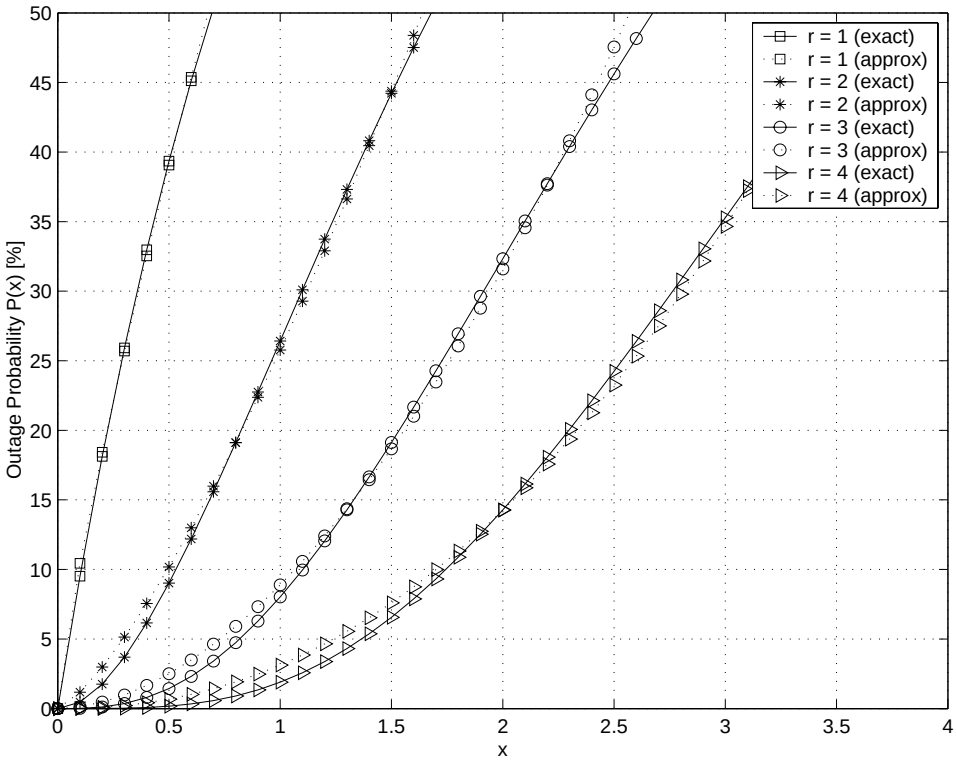


Figure 2.27: Exact and approximate outage probability for various parameters $r$; $\gamma(r,x)/\Gamma(r) \approx ax^b$ for linear $x$.

## 2.6 Conclusions

### 2.6.1 Summary

This chapter has analysed capacities and associated outage probabilities of MIMO channels of different types. Although the derived capacity limits can only be approached with transceivers of infinite complexity, an understanding of their behaviour is vital in designing optimum MIMO communication systems. The analysis in Sections 2.3−2.5 will prove very useful in assigning optimum resources to VAA-type communication systems, such as distributed-MIMO multi-stage systems. It was the aim to maintain a logical thread throughout the analysis, from the introductory notes to the derivation of closed form and approximate expressions for capacities and associated outage probabilities. Essential foundations have been given, with generally known results kept to a minimum.

In Section 2.1, a brief historical background to the evolvement of capacity was given, ranging from its infancy to the neat information theory developed by Shannon. His understanding and definition of capacity was then briefly reiterated in Section 2.2 to allow for a proper understanding of that subject in later sections. In the same section, the fundamental difference between capacity and its outage probability was highlighted. Both concepts proved vital for the remaining sections.

In Section 2.3, the traditional flat Rayleigh fading MIMO channel in its ergodic and non-ergodic realisation was dealt with. The underlying theory was briefly introduced, after which a closed solution to Telatar's MIMO capacity expression has been developed. The integral that has been solved was referred to as the capacity integral, as it proved useful in a variety of following MIMO capacity problems. For the sake of completeness, the outage probability of generic MIMO channels has been characterised.

The two major problems associated with MIMO systems, i.e. complexity and difficulties of analysing it analytically for more general communication scenarios, have been overcome by deploying Space-Time Block Codes. These are known to yield orthogonalised MIMO (O-MIMO) channels, and hence simplifying analysis significantly, as shown throughout Section 2.4. In there, the capacities (i.e. maximum mutual information for given STBC processing and channel coefficients) and associated outage probabilities of a wide range of O-MIMO Rayleigh and Nakagami fading channels were derived. The cases of equal, unequal and generic channel coefficients were dealt with, which allow assessing the capacity behaviour of distributed O-MIMO communication systems with links subject to different pathloss or shadowing. Finally, O-MIMO channels were shown to yield significantly lower capacities than their traditional MIMO channel counterparts, induced by the lower deployment complexity.

The exposed capacity behaviour of MIMO and O-MIMO channels will prove vital in deploying VAA-type communication systems. However, the optimisation of resources determining the capacity by utilising the derived closed form capacity expressions of Sections 2.3 and 2.4, was shown to be impossible. In Section 2.5, sufficiently precise functional approximations have thus been suggested for the logarithm occurring in the MIMO capacity expressions. This allowed the decoupling of the fairly intricate expression related to MIMO capacity gains from terms requiring optimisation, such as transmission power or bandwidth. Closed solutions of the approximate capacity have also been developed for a variety of different communication conditions. In the same section, an approximation for the outage probability has been exposed which will also be useful for the allocation of fractional resources over non-ergodic channels.

### 2.6.2 Contributions

The field of MIMO Information Theory is currently one of the biggest and most flourishing areas of research. However, only essential fundamentals on MIMO theory have been incorporated into this chapter, whereas the majority of the exposed analysis was the contribution of the author. The contributions to the research community can be summarised as follows:

1. A closed solution to the MIMO capacity over ergodic flat Rayleigh fading channels with equal channel gains has been developed.

2. A closed solution to the MIMO capacity over space-time block encoded ergodic flat Rayleigh fading channels with unequal channel gains has been developed, as well its associated outage probability over a non-ergodic channel.

3. A closed solution to the MIMO capacity over space-time block encoded ergodic flat Nakagami fading channels with unequal channel gains has been developed, as well its associated outage probability over a non-ergodic channel.

4. A sufficiently precise functional approximation has been suggested for the logarithm occurring in the MIMO capacity expressions. This allowed the fairly intricate expression related to MIMO capacity gains to be decoupled from terms requiring optimisation, such as transmission power or bandwidth. Closed solutions of the approximate capacity have also been developed for a variety of different communication conditions.

5. A sufficiently precise functional approximations to the outage probability involving the complete and incomplete Gamma functions has been suggested, as well as its precision assessed.

### 2.6.3 Future Research

Numerous questions and problems remain open in the field of MIMO information theory. Related to the problematic of distributed-MIMO capacity, the following topics are deemed to be worthwhile pursuing as future research:

1. Fractional Transmit Power Allocation. A rigorous mathematical assessment of the precision of the conjectured fractional transmit power allocation (2.109) for fixed or quasi-static channels is still an open problem.

2. Generic Eigenvalue Distribution. A very challenging research area is the derivation of the pdf of the eigenvalues occurring in MIMO channels of arbitrary statistics, correlation and channel gains.

3. Ricean Fading. Although Ricean fading is well approximated by Nakagami fading, closed capacity expressions for the Ricean case are desirable.

### 2.6.4 Deployment Guidelines

The following guidelines give a technical summary on the derived dependencies. They can prove useful for general MIMO system understanding, as well as in subsequent chapters when dealing with VAA-type communication systems. Furthermore, since these guidelines might be read by people not that familiar with statistics, some terminology has been simplified, e.g. "ergodic" $\rightarrow$ "fast-fading".

**Guidelines based on MIMO Capacity Behaviour**

1. Fast-Fading Channels: Having more transmit antennas $t$ than receive antennas $r$ is not worth deploying.

   EXAMPLE: With one receive antenna and an SNR of 10dB, the capacity is approximately 3 bits/s/Hz irrespective of the number of transmit antennas.

2. Fast-Fading Channels: Having more receive antennas $r$ than transmit antennas $t$ is worth deploying; however, a higher capacity can be achieved if the elements are equally distributed between transmitter and receiver.

   EXAMPLE: With one transmit antenna and an SNR of 10dB, the capacity is 3 bits/s/Hz for $r = 1$, 4 bits/s/Hz for $r = 2$ and 5 bits/s/Hz for $r = 4$. The increase follows a logarithmic dependency.

3. Fast-Fading Channels: Having $r = t$ yields the highest capacity, and is hence optimum.

   EXAMPLE: With an SNR of 10dB, the capacity is 3 bits/s/Hz for $1 \times 1$, 6 bits/s/Hz for $2 \times 2$ and 12 bits/s/Hz for $4 \times 4$. The increase is hence linear.

4. Slow-Fading Channels: For a fixed configuration of $t \times r$ and a desired rate $\Phi$ in [bits/s/Hz], increasing the transmit power results in a higher reliability.

   EXAMPLE: For a desired rate of 2 bits/s/Hz and a $2 \times 1$ MIMO system, operating at 5dB allows the system to support 2 bits/s/Hz in 46% of all times, whereas operating at 10dB increases the reliability to 88%.

5. Slow-Fading Channels: For a fixed configuration of $t \times r$ and a fixed SNR, increasing the desired rate results in a lower reliability.

   EXAMPLE: For an SNR of 10dB and a $2 \times 1$ MIMO system, a rate of 2 bits/s/Hz can be supported in 88% of all cases, whereas a rate of 4 bits/s/Hz only in 20%.

6. Slow-Fading Channels: For a fixed SNR and fixed communication rate, increasing the number of receive antennas always results in a higher communication reliability, whereas the optimum choice of the number of transmit antennas depends on the SNR and rate. Generally, higher rates should be supported by one transmit element only, whereas lower rates by as many as possible.

   EXAMPLE: For an SNR of 10dB and a rate of 2 bits/s/Hz, the $8 \times 1$ MIMO system offers 100% reliability, whereas the $1 \times 1$ MIMO system only 75%. For a higher rate of 4 bits/s/Hz, the $8 \times 1$ MIMO system offers only 10% reliability, whereas the $1 \times 1$ MIMO system only 22%. Since systems are traditionally designed to yield a high reliability, the maximum number of elements should be chosen in any MIMO configuration.

**Guidelines based on O-MIMO Capacity Behaviour**

1. Generally: The capacity of an O-MIMO channel cannot exceed the capacity of an equivalent Gaussian channel. The role of the deployed STBC is to reduce the detrimental effect of fading only, hence merely leading to diversity gains.

   EXAMPLE: The capacity of a $4 \times 2$ O-MIMO channel cannot be greater than the capacity of a $1 \times 2$ Gaussian channel (2 Gaussian channels in parallel).

2. Generally: In the case of uncorrelated Rayleigh fading, the capacity of a MIMO channel exceeds the capacity of an O-MIMO channel. The difference between both capacities lessens with an increase in the LOS component, i.e. predominant Ricean/Nakagami fading.

   EXAMPLE: Assuming a $2 \times 2$ communication scenario operating at 10dB, the loss in capacity from a MIMO to a O-MIMO communication system mounts to approximately 30% for the case of no LOS component, i.e. Nakagami $f = 1$ or Ricean $K \to -\infty$dB. In the case of strong LOS with Nakagami $f = 6$ or Ricean $K = 10$dB, the loss in capacity mounts only to 10%.

3. Fast-Fading: The STBC rate $R$ has a predominant influence, i.e. it is only worth deploying full-rate STBCs for any channel conditions. The only full-rate STBC is the Alamouti scheme.

   EXAMPLE: For a O-MIMO system with two receivers operating at an SNR of 10dB, the equivalent Gaussian channel supports a rate of 4.2 bits/s/Hz, the Alamouti scheme ($t = 2$) 4.1 bits/s/Hz, the 3/4-rate schemes ($t = 3, 4$) 3.6 bits/s/Hz and the 1/2-rate schemes ($t = 3, 4$) only 2.6 bits/s/Hz.

4. Fast-Fading: STBC diversity gains can be traded against the strength of LOS conditions.

   EXAMPLE: Assuming a system supporting 3.3 bits/s/Hz at 10dB with one receive antenna, then for weak LOS conditions with $f = 2$ two transmit antennas should be deployed, whereas for stronger LOS conditions with $f = 4$ only one transmit antenna suffices. If in the latter case two transmit antennas were deployed then a rate of 3.4 bits/s/Hz could be deployed.

5. Slow-Fading: The same tendencies as for the general MIMO channels hold. Therefore, to maintain a rate with high reliability, the 3/4-rate STBC with four transmit antennas should be used.

   EXAMPLE: To maintain a rate of 2 bits/s/Hz with 90% reliability, a $1 \times 1$ SISO system requires an SNR of 14.5dB and a $4 \times 1$ O-MIMO system with 3/4-rate STBC only 9.5dB, leading to a power savings of 4dB.

6. Distributed Cases: Deploying distributed O-MIMO communication systems may not yield optimum performance, however, it yields a more robust system. If one or more links of the O-MIMO system are shadowed then, without the distributed deployment, the capacity and reliability will be very low; whereas for a distributed deployment, the capacity and reliability are fairly unaffected by shadowing. This is the case because capacity and reliability are dominated by the weakest link.

   EXAMPLE: A distributed Alamouti scheme operating at 10dB (if both links are equally strong) can support a rate of at least 3 bits/s/Hz, whereas if only either of the links was deployed in a SISO system then the rates would break down for the weak link, e.g. 1 bit/s/Hz when the link is 12dB weaker than the stronger of the two.

## 2.7 Appendix

**Derivation I.** An approximate fractional power allocation to each transmit element in the case of fixed (quasi-static) channel coefficients is exposed here. The author could not derive the allocation strategy, which is the the reason why the allocation is stated as a conjecture. It is hence the aim to find approximate transmit power allocations $\epsilon_{i\in(1,t)}$ such that

$$C = \sum_{i=1}^{t} \log_2 \left(1 + \epsilon_i \lambda_i \frac{S}{N}\right) \tag{2.108}$$

is maximised, which can be achieved by the allocation strategy

$$\epsilon_i = \frac{\prod_{j=1, j\neq i}^{t} \lambda_j^{-1/2}}{\sum_{k=1}^{t} \prod_{j=1, j\neq k}^{t} \lambda_j^{-1/2}} \tag{2.109}$$

Figure 2.28 depicts the achieved normalised capacity in [bits/s/H] versus the SNR in [dB] for $4 \times 4$ MIMO communication scenario, where $\mathbf{H}$ was chosen randomly and then fixed to perform the allocation process. The optimum allocation was obtained following the strategy developed in Section 2.3.2. The near-optimum capacity was achieved by deploying the conjectured fractional power allocation (2.109). Clearly, the exposed allocation strategy yields near-optimum performance. Furthermore, the case of equal power allocation is shown to be inferior to the other two allocation strategies.

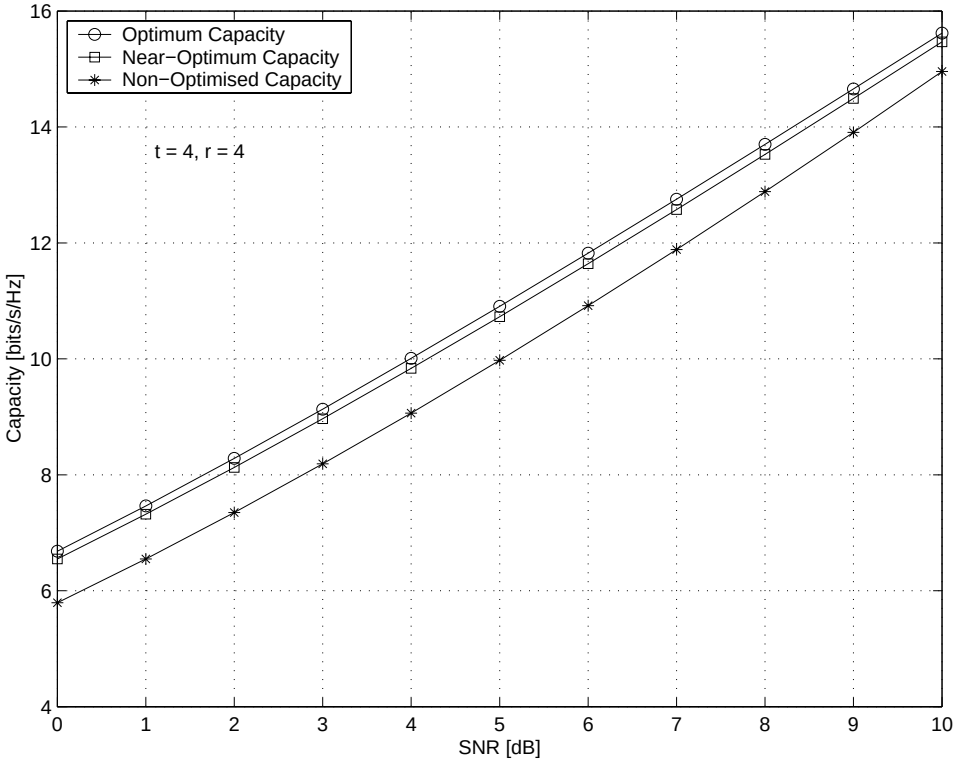


Figure 2.28: Achieved capacity for various fractional power allocation strategies; $\mathbf{H}$ is fixed.

**Derivation II.** It is proven here that

$$K_i = \prod_{i'=1, i' \neq i}^{u} \frac{\gamma_i}{\gamma_i - \gamma_{i'}} \tag{2.110}$$

Without loss of generality, $K_1$ is derived here according to [50]. To this end, the fractional expansion is equated to the product expression, i.e.

$$\sum_{i'=1}^{u} \frac{K_{i'}}{1 - \gamma_{i'} s} \equiv \prod_{i'=1}^{u} \frac{1}{1 - \gamma_{i'} s} \tag{2.111}$$

$$\frac{K_1}{1 - \gamma_1 s} + \frac{K_2}{1 - \gamma_2 s} + \ldots + \frac{K_u}{1 - \gamma_u s} = \frac{1}{1 - \gamma_1 s} \cdot \frac{1}{1 - \gamma_2 s} \cdot \ldots \cdot \frac{1}{1 - \gamma_u s} \tag{2.112}$$

To obtain $K_1$, (2.112) is multiplied by $(1 - \gamma_1 s)$ to yield

$$K_1 + K_2 \frac{1 - \gamma_1 s}{1 - \gamma_2 s} + \ldots + K_u \frac{1 - \gamma_1 s}{1 - \gamma_u s} = \frac{1}{1 - \gamma_2 s} \cdot \ldots \cdot \frac{1}{1 - \gamma_u s} \tag{2.113}$$

after which $s$ is set to $s = 1/\gamma_1$ to arrive at

$$K_1 = \frac{1}{1 - \frac{\gamma_2}{\gamma_1}} \cdot \ldots \cdot \frac{1}{1 - \frac{\gamma_u}{\gamma_1}} \tag{2.114}$$

$$= \prod_{i'=2}^{u} \frac{\gamma_1}{\gamma_1 - \gamma_{i'}} \tag{2.115}$$

The same procedure is repeated for any $K_i$ to derive (2.110).

**Derivation III.** Following the approach exposed in [50], it is proven here that

$$K_{i,j} = \frac{1}{(\nu_i - j)! \, (-\hat{\gamma}_i)^{\nu_i - j}} \frac{\partial^{\nu_i - j}}{\partial s^{\nu_i - j}} \left[ \prod_{i'=1, i' \neq i}^{g} \frac{1}{(1 - s\hat{\gamma}_{i'})^{\nu_{i'}}} \right]_{s = 1/\hat{\gamma}_i} \tag{2.116}$$

if the partial fractions are applied to (2.79) which, expanded into its partial fractions, can be expressed as

$$\sum_{i'=1}^{g} \sum_{j'=1}^{\nu_{i'}} \frac{K_{i',j'}}{(1 - \hat{\gamma}_{i'} s)^{j'}} \equiv \prod_{i'=1}^{g} \frac{1}{(1 - \hat{\gamma}_{i'} s)^{\nu_{i'}}}$$

$$\left[ \frac{K_{1,1}}{(1 - \hat{\gamma}_1 s)^1} + \ldots + \frac{K_{1,\nu_1}}{(1 - \hat{\gamma}_1 s)^{\nu_1}} \right] + \ldots + \left[ \ldots + \frac{K_{g,\nu_g}}{(1 - \hat{\gamma}_g s)^{\nu_g}} \right] = \prod_{i'=1}^{g} \frac{1}{(1 - \hat{\gamma}_{i'} s)^{\nu_{i'}}} \tag{2.117}$$

To obtain coefficient $K_{1,\nu_1}$, (2.117) is multiplied with $(1 - \hat{\gamma}_1 s)^{\nu_1}$ after which $s$ is set to $s = 1/\hat{\gamma}_1$ to arrive at

$$K_{1,\nu_1} = \prod_{i'=2}^{g} \frac{1}{\left(1 - \frac{\hat{\gamma}_{i'}}{\hat{\gamma}_1}\right)^{\nu_{i'}}} \tag{2.118}$$

Similarly, the coefficients $K_{i,\nu_i}$ can be obtained as

$$K_{i,\nu_i} = \prod_{i'=1, i' \neq i}^{g} \frac{1}{\left(1 - \frac{\hat{\gamma}_{i'}}{\hat{\gamma}_i}\right)^{\nu_{i'}}} \tag{2.119}$$

Furthermore, to obtain coefficient $K_{1,\nu_1-1}$, (2.117) is multiplied with $(1-\hat{\gamma}_1 s)^{\nu_1}$, differentiated w.r.t. $s$, after which $s$ is set to $s = 1/\hat{\gamma}_1$ to arrive at

$$K_{1,\nu_1-1} = \frac{1}{(-\hat{\gamma}_1)} \frac{\partial}{\partial s} \left[ \prod_{i'=2}^{g} \frac{1}{(1-s\hat{\gamma}_{i'})^{\nu_{i'}}} \right]_{s=1/\hat{\gamma}_1} \tag{2.119}$$

Similarly, the coefficients $K_{i,\nu_i-1}$ are obtained as

$$K_{i,\nu_i-1} = \frac{1}{(-\hat{\gamma}_i)} \frac{\partial}{\partial s} \left[ \prod_{i'=1,i'\neq i}^{g} \frac{1}{(1-s\hat{\gamma}_{i'})^{\nu_{i'}}} \right]_{s=1/\hat{\gamma}_i} \tag{2.120}$$

The same procedure is repeated for coefficients $K_{1,j}$. Hence, coefficient $K_{1,1}$ is obtained by multiplying (2.117) with $(1-\hat{\gamma}_1 s)^{\nu_1}$, differentiated $(\nu_1 - 1)$ times w.r.t. $s$, after which $s$ is set to $s = 1/\hat{\gamma}_1$ to arrive at

$$K_{1,1} = \frac{1}{(\nu_1-1)!\,(-\hat{\gamma}_1)^{\nu_1-1}} \frac{\partial^{\nu_1-1}}{\partial s^{\nu_1-1}} \left[ \prod_{i'=2}^{g} \frac{1}{(1-s\hat{\gamma}_{i'})^{\nu_{i'}}} \right]_{s=1/\hat{\gamma}_1} \tag{2.121}$$

Similarly, the coefficients $K_{i,1}$ are obtained as

$$K_{i,1} = \frac{1}{(\nu_i-1)!\,(-\hat{\gamma}_i)^{\nu_i-1}} \frac{\partial^{\nu_i-1}}{\partial s^{\nu_i-1}} \left[ \prod_{i'=1,i'\neq i}^{g} \frac{1}{(1-s\hat{\gamma}_{i'})^{\nu_{i'}}} \right]_{s=1/\hat{\gamma}_i} \tag{2.122}$$

That finalises the proof that $K_{i,j}$ is given by (2.116). Note that the $(\nu_i - j)^{th}$ derivative of $\prod_{i'=1,i'\neq i}^{g} (1-s\hat{\gamma}_{i'})^{-\nu_{i'}}$ in (2.116) is easily derived in closed form. The first order derivative is obtained as

$$\frac{\partial}{\partial s} \left[ \prod_{i'=1,i'\neq i}^{g} \frac{1}{(1-s\hat{\gamma}_{i'})^{\nu_{i'}}} \right] = \left[ \prod_{i'=1,i'\neq i}^{g} \frac{1}{(1-s\hat{\gamma}_{i'})^{\nu_{i'}}} \right] \left[ \sum_{i'=1,i'\neq i}^{g} \frac{\nu_{i'}\hat{\gamma}_{i'}}{1-s\hat{\gamma}_{i'}} \right] \tag{2.123}$$

To enhance readability, the following symbolic notation is introduced

$$[\Pi] \triangleq \prod_{i'=1,i'\neq i}^{g} \frac{1}{(1-s\hat{\gamma}_{i'})^{\nu_{i'}}} \tag{2.124}$$

$$[\Sigma] \triangleq \sum_{i'=1,i'\neq i}^{g} \frac{\nu_{i'}\hat{\gamma}_{i'}}{1-s\hat{\gamma}_{i'}} \tag{2.125}$$

$$[\Sigma^n] \triangleq \sum_{i'=1,i'\neq i}^{g} \frac{\nu_{i'}\,(\hat{\gamma}_{i'})^n}{(1-s\hat{\gamma}_{i'})^n} \tag{2.126}$$

$$\partial^n [\cdot] \triangleq \frac{\partial^n}{\partial s^n} [\cdot] \tag{2.127}$$

With the introduced notation the following holds

$$\partial[\Sigma^n] = n[\Sigma^{n+1}] \tag{2.128}$$

$$\partial[\Sigma]^m = m[\Sigma]^{m-1}[\Sigma^2] \tag{2.129}$$

and generally

$$\partial[\Xi][\Psi] = \partial[\Xi] \cdot [\Psi] + [\Xi] \cdot \partial[\Psi] \tag{2.130}$$

This allows one finally to rewrite (2.123) and, inductively, any higher order derivative as

$$\begin{aligned}
\partial[\Pi] &= [\Pi][\Sigma] && (2.131)\\
\partial^2[\Pi] &= \partial[\Pi][\Sigma] && (2.132)\\
&= \partial[\Pi] \cdot [\Sigma] + [\Pi] \cdot \partial[\Sigma] \\
&= [\Pi]\left([\Sigma]^2 + [\Sigma^2]\right) \\
\partial^3[\Pi] &= \partial\left[[\Pi]\left([\Sigma]^2 + [\Sigma^2]\right)\right] && (2.133)\\
&= \partial[\Pi] \cdot \left([\Sigma]^2 + [\Sigma^2]\right) + [\Pi] \cdot \partial\left([\Sigma]^2 + [\Sigma^2]\right) \\
&= [\Pi]\left([\Sigma]^3 + 3[\Sigma][\Sigma^2] + 2[\Sigma^3]\right) \\
\partial^4[\Pi] &= [\Pi]\left([\Sigma][\Sigma]^3 + 6[\Sigma]^2[\Sigma^2] + 8[\Sigma][\Sigma^3] + 3[\Sigma^2]^2 + 6[\Sigma^4]\right) && (2.134)\\
&\vdots
\end{aligned}$$

# Chapter 3

# Resource Allocation Strategies

## 3.1 Introduction

It is the aim of this chapter to analyse the behaviour of distributed-MIMO multi-stage communication networks with the aid of the theory developed in the previous chapter. An example realisation of the named communication network is depicted in Figure 3.1. Of major interest here is to maximise the end-to-end data throughput by optimally assigning resources in terms of frame duration, frequency band and transmission power to each of the terminals. These resources are usually constrained, thus calling for effective allocation strategies. Since resources have to be shared among all terminals involved, the allocation strategies to be developed are referred to as fractional resource allocation strategies.

The two major approaches to accomplish a relaying network are transparent or regenerative relaying. For the transparent case, a relaying terminal receives a signal stream on one frequency band and directly translates it for re-transmission onto another. In the regenerative case, a relaying terminal receives a signal stream, processes it and re-transmits it. From a capacity perspective it is clear that regenerative relaying outperforms transparent relaying, which is confirmed by [51] for the particular communication scenario of SISO relaying over flat Rayleigh fading channels. Additionally, regenerative relaying allows the deployment of MIMO capacity enhancement technologies at each relaying stage. These are the reasons why regenerative relaying is considered in this thesis. It is therefore the aim to allocate fractional resources to each relaying terminal so as to maximise the end-to-end throughput in dependency of prevailing channel conditions.

The problem formulation to similar resource allocation problems with partial solutions to achieve maximum throughput has been analysed in [27] and [52]-[59]. A generic operational mode of a wireless network is defined in [27] that covers both routing, scheduling and power control. Joint routing and scheduling is considered in [52], where the total throughput is maximised by decomposing the joint optimisation problem into a pure scheduling and a pure routing problem. In [53], a joint scheduling-power control solution to the multiple access problem in wireless ad-hoc networks is introduced.

In [54], a jointly optimal scheduling, routing and power control algorithm achieving max-min fair rate allocation in one-dimensional networks is presented. The capacity regions for wireless ad-hoc networks with an arbitrary number of nodes and topology are studied in [55]. Here, the transceivers used are capable of variable-rate adaptation by automatically adjusting the transmission rate to match the SINR at the receiver. In [56], the capacity region and optimal power allocation scheme for a multi-user fading broadcast channel is derived in which minimum rates must be maintained for each user in all fading states.

In [57] and [58], three types of capacity (ergodic, zero-outage and outage with nonzero outage) regions for fading broadcast channels and their corresponding optimal resource allocation strategies for different spectrum-sharing techniques are analysed. The optimal power allocation that achieves the boundary of the ergodic capacity region is derived by solving an optimisation problem over a set of time-invariant Gaussian broadcast channels with a constrained total average transmit power. Finally, the capacity region of the downlink broadcast channel in fading and additive white Gaussian noise for time-division, frequency-division, and code-division is studied in [59].

All solutions to the respective optimisation problems, however, require some form of numerical optimisation. It is the aim of this chapter to introduce for the first time explicit resource allocation strategies for regenerative distributed-MIMO multi-stage communication scenarios constrained by a total utilised power $S$, bandwidth $W$ and frame duration $T$.

This chapter is organised as follows. In Section 3.1, the system assumptions are introduced, as well as the notation to be used throughout the remainder of the chapter. It is also demonstrated how to relate the obtained fractional bandwidth and power of an FDMA-based system with the fractional frame duration and power of a TDMA-based system. Subsequent analysis is therefore focused only onto FDMA-based systems.

Analysis then splits into ergodic and non-ergodic flat fading channels, the optimum fractional resource allocation strategies for each are then introduced in Section 3.2 and 3.3, respectively. In each of the sections, the following communication scenarios have been analysed in sufficient depth: (1) distributed-MIMO multi-stage relaying without resource reuse, (2) distributed-MIMO multi-stage relaying with resource reuse, and (3) distributed O-MIMO multi-stage relaying with and without resource reuse. A network with resource reuse allows allocating, e.g., the same fractional bandwidth to terminals which have a sufficient spatial separation. That is shown to influence the fractional resource allocation strategy.

In Section 3.4, it is then shown that the very same algorithms are also applicable to frequency selective fading channels, which makes them applicable to currently deployed CDMA and OFDMA based communication systems.

Finally, conclusions are drawn in Section 3.5, which includes a summary of the results of this chapter, the research contributions, and future research.

## 3.2 System Model

### 3.2.1 General Deployment

The description here relates to the generalised VAA multi-stage communication system as depicted in Figure 3.1. Consider, a source mobile terminal (s-MT) communicating with a target mobile terminal (t-MT) via a given number of relaying mobile terminals (r-MTs). Spatially adjacent r-MTs are grouped into VAAs, thereby forming a relaying VAA (r-VAA) tier. The s-MT and t-MT themselves might be a member of a VAA, henceforth referred to as source VAA (s-VAA) and target VAA (t-VAA), respectively. The system of a s-VAA communicating with a t-VAA via several tiers of r-VAAs is referred to as a VAA multi-stage communication system. The optimum choice of r-MTs, as well as their optimum grouping into VAAs, is beyond the scope of this thesis. It is therefore assumed that the fractional resource allocation algorithms developed here are applied to the given topology.

The s-MT, t-MT and r-MTs may possess any number of antenna elements, depicted as large dots in Figure 3.1. Furthermore, the MTs may or may not cooperate among each other within the same VAA tier. The cooperative link is shown as a dash-dotted line. Each r-MT of the same r-VAA transmits the prior agreed spatial branch of a space-time code word, where the encoding bases on the received and detected symbol from the previous r-VAA tier. The resulting MIMO sub-channels are shown as grey lines.

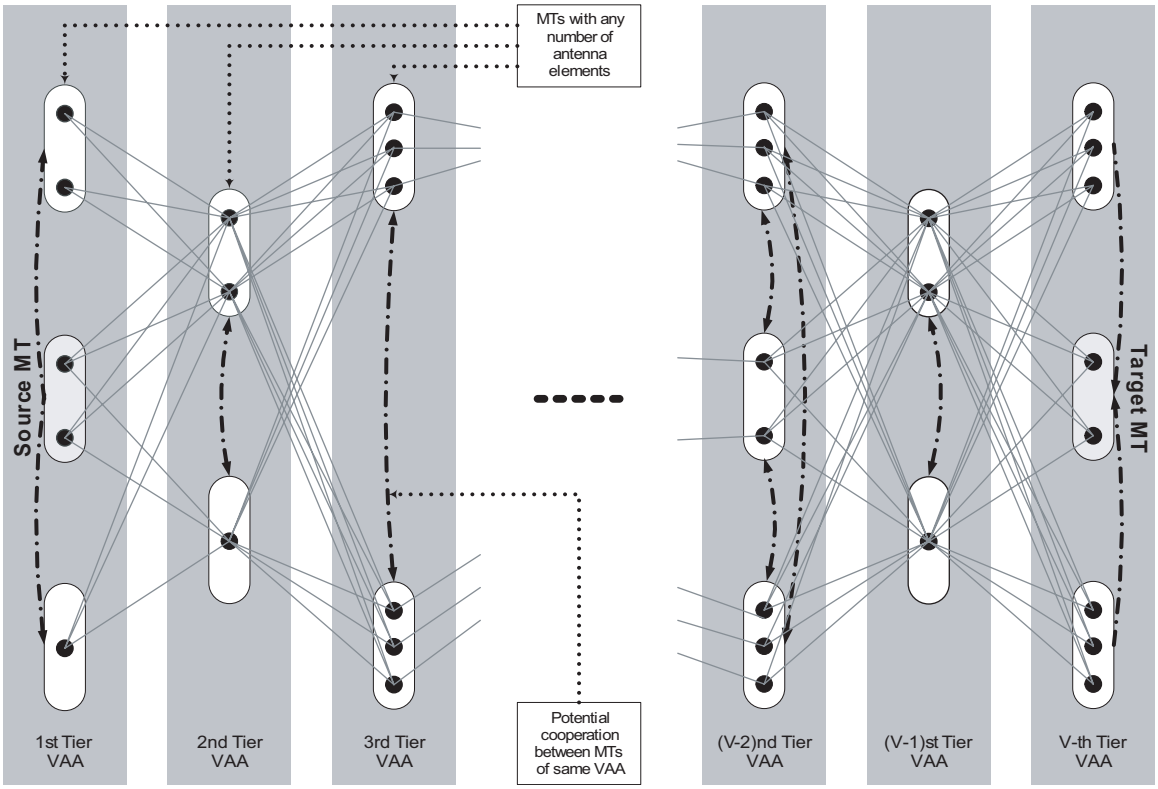


Figure 3.1: Distributed-MIMO multi-stage communication system.

Clearly, a cooperative deployment yields a higher capacity; however, at the expense of additional complexity, relaying power and bandwidth. The latter two are assumed to be negligible in the current analysis, as justified in Section 2.4.2. The increase in capacity is thus due to more complex transceivers only, which have to accomplish intra (cooperation) and inter (multi-stage) VAA relaying. It is assumed here that the intra (cooperation) VAA communication process is error-free. Note further that not all available antenna elements need to be active for the intra and/or inter VAA relaying process.

With reference to eq. (2.8), regenerative relaying allows the utilisation of two access methodologies: frequency division multiple access (FDMA) and time division multiple access (TDMA). FDMA-based regenerative relaying implies that the totally available bandwidth $W$ is orthogonally or non-orthogonally partitioned among the relaying VAA tiers, as depicted in Figure 3.2; communication may occur continuously over the entire frame duration $T$. On the other hand, TDMA-based regenerative relaying implies that the total frame duration $T$ is orthogonally or non-orthogonally partitioned into slots among the relaying VAA tiers, as depicted in Figure 3.3; communication occurs over the entire bandwidth $W$.

For orthogonal relaying, available resources are divided such that no interference between the relaying stages occurs. Thus, bandwidth/frame has to be fractioned into non-overlapping frequency-bands/slots such that at any time they are used by only one relaying link. On the other hand, non-orthogonal relaying allows resources to be re-used among stages, which leads to interference between the relaying VAA tiers.

The encoding, distributed relaying and decoding process is described for an FDMA-based relaying system as follows.

**Source MT.** In an FDMA-based relaying system, the s-MT continuously broadcasts the data to the remaining r-MTs in the first relaying VAA tier, utilising negligible power and bandwidth, and possibly not deploying all of its available antenna elements.

**First Relaying VAA Tier.** The first VAA relaying tier is formed by $q_1$ spatially adjacent MTs (including the s-MT). Each of the involved MTs possesses $n_{1,i}$ antenna elements for inter VAA relaying purposes, where the first subscript relates to the first VAA relaying tier and $1 \leq i \leq q_1$.

After cooperation between the s-MT and the remaining r-MTs of the first relaying VAA tier, the data is space-time encoded according to a given code book with $t_1 = \sum_{i=1}^{q_1} n_{1,i}$ spatial dimensions. Each MT then transmits only $n_{1,i\in(1,q_1)}$ spatial dimensions such that no transmitted codeword is duplicated. Transmission from the first relaying VAA tier is accomplished at frequency band $W_1$ with total transmission power $S_1$.

**Second Relaying VAA Tier.** The second VAA relaying tier is formed by $q_2$ spatially adjacent MTs such that their inclusion into the VAA yields capacity benefits to the communication system.

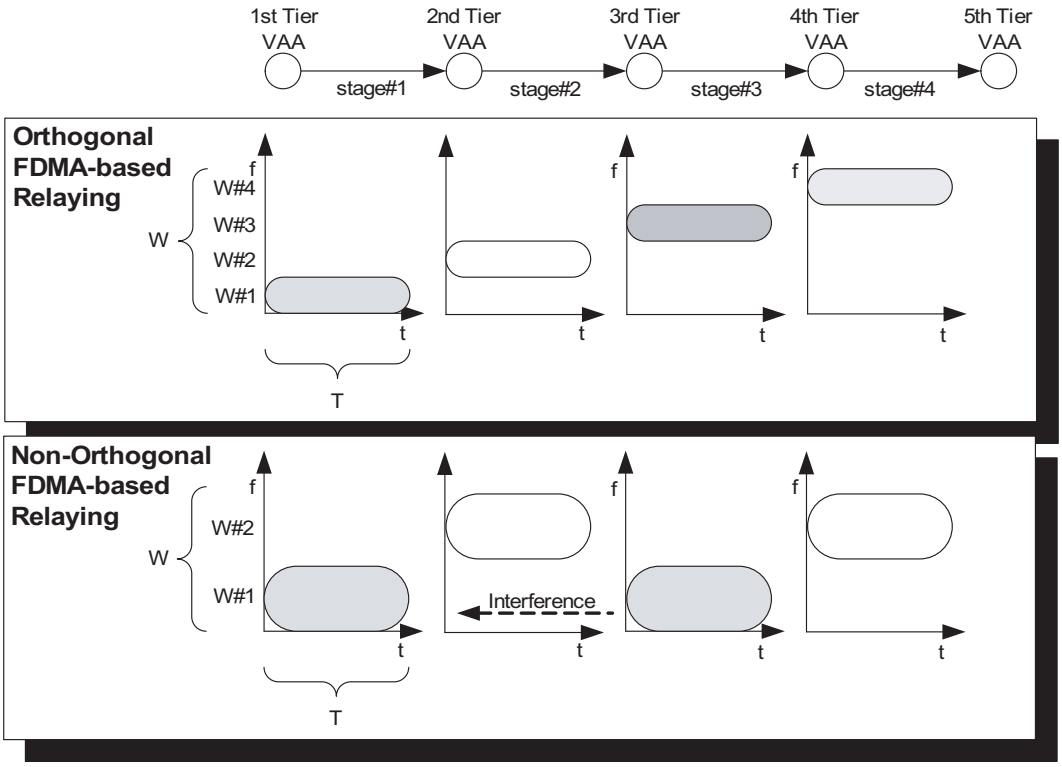


Figure 3.2: Principle of FDMA-based orthogonal and non-orthogonal relaying.

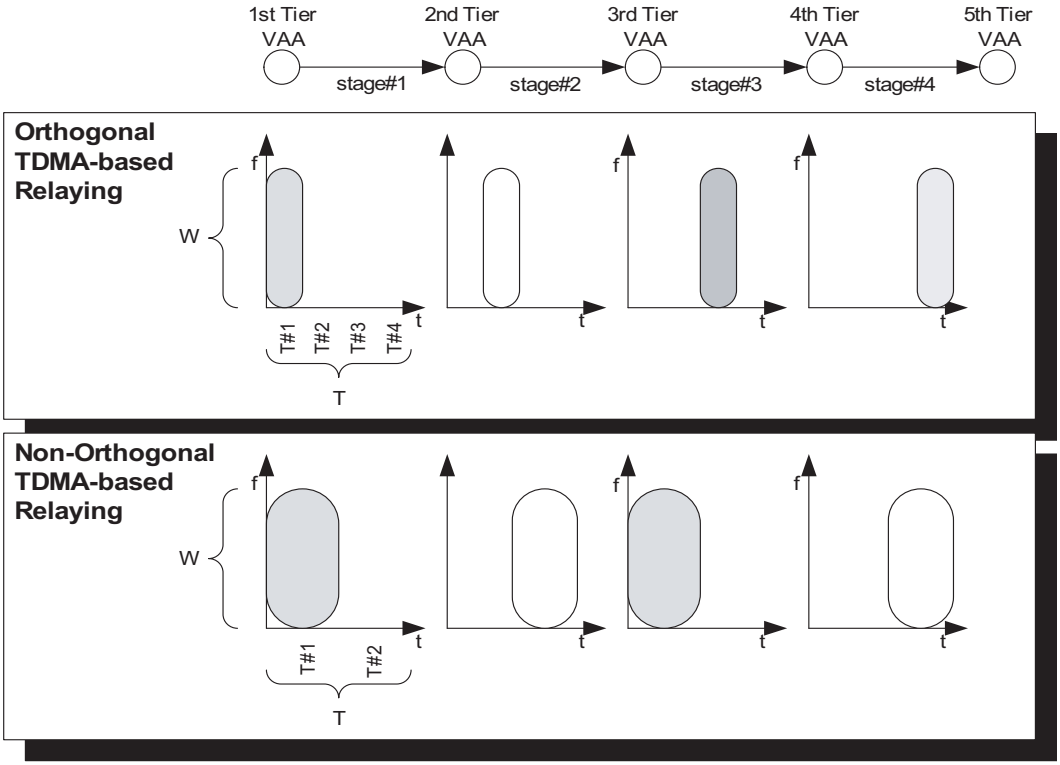


Figure 3.3: Principle of TDMA-based orthogonal and non-orthogonal relaying.

Each of the $q_2$ MTs possesses $n_{2,i\in(1,q_2)}$ antenna elements. Some MTs may cooperate among each other, thereby forming $Q_2$ clusters, where $1 \leq Q_2 \leq q_2$. The case of $Q_2 = 1$ represents the scenario where all MTs cooperate, whereas $Q_2 = q_2$ means that none of the MTs cooperate. The former case clearly yields the best performance, however, at the expense of additional transceiver complexity to realise the cooperation; also, additional bandwidth and power are required to accomplished the relaying process. The later case yields less gains; however, it will be shown that the performance of such a system still outperforms a traditional SISO relaying system.

The $j^{th}$ cluster is assumed to contain $r_{2,j}$ receive antennas, where $1 \leq j \leq Q_2$ and $\sum_{i=1}^{q_2} n_{2,i} = \sum_{j=1}^{Q_2} r_{2,j}$. Therefore, $Q_2$ MIMO channels are created, each with $t_1$ transmit antennas and $r_{2,j\in(1,Q_2)}$ receive antennas.

After cooperation, the data is space-time decoded and re-encoded according to a given code book with $t_2 = \sum_{i=1}^{q_2} n_{2,i}$ spatial dimensions. Again, each MT then re-transmits only $n_{2,i\in(1,q_2)}$ spatial dimensions such that no re-transmitted code word is duplicated. Re-transmission from the second relaying VAA tier is accomplished at frequency band $W_2$ with total transmission power $S_2$.

**$\mathbf{v}^{th}$ Relaying VAA Tier.** The reception, cooperation, de-coding, re-encoding and re-transmission process is congruent to the proceedings described above. Again, $Q_v$ MIMO channels are created. All of these MIMO channels will have $t_{v-1}$ transmit antennas and $r_{v,j\in(1,Q_v)}$ receive antennas. After cooperation, the data is space-time decoded and re-encoded according to a given code book with $t_v = \sum_{i=1}^{q_v} n_{v,i}$ spatial dimensions. Re-transmission from the $v^{th}$ relaying VAA tier is accomplished at frequency band $W_v$ with total power $S_v$.

**$\mathbf{V}^{th}$ Relaying VAA Tier.** The final relaying tier contains the t-MT. Similar to the $1^{st}$ tier, only cooperative MTs are considered here (no cooperation between the r-MTs and the t-MT would terminate the data flow in the respective r-MTs). Therefore, there will be one MIMO channel with $t_{V-1}$ transmit antennas and $\sum_{i=1}^{q_V} n_{V,i}$ receive antennas.

**Target MT.** After cooperation between the r-MTs and the t-MT, the data is space-time decoded and passed on to the information sink in the t-MT.

A TDMA-based system operates exactly like the above-described FDMA-based relaying system, with the only difference that all fractional bandwidths $W_{v\in(1,K)}$ need to be replaced by fractional frame durations $T_{v\in(1,K)}$. Here, $K$ denotes the number of relaying stages and is related to the number of VAA relaying tiers via $K = V - 1$.

For any scenario, the total communication duration is normalised to $T$ and the total bandwidth to $W$. For orthogonal TDMA and FDMA-based relaying systems, $T = \sum_{v=1}^{K} T_v$ and $W = \sum_{v=1}^{K} W_v$ respectively. For non-orthogonal (interfering) relaying systems, the sum of all utilised fractional resources need to add-up to $T$ and $W$ respectively.

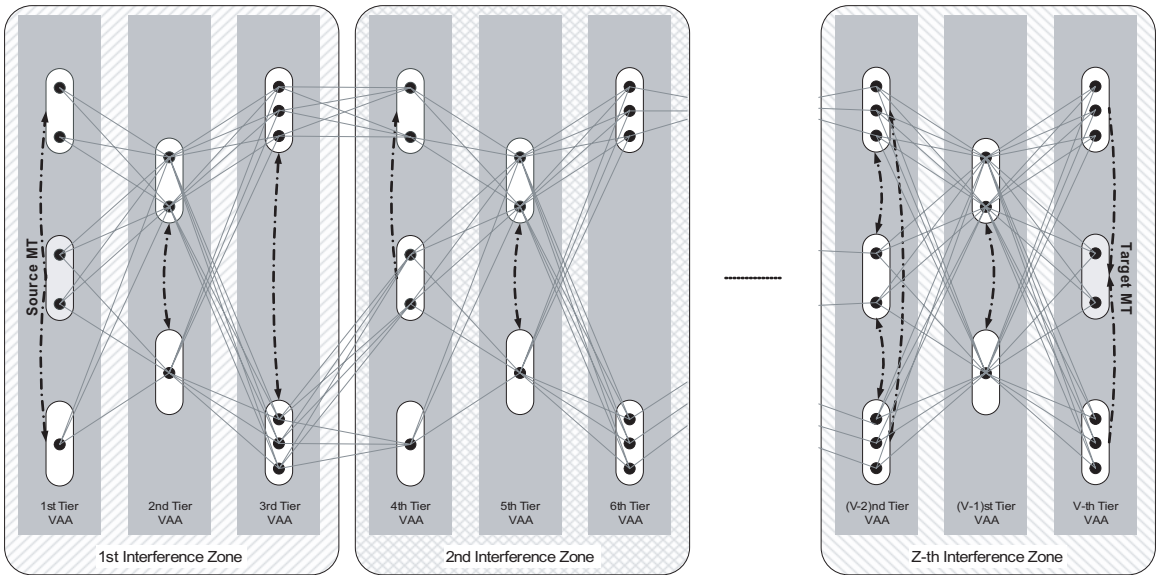


Figure 3.4: Distributed MIMO Multi-Stage communication system with resource reuse within the respective interference zones.

### 3.2.2 Extension to Resource Reuse Networks

The introduced communication scenario is easily extended to the case where resources in terms of fractional frame duration or bandwidth are reused after a given number of relaying VAA tiers, without yielding any interference to the other stages utilising the same resources. The concept is similar to the frequency re-use concept in cellular systems, which relies on the radio propagation inherent pathloss.

The suggested system deployment is depicted in Figure 3.4 with $Z$ interference zones. Within each such interference zone, the same resources may be reused without introducing interference to adjacent interference zones.

### 3.2.3 Equivalence between TDMA and FDMA

To simplify subsequent analysis, it is proven here that TDMA and FDMA-based SISO relaying systems are equivalent in terms of fractional resource allocations. The outlined analysis is equally applicable to multi-stage distributed-MIMO systems.

In TDMA-based relaying, only a fraction $\alpha^{(t)}$ of the total frame length $T$ is allocated to a MT; whereas in FDMA, only a fraction $\alpha^{(f)}$ of the total bandwidth $W$. Traditionally, a given fractional power is allocated to each MT; however, as illustrated in Figure 3.5, fractional energy is the appropriate figure to be considered. Here, hop #1 and hop #3 transmit with the same average power $S_1 = S_3$, whereas hop #2 transmits with power $S_2$. The energy consumed by hop #1, however, is much smaller than of hop #3, and equates the energy consumed by hop #2.

The energy $E$ to transmit information from source to sink needs therefore to be constrained, so as to allow for a fair comparison between different relaying schemes. Since the Shannon capacity is related to the signal and noise powers, appropriate translations to the energies have to be performed.

Given a TDMA-based multi-hop SISO communication scenario with $K$ hops, the capacity of the $v^{th}$ hop can be expressed as

$$C_v^{(t)} = \alpha_v^{(t)} \cdot W \cdot \mathrm{E}_{\lambda_v} \left\{ \log_2 \left( 1 + \frac{\lambda_v \cdot \gamma_v \cdot S_v}{N_v} \right) \right\} \tag{3.1}$$

where $\alpha_v^{(t)}$ is the fractional frame duration, $\gamma_v$ is the pathloss associated with the $v^{th}$ link, and $\lambda_v$ the random fading with given statistics $pdf_{\lambda_v}(\lambda_v)$. The transmit power into the $v^{th}$ hop is denoted as $S_v$ and the captured noise power at the receiver is $N_v$. The later can also be expressed as $N_v = N_0 \cdot W_v$, where $N_0$ is the noise power spectral density and $W_v$ is the allocated fractional bandwidth. For a TDMA-based relaying system, the following holds:

$$E_v = \beta_v^{(E_t)} E, \quad T_v = \alpha_v^{(t)} T, \quad W_v = W \tag{3.2}$$

where $\beta_v^{(E_t)}$ is the fraction of the total energy $E$ allocated to the $v^{th}$ hop leading to a fractional energy $E_v$. Furthermore, $T_v$ is the fractional frame duration of a total frame duration $T$. The total power $S$ relates to the total energy $E$ via $S = E/T$; furthermore, $N = N_0 \cdot W$. Inserting (3.2) into (3.1) yields for the capacity

$$C_v^{(t)} = \alpha_v^{(t)} \cdot W \cdot \mathrm{E}_{\lambda_v} \left\{ \log_2 \left( 1 + \lambda_v \cdot \gamma_v \cdot \frac{\beta_v^{(E_t)}}{\alpha_v^{(t)}} \cdot \frac{S}{N} \right) \right\} \tag{3.3}$$

with constraints

$$\sum_{v=1}^{K} \alpha_v^{(t)} \equiv 1, \qquad \sum_{v=1}^{K} \beta_v^{(E_t)} \equiv 1 \tag{3.4}$$

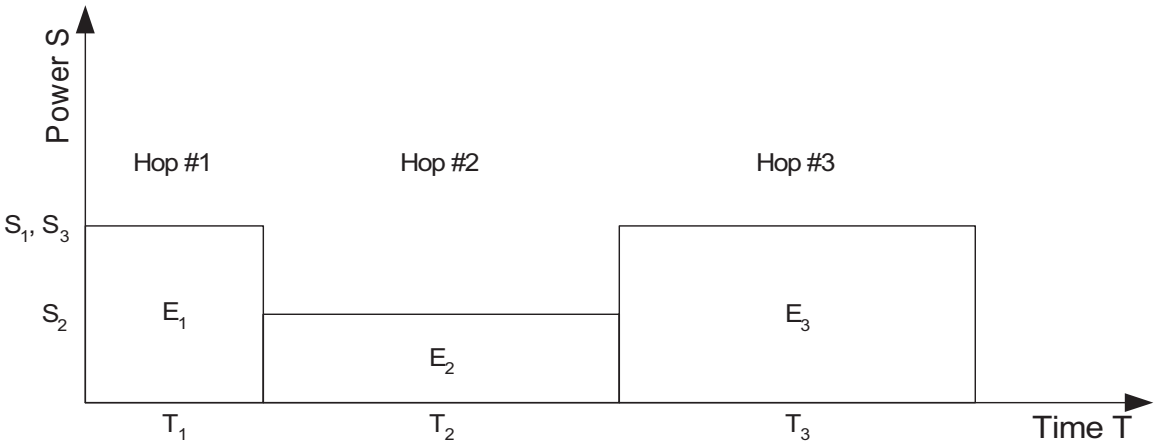


Figure 3.5: Relationship between power, energy and frame duration at each hop.

From (3.2) it is easily seen that a fractional power $\beta_v^{(P_t)} = \beta_v^{(E_t)}/\alpha_v^{(t)}$ has to be allocated to the $v^{th}$ hop, to which the constraint $\sum_{v=1}^{K} \alpha_v^{(t)} \beta_v^{(P_t)} \equiv 1$ applies.

Given an FDMA-based multi-hop SISO communication scenario with $K$ hops, the capacity of the $v^{th}$ hop can be expressed as

$$C_v^{(f)} = \alpha_v^{(f)} W \cdot \mathrm{E}_{\lambda_v} \left\{ \log_2 \left( 1 + \frac{\lambda_v \cdot \gamma_v \cdot S_v}{N_v} \right) \right\} \tag{3.5}$$

where $\alpha_v^{(f)}$ denotes the fractional bandwidth. Furthermore,

$$E_v = \beta_v^{(E_f)} E, \quad T_v = T, \quad W_v = \alpha_v^{(f)} W \tag{3.6}$$

where $\beta_v^{(E_f)}$ is the fractional energy. This yields for the FDMA-based relaying system

$$C_v^{(f)} = \alpha_v^{(f)} W \cdot \mathrm{E}_{\lambda_v} \left\{ \log_2 \left( 1 + \lambda_v \cdot \gamma_v \cdot \frac{\beta_v^{(E_f)}}{\alpha_v^{(f)}} \cdot \frac{S}{N} \right) \right\} \tag{3.7}$$

with constraints

$$\sum_{v=1}^{K} \alpha_v^{(f)} \equiv 1, \qquad \sum_{v=1}^{K} \beta_v^{(E_f)} \equiv 1 \tag{3.8}$$

From (3.6) it is easily seen that a fractional power $\beta_v^{(P_f)} = \beta_v^{(E_f)}$ has to be allocated to the $v^{th}$ hop, to which the constraint $\sum_{v=1}^{K} \beta_v^{(P_f)} \equiv 1$ applies.

Comparing (3.3) with (3.7), and the respective constraints (3.4) and (3.8), demonstrates that with given constraints on frame duration, bandwidth and energy to deliver information from source to sink, either relaying access methodology leads to the same capacity expression. In other words, if a fractional bandwidth $\alpha_v^{(f)}$ and energy $\beta_v^{(E_f)}$ is found to be optimum for an FDMA-based relaying system, then a fractional frame duration $\alpha_v^{(t)} = \alpha_v^{(f)}$ and energy $\beta_v^{(E_t)} = \beta_v^{(E_f)}$ will also be optimum for a TDMA-based relaying system. Although rigorously derived here, this could have been expected as the Shannon capacity of either systems ought not to differ.

Since traditionally fractional transmission powers are allocated to relaying terminals, subsequent analysis will refer to $\alpha_v^{(t)}$ and $\beta_v^{(P_t)}$ for TDMA-based relaying systems, and $\alpha_v^{(f)}$ and $\beta_v^{(P_f)}$ for FDMA-based relaying systems. As demonstrated above, $\sum_{v=1}^{K} \alpha_v^{(t)} \beta_v^{(P_t)} \equiv 1$ and $\sum_{v=1}^{K} \beta_v^{(P_f)} \equiv 1$, where the latter is clearly the more desirable constraint from an analysis point of view. Further analysis will therefore concentrate on FDMA-based relaying only. To simplify notation, the superscripts are dropped which yields for the constraints on fractional bandwidth and transmission power of an FDMA-based system

$$\sum_{v=1}^{K} \alpha_v \equiv 1 \tag{3.9}$$

$$\sum_{v=1}^{K} \beta_v \equiv 1 \tag{3.10}$$

An equivalent TDMA-based relaying system therefore requires a fractional frame duration $\alpha_v$ and transmission power $\beta_v/\alpha_v$. This will frequently be used in subsequent analysis.

## 3.3 Maximum Throughput for Ergodic Channels

Throughput is defined as the information delivered from source towards sink. This requires a certain duration of communication $T$ and frequency band $W$. Subsequent analysis will therefore refer to the normalised (spectral) throughput $\Theta$ in [bits/s/Hz].

An ergodic channel offers a normalised capacity $C$ in [bits/s/Hz] with 100% reliability, which allows relating capacity and throughput via $\Theta = C$. Therefore, maximising the throughput $\Theta$ is equivalent to maximising the capacity $C$. As defined by Shannon, capacity relates to error-free transmission. Hence, if a certain capacity was to be provided from source to sink, all channels involved must guarantee error-free transmission. From this it is clear that the end-to-end capacity $C$ is dictated by the capacity of the weakest link.

For a VAA multi-stage relaying network with $V$ relaying tiers as depicted in Figure 3.1, there will be $V - 1 = K$ stages each comprised of multiple MIMO channels. At each of the stages, partial cooperation may take place on the receiving side. As an example, the transmission stage from the $v^{th}$ VAA relaying tier to the $(v+1)^{st}$ is enlarged in Figure 3.6, where the three receiving terminals cooperate such as to yield two clusters. Generally, the clustering yields $Q_{v+1}$ MIMO channels with $t_v$ transmit antennas and $r_{v+1,j\in(1,Q_{v+1})}$ receive antennas. For the example below, $Q_{v+1} = 2$, $t_v = 5$, $r_{v+1,1} = 3$ and $r_{v+1,2} = 3$.

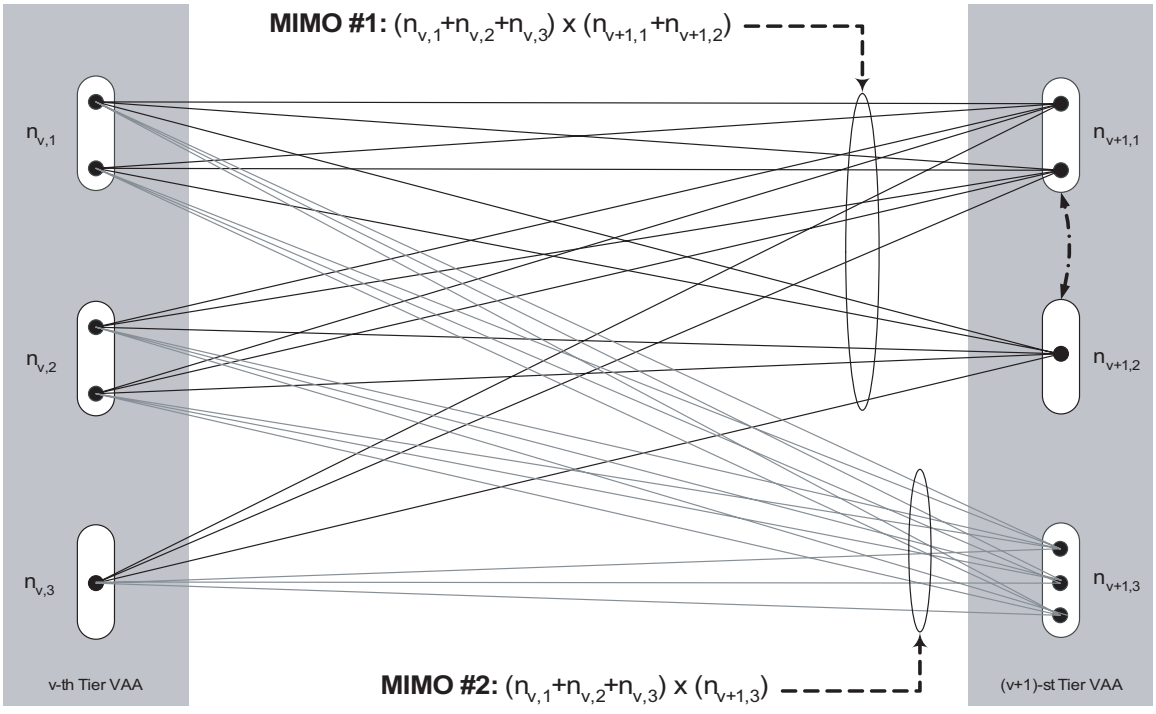


Figure 3.6: Established MIMO channels from the $v^{th}$ to the $(v+1)^{st}$ VAA relaying tier.

Prior to optimising the end-to-end capacity, the weakest of all $Q_{v+1}$ MIMO channels has to be determined at each relaying stage. If the distances between the r-MTs of the same relaying VAA tier are negligible compared to the inter-VAA distances, then the strength of a MIMO channel can be measured by the number of receive antennas. It is generally desirable to guarantee mutual cooperation between terminals such that all created MIMO channels offer the same capacity, which can be achieved if they have the same number of receive antennas. In Figure 3.6 for example, two r-MTs cooperate with a total of three receive antennas, which equates to the number of receive antennas of the non cooperating r-MT, hence achieving an optimal relaying solution.

Since optimisation has to be performed on the weakest link (or one of the equally strong links) at each of the $K$ relaying stages, notation can be simplified further. To this end, it is assumed that the $v^{th}$ relaying stage has $t_v$ antennas acting as transmitters and, to simplify subsequent notation, $r_v \triangleq \min_{j\in(1,Q_{v+1})}\{r_{v+1,j}\}$ antennas acting as receivers. This is henceforth denoted as $(t_1 \times r_1)/(t_2 \times r_2)/\ldots/(t_K \times r_K)$.

The capacity $C_v$ of the $v^{th}$ relaying stage is hence determined by $t_v$ and $r_v$, and the occurring channel conditions. It is thus the aim to find for all $v = 1,\ldots,K$ stages the fractional allocations of bandwidth $\alpha_v$ and power $\beta_v$ for given channel conditions $\lambda_v$ and $\gamma_v$ so as to maximise the minimum capacity $C$, i.e.

$$C = \sup_{\boldsymbol{\alpha},\boldsymbol{\beta}}\Big\{\min\big\{C_1(\alpha_1,\beta_1,\lambda_1,\gamma_1),\ldots,C_K(\alpha_K,\beta_K,\lambda_K,\gamma_K)\big\}\Big\} \tag{3.11}$$

where the optimisation is performed over the fractional sets $\boldsymbol{\alpha} \triangleq (\alpha_1,\ldots,\alpha_K)$ and $\boldsymbol{\beta} \triangleq (\beta_1,\ldots,\beta_K)$. Furthermore, $C_v(\alpha_v,\beta_v,\lambda_v,\gamma_v)$ denotes the dependency of the capacity in the $v^{th}$ link on the fractional resource allocations $\alpha_v$ and $\beta_v$, and on the channel conditions $\lambda_v$ and $\gamma_v$. Fractional capacity allocation strategies satisfying (3.11) under applicable constraints are derived below.

### 3.3.1 Algorithms for MIMO Relaying without Resource Reuse

With the parameter constraints given by (3.9) and (3.10), increasing one capacity inevitably requires decreasing the other capacities. The minimum is maximised if all capacities are equated and then maximised. The normalised capacity of the $v^{th}$ stage is given as

$$C_v \;=\; \alpha_v \cdot \mathrm{E}_{\lambda_v}\left\{m_v \log_2\left(1+\lambda_v \frac{\gamma_v}{t_v}\frac{\beta_v}{\alpha_v}\frac{S}{N}\right)\right\} \tag{3.12}$$

where the expectation is evaluated with any of the applicable pdfs derived in Chapter 2. Thus, $\alpha_v$ is obtained by equating (3.12) for all $v = 1,\ldots,K$, which is derived in Appendix 3.7 (Derivation I) to be

$$\alpha_v = \frac{\prod_{w\neq v}\mathrm{E}_{\lambda_w}\left\{m_v \log_2\left(1+\lambda_w \frac{\gamma_w}{t_w}\frac{\beta_w}{\alpha_w}\frac{S}{N}\right)\right\}}{\sum_{k=1}^{K}\prod_{w\neq k}\mathrm{E}_{\lambda_w}\left\{m_v \log_2\left(1+\lambda_w \frac{\gamma_w}{t_w}\frac{\beta_w}{\alpha_w}\frac{S}{N}\right)\right\}} \tag{3.13}$$

The end-to-end capacity $C = C_1 = \ldots = C_K$ is obtained by inserting (3.13) into (3.12), i.e.

$$C = \frac{\prod_{w=1}^{K} \mathrm{E}_{\lambda_w} \left\{ m_v \log_2 \left( 1 + \lambda_w \frac{\gamma_w}{t_w} \frac{\beta_w}{\alpha_w} \frac{S}{N} \right) \right\}}{\sum_{k=1}^{K} \prod_{w \neq k} \mathrm{E}_{\lambda_w} \left\{ m_v \log_2 \left( 1 + \lambda_w \frac{\gamma_w}{t_w} \frac{\beta_w}{\alpha_w} \frac{S}{N} \right) \right\}} \tag{3.14}$$

Equation (3.14) is conveniently expressed as

$$C = \left[ \sum_{k=1}^{K} \frac{1}{\mathrm{E}_{\lambda_k} \left\{ m_v \log_2 \left( 1 + \lambda_k \frac{\gamma_k}{t_k} \frac{\beta_k}{\alpha_k} \frac{S}{N} \right) \right\}} \right]^{-1} \tag{3.15}$$

which constitutes a $2K$-dimensional optimisation problem with respect to (w.r.t.) the fractional bandwidth and power allocations $\alpha_k$ and $\beta_k$, respectively.

**Exact Optimisation via Lagrangian**

Using Lagrange's method [60] for maximising (3.15) under constraints (3.9) and (3.10), suggests the Lagrangian

$$\mathcal{L} = \left[ \sum_{k=1}^{K} \frac{1}{\mathrm{E}_{\lambda_k} \left\{ m_v \log_2 \left( 1 + \lambda_k \frac{\gamma_k}{t_k} \frac{\beta_k}{\alpha_k} \frac{S}{N} \right) \right\}} \right]^{-1} + \iota \left[ 1 - \sum_{k=1}^{K} \alpha_k \right] + \kappa \left[ 1 - \sum_{k=1}^{K} \beta_k \right] \tag{3.16}$$

which is differentiated w.r.t. $\alpha_k$ $K$ times and then w.r.t $\beta_k$ another $K$ times. The resulting $2K$ equations are equated to zero and the system of equations is resolved in favour of any $\alpha_k$ and $\beta_k$, where $\iota$ and $\kappa$ are chosen so as to satisfy (3.9) and (3.10).

Clearly, a pdf given in the form of (2.32) leads to $2K$ equations which are not explicitly resolvable in favour of the sought variables. This is the main reason why no explicit resource allocation strategy has been developed to date, where only numerical optimisation routines can be found in the literature.

**Optimised Fractional Bandwidth and Optimised Fractional Power**

An explicit resource allocation algorithm has been developed by the author, which yields a close to optimum solution, the precision of which is being assessed below. To this end, it is suggested to reduce the $2K$ dimensional optimisation problem (3.15) to a $K$-dimensional optimisation problem by optimising w.r.t. $\frac{\beta_k}{\alpha_k}$, the ratio between the fractional power and bandwidth allocation. In Appendix 3.7 (Derivation II) it is shown that

$$\sum_{k=1}^{K} \frac{\beta_k}{\alpha_k} \approx K \tag{3.17}$$

Applying approximation (2.98) and taking (3.17) into account, (3.15) can be simplified to

$$C \approx \left[ \frac{1}{\Lambda(t_1, r_1) \sqrt{\gamma_1 \frac{S}{N}} \sqrt{K - \sum_{k=2}^{K} \frac{\beta_k}{\alpha_k}}} + \sum_{k=2}^{K} \frac{1}{\Lambda(t_k, r_k) \sqrt{\gamma_k \frac{S}{N}} \sqrt{\frac{\beta_k}{\alpha_k}}} \right]^{-1} \tag{3.18}$$

which constitutes now a $(K-1)$-dimensional optimisation problem w.r.t. $\frac{\beta_k}{\alpha_k}$ with $k = 2,\ldots,K$. The approximate capacity gain $\Lambda(t,r)$ in dependency of the number of transmit antennas $t$ and receive antennas $r$ can be taken from (2.105) for the appropriate communication scenarios. The maximum end-to-end capacity is obtained by equating the first derivative of $C$ w.r.t. $\frac{\beta_2}{\alpha_2},\ldots,\frac{\beta_K}{\alpha_K}$ to zero. Instead of maximising $C$ it is more convenient to minimise $1/C$, i.e.

$$\frac{\partial\left(\frac{1}{C}\right)}{\partial\left(\frac{\beta_2}{\alpha_2}\right)} = \ldots = \frac{\partial\left(\frac{1}{C}\right)}{\partial\left(\frac{\beta_K}{\alpha_K}\right)} \equiv 0 \tag{3.19}$$

After partial differentiation, one obtains

$$\frac{1}{\Lambda(t_1,r_1)\sqrt{\gamma_1\frac{S}{N}}\left[K-\sum_{v=2}^{K}\frac{\beta_v}{\alpha_v}\right]^{\frac{3}{2}}} - \frac{1}{\Lambda(t_2,r_2)\sqrt{\gamma_2\frac{S}{N}}\left[\frac{\beta_2}{\alpha_2}\right]^{\frac{3}{2}}} = 0 \tag{3.20}$$

$$\vdots$$

$$\frac{1}{\Lambda(t_1,r_1)\sqrt{\gamma_1\frac{S}{N}}\left[K-\sum_{v=2}^{K}\frac{\beta_v}{\alpha_v}\right]^{\frac{3}{2}}} - \frac{1}{\Lambda(t_K,r_K)\sqrt{\gamma_K\frac{S}{N}}\left[\frac{\beta_K}{\alpha_K}\right]^{\frac{3}{2}}} = 0 \tag{3.21}$$

The $K-1$ equations can be resolved for any $\beta_v/\alpha_v$ which yields, as demonstrated in Appendix 3.7 (Derivation III)

$$\frac{\beta_v}{\alpha_v} \approx K \cdot \frac{\prod_{w\neq v}\sqrt[3]{\gamma_w\cdot\Lambda^2(t_w,r_w)}}{\sum_{k=1}^{K}\prod_{w\neq k}\sqrt[3]{\gamma_w\cdot\Lambda^2(t_w,r_w)}} \tag{3.22}$$

The fractional bandwidth allocations $\alpha_{v=(1,\ldots,K)}$ can now be obtained by substituting (3.22) into (3.13). The fractional power allocations $\beta_{v=(1,\ldots,K)}$ can finally be obtained by inserting the prior obtained $\alpha_v$ into (3.22) and solving for $\beta_v$.

Since the derived fractional resource allocation rules are the result of various approximations, they have to be applied with care.

First, one has to make sure that the constraints (3.9) and (3.10) hold for the derived $\alpha_v$ and $\beta_v$. Therefore, it is suggested to derive $K-1$ coefficients $\alpha_v$ and $\beta_v$, and then obtain the remaining two $\alpha_v$ and $\beta_v$ from (3.9) and (3.10). Second, it is suggested to obtain the $K-1$ coefficients $\alpha_v$ and $\beta_v$ from the first $K-1$ strongest links, where the strength is determined by $\gamma_w\cdot\Lambda^2(t_w,r_w)$. Third, the obtained $K$ capacities $C_{v\in(1,K)}$ are not entirely equal, which is again due to the approximations deployed. The end-to-end capacity utilising the above-given technique is hence obtained by choosing the minimum of all $C_v$.

The flowchart in Figure 3.7 summarises the method in obtaining the fractional bandwidth and power allocations.

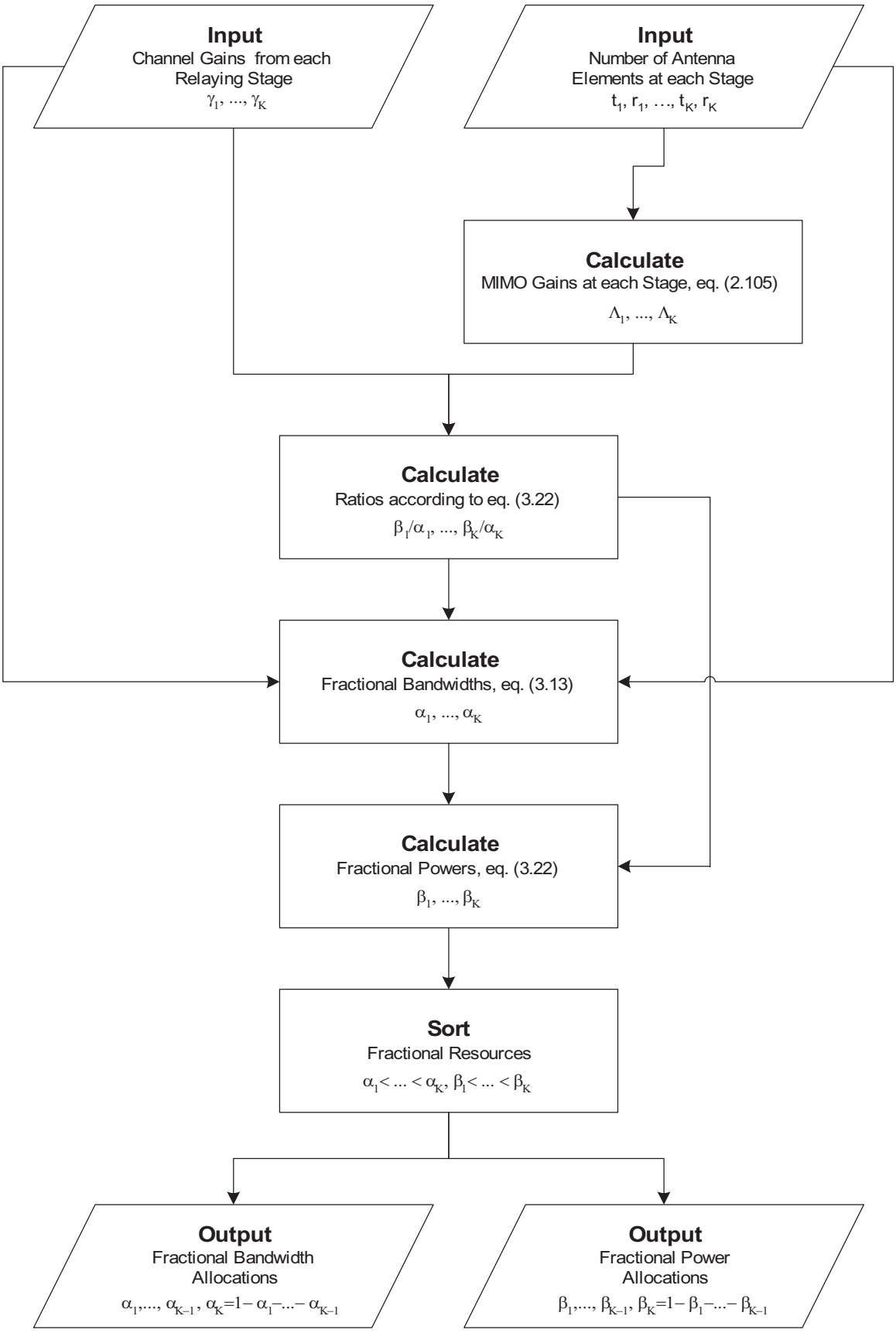


Figure 3.7: Flowchart specifying the algorithmic method for determining the fractional bandwidth and power.

**Equal Fractional Bandwidth and Optimised Fractional Power**

To compare the performance benefits of the above-developed fractional resource allocation algorithm, a similar algorithm is developed here with the fractional power allocation optimised only. With the fractional power $\beta_v$ to be optimised and equal bandwidth $\alpha_v = 1/K$, (3.12) turns into

$$C_v = \frac{1}{K} \cdot \mathrm{E}_{\lambda_v} \left\{ m_v \log_2 \left( 1 + \lambda_v \beta_v K \frac{\gamma_v}{t_v} \frac{S}{N} \right) \right\} \tag{3.23}$$

$$\approx \sqrt{\beta_v} \sqrt{\frac{\gamma_v}{K}} \sqrt{\frac{S}{N}} \, \Lambda(t_v, r_v) \tag{3.24}$$

Equating all capacities $C_v$ given by (3.24) and applying constraint (3.10) allows one to resolve the set of equations in favour of any $\beta_v$ as

$$\beta_v \approx \frac{\prod_{w \neq v} \gamma_w \cdot \Lambda^2(t_w, r_w)}{\sum_{k=1}^{K} \prod_{w \neq k} \gamma_w \cdot \Lambda^2(t_w, r_w)} \tag{3.25}$$

which, when inserted into (3.23), yields the end-to-end capacity $C$. Again, the obtained capacities $C_v$ do not entirely coincide because of the approximation chosen. The end-to-end capacity will therefore be dominated by the smallest of all. Note finally that the case of optimised bandwidth and equal power has not been considered here because of negligible applicability.

**Equal Fractional Bandwidth and Equal Fractional Power**

Finally, the trivial case of equal fractional bandwidth and power yields for the capacity at each stage $C_v = \frac{1}{K} \cdot \mathrm{E}_{\lambda_v} \left\{ m_v \log_2 \left( 1 + \lambda_v \frac{\gamma_v}{t_v} \frac{S}{N} \right) \right\}$, and the end-to-end capacity $C$ is obtained by choosing the minimum of all $C_v$.

### 3.3.2 Performance of MIMO Relaying without Resource Reuse

The developed fractional resource allocation algorithms are assessed below for various VAA relaying scenarios. The simplest scenario is the 2-stage relaying scenario with only one relaying VAA tier. In addition to this, the 3-stage relaying configuration is assessed. More relaying stages have not been analysed here due to the lengthy numerical optimisation. The obtained graphs are generally labelled on the parameter $p$ defined as

$$p \triangleq \left[ 10 \log_{10} \left( \frac{\gamma_1}{\gamma_1} \right), 10 \log_{10} \left( \frac{\gamma_2}{\gamma_1} \right), \ldots, 10 \log_{10} \left( \frac{\gamma_K}{\gamma_1} \right) \right] \tag{3.26}$$

which characterises the relative strength in dB of the $K$ relaying stages with respect to the first stage.

**The 2-Stage VAA Relaying Scenario**

The precision and applicability of the derived resource allocation strategies is assessed here for various antenna configurations of the 2-stage VAA relaying scenario.

**a) Single Antenna Element.** The derived resource allocation strategies are obviously also applicable to traditional relaying networks with one antenna element per MT. The precision of the developed fractional resource allocation algorithm is assessed in Figure 3.8. It depicts the optimum end-to-end capacity obtained via numerical optimisation on (3.16) and the approximate end-to-end capacity obtained from (3.22), (3.13) and (3.12) versus the SNR in the first relaying stage. The graphs are labelled on the parameter $p$ as defined in (3.26) with $K = 2$, where the second relaying channel is 10dB and 5dB stronger than the first one, equally strong than the first one, and 5dB and 10dB weaker than the first one.

It can be observed that the exact and developed end-to-end capacities almost coincide. The error was found not to exceed 3% for any of the depicted cases. The developed explicit resource allocations are hence a powerful tool in obtaining a near-to-optimum end-to-end capacity without the need for lengthy numerical optimisations. The algorithm is shown to be applicable for channels with attenuations differing by magnitudes.

Figure 3.9 compares the obtained end-to-end capacities of various allocation strategies, where the curves are labelled on $p = \big([0, 10], [0, 0], [0, -10]\big)$dB. The numerically obtained optimum allocation strategy is depicted together with the developed strategies of optimised bandwidth and power, equal power but optimised bandwidth, and equal bandwidth and equal power. When both links are equally strong, i.e. $p = [0, 0]$dB, then all of the considered allocation strategies yield the same end-to-end capacity. This is obvious because for the given symmetric communication scenario, resources have to be shared equally between the relaying terminals.

When the second link is 10dB weaker, i.e. $p = [0, -10]$dB, then optimising bandwidth and power or optimising power only yields close to optimum performance. This is because for low SNR, $\log(1+x) \approx x$, which, with reference to (3.12), makes the optimisation problem independent of the bandwidth $\alpha_v$. When no optimisation is performed then the end-to-end capacity is dictated by the weakest link, here the second link which is 10 times weaker than the first one. The capacity is considerably lower than for the optimised cases; at an SNR of 6dB a loss in rate of 40% can be observed, whereas at a rate of 0.4 bits/s/Hz approximately 40% more power is required.

When the second link is 10dB stronger, i.e. $p = [0, 10]$dB, then optimising bandwidth and power yields close to optimum performance, whereas only optimising power does not. This is because for high SNR, the dependence of the end-to-end capacity on the bandwidth $\alpha_v$ increases. At an SNR of 6dB, a relative loss of approximately 10% occurs. As for the case where no optimisation is performed, the end-to-end capacity is dictated by the first link which yields the same end-to-end capacity as for $p = [0, 0]$dB. Here, a relative loss of 30% occurs at an SNR of 6dB, or 50% more power is required to maintain a rate of 1 bit/s/Hz. Note that the absolute loss in bits/s/Hz is much higher as for the case of $p = [0, -10]$dB.

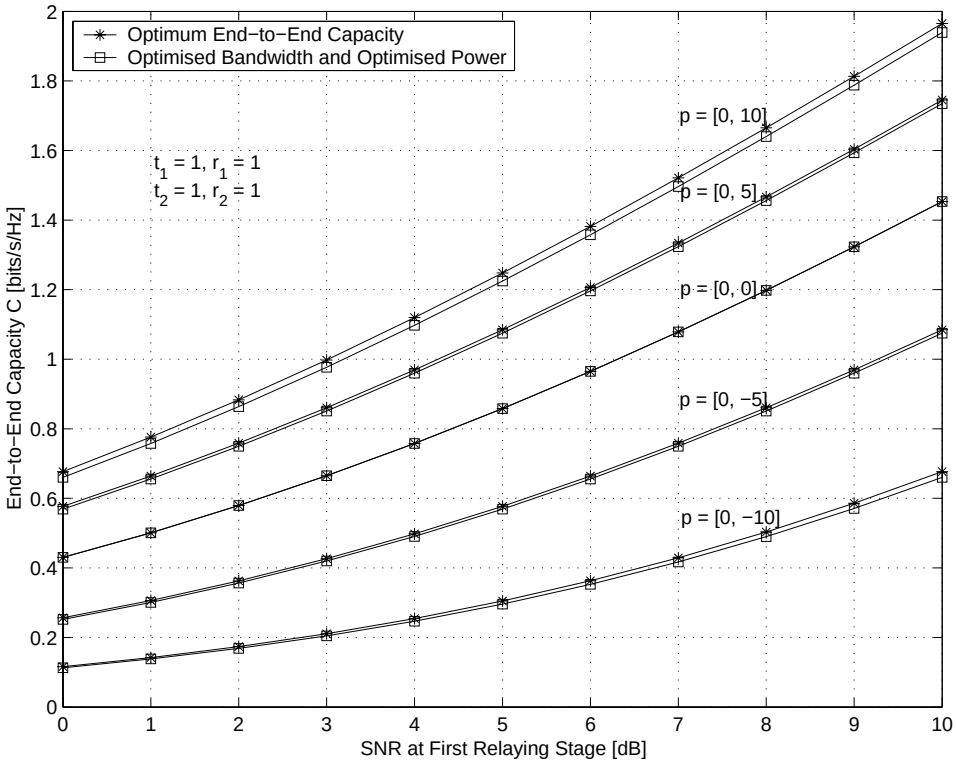


Figure 3.8: Comparison between optimum end-to-end capacity and the capacity obtained with the aid of the fractional resource allocation algorithm for a 2-stage network.

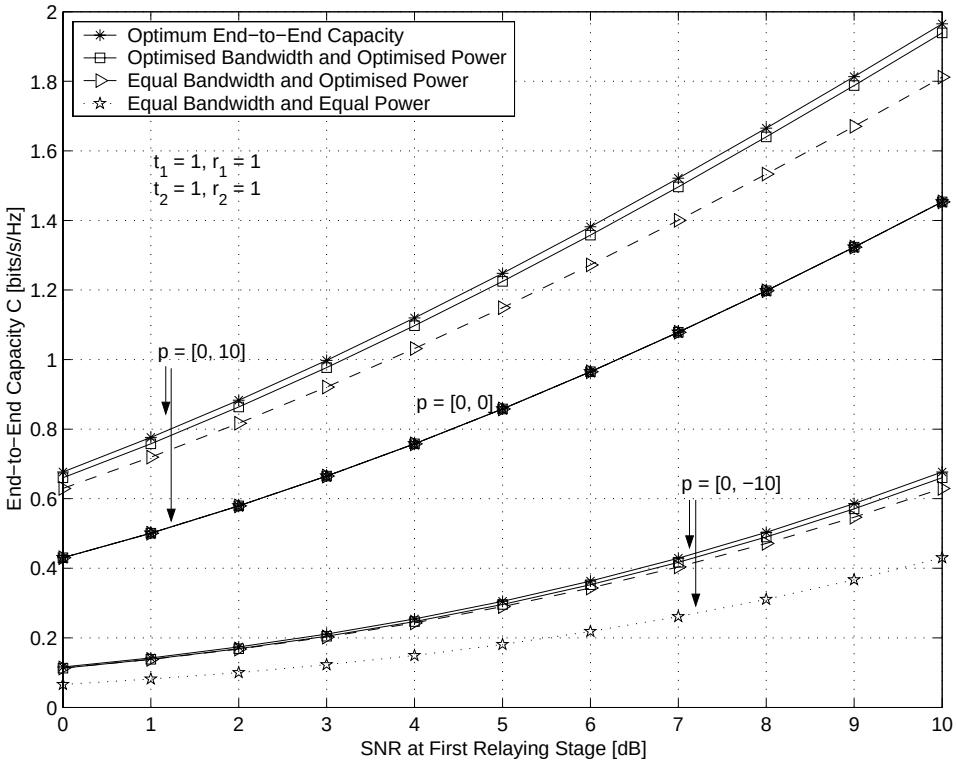


Figure 3.9: Achieved end-to-end capacity of various fractional resource allocation strategies for a 2-stage network.

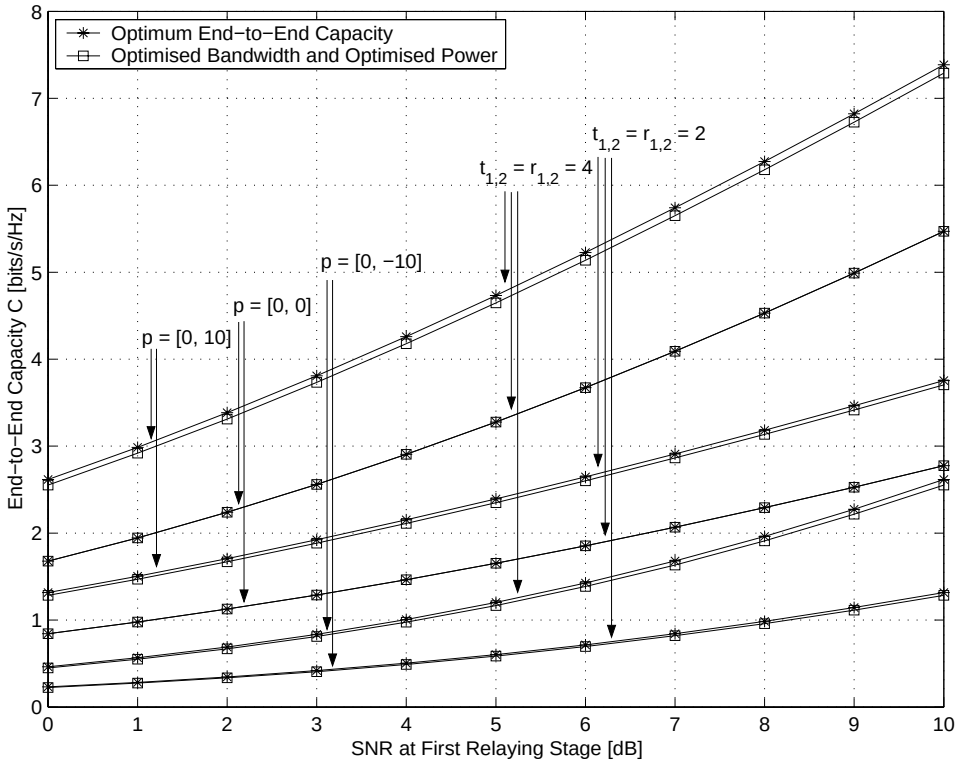


Figure 3.10: Comparison between optimum end-to-end capacity and the capacity obtained with the aid of the fractional resource allocation algorithm for a 2-stage network with a varying number of transmit and receive antennas.

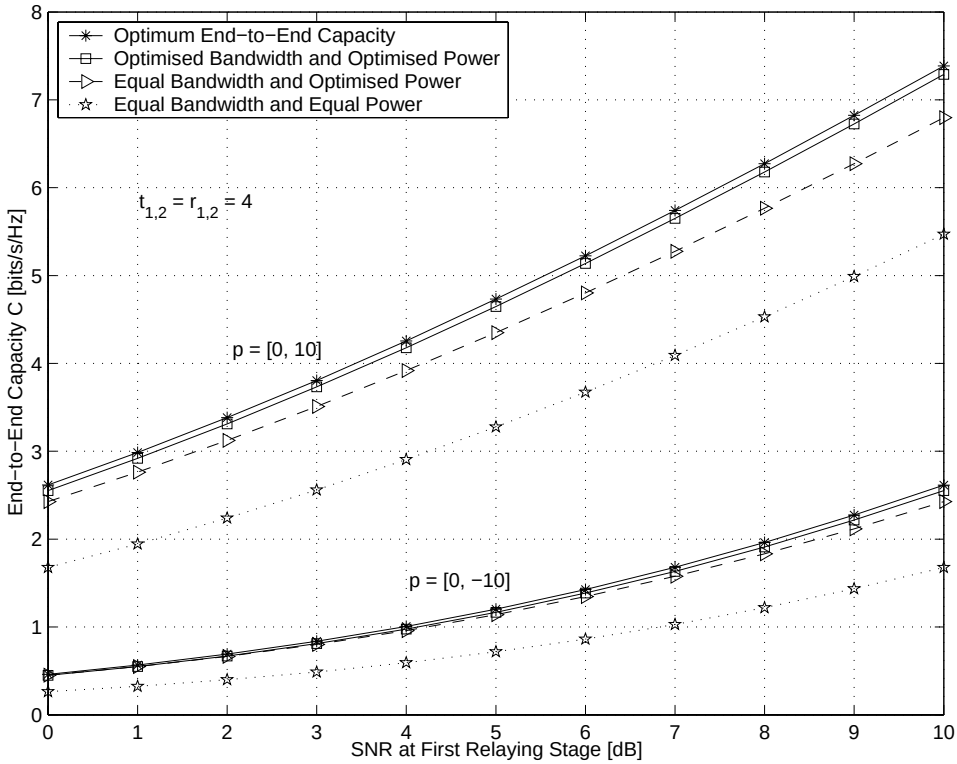


Figure 3.11: Achieved end-to-end capacity of various fractional resource allocation strategies for a 2-stage network.

For decreasing differences in the attenuations between the links, the relative and absolute errors in the maximum achievable end-to-end capacities of all developed allocation strategies decrease. The example of 10dB difference has been chosen to obtain some upper bounds on the occurring errors.

**b) Multiple Antenna Elements.** The algorithms are now scrutinised for communication scenarios where the MTs possess multiple but equal number of antenna elements. Figure 3.10 is the equivalent to Figure 3.8, with the only difference that each MT possesses two or four transmit and receive antennas. Again, the occurring errors between derived allocation strategy and an optimum allocation is below 3%.

Figure 3.11 is the equivalent of Figure 3.9, with the only difference that each terminal possesses 4 antenna elements; note that the $p = [0, 0]$dB case has been omitted here due to the symmetric communication scenario. The same comments on the precision of the algorithms as above apply. For a second link being 10 times weaker than the first link, the allocation of optimised bandwidth/power and power only yield close to optimum performance, whereas no optimisation leads to a loss of 40% at an SNR of 6dB, or approximately 75% more power is required to maintain 1 bit/s/Hz. When the second link is 10 times stronger than the first one, then the losses from optimum to optimised power only is about 8%, whereas from optimum to no optimisation a loss of about 30% occurs at an SNR of 6dB or, alternatively, 85% more power is needed to accomplish 4 bits/s/Hz.

The demonstrated performance gains and power savings clearly underline the merit of the developed fractional resource allocation algorithms.

**c) Differing Antenna Elements.** The importance of the developed strategy, however, becomes apparent when the 2-stage communication scenario is optimised for terminals with a different number of antenna elements. The precision of the fractional resource allocation algorithm, as well as its performance gains when compared to sub-optimal solutions, is exposed in Figures 3.12 and 3.13.

In particular, Figure 3.12 depicts the case where a s-MT with one antenna element communicates with a t-MT (or t-VAA) with three elements via a relaying stage, which effectively provides two relaying antennas. The asymmetry of the gains provided by the respective distributed-MIMO relaying stages causes the sub-optimum allocation strategies not to overlap with the optimum one for $p = [0, 0]$dB. Furthermore, non-linearities can be observed in the end-to-end capacity for the case of optimised power only, which is due to the approximation utilised in the derivation of the allocation strategy. In fact, one can observe a breakpoint which divides the zones where one or the other approximate capacity dominates the end-to-end capacity.

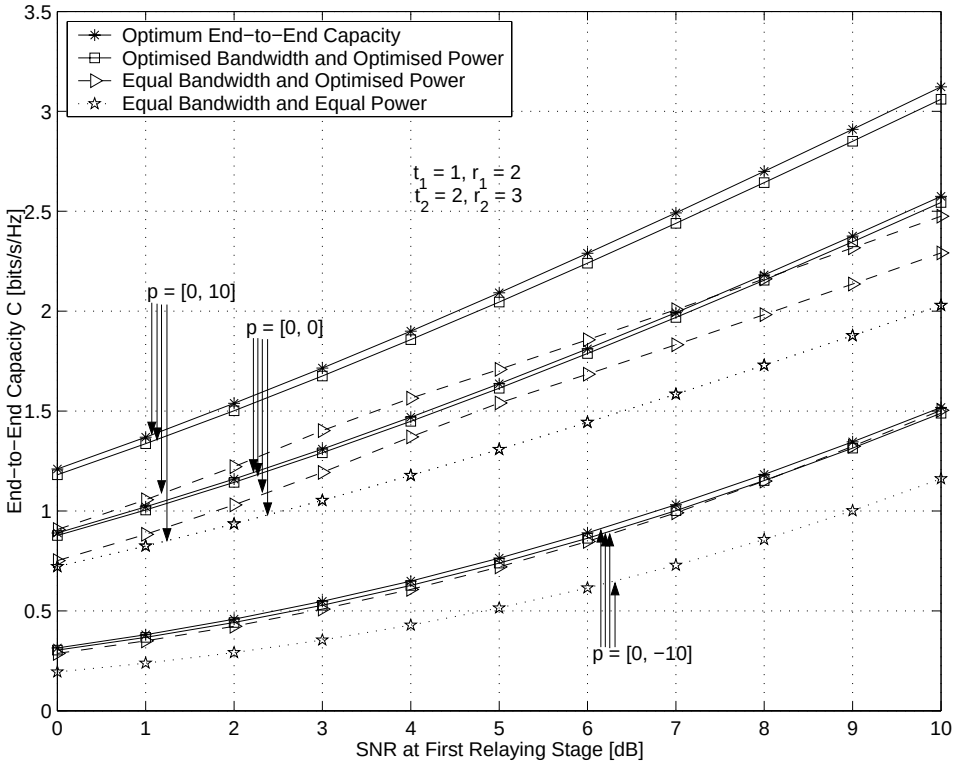


Figure 3.12: Achieved end-to-end capacity of various fractional resource allocation strategies for a 2-stage network.

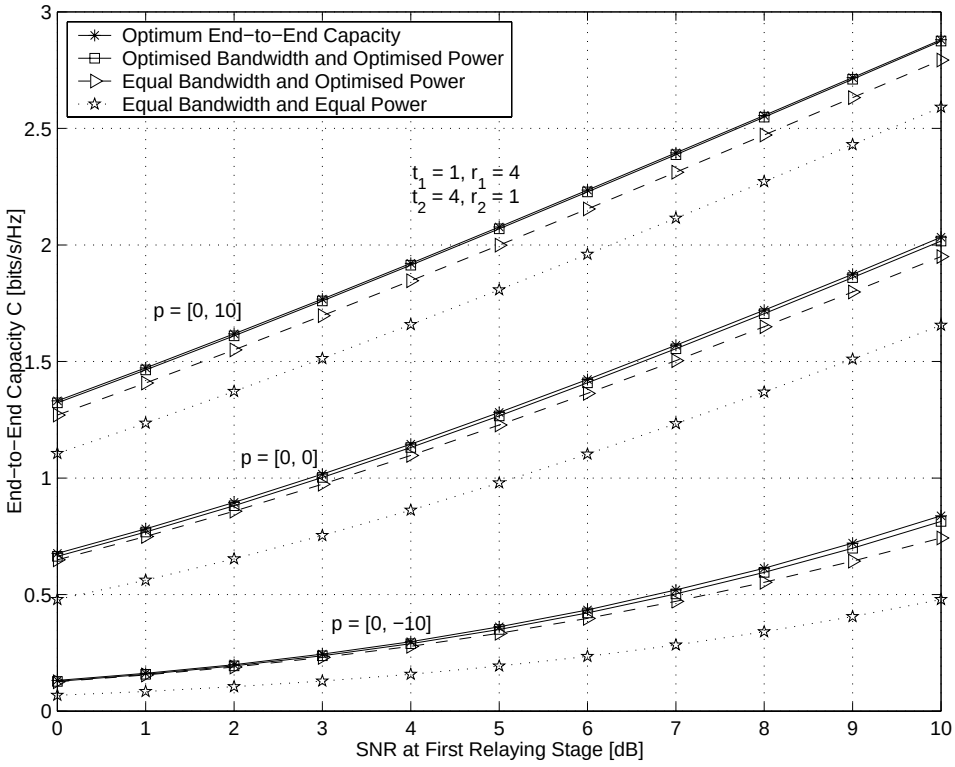


Figure 3.13: Achieved end-to-end capacity of various fractional resource allocation strategies for a 2-stage network.

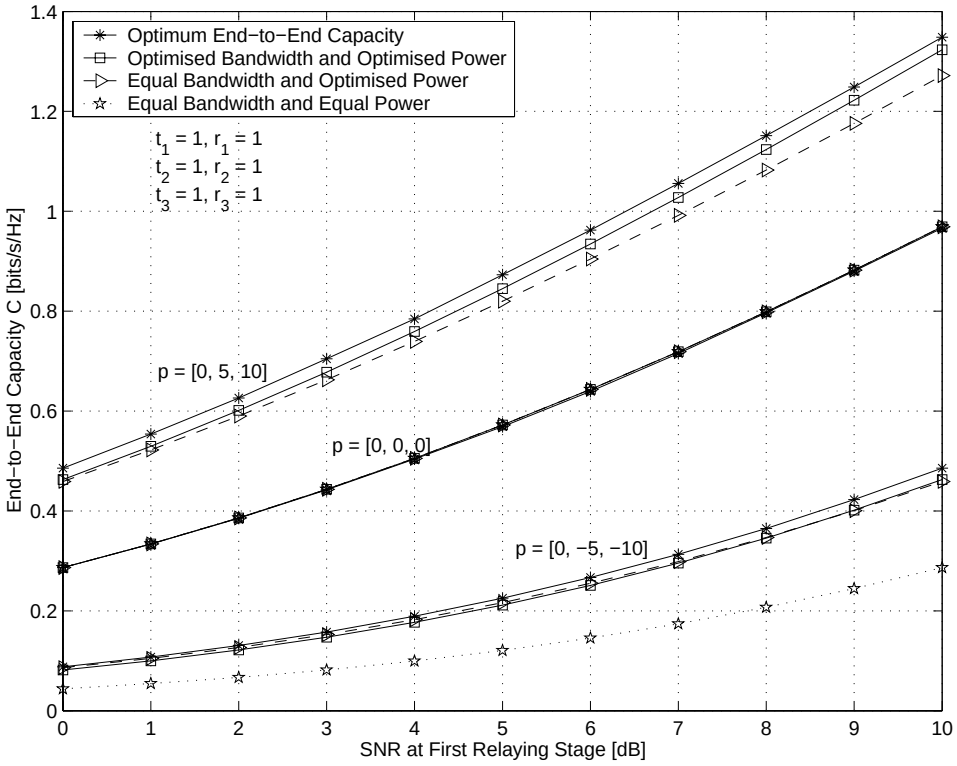


Figure 3.14: Achieved end-to-end capacity of various fractional resource allocation strategies for a 3-stage network.

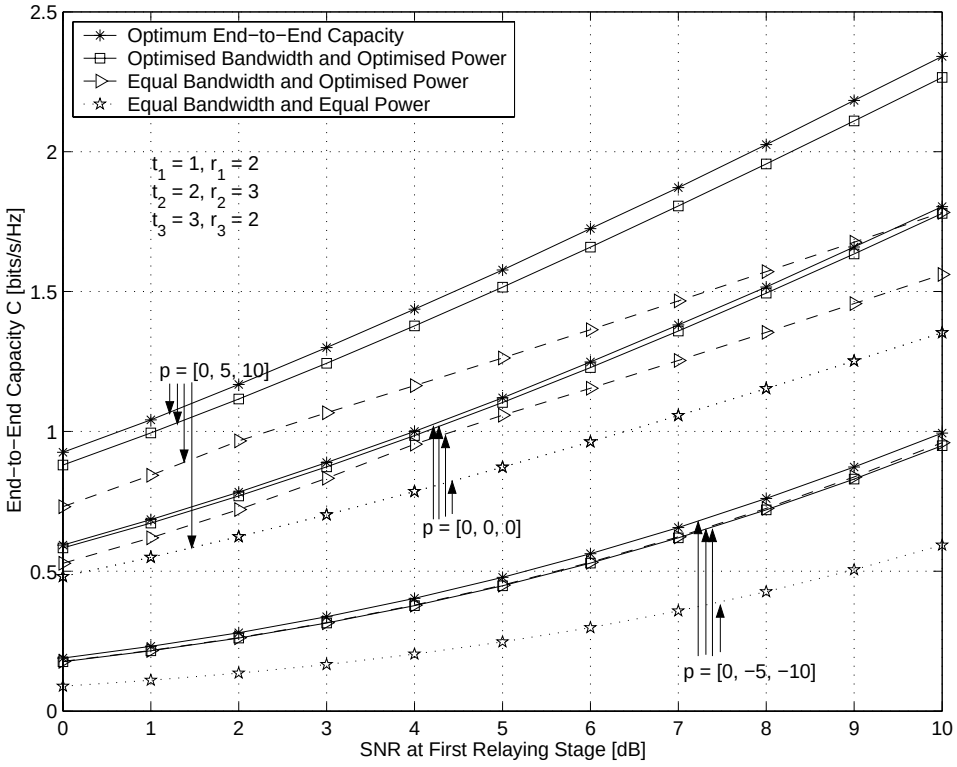


Figure 3.15: Achieved end-to-end capacity of various fractional resource allocation strategies for a 3-stage network.

However, the optimised fractional bandwidth and power allocation strategy yields close to optimum performance, even if the link attenuations and the created MIMO configurations differ significantly. Additionally, the gains obtained from a bandwidth/power optimised system when compared to a power optimised or non-optimised system increase with the balance between both links decreasing. For instance, for $p = [0, 10]$dB, the first $(1 \times 2)$ MIMO link is much weaker than the second $(2 \times 3)$ link. At an SNR of 6dB the capacity losses of a power optimised system is then 20% and of a non-optimised system a considerable 40%. Alternatively, the power required to maintain 2 bits/s/Hz is about 55% higher for the power optimised system, whereas a non-optimised system requires 120% (!) more power.

Figure 3.13 depicts a $(1 \times 4)/(4 \times 1)$ scenario. The same tendencies as already described can be observed; additionally, the precision of the developed fractional bandwidth/power allocation strategy is once more corroborated.

#### The 3-Stage VAA Relaying Scenario

The 3-stage relaying scenario is dealt with in less detail as for the 2-stage case, which is due to the increased simulation times and the increased number of potentially different communication scenarios. To this end, Figures 3.14 and 3.15 depict the performance of the developed resource allocation algorithms for the 3-stage communication scenario.

Explicitly, Figure 3.14 deals with the case of only one antenna element per MT, i.e. a $(1 \times 1)/(1 \times 1)/(1 \times 1)$ relaying scenario. The case of equally strong links when $p = [0, 0, 0]$dB yields an equal performance for any of the allocation strategies, which is again due to the scenario's symmetry. The allocation strategies, however, deviate from the numerically obtained optimum when the links are unbalanced; the error was found to be below 3%. Figure 3.15 shows the performance of the allocation strategies for the relaying scenario of $(1 \times 2)/(2 \times 3)/(3 \times 2)$. Here, the approximation error was found not to exceed 5%.

The scrutinised communication scenarios hence confirm the applicability and precision of the developed explicit fractional bandwidth and power allocation strategy. The optimised systems were shown to perform near-optimum, with drastic gains in communication rates at a given SNR, or power savings at a given communication rate.

### 3.3.3 MIMO Relaying with Resource Reuse

The reuse of resources under the assumption of orthogonal relaying is analysed here. With reference to Figure 3.4, there are $Z$ interference zones within which the reuse of resources would cause interference. It is further assumed that the optimum formation of VAA relaying stages is accomplished according to the description at the beginning of Section 3.3, which implies that each of the $v \in (1, K)$ stages is assigned $t_v$ transmit and $r_v$ receive elements.

Defining as $K_{z\in(1,Z)}$ the number of stages in the $z^{th}$ interference zone, then the capacity of the $v^{th}$ stage is given through (3.12); however, end-to-end capacity optimisation is now performed under the following constraints

$$\sum_{v=1+K_{z-1}}^{K_z+K_{z-1}} \alpha_v \equiv 1, \quad z = 1, \ldots, Z \tag{3.27}$$

$$\sum_{v=1}^{K} \beta_v \equiv 1 \tag{3.28}$$

where $K_0 \triangleq 0$ and $\sum_{z=1}^{Z} K_i = K$. Put in words, the power (energy) required to deliver information from source to sink is still normalised taking all relaying stages into account; however, the fractional bandwidths are now only normalised over one interference zone.

Optimising (3.12) under the set of constraints (3.27) and (3.28) is again not feasible utilising a Lagrangian approach. Furthermore, the author could attain a satisfactory solution optimising fractional bandwidth and power for special communication scenarios only. The lack of generality is the reason why this case has been excluded from further analysis. However, a sufficiently precise solution could be derived when optimising power only.

**Equal Fractional Bandwidth and Optimised Fractional Power**

Equal fractional bandwidth implies that the same bandwidth is assigned to each relaying stage within an interference zone. With the fractional power $\beta_v$ to be optimised and equal bandwidth per interference zone, i.e. $\alpha_{v\in(1+K_{z-1},K_z+K_{z-1})} = 1/K_z$, (3.12) turns into

$$C_{v\in(1+K_{z-1},K_z+K_{z-1})} = \frac{1}{K_z} \cdot \mathrm{E}_{\lambda_v} \left\{ m_v \log_2 \left( 1 + \lambda_v \beta_v K_z \frac{\gamma_v}{t_v} \frac{S}{N} \right) \right\} \tag{3.29}$$

$$\approx \sqrt{\beta_v} \sqrt{\frac{\gamma_v}{K_z}} \sqrt{\frac{S}{N}} \, \Lambda(t_v, r_v) \tag{3.30}$$

for $z = 1, \ldots, Z$. Equating all capacities $C_v$ given by (3.30) and applying constraint (3.28) allows one to resolve the set of equations in favour of any $\beta_v$ as

$$\beta_v \approx \frac{\prod_{z=1}^{Z} \prod_{w=1+K_{z-1}, w\neq v}^{K_z+K_{z-1}} \gamma_w \cdot \Lambda^2(t_w, r_w)/K_z}{\sum_{k=1}^{K} \prod_{z=1}^{Z} \prod_{w=1+K_{z-1}, w\neq k}^{K_z+K_{z-1}} \gamma_w \cdot \Lambda^2(t_w, r_w)/K_z} \tag{3.31}$$

which, when inserted into (3.29), yields the end-to-end capacity $C$ for a relaying system allowing a reuse of resources. Since the obtained capacities $C_v$ do not entirely coincide, the end-to-end capacity will again be dominated by the smallest of all.

**Equal Fractional Bandwidth and Equal Fractional Power**

The trivial case of equal fractional bandwidth per interference zone and equal power for each relaying stage yields for the capacity at each stage

$$C_{v\in(1+K_{z-1},K_z+K_{z-1})} = \frac{1}{K_z} \cdot \mathrm{E}_{\lambda_v} \left\{ m_v \log_2 \left( 1 + \lambda_v \frac{K_z}{K} \frac{\gamma_v}{t_v} \frac{S}{N} \right) \right\} \tag{3.32}$$

and the end-to-end capacity $C$ is obtained by choosing the minimum of all $C_v$.

**Performance**

The performance of the fractional power allocation strategy is investigated here. Clearly, the number of potential scenarios is much greater than for the case without resource reuse. This is the reason why only a few selected scenarios are scrutinised.

Figure 3.16 depicts the achieved end-to-end capacity for a 2-stage $(1 \times 4)/(4 \times 1)$ communication scenario with frequency reuse. To allow for such configuration, the relaying stage requires 8 antenna elements, because transmission and reception at the same time and frequency is not feasible.

The optimum end-to-end capacity is obtained via numerical optimisation of (3.12) under constraints (3.27) and (3.28), i.e. bandwidth and power are optimised numerically. The capacity for equal bandwidth and optimum power is obtained utilising (3.31) inserted into (3.29) with $Z = 2$ and $K_1 = K_2 = 1$, whereas the capacity for non-optimised bandwidth or power is obtained from (3.32). From Figure 3.16 it is clear that the derived fractional power allocation strategy performs very well, even for highly unbalanced communication links. The error was again found not to exceed 3%.

Furthermore, for the chosen antenna configuration and an SNR in the first link of 6dB, the gain due to the deployed fractional power allocation mounts to approximately 100%, 30% and 15% for $p = [0, -10]$dB, $p = [0, 0]$dB and $p = [0, 10]$dB, respectively, when compared to a non-optimised system. The power savings mount to 50%, 30%, 20% at a rate of 0.5 bits/s/Hz for $p = [0, -10]$dB, 2 bits/s/Hz for $p = [0, 0]$dB and 4 bits/s/Hz for $p = [0, 10]$dB, respectively, when compared to a non-optimised system.

Note that resource reuse allows achieving higher end-to-end capacities when compared to systems without resource reuse. This becomes apparent when comparing the absolute values of the achieved end-to-end capacities of Figure 3.16 with the ones of Figure 3.13, which deal with a $(1 \times 4)/(4 \times 1)$ system with and without resource reuse, respectively.

Finally, Figure 3.17 depicts the case of a highly asymmetric $(1\times2)/(2\times3)/(3\times2)$ scenario with $Z = 2$ and $K_1 = 1$, $K_2 = 2$. The precision of the developed fractional power allocation strategy is clearly limited; nonetheless, it still yields significant gains when compared to a non-optimised system. At an SNR of 6dB, the loss in precision of the fractional power allocation algorithm when compared to the numerically obtained optimum is approximately 10%, 11% and 12% for $p = [0, -10]$dB, $p = [0, 0]$dB and $p = [0, 10]$dB, respectively. The gain when compared to a non-optimised system, however, is approximately 70%, 20% and 50% for $p = [0, -10]$dB, $p = [0, 0]$dB and $p = [0, 10]$dB, respectively.

Here, the power savings mount to 60%, 30%, 100% at a rate of 0.5 bits/s/Hz for $p = [0, -10]$dB, 1.5 bits/s/Hz for $p = [0, 0]$dB and 1.5 bits/s/Hz for $p = [0, 10]$dB, respectively, when compared to a non-optimised system.

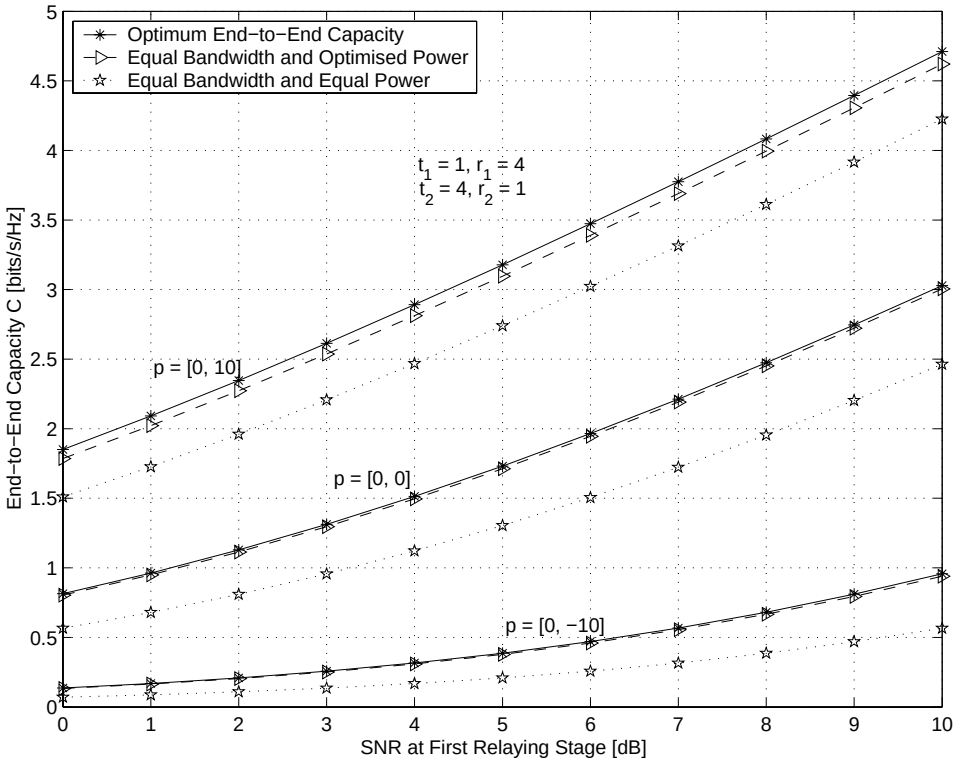


Figure 3.16: Achieved end-to-end capacity of various fractional resource allocation strategies for a 2-stage relaying network with resource reuse.

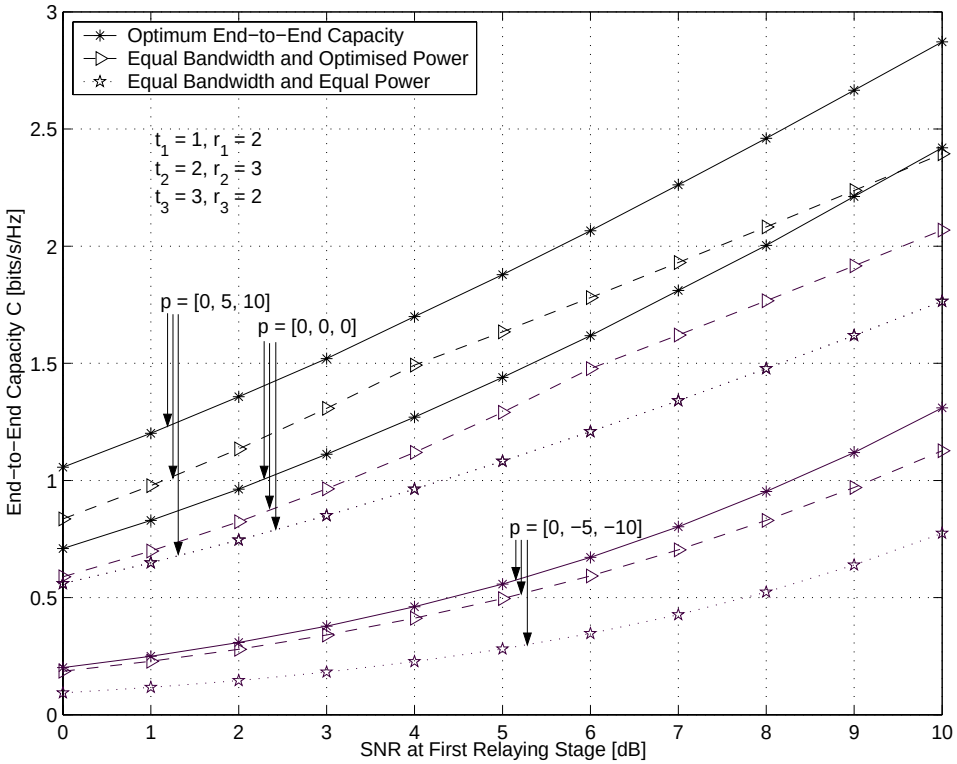


Figure 3.17: Achieved end-to-end capacity of various fractional resource allocation strategies for a 3-stage relaying network with resource reuse.

### 3.3.4 O-MIMO Relaying

Similar fractional allocation strategies with and without resource reuse can also be derived for relaying networks deploying O-MIMO. The derivations for an O-MIMO channel with equal sub-channel gains differ slightly from the case with unequal sub-channel gains. Here, the cases of equal sub-channel gains for Rayleigh and Nakagami fading channels is considered, as well as the case of unequal sub-channel gains for Rayleigh fading only. The analysis can easily be extended to the cases of generic attenuations for the Rayleigh and Nakagami fading cases; however, it was omitted here because the principle is already sufficiently outlined with the case of unequal gains over a Rayleigh fading O-MIMO channel.

#### Equal Sub-Channel Gains

For equal sub-channel gains, $\Lambda(t_v, r_v)$ occurring in the above analysis is simply replaced by the respective expressions in (2.105). Furthermore, the exact capacities, denoted by the expectations in the above analysis, are calculated utilising (2.73) for the case of Rayleigh fading and (2.89) for the case of Nakagami fading with equal channel gains. The performance is demonstrated with the aid of Figures 3.18 and 3.19. Note that for these examples not more than two transmit antennas (Alamouti scheme) were studied, because a deployment of STBCs with a rate less than one is not worthy when considering ergodic channels, as shown in Section 2.4.2.

Explicitly, Figure 3.18 shows the attained capacity of a 2-stage relaying system versus the SNR in the first link for various resource allocation algorithms over Rayleigh fading channels. In the first stage, a SIMO communication is realised with one transmit and two receive elements. The second stage utilises Alamouti encoding with two transmit and four receive elements, the rate hence being $R_2 = 1$. Clearly, the developed fractional power and bandwidth allocation algorithm performs close to optimum, even for highly asymmetric communication links. As observed before, sub-optimum resource allocation strategies, such as optimising power only or allocating equal resources to each link, exhibit a poorer performance. As an example, for the highly asymmetric scenario of $t_2 > t_1$, $r_2 > r_1$ and the second link being 10dB stronger than the first link, the developed fractional capacity allocation strategy performs by 30% better than the strategy of equal resources at an SNR of 6dB in the first link. Furthermore, 80% transmission power can be saved when operating at 2 bits/s/Hz.

Figure 3.19 is the equivalent to Figure 3.18 with the only difference that Nakagami channels are deployed, where $f_1 = 5$ (strong LOS) in the first and $f_2 = 1$ (Rayleigh) in the second stage. Again, the developed fractional resource allocation algorithm performs near optimum. It can further be observed that the absolute capacities are slightly improved with respect to the Rayleigh fading case, which is due to strong LOS channels in the first link.

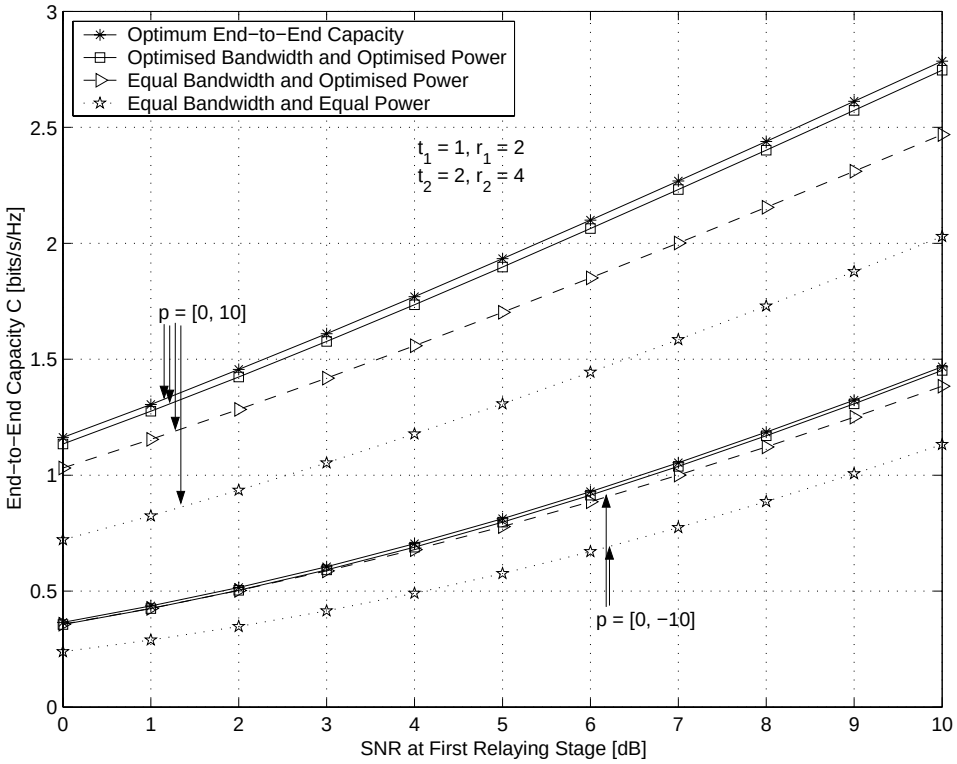


Figure 3.18: Achieved end-to-end capacity of various fractional resource allocation strategies for a 2-stage relaying network over O-MIMO Rayleigh channels.

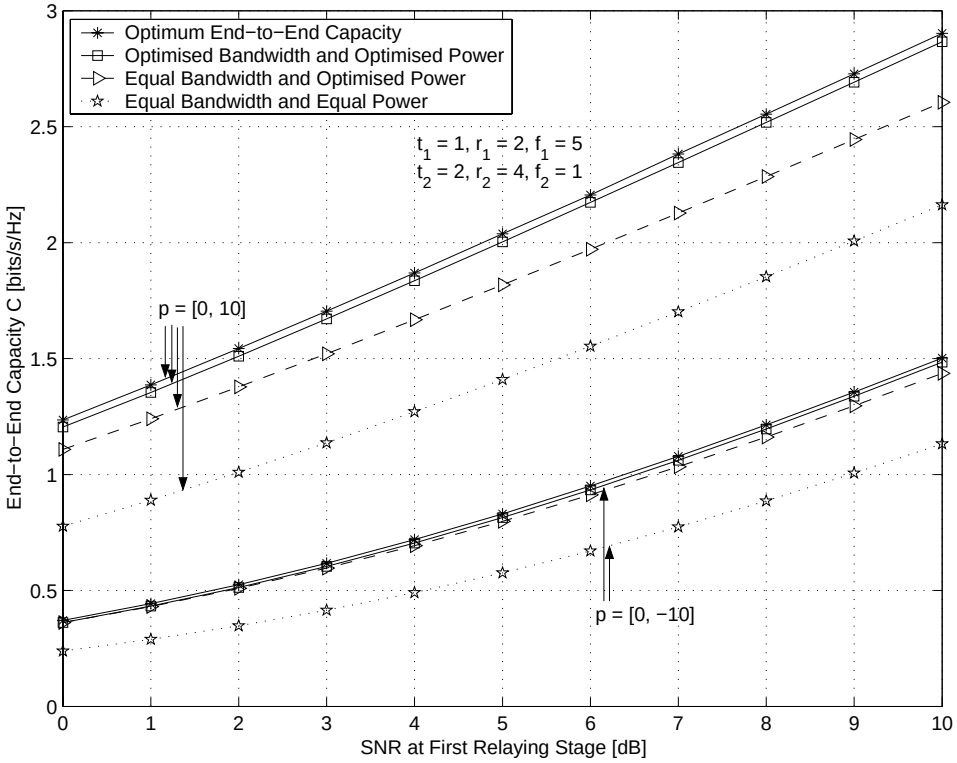


Figure 3.19: Achieved end-to-end capacity of various fractional resource allocation strategies for a 2-stage relaying network over O-MIMO Nakagami channels.

**Unequal Sub-Channel Gains**

If the channel attenuations within the $v^{th}$ stage are different, then the fractional power $\beta_v$ allocated to that stage can be distributed among the transmitting elements in an optimum manner. Since the distribution will influence the achieved capacity in the $v^{th}$ stage, the end-to-end capacity optimisation process will also depend on it. This requires an optimum distribution of power among the transmitting elements in each stage to be found, only after which the above-derived allocation strategies can be applied.

The optimum power distribution is achieved by deploying water-filling in the spatial domain, c.f. Section 2.3.2. Because of the fairly intricate expressions, neither an explicit nor an iterative expression could be derived which determines an optimum allocation of power to each transmit element. For slightly differing channel gains, it is hence suggested to allocate equal transmit power to all transmit elements and use the average of all channel gains as the input to the respective equations for the $v^{th}$ relaying stage, i.e. $\gamma_v \approx \sum_{i=1}^{u_v} \gamma_{v,i}/u_v$, where $u_v$ is the number of sub-channels in the $v^{th}$ stage, and $\gamma_{v\in(1,K),i\in(1,u_v)}$ are the associated channel gains.

If, however, the channel attenuations within the same relaying stage differ drastically, a numerical optimisation has to be performed. Interestingly, an approximate expression for the power distribution could be obtained, the analysis of which is deemed to be an interesting topic of future research.

To this end, the reader is reminded that with $t_v$ transmit and $r_v$ receive elements, there are $u_v = t_v \cdot r_v$ channels with unequal gain. It is hence the aim to allocate a fractional power $\epsilon_{v\in(1,K),i\in(1,t_v)}$ to each transmit element, where at any stage $v$

$$\sum_{i=1}^{t_v} \epsilon_{v,i} \equiv 1 \tag{3.33}$$

Since the power is distributed among the $t_v$ transmit antennas only, and not among all $u_v$ sub-channels, eq. (2.78) needs to be rewritten as

$$C_v = R_v \sum_{i=1}^{t_v} \sum_{j=1}^{r_v} K_{(i-1)r_v+j} \cdot \hat{C}_0 \left( \frac{\epsilon_{v,i} \cdot \gamma_{(i-1)r_v+j}}{R_v} \frac{S}{N} \right) \tag{3.34}$$

where, with reference to (2.76), the coefficients $K_{(i-1)r_v+j}$ can be calculated as

$$K_{(i-1)r_v+j} = \prod_{i'=1}^{t_v} \prod_{j'=1}^{r_v} \left. \frac{\epsilon_{v,i} \cdot \gamma_{(i-1)r_v+j}}{\epsilon_{v,i} \cdot \gamma_{(i-1)r_v+j} - \epsilon_{v,i'} \cdot \gamma_{(i'-1)r_v+j'}} \right|_{(i'-1)r_v+j' \neq (i-1)r_v+j} \tag{3.35}$$

It is conjectured here that the allocation $\epsilon_{v\in(1,K),i\in(1,t_v)}$, which maximises (3.34) satisfying constraint (3.33), can be approximated by

$$\epsilon_{v,i} \approx \frac{\prod_{i'=1,i'\neq i}^{t_v} \left( \sum_{j=1}^{r_v} \gamma_{(i'-1)r_v+j} \right)^{-3}}{\sum_{k=1}^{t_v} \prod_{i'=1,i'\neq k}^{t_v} \left( \sum_{j=1}^{r_v} \gamma_{(i'-1)r_v+j} \right)^{-3}} \tag{3.36}$$

The approximation becomes apparent for very unbalanced channel gains, where the optimum water-filling algorithm would allocate no power at all to the weakest sub-channels, eq. (3.36), however, only suggests an asymptotically close to zero power allocation.

The performance of the conjectured transmit power distribution is assessed by means of Figure 3.20 for the simple case of two transmit and one receive antenna, operating at an SNR of 6dB. Since only one stage is investigated here, the subscript $v$ is omitted to simplify notation. Depicted is the power allocation $\epsilon_1$ to the first transmit antenna versus the relative channel gain $\gamma_1$ in the first sub-channel which, in this example, is the only sub-channel from the first transmit antenna. The relative channel gain $\gamma_2$ in the second sub-channel has either been kept constant to $\gamma_2 = 1$ or changed in dependency of $\gamma_1$, i.e. $\gamma_2 = 2 - \gamma_1$. In Figure 3.20 the numerically obtained exact power allocation is compared against the conjectured power allocation given through (3.36).

It can be observed that in the region where both channel gains are approximately equal, the conjectured power distribution strategy performs near-optimum. For this particular case it was found that this region is spanned by ratios between both gains which do not exceed 2:1. From the figure it is also apparent that if one channel gain is much bigger than the other, then the optimum allocation yields no power for the weaker link, whereas the conjectured distribution strategy does allocate some power.

However, the loss in precision has little impact onto the capacity of the respective stage as demonstrated by means of Figures 3.21−3.22. Figure 3.21 depicts the achieved capacity for a deployed Alamouti scheme with 2 transmit and 1 receive antenna versus the relative channel gain $\gamma_1$ in the first sub-channel, operating at an SNR of 6dB. The channel gain in the second link is accordingly $\gamma_2 = 2-\gamma_1$. Three transmit power distribution algorithms are compared: first, a numerically obtained optimum allocation; second, the conjectured allocation; and third, an equal transmit power allocation as suggested for approximately equal channel gains. It can be observed that optimum and conjectured allocation virtually yield the same capacity over the entire range of $\gamma_1$, whereas an equal transmit power allocation is only close to optimum for both channel gains being approximately equal. For example, a ratio between both channel gains of 1:4 yields a loss of 15% when the equal transmit power distribution is deployed, instead of the optimum or near-optimum allocation.

Figure 3.22 demonstrates the validity of the conjecture if more than one receive antenna is present. Here, the case of two transmit and two receive antennas is assumed, where the respective channel gains are (fairly arbitrary) determined as follows: $\gamma_2 = 1.5$, $\gamma_3 = 2 - \gamma_1$, $\gamma_4 = 0.5$. It is further assumed that $\gamma_1$ and $\gamma_2$ are the gains of the sub-channels spanned from the first transmit antenna towards the two receive antennas; similarly, $\gamma_3$ and $\gamma_4$ are the gains from the second transmit antenna towards the two receive antennas. The algorithm is again found to perform near optimum.

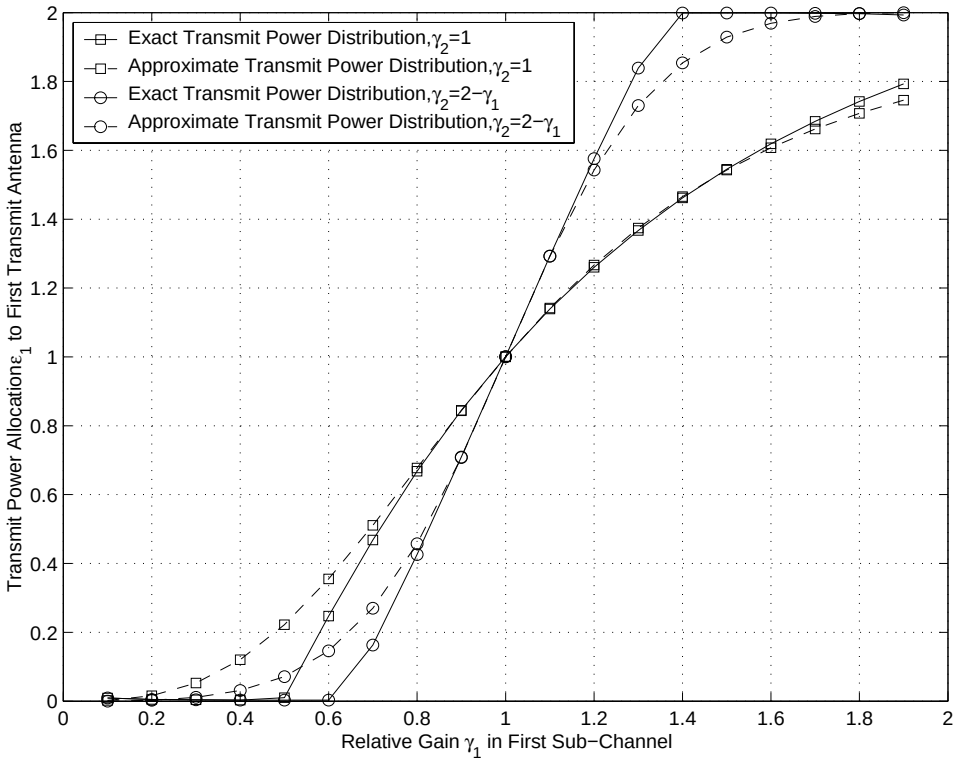


Figure 3.20: Example assessment of conjectured near-optimum transmit power distribution; SNR=6dB.

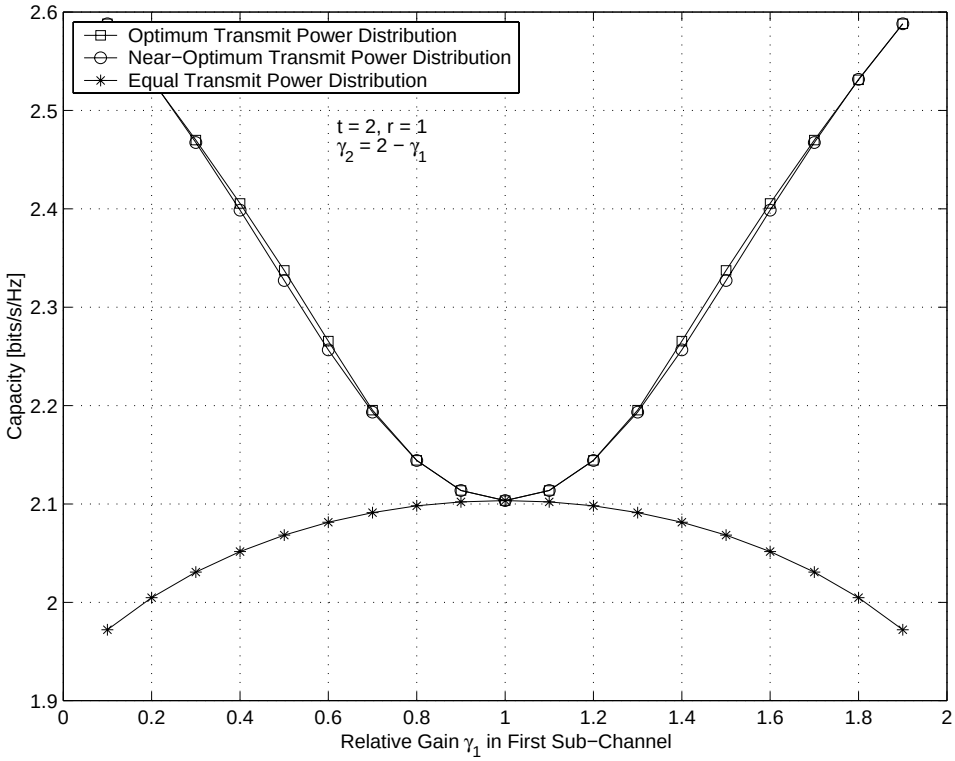


Figure 3.21: Achieved capacity for various power distribution algorithms with deployed Alamouti scheme and one receive antenna; SNR=6dB.

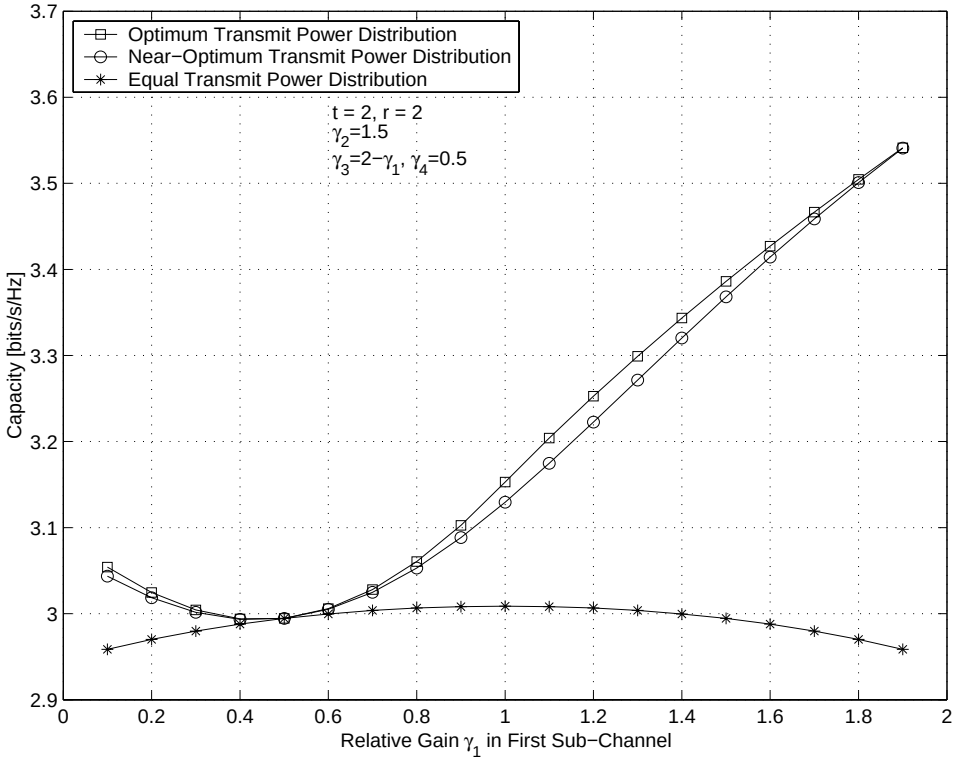


Figure 3.22: Achieved capacity for various power distribution algorithms with deployed Alamouti scheme and two receive antennas; SNR=6dB.

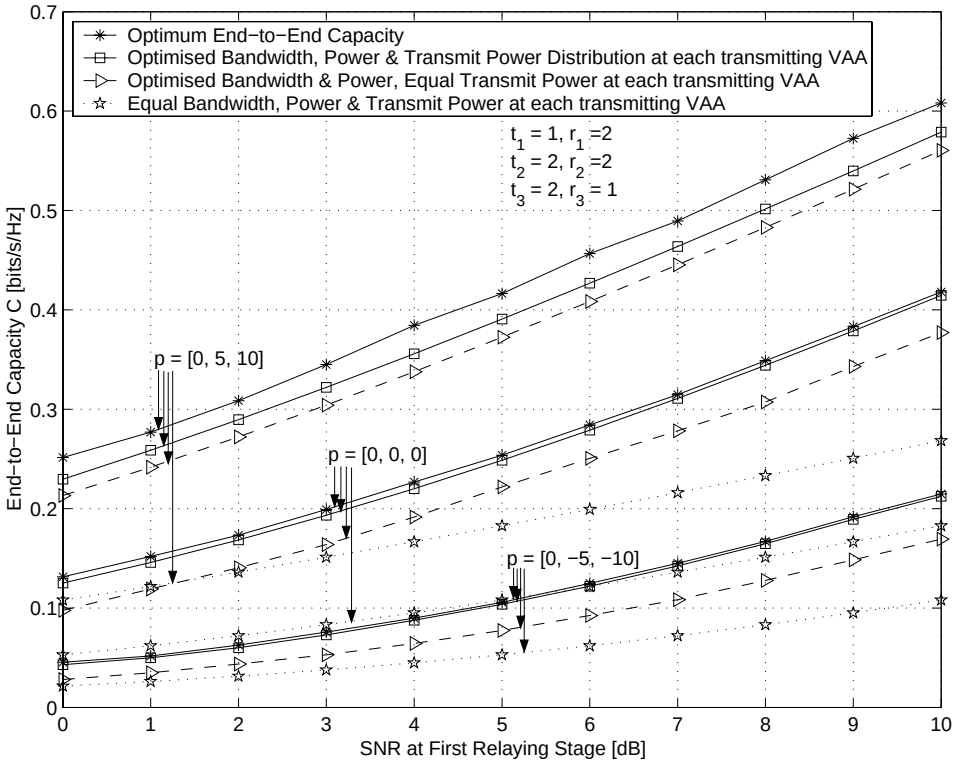


Figure 3.23: Achieved end-to-end capacity of various fractional resource allocation strategies for a 3-stage relaying network over O-MIMO Rayleigh channels.

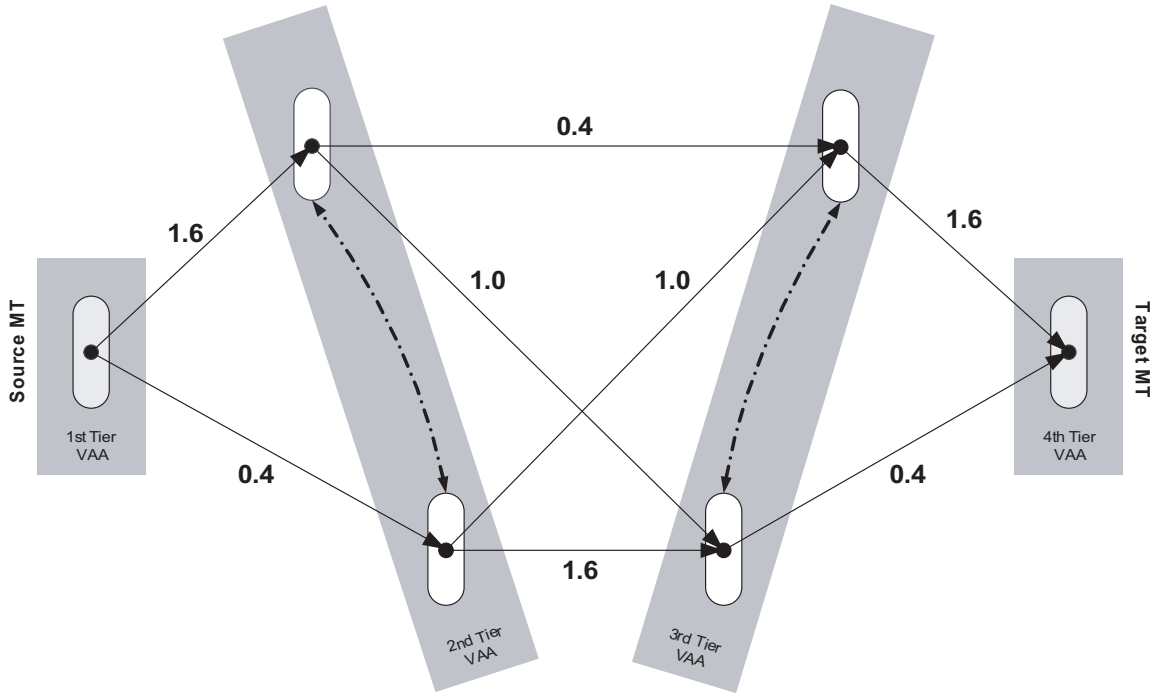


Figure 3.24: 3-Stage distributed O-MIMO communication scenario.

The conjectured low complexity power distribution algorithm (3.36) renders numerical optimisation within the MTs superfluous, and yet accomplishes near-optimum performance. With the obtained near-optimum capacities in each stage, the end-to-end capacity maximising fractional power and bandwidth are obtained following the analysis outlined in Section 3.3.1. The only difference is that in each stage (2.105) has to be replaced by

$$\Lambda(t_v, r_v) = \frac{\sqrt{R_v \pi}}{\sqrt{t_v}} \sum_{i=1}^{t_v} \sum_{j=1}^{r_v} K_{(i-1)r_v+j} \cdot \sqrt{\epsilon_{v,i} \cdot \gamma_{v,(i-1)r_v+j}} \tag{3.37}$$

The applicability of the developed algorithms is assessed by means of a 3-stage distributed O-MIMO communication scenario as depicted in Figure 3.24. Here, each of the terminals possesses only one antenna element. The s-MT communicates with the t-MT via two VAA relaying tiers. The s-MT, being part of the first tier VAA, broadcasts data to the second tier VAA. A mutual cooperation of the r-MTs within the second tier VAA accomplishes a $(1 \times 2)$ MIMO channel. The data is then Alamouti encoded and transmitted to the third tier VAA, cooperation within which leads to a $(2 \times 2)$ O-MIMO channel. Finally, the data is again Alamouti encoded, which reaches the t-MT via a $(2 \times 1)$ O-MIMO channel. The spatial distribution is such that the relative channel gains are different for each link, which is reflected by different labels to each occurring wireless link in Figure 3.24. In the second stage, for instance, the relative gains are $\gamma_{2,1} = 0.4$ and $\gamma_{2,2} = 1.0$ from the first r-MT and $\gamma_{2,3} = 1.0$ and $\gamma_{2,4} = 1.6$ from the second r-MT, both of which accomplish a distributed space-time block encoding with an outer Shannon channel code.

The prior developed analysis allows the assignment of fractional resources to each MT such as to accomplish near-optimum end-to-end capacity, the precision of which is assessed in Figure 3.23. Depicted is the achieved end-to-end capacity versus the SNR in the first link; the curves are labelled on $p$, where $p = [0, 5, 10]$dB, $p = [0, 0, 0]$dB and $p = [0, -5, -10]$dB. The optimum end-to-end capacity is obtained via numerical optimisation, where both the fractional bandwidth and power allocation per stage are optimised, as well as the distribution of the assigned power among the transmit elements.

Three further allocation strategies are compared against the optimum one. The first one is the developed strategy of determining the near-optimum distribution of the power among the transmit elements in each VAA relaying tier (here only the second and third) according to (3.36), after which the fractional bandwidth and power is obtained according to (3.22) and (3.13) assuming an O-MIMO Rayleigh fading channel with unequal channel gains. For the second strategy, only the fractional resources per VAA relaying tier are determined; thus, no water-filling is accomplished at each stage. The third strategy assumes no optimisation at all, and resources are equally distributed among the MTs.

From Figure 3.23 it is clear that the first allocation strategy yields a near-optimum end-to-end capacity. Furthermore, optimising the distribution of the transmit power per relaying tier yields an additional performance benefit, e.g. a 10% rate gain at an SNR of 6dB or, alternatively, a 30% power gain at 0.2 bits/s/Hz for $p = [0, 0, 0]$dB. Performing no optimisation at all yields by far the worst performance, e.g. the loss in rate mounts to 30% at an SNR of 6dB or, alternatively, 50% on transmission power is lost if a rate of 0.2 bits/s/Hz was to be maintained for $p = [0, 0, 0]$dB.

In summary, sufficiently precise fractional bandwidth and power allocation algorithms have been developed for a variety of distributed-MIMO multi-stage networks communicating over ergodic channels. The exposed algorithms are of very low complexity, yet they perform near-optimum. That renders a numerical optimisation within each mobile terminal superfluous.

Note that the complexity of numerical optimisation routines is prohibitively high and hence not applicable. For example, to find an optimum fractional bandwidth and power allocation for a simple example as depicted in Figure 3.24, the numerical optimisation required 5min per point on a Pentium III, 800MHz. That is in contrast to the developed algorithms, which take a fraction of a second to be calculated.

Finally, the reader is reminded that the fractional bandwidth and power allocations developed are easily translated into fractional frame duration and power allocations according to the analysis exposed in Section 3.2.3. That is, a fractional bandwidth $\alpha_v$ translates into a frame duration $\alpha_v$, whereas a fractional transmission power $\beta_v$ for an FDMA-based system translates into a transmission power $\beta_v/\alpha_v$ for a TDMA-based system.

## 3.4 Maximum Throughput for Non-Ergodic Channels

As thoroughly illuminated in Chapter 2, the capacitive behaviour of a non-ergodic channel is entirely characterised by the rate $\Phi$ supported with probability $1-P_{out}(\Phi)$. The normalised (spectral) throughput $\Theta$ measured in [bits/s/Hz] is shown in Appendix 3.7 (Derivation IV) to be

$$\Theta \propto \Phi \cdot \big(1 - P_{out}(\Phi)\big) \tag{3.38}$$

where the outage probability $P_{out}(\Phi)$ has been developed for various communication scenarios in closed form in Chapter 2. Clearly, for each dependency $P_{out}$ on $\Phi$, there exists an optimum rate $\Phi$ such as to maximise the throughput $\Theta$ according to (3.38). Such rate $\Phi$ is found by differentiating (3.38) to arrive at

$$1 - P_{out}(\Phi) = \Phi \cdot \frac{\partial}{\partial \Phi} P_{out}(\Phi) \tag{3.39}$$

which, with respect to the closed form expressions of the outage probabilities introduced in Chapter 2, has proven to be impossible to obtain in explicit form. To this end, the approximation of the outage probability introduced in Section 2.5.2 proves vital.

### 3.4.1 Transformation into Equivalent Ergodic Problem

It is demonstrated here, that the problem related to finding the maximum end-to-end throughput over non-ergodic channels can be reduced to the developed analysis for ergodic channels. The reduction comes at the expense of loss in precision, which is due to the tractable approximations introduced in Section 2.5.2 to express the outage probability, i.e.

$$\gamma(r, x)/\Gamma(r) \approx a x^b \tag{3.40}$$

where $r \in \mathbb{N}$ is a parameter. The constants $a$ and $b$ are chosen such as to minimise the approximation error; they depend on $r$ and are tabled in Table 2.3 of Chapter 2.

#### The SIMO Channel

With approximation (3.40), the outage capacity of a SIMO channel given by (2.55) can be expressed as

$$\begin{aligned} P_{out}(\Phi) &= \gamma\Big(r, \big(2^{\Phi}-1\big)\Big/\big(S/N\big)\Big)\Big/\Gamma(r) && (3.41)\\ &\approx a \cdot \left(\frac{2^{\Phi}-1}{S/N}\right)^{b} && (3.42) \end{aligned}$$

where $a = a(r)$ and $b = b(r)$. It is easily resolved in favour of $\Phi$ as

$$\Phi\left(P_{out}\right) \approx \log_2\left(1 + \sqrt[b]{\frac{P_{out}}{a}}\frac{S}{N}\right) \tag{3.43}$$

The throughput $\Theta$ can hence be approximated as

$$\Theta \approx (1 - P_{out}) \cdot \log_2 \left( 1 + \sqrt[b]{\frac{P_{out}}{a}} \frac{S}{N} \right) \tag{3.44}$$

$$\approx (1 - P_{out}) \cdot \sqrt[2b]{\frac{P_{out}}{a}} \sqrt{\frac{S}{N}} \tag{3.45}$$

where approximation (3.45) is due to the square root approximation of the logarithm. The throughput-maximising outage probability is now obtained by differentiating (3.44) along $P_{out}$. After some elementary manipulations, this yields

$$P_{out} \approx \frac{1}{1 + 2b} \tag{3.46}$$

which is a remarkable result because the outage probability is shown to be approximately independent from the SNR, and hence from fractional power and bandwidth allocations. The precision of (3.46) is assessed with the aid of Figure 3.25, which depicts a comparison between the numerically obtained exact throughput-maximising outage probability and the one given by (3.46) versus the number of receive elements at an SNR of 3dB, 6dB and 9dB. It is observed that the approximation error does not exceed 10% for the SNRs chosen.

Inserting (3.46) into (3.44), and allocating a fractional bandwidth $\alpha_v$ and a fractional power $\beta_v$ to the $v^{th}$ relaying stage, the throughput of that stage experiencing a pathloss $\gamma_v$ can be expressed as

$$\Theta_v \approx \alpha_v \cdot \left( \frac{2b}{1 + 2b} \right) \cdot \log_2 \left( 1 + \frac{\gamma_v}{\sqrt[b]{a(1 + 2b)}} \frac{\beta_v}{\alpha_v} \frac{S}{N} \right) \tag{3.47}$$

Again, the end-to-end throughput will be dictated by the weakest link. The maximum end-to-end throughput is hence achieved by equating the throughputs of all stages, and maximising the set of equations with respect to the fractional bandwidth and power allocations.

With reference to the ergodic cases it is shown here that, except for some multiplicative factors, maximising the end-to-end throughput over non-ergodic channels is equivalent to the problem of maximising the end-to-end capacity over ergodic channels. That allows applying exactly the same fractional resource allocation strategies as derived before.

### The MISO Channel

The precision of the approximated throughput-maximising outage probability given by (3.46) suffers slightly for the MISO case, which is illustrated by means of Figure 3.26. Nonetheless, it proves applicable to the optimisation problems as will be demonstrated below. Similarly to the SIMO channel, the throughput of the $v^{th}$ MISO stage can hence be derived as

$$\Theta_v \approx \alpha_v \cdot \left( \frac{2b}{1 + 2b} \right) \cdot \log_2 \left( 1 + \frac{\gamma_v}{t \cdot \sqrt[b]{a(1 + 2b)}} \frac{\beta_v}{\alpha_v} \frac{S}{N} \right) \tag{3.48}$$

where $a = a(t)$ and $b = b(t)$. The very same conclusions as for the SIMO channel hold.

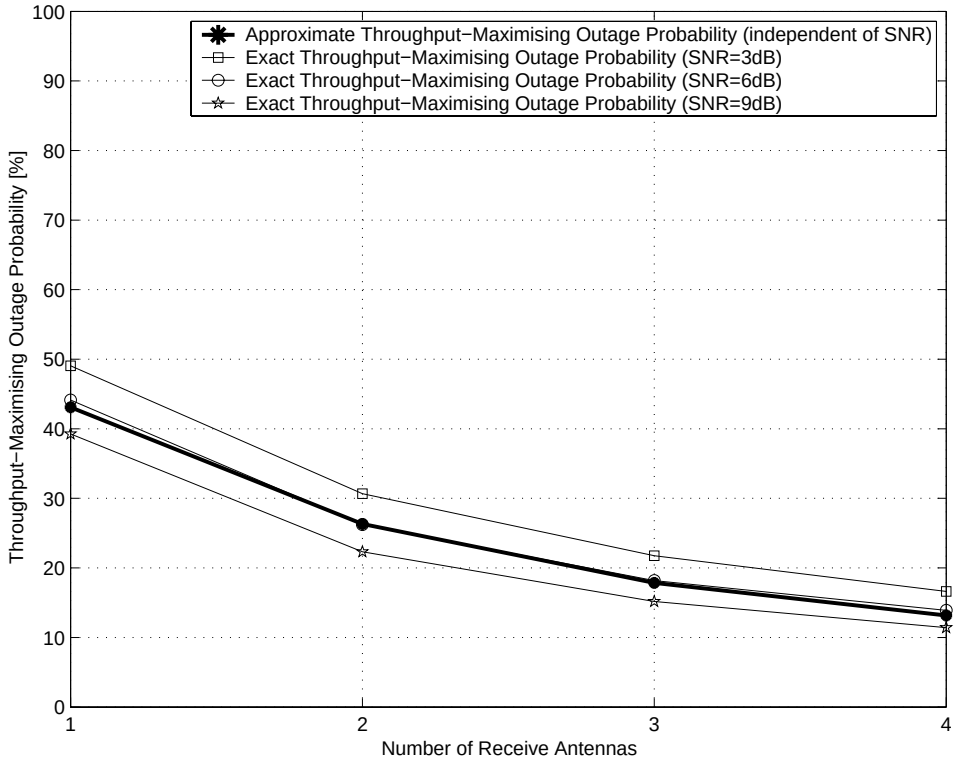


Figure 3.25: Comparison between exact and approximate throughput-maximising outage probability versus the number of receive elements for a SIMO channel.

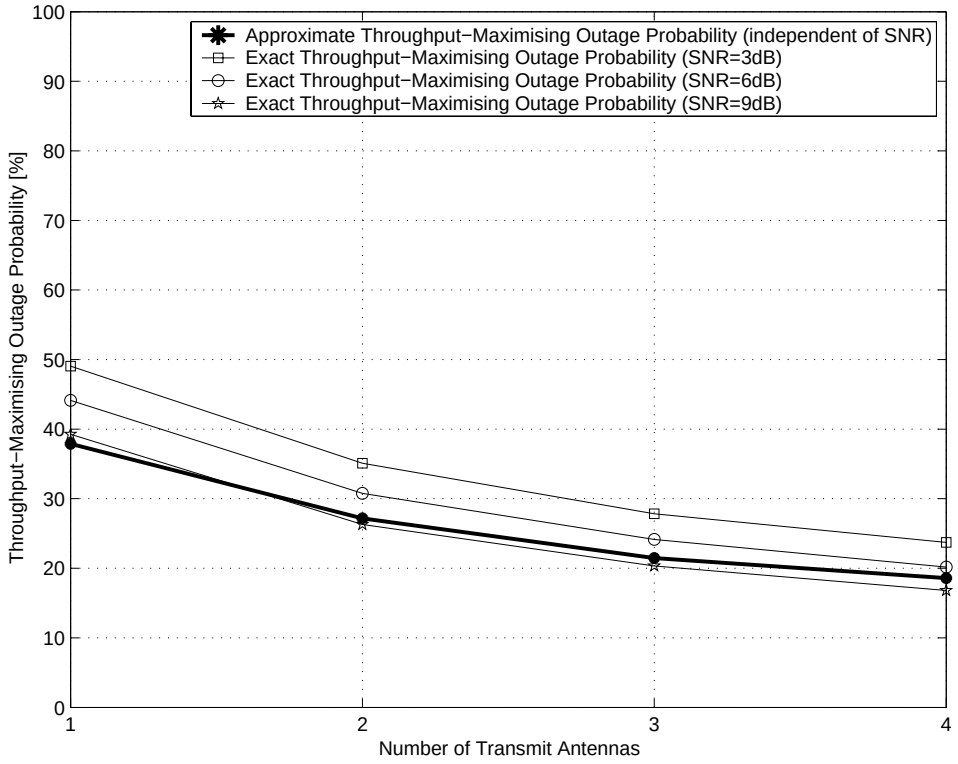


Figure 3.26: Comparison between exact and approximate throughput-maximising outage probability versus the number of transmit elements for a MISO channel.

### The MIMO Channel

The MIMO channel is not dealt with because there is no closed-form expression for the outage probability over MIMO channels. An upper bound on the outage probability, however, is obtained by replacing the available $t \times r$ MIMO channel with a $1 \times r$ SIMO channel, on which all optimisation problems are performed.

### The O-MIMO Channel

For a STBC transmission over a channel with equal channel gains, the throughput of the $v^{th}$ stage can similarly be derived as

$$\Theta_v \approx \alpha_v \cdot R \cdot \left(\frac{2b}{1+2b}\right) \cdot \log_2\left(1 + \frac{1}{tR}\frac{\gamma_v}{\sqrt[b]{a(1+2b)}}\frac{\beta_v}{\alpha_v}\frac{S}{N}\right) \tag{3.49}$$

where $a = a(u)$ and $b = b(u)$ for Rayleigh fading, and $a = a(uf)$ and $b = b(uf)$ for Nakagami fading with fading parameter $f$, and $u = t \cdot r$. The Rayleigh fading case with unequal channel coefficients and no transmit power optimisation is obtained as

$$\Theta_v \approx \alpha_v \cdot R \cdot \left(\frac{2b}{1+2b}\right) \cdot \log_2\left(1 + \frac{1}{tR}\frac{\gamma_v}{\sqrt[b]{a(1+2b)}}\frac{1}{\sqrt[b]{\sum_{i=1}^{u} K_i/\gamma_i^b}}\frac{\beta_v}{\alpha_v}\frac{S}{N}\right) \tag{3.50}$$

where $a = a(1)$ and $b = b(1)$. If an optimum fractional transmit power $\epsilon_{i\in(1,t)}$ is deployed, then the above equation can be written as

$$\Theta_v \approx \alpha_v R \left(\frac{2b}{1+2b}\right) \log_2\left(1 + \frac{1}{tR}\frac{\gamma_v}{\sqrt[b]{a(1+2b)}}\frac{1}{\sqrt[b]{\sum_{i=1}^{t}\sum_{j=1}^{r}\frac{K_{(i-1)r+j}}{(\epsilon_i \cdot \gamma_{(i-1)r+j})^b}}}\frac{\beta_v}{\alpha_v}\frac{S}{N}\right) \tag{3.51}$$

with $K_{(i-1)r+j}$ given by (3.35).

The cases of generic Rayleigh and Nakagami fading cannot be obtained in a similar fashion which is due to the differing exponent of each summand when applying the approximated lower incomplete Gamma function to, e.g., eq. (2.95). That is not deemed to be a serious limitation, as realistic scenarios with unequal channel gains can always be approximated by a channel with equal gains.

### A General Expression

The throughput of any of the aforementioned examples can be generalised to

$$\Theta_v \approx \alpha_v A_v \cdot \log_2\left(1 + \gamma_v \frac{B_v}{t_v}\frac{\beta_v}{\alpha_v}\frac{S}{N}\right) \tag{3.52}$$

where the respective $A_v$ and $B_v$ are found by comparing (3.52) with (3.47)−(3.51). Eq. (3.52) proves useful in deriving general fractional resource allocation algorithms, which can then be applied to the required communication scenario.

### 3.4.2 MIMO Relaying without Resource Reuse

The throughput of the $v^{th}$ SIMO stage with fractional bandwidth $\alpha_v$ and fractional power $\beta_v$ experiencing a channel attenuation $\gamma_v$ is, with reference to (3.38) and (2.55), given as

$$\Theta_v = \Phi_v \cdot \left[1 - \gamma\left(r_v, \frac{2^{\Phi_v/\alpha_v} - 1}{\gamma_v \frac{\beta_v}{\alpha_v}\frac{S}{N}}\right) \Big/ \Gamma(r_v)\right] \tag{3.53}$$

Utilising approximation (3.40), the throughput-maximising rate $\Phi_v$ over the $v^{th}$ stage can be approximated as

$$\Phi_v \approx \alpha_v \log_2\left(1 + \frac{\gamma_v}{\sqrt[b]{a(1+2b)}}\frac{\beta_v}{\alpha_v}\frac{S}{N}\right) \tag{3.54}$$

where $a = a(r_v)$ and $b = b(r_v)$. It is hence the aim to find fractional bandwidth and power such as to maximise the end-to-end throughput. To this end, the allocation strategies of optimised fractional bandwidth and power, equal bandwidth and optimised power, and equal bandwidth and power are dealt with below.

#### Optimised Fractional Bandwidth and Optimised Fractional Power

The fractional bandwidth allocation $\alpha_v$ can be found analogously as for the scenario of MIMO relaying without resource reuse over ergodic channels. It is given as

$$\alpha_v = \frac{\prod_{w\neq v} A_w \log_2\left(1 + \gamma_w \frac{B_w}{t_w}\frac{\beta_w}{\alpha_w}\frac{S}{N}\right)}{\sum_{k=1}^{K}\prod_{w\neq k} A_w \log_2\left(1 + \gamma_w \frac{B_w}{t_w}\frac{\beta_w}{\alpha_w}\frac{S}{N}\right)} \tag{3.55}$$

where the ratio between fraction power $\beta_w$ and fractional bandwidth $\alpha_w$ is found to be

$$\frac{\beta_v}{\alpha_v} \approx K \cdot \frac{\prod_{w\neq v}\sqrt[3]{\gamma_w/t_w \cdot A_w^2 B_w}}{\sum_{k=1}^{K}\prod_{w\neq k}\sqrt[3]{\gamma_w/t_w \cdot A_w^2 B_w}} \tag{3.56}$$

The fractional bandwidth $\alpha_v$ of each stage is hence obtained by inserting (3.56) into (3.55). Furthermore, there are two ways of determining the optimum communication rate. First, eq. (3.55) and (3.56) are inserted into (3.53), after which a simple numerical sweep across the rate is performed within each terminal to determine the rate $\Phi_v$ which yields maximum throughput. Second, eq. (3.55) and (3.56) are inserted into (3.54), which determines the approximate communication rate. The throughput is then determined by inserting the obtained rate, together with fractional bandwidth and power into (3.54). For either case, the total end-to-end throughput is determined by the minimum of the approximate $\Theta_v$.

#### Equal Fractional Bandwidth and Optimised Fractional Power

With reference to the ergodic case, fractional resources are assigned to each stage such that

$$\alpha_v = 1/K \tag{3.57}$$

$$\beta_v \approx \frac{\prod_{w\neq v}\gamma_w/t_w \cdot A_w^2 B_w}{\sum_{k=1}^{K}\prod_{w\neq k}\gamma_w/t_w \cdot A_w^2 B_w} \tag{3.58}$$

Inserted into (3.54), this yields the approximate rate required to communicate at the $v^{th}$ stage to achieve maximum throughput, which is then given through (3.53). Remember that the obtained throughputs $\Theta_v$ do not entirely coincide because of the approximation chosen. The end-to-end throughput will therefore be dominated by the smallest of all.

**Equal Fractional Bandwidth and Equal Fractional Power**

In this case, resources in terms of fractional bandwidth and power are allocated such that

$$\alpha_v = 1/K \tag{3.59}$$

$$\beta_v = 1/K \tag{3.60}$$

which is expected to yield inferior performance when compared to any of the previous resource allocation algorithms.

**Performance**

The derived allocation strategies for general MIMO channels without resource reuse are assessed by means of Figures 3.27−3.29, which depict the throughput behaviour for a 2-stage relaying network only. The 3-stage case was found to exhibit the same characteristics and was thus omitted here; more stages require a numerical optimisation of several weeks with current computing power.

Explicitly, Figure 3.27 depicts the normalised end-to-end throughput in [bits/s/Hz] versus the SNR in [dB] in the first link. The throughput of a numerically obtained optimum resource allocation is compared against the throughput achieved by the developed fractional resource allocation strategies. It can be seen that optimised fractional power and bandwidth, given through (3.55) and (3.56), yields near-optimum end-to-end throughput for any of the chosen communication configurations. Similar to the ergodic case, optimising fractional power only yields a slightly inferior performance when compared to the aforementioned cases. Finally, optimising neither fractional bandwidth nor power results in drastic end-to-end performance losses. For $p = [0, 10]$dB, for example, the gains in communication rate are more than 40% at an SNR of 6dB or, alternatively, 65% less power is needed to support 0.6 bits/s/Hz.

The curves in Figure 3.27 have been obtained by applying the respective fractional resources to (3.53), after which a numerical sweep has been performed to obtain the throughput-maximising rate at each stage. In contrast to this, Figure 3.28 depicts the same communication scenario as above with the only difference that the approximate throughput-maximising rate is found first via (3.54) with the respective fractional resources, after which the approximate throughput is determined again through (3.54). The precision of that approach suffers negligibly at the benefit of no optimisation required to assign fractional resources and to determine the near-optimum communication rate.

Finally, Figure 3.29 depicts the throughput behaviour of the asymmetric 2-stage communication scenario with four antenna elements in the relaying tier, i.e. $(1\times4)/(4\times1)$. The developed fractional resource allocation strategies were again found to perform sufficiently well.

### 3.4.3 MIMO Relaying with Resource Reuse

It is the aim here to develop fractional resource allocation strategies which maximise the end-to-end throughput over non-ergodic channels where resources in terms of fractional bandwidths are reused in $Z$ interference zones. As for the ergodic case, no satisfactory fractional bandwidth and power allocation strategy could be derived. For that reason, the case of equal bandwidth and optimised power is dealt with only.

#### Equal Fractional Bandwidth and Optimised Fractional Power

Equal fractional bandwidth implies that the same bandwidth is assigned to each relaying stage within an interference zone. With reference to the ergodic case, this leads to the following fractional bandwidth and power allocation

$$\alpha_{v\in(1+K_{z-1},K_z+K_{z-1})} = 1/K_z \tag{3.61}$$

$$\beta_v \approx \frac{\prod_{z=1}^{Z}\prod_{w=1+K_{z-1},w\neq v}^{K_z+K_{z-1}}\gamma_w/t_w\cdot A_w^2B_w/K_z}{\sum_{k=1}^{K}\prod_{z=1}^{Z}\prod_{w=1+K_{z-1},w\neq k}^{K_z+K_{z-1}}\gamma_w/t_w\cdot A_w^2B_w/K_z} \tag{3.62}$$

which, when inserted into (3.53), allows determining the throughput-maximising rate. The smallest of all $\Theta_v$ then determines the end-to-end throughput.

#### Equal Fractional Bandwidth and Equal Fractional Power

The trivial case of equal fractional bandwidth per interference zone and equal power for each relaying stage yields for the fractional resources

$$\alpha_{v\in(1+K_{z-1},K_z+K_{z-1})} = 1/K_z \tag{3.63}$$

$$\beta_v = 1/K \tag{3.64}$$

which, when inserted into (3.53), allows determining the throughput-maximising rate. The smallest of all $\Theta_v$ then determines the end-to-end throughput.

#### Performance

The performance of the developed algorithms is exposed in Figure 3.30, which depicts the end-to-end throughput versus the SNR in the first link for a 3-stage $(1\times4)/(4\times1)/(1\times1)$ relaying network where the fractional bandwidth is reused in the third stage. Although only the power was optimised, the performance is near-optimum for any of the chosen channel conditions, i.e. $p=[0,5,10]$dB, $p=[0,0,0]$dB and $p=[0,-5,-10]$dB.

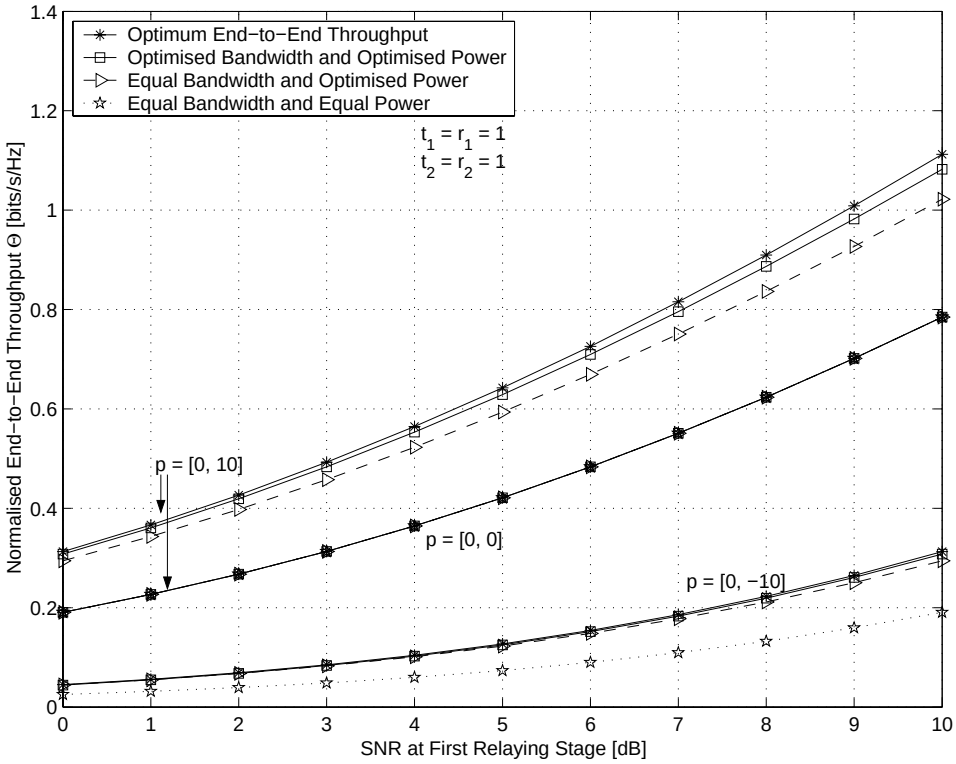


Figure 3.27: Achieved end-to-end throughput of various fractional resource allocation strategies utilising a simple numerical optimisation of the rate in each stage for a 2-stage network.

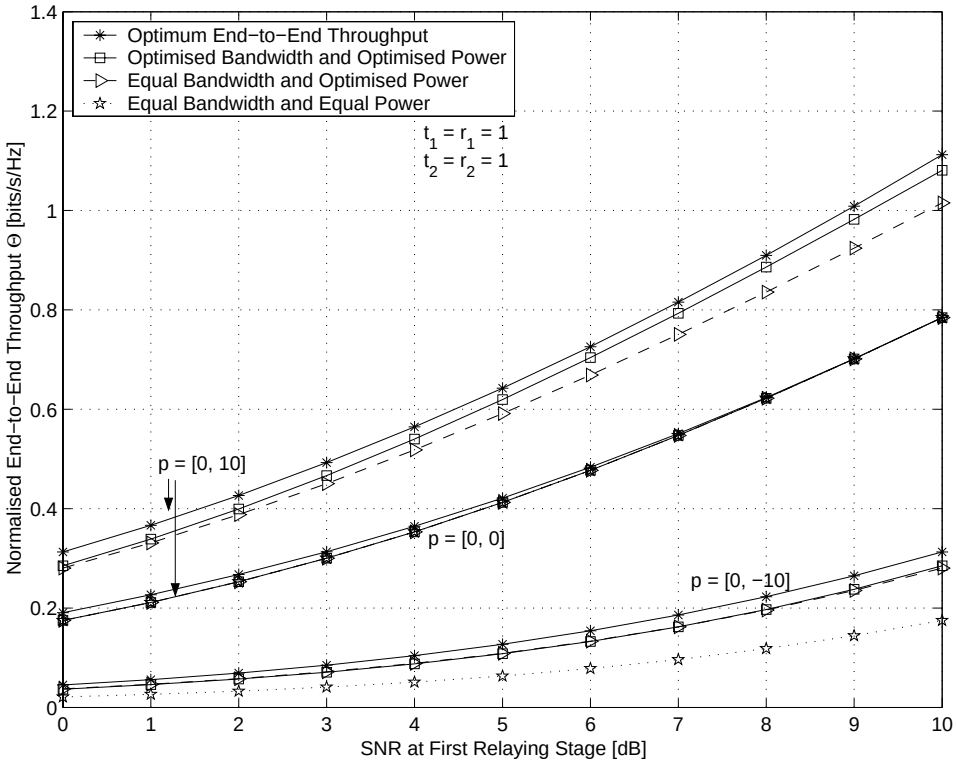


Figure 3.28: Achieved end-to-end throughput of various fractional resource allocation strategies utilising an approximation for the rate in each stage for a 2-stage network.

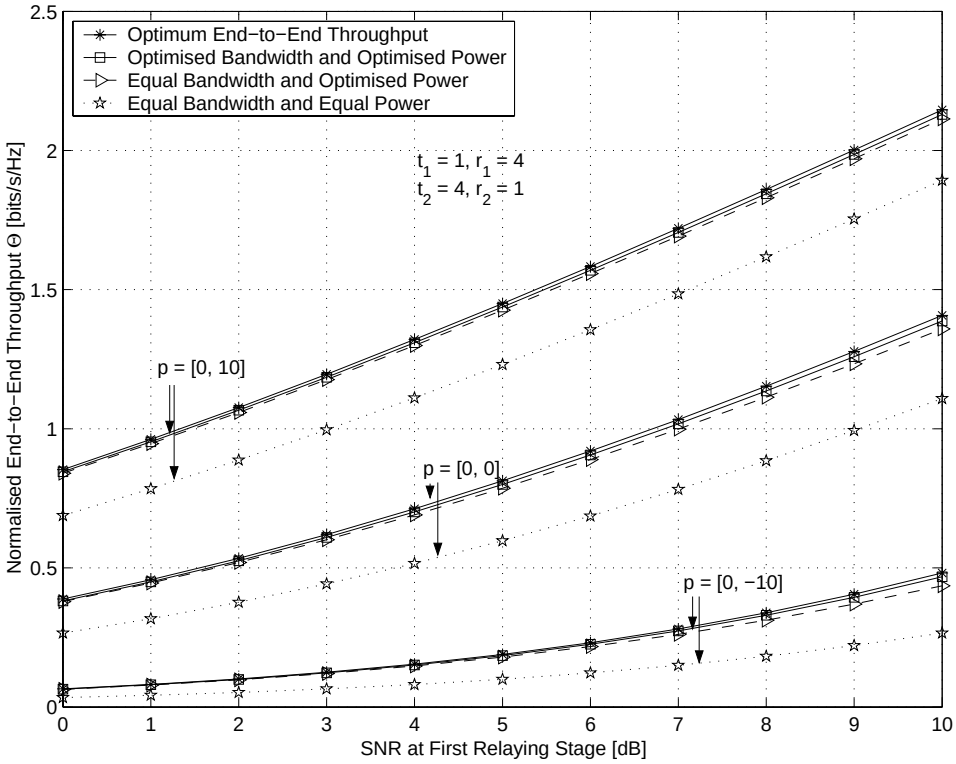


Figure 3.29: Achieved end-to-end throughput of various fractional resource allocation strategies for a 2-stage network.

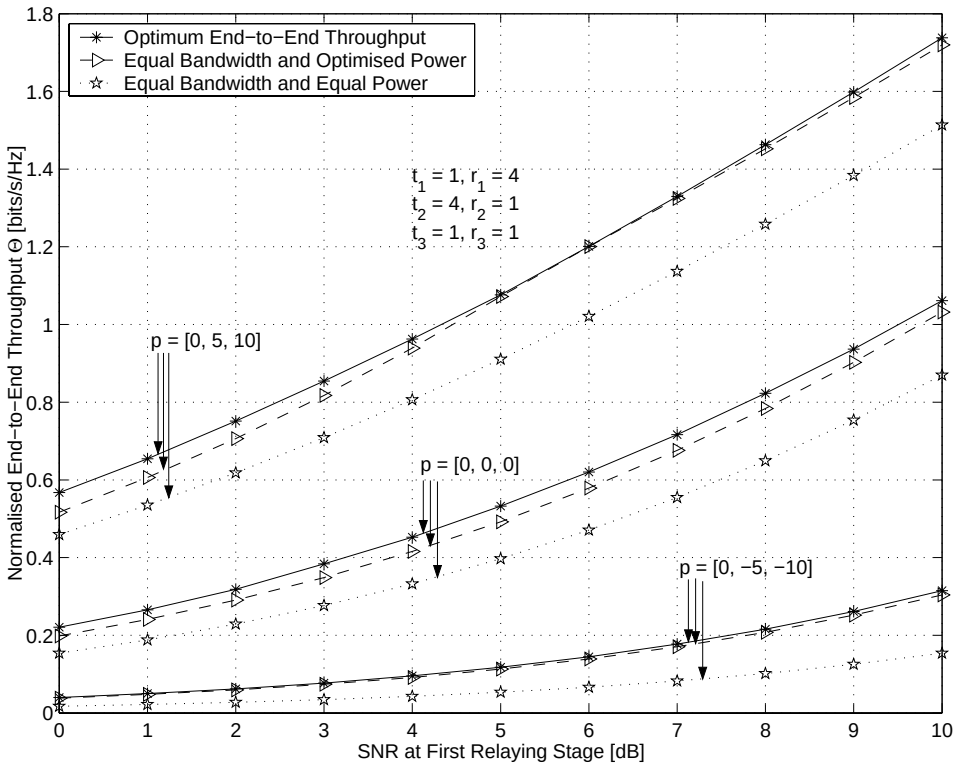


Figure 3.30: Achieved end-to-end throughput of various fractional resource allocation strategies for a 3-stage network with resource reuse.

### 3.4.4 O-MIMO Relaying

The fractional resource allocation strategies over O-MIMO channels with and without resource reuse are derived in the same fashion as for the above MIMO channels. Additionally, reference can be taken from the allocation strategies developed for ergodic O-MIMO channels. Again, the allocation for O-MIMO channels with equal channel gains differs from the case of unequal channel gains. The cases of Rayleigh and Nakagami fading with equal channel gains are dealt with below, as well as the case of unequal channel gains for Rayleigh fading only. Note that, in contrast to the ergodic counterpart, the exposed approach is not applicable to generic channel gains obeying any fading statistics.

#### Equal Sub-Channel Gains

For equal sub-channel gains, the coefficients $A_v$ and $B_v$ have to be replaced for the respective fractional resource allocation strategy throughout (3.55)−(3.58). These can be determined from (3.49) as

$$A_v = R_v \cdot \left( \frac{2b_v}{1+2b_v} \right) \tag{3.65}$$

$$B_v = \frac{1}{R_v} \frac{1}{\sqrt[b_v]{a_v(1+2b_v)}} \tag{3.66}$$

where $a_v = a_v(u_v)$ and $b_v = b(u_v)$ for the Rayleigh fading case, and $a_v = a_v(u_v f_v)$ and $b_v = b(u_v f_v)$ for the Nakagami fading case. The performance is demonstrated with the aid of Figure 3.31. In contrast to the ergodic case, the deployment of more than two transmit antennas yields benefits, which is the reason why this has been considered here.

Explicitly, Figure 3.31 shows the attained end-to-end throughput of a 2-stage relaying system versus the SNR in the first link for various resource allocation algorithms over O-MIMO Rayleigh fading channels. In the first stage, a SIMO communication is realised with one transmit and four receive elements. The second stage deploys a sporadic 3/4-rate STBC four transmit and 1 receive element.

Clearly, the developed fractional power and bandwidth allocation algorithm performs close to optimum, even for highly asymmetric communication links. As observed before, sub-optimum resource allocation strategies, such as optimising power only or allocating equal resources to each link, exhibit a poorer performance. Furthermore, as expected, the realised end-to-end throughput utilising STBCs is inferior to the respective general MIMO cases depicted in Figure 3.29.

#### Unequal Sub-Channel Gains

Similar to the ergodic case, unequal sub-channel gains require the application of spatial water-filling to the transmit power at each relaying stage prior to optimising fractional bandwidth and power.

It is hence the aim to find fractional transmit power allocations $\epsilon_{v\in(1,K),i\in(1,t)}$ such as to maximise

$$\Theta_v \quad = \quad \Phi_v \cdot \left[ 1 - \sum_{i=1}^{t_v} \sum_{j=1}^{r_v} K_{(i-1)r_v+j} \cdot \gamma \left( 1, \frac{2^{\Phi_v/R_v/\alpha_v} - 1}{\frac{\epsilon_{v,i} \cdot \gamma_{v,(i-1)r_v+j}}{R_v} \frac{\beta_v}{\alpha_v} \frac{S}{N}} \right) \right] \tag{3.67}$$

with $K_{(i-1)r_v+j}$ given by (3.35). A Lagrangian approach is unfortunately again not possible. Interestingly, as for the ergodic case, a near-optimum water-filling strategy could be attained by the author which is dealt with in the Appendix 3.7 (Derivation V) to this chapter. The therein conjectured fractional transmit power allocation, however, is fairly complex to deal with. Since algorithmic simplicity is vital for a successful application of the derived strategies, a simplistic approach similar to the ergodic case is suggested here. That implies that equal transmit power is allocated to all transmit elements and the average of all channel gains is used as an input to the respective equations for the $v^{th}$ relaying stage, i.e.

$$\gamma_v \approx \sum_{i=1}^{u_v} \gamma_{v,i}/u_v \tag{3.68}$$

where $u_v$ is the number of sub-channels in the $v^{th}$ stage, and $\gamma_{v\in(1,K),i\in(1,u_v)}$ are the associated channel gains. Thereafter, the above derived fractional resource allocation strategies are deployed to obtain maximum throughput.

The applicability of (3.68) is assessed for the scenario as depicted in Figure 3.24. To this end, Figure 3.32 depicts the achieved end-to-end throughput versus the SNR in the first link; the curves are labelled on $p$, where $p = [0, 5, 10]$dB, $p = [0, 0, 0]$dB and $p = [0, -5, -10]$dB. The optimum end-to-end capacity is obtained via numerical optimisation, where both the fractional bandwidth and power allocation per stage are optimised, as well as the distribution of the assigned power among the transmit elements.

Two further allocation strategies are compared against the optimum one. The first one deploys (3.68), after which the fractional bandwidth and power is obtained for (3.50) assuming an O-MIMO Rayleigh fading channel with equal channel gains. The second strategy assumes no optimisation at all, and resources are equally distributed among the MTs.

From Figure 3.32 it is clear that the suggested averaging approach still yields a near-optimum end-to-end throughput. Performing no optimisation at all results in significant performance losses, e.g. the loss in rate mounts to 60% at an SNR of 6dB or, alternatively, 65% less transmission power is required if a rate of 0.8 bits/s/Hz was to be maintained for $p = [0, 5, 10]$dB.

In summary, sufficiently precise fractional bandwidth and power allocation algorithms have been developed for a variety of distributed-MIMO multi-stage networks communicating over non-ergodic channels. The exposed algorithms are of very low complexity, yet they perform near-optimum. That renders a numerical optimisation within each mobile terminal superfluous.

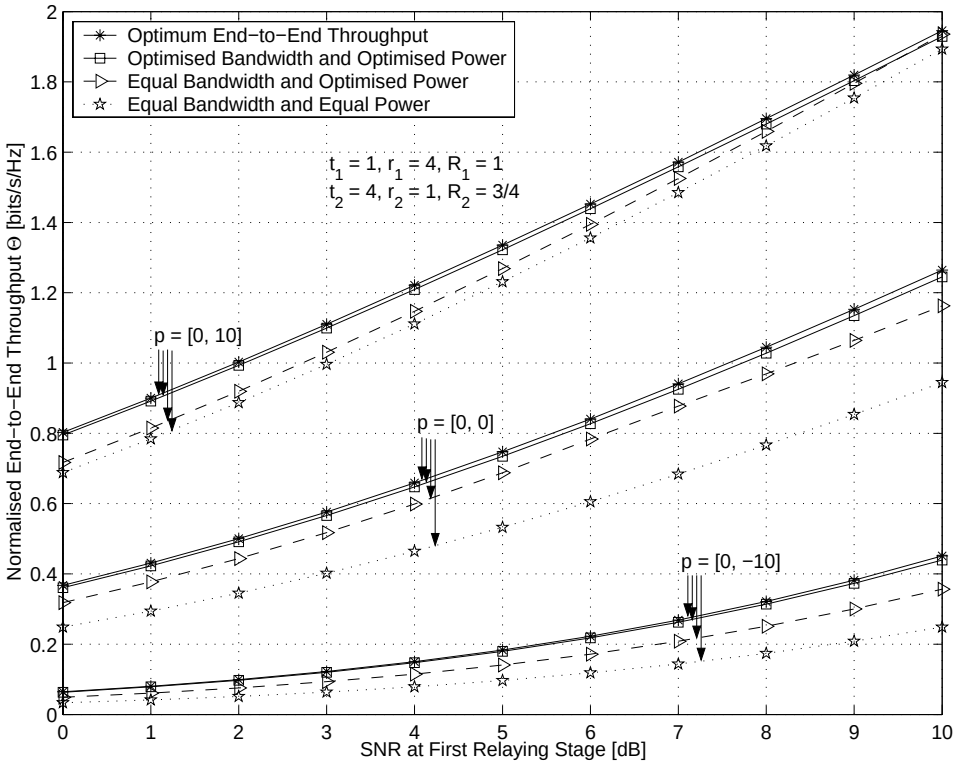


Figure 3.31: Achieved end-to-end throughput of various fractional resource allocation strategies over Rayleigh O-MIMO channels for a 2-stage network.

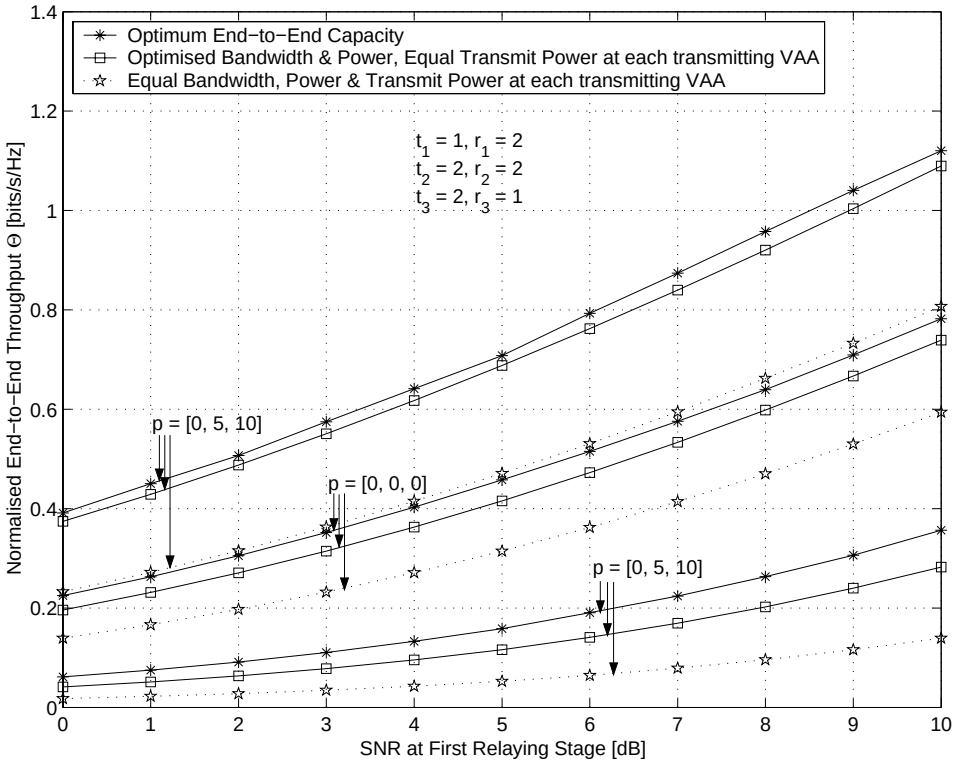


Figure 3.32: Achieved end-to-end throughput versus SNR in the first link for a 3-stage O-MIMO relaying network with unequal channel gains as specified in Figure 3.24.

## 3.5 Frequency Selective Channels

The analysis of this chapter has so far concentrated on the narrowband fading channels. It was hence assumed that the symbol duration is much larger than the delay spread of the channel. Modern communication systems, however, accomplish symbol durations much shorter than the channel delay spread. This yields a frequency selective channel, which requires special attention. Further analysis concentrates on general frequency selective MIMO channels, after which the analysis of OFDM-based systems is illuminated.

### 3.5.1 Generic Frequency Selectivity

A frequency selective channel is characterised by the frequency dependent channel transfer function $\mathbf{H}(f)$ over a given bandwidth $W$. The cause of frequency selectivity, as well as its dependency on the system assumptions is beyond the scope of this thesis. The interested reader is referred to the vast amount of excellent contributions available in this field, e.g. [37, 61].

The analysis exposed below is mainly based on the concise and insightful contribution by [62], wherein it is shown that the capacity of a frequency selective channel assuming perfect channel state information at the receiver is given as

$$C = \max_{\mathbf{S}(f)} \int_W \mathrm{E}_{\mathbf{H}(f)} \left\{ \log_2 \det \left( \mathbf{I}_r + \frac{\mathbf{H}(f)\mathbf{S}(f)\mathbf{H}^{\mathrm{H}}(f)}{N} \right) \right\} df \tag{3.69}$$

where capacity maximising codewords $\mathbf{x}(f)$ have to be determined with a given covariance matrix

$$\mathbf{S}(f) = \mathrm{E}\{\mathbf{x}(f)\mathbf{x}^{\mathrm{H}}(f)\} \tag{3.70}$$

which satisfies the power constraint

$$\int_W \mathrm{tr}\big(\mathbf{S}(f)\big) df \leq S \tag{3.71}$$

In [62] it is shown that the statistics of $\mathbf{H}(f)$ do not depend on the frequency $f$, which reduces the wideband capacity (3.69) to the narrowband capacity given by (2.23). Explicitly, Theorem 6 in [62] states that "frequency selectivity does not affect the ergodic capacity of wideband MIMO channels".

That is an important result, as the entire analysis developed for the ergodic narrowband channels can directly be translated to the wideband case. The analysis of non-ergodic frequency selective MIMO channels, however, is very intricate. It is deemed to be an interesting topic of future research.

In summary, the same fractional bandwidth, frame duration and power allocation strategies hold for the ergodic wideband case as for the ergodic narrowband case. Therefore, no matter the obtained fractional bandwidth $\alpha$, the same capacity can be achieved irrespective of the frequency selectivity of the channel.

### 3.5.2 OFDMA-Based Systems

In practical systems, frequency selectivity causes inter symbol interference (ISI) which is known to affect the system performance in a detrimental manner. Practical wideband transceivers therefore utilise either code division multiple access (CDMA) or orthogonal frequency division multiple access (OFDMA) as an access technique to mitigate a frequency selective channel. That applies to SISO, as well as MIMO channels.

An analysis of the functioning and capacity of CDMA-based systems is certainly beyond the scope of this thesis. The interested reader is, e.g., referred to [63, 64]. It shall only be noted that TDMA-based relaying is easier implemented in a CDMA-based channel access system. Note finally that the same fractional frame duration and power allocation strategies hold as already derived for the narrowband ergodic and non-ergodic cases.

Of higher practical importance for a deployment in high-data rate relaying networks, is OFDMA. It is understood to be orthogonal frequency division multiplexing (OFDM) combined with TDMA or FDMA as a channel access or relaying scheme. An OFDM symbol devides a wideband signal of bandwidth $W$ into $L$ independent sub-carriers of bandwidth $W/L$. Each of the sub-carriers is narrowband and hence does not exhibit any ISI. Such advantageous property comes at the expense of a required transform, namely the Fourier transform, and an additional cyclic prefix which diminishes the spectral efficiency of the system. The analysis of the functioning of an OFDM system is beyond this thesis, where the interested reader is referred to [65].

A TDMA-based relaying approach allows one to apply the previously derived fractional frame duration and power allocation strategies without any changes. That means that the $v^{th}$ relaying stage transmits a given number of OFDM symbols with power $\beta_v/\alpha_v$ over a fractional frame duration of length $\alpha_v$, where each OFDM symbol occupies the entire bandwidth $W$. Note that the discrete nature of samples representing an OFDM symbol in time allows only discrete realisations of $\alpha_v$. This poses no limitations in the time domain where the absolute fractional frame durations of $\alpha_v$ can be adjusted such as to maintain the theoretically derived ratios between all $\alpha_v$ at arbitrary precision.

An FDMA-based relaying system, however, is fairly restricted by the discrete number of samples representing an OFDM symbol in frequency. Here, only a discrete fraction $\alpha_v$ of all sub-carriers is utilised to form an OFDM symbol to be transmitted at each stage. Additionally, a simple implementation of OFDM requires the number of sub-carriers to be a power of two, which facilitates a fast Fourier transform. That may cause additional losses in precision.

For example, the channel conditions in a 2-stage relaying network are assumed to yield $\alpha_1 = 1/3$ and $\alpha_2 = 2/3$. With 64 sub-carriers available, an optimum allocation requires $21.\overline{3}$ sub-carriers to be used for the first stage, and $42.\overline{6}$ sub-carriers for the second stage. That is technically not feasible; instead, 21 and 43 sub-carriers will be allocated to each stage, respectively. The loss in precision for this case is only 1%. For an increasing number of sub-carriers, the allocation error will clearly decrease. However, if the number of sub-carriers has to be a power of two, then the allocation yields 32 and 32 sub-carriers for each stage, which causes a maximum allocation error of 50%.

Figure 3.33 assesses the degradation in performance due to the discrete number of OFDM sub-carriers available. The studied communication scenario is equivalent to the case analysed in Figure 3.18. It shows the attained capacity of a $(1 \times 2)/(2 \times 4)$ O-MIMO relaying system versus the SNR in the first link for various resource allocation algorithms over Rayleigh fading channels. Not to clutter the figure, only the channel distribution of $p = [0, 10]$dB is studied. Furthermore, to enhance the resolution, only an SNR from 6dB to 10dB has been considered.

It can be observed that with only four sub-carriers available, the precision of the derived fractional resource allocation suffers dramatically. For an increasing SNR, this case even approaches the non-optimised case. However, increasing the number of sub-carriers already to 16, the precision of the algorithm is almost restored. Finally, with 32 sub-carriers, there is virtually no difference between the discrete and continuous fractional bandwidth allocation. Note that the fractional transmission power remains a continuous value. It can therefore be concluded that with currently prevailing OFDM systems with a fairly large number of sub-carriers, the precision of the developed fractional allocation algorithms will not suffer. That is a very attractive property, as it allows applying the deduced strategies to any OFDM-based relaying system.

Figure 3.34 demonstrates the loss in precision if the number of allocated sub-carriers have to be a fraction of two. The fractional bandwidth in the first hop is found to be $\alpha_1 \approx 0.65$ in the studied SNR region and for $p = [0, 10]$dB. Having four sub-carriers, the only feasible fractional bandwidth allocation is to allocate two sub-carriers to the first hop, and another two to the second one. The same applies for the case of 16 and 32 sub-carriers, i.e. fractional resources have to be equally shared unless some sub-carriers remain unused. This resource sharing rule will apply to any number of sub-carriers which, with reference to Figure 3.34, causes a drastic performance degradation. Here, a rate loss of 20% occurs at an SNR of 6dB or, alternatively, 35% more power is required to maintain 2 bits/s/Hz.

This section only hinted at the potential application of the developed fractional resource allocation strategies, which were found to be applicable to realistic transceiver systems based on CDMA or OFDMA.

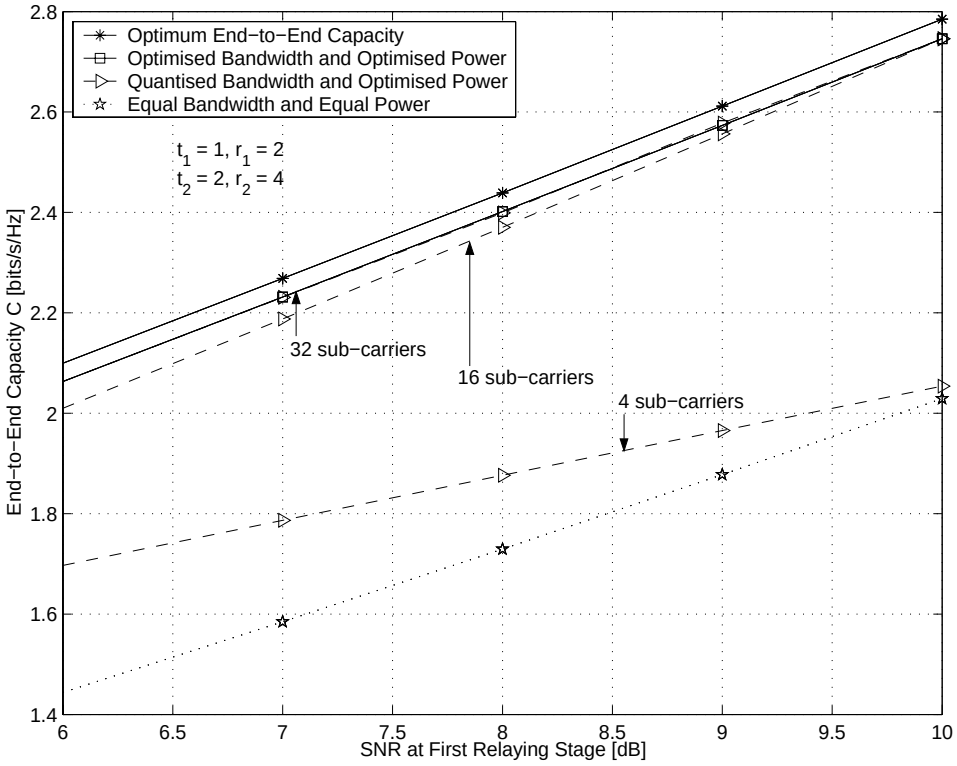


Figure 3.33: Achieved end-to-end capacity with quantised fractional bandwidth for a 2-stage relaying network over O-MIMO Rayleigh channels.

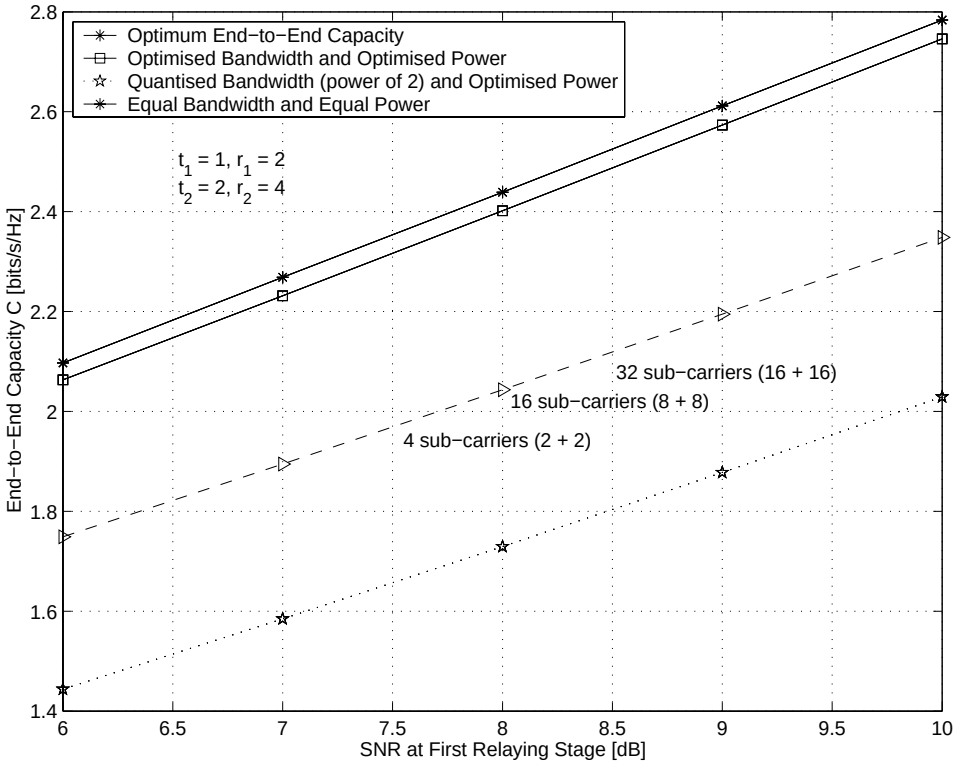


Figure 3.34: Achieved end-to-end capacity with quantised fractional bandwidth of power of two for a 2-stage relaying network over O-MIMO Rayleigh channels.

## 3.6 Conclusions

### 3.6.1 Summary

The analysis in this chapter exposed a variety of techniques deemed to be vital in providing maximum throughput in distributed-MIMO multi-stage relaying networks. The developed techniques heavily relied upon the analysis provided in Chapter 2, which was applied here to derive low-complexity near-optimal fractional resource allocation strategies matched to the prevailing communication scenario. Again, it was the aim to maintain a logical proceeding throughout the chapter, ranging from a thorough introduction to the topic, to the development of different strategies for ergodic and non-ergodic communication channels, towards a discussion on the implication of frequency selective channels.

In Section 3.1, a sufficiently concise introduction to the topic of resource allocation has been given. It was shown that the problem formulation *per sé* has already been known for some years; however, no satisfactory explicit resource allocation strategies had been developed so far. All previous analyses were of a theoretical nature, the solution to which had to be obtained numerically. The explicit fractional allocation strategies developed here were hence justified and put into the context of existing techniques.

The role of Section 3.2 was manyfold; first, the general system model comprising a regenerative distributed-MIMO multi-stage relaying network without resource reuse was thoroughly introduced; second, this deployment model was then extended to networks where resource reuse is allowed; and third, the equivalence between TDMA and FDMA-based relaying networks was proven. The latter allowed the simplification of subsequent analysis, since the fractional resource allocations developed for one access scheme are easily translatable to the other one. The analysis throughout the remaining part of the chapter thus concentrates on FDMA-based relaying, where fractional bandwidths $\alpha$ and fractional powers $\beta$ were derived. An equivalent TDMA-based system requires fractional frame durations $\alpha$ and fractional powers $\beta/\alpha$.

Section 3.3 constitutes an important milestone as it derives the explicit fractional resource allocation rules for ergodic channels such as to maximise the end-to-end throughput which, in the ergodic case only, is equivalent to the end-to-end capacity. The cases of distributed MIMO and O-MIMO relaying with and without resource have been considered. The derivation of the explicit algorithms relied on the approximation of MIMO capacity, as shown in Section 2.5. The developed algorithms were extensively tested over a variety of scenarios, i.e. a different number of relaying stages, different number of antennas per stage, different channel attenuations and statistics. Despite the utilised approximation, the algorithms were found to yield near-optimum end-to-end throughput. The latter was obtained via lengthy numerical optimisation.

Section 3.4 explored fractional allocation strategies for non-ergodic channels to maximise end-to-end throughput. To this end, the problem has been transformed to the previously analysed ergodic case by means of the approximation shown in Section 2.5. Again, the developed explicit fractional allocation strategies were shown to yield near-optimum throughput for distributed MIMO and O-MIMO relaying systems.

So far, analysis has been applicable to the flat fading channel. This constraint has been loosened in Section 3.5, in which the analysis has been extended to frequency selective channels. It has been shown that frequency selectivity does not influence the ergodic capacity, which allows the application of previously derived fractional resource allocation strategies also to these type of channels. The section is finalised with a brief glimpse into the capacity behaviour of realistic systems, here an OFDMA system. The application of the developed fractional bandwidth allocation to the selection of the number of utilised sub-carriers has been dealt with. It was shown that for an increasing number of sub-carriers, the allocation error caused by the discrete nature of the number of available sub-carriers diminishes. It has also been shown that if the number of chosen sub-carriers must be a power of two, such as to facilitate a fast Fourier transform, then the allocation error caused may seriously diminish the potential end-to-end capacity.

### 3.6.2 Contributions

This chapter opens the way to explicit fractional resource allocation strategies for large-scale distributed-MIMO multi-stage communication networks. To this end, the research contributions can be summarised as follows:

1. An explicit algorithm has been developed which yields near-optimum fractional bandwidth, optimum frame duration and optimum power allocations over ergodic MIMO channels without resource reuse. It is summarised as a flowchart in Figure 3.7. Similar flowcharts hold for the algorithms listed below.

2. An explicit algorithm has been developed which yields equal fractional bandwidth or equal frame duration but optimum power allocations over ergodic MIMO channels without resource reuse.

3. An explicit algorithm has been developed which yields equal fractional bandwidth or equal frame duration but optimum power allocations over ergodic MIMO channels with resource reuse.

4. All of the above-mentioned algorithms were developed for O-MIMO channels with equal and unequal channel gains.

5. Additionally, a near-optimum transmit power distribution per relaying stage has been conjectured for O-MIMO channels with unequal channel gains (similar to the water-filling principle).

6. The problem of finding optimum resources for non-ergodic channel has been transformed to the ergodic cases; therefore, all of the above-mentioned allocation strategies are applicable to communication scenarios over non-ergodic channels.

### 3.6.3 Future Research

Numerous questions and problems remain open in the field of MIMO information theory. Related to the problematic of distributed-MIMO capacity, the following topics are deemed to be worthwhile pursuing as future research:

1. Conjecture on Optimum Transmit Power. A rigorous analysis of the conjectured near-optimum fractional transmit power allocation for ergodic (equation (3.36)) and non-ergodic (equation (3.87)) channels still needs to be performed.

2. Throughput Generic Rayleigh/Nakagami. The developed approximation failed for the outage probability of generic Rayleigh and Nakagami fading channels. It is thus desirable to obtain a satisfactory solution for the near-optimum end-to-end throughput for these type of fading channels.

3. Multi-User. So far, only the case of a single source wishing to communicate with a single sink has been considered. The problem formulation and its solution(s) needs to be generalised to the multi-user environment.

4. Realistic Systems. CDMA and OFDMA-based system should further be explored in terms of optimised resource allocation for various communication conditions.

5. Impact of Correlation. So far, uncorrelated channels have been assumed. A further study could incorporate fractional resource assignments in dependency of the prevailing channel correlation.

6. Impact of Beamforming. Similarly, a deployment of beamforming could be investigated from a Shannon point of view.

7. Local Channel Knowledge. So far, it has been assumed that each terminal has a universal knowledge of the channel attenuations of the entire relaying chain. Of interest could be the development of optimised resource allocation strategies the input to which incorporates only adjacent channel gains, which are reported via feedback channels.

8. Resource Reuse. A development of optimum resource reuse zones could be important.

## 3.7 Appendix

**Derivation I.** To prove (3.13), all capacities given by (3.12) are equated, which yields $C = C_1 = \ldots = C_K$. Without loss of generality, (3.13) is proven for $v = K$. With the constraint given by (3.9), the $K$ equated capacities can be written as

$$\begin{aligned}
\left(1 - \sum_{v=2}^{K} \alpha_v\right) \mathrm{E}_{\gamma_1}\left\{m_1 \log_2\left(1 + \gamma_1 \frac{\beta_1}{\alpha_1}\frac{S}{N}\right)\right\} &= \alpha_K \mathrm{E}_{\gamma_K}\left\{m_K \log_2\left(1 + \gamma_K \frac{\beta_K}{\alpha_K}\frac{S}{N}\right)\right\} \\
\alpha_2 \mathrm{E}_{\gamma_2}\left\{m_2 \log_2\left(1 + \gamma_2 \frac{\beta_2}{\alpha_2}\frac{S}{N}\right)\right\} &= \alpha_K \mathrm{E}_{\gamma_K}\left\{m_K \log_2\left(1 + \gamma_K \frac{\beta_K}{\alpha_K}\frac{S}{N}\right)\right\} \\
&\vdots \\
\alpha_{K-1} \mathrm{E}_{\gamma_{K-1}}\left\{m_{K-1} \log_2\left(1 + \gamma_{K-1} \frac{\beta_{K-1}}{\alpha_{K-1}}\frac{S}{N}\right)\right\} &= \alpha_K \mathrm{E}_{\gamma_K}\left\{m_K \log_2\left(1 + \gamma_K \frac{\beta_K}{\alpha_K}\frac{S}{N}\right)\right\}
\end{aligned}$$

The above-given equations can be rewritten as

$$\alpha_2 = \alpha_K \cdot \frac{\mathrm{E}_{\gamma_K}\left\{m_K \log_2\left(1 + \gamma_K \frac{\beta_K}{\alpha_K}\frac{S}{N}\right)\right\}}{\mathrm{E}_{\gamma_2}\left\{m_2 \log_2\left(1 + \gamma_2 \frac{\beta_2}{\alpha_2}\frac{S}{N}\right)\right\}} \tag{3.72}$$

$$\vdots$$

$$\alpha_{K-1} = \alpha_K \cdot \frac{\mathrm{E}_{\gamma_K}\left\{m_K \log_2\left(1 + \gamma_K \frac{\beta_K}{\alpha_K}\frac{S}{N}\right)\right\}}{\mathrm{E}_{\gamma_{K-1}}\left\{m_{K-1} \log_2\left(1 + \gamma_{K-1} \frac{\beta_{K-1}}{\alpha_{K-1}}\frac{S}{N}\right)\right\}} \tag{3.73}$$

which inserted into the top equation yields

$$\left(1 - \sum_{v=2}^{K} \alpha_K \cdot \frac{\mathrm{E}_{\gamma_K}\left\{m_K \log_2\left(1 + \gamma_K \frac{\beta_K}{\alpha_K}\frac{S}{N}\right)\right\}}{\mathrm{E}_{\gamma_v}\left\{m_v \log_2\left(1 + \gamma_v \frac{\beta_v}{\alpha_v}\frac{S}{N}\right)\right\}}\right) = \alpha_K \cdot \frac{\mathrm{E}_{\gamma_K}\left\{m_K \log_2\left(1 + \frac{\beta_K}{\alpha_K} \cdot \gamma_K \cdot \frac{S}{N}\right)\right\}}{\mathrm{E}_{\gamma_1}\left\{m_1 \log_2\left(1 + \frac{\beta_1}{\alpha_1} \cdot \gamma_1 \cdot \frac{S}{N}\right)\right\}}$$

Resolving for $\alpha_K$ gives

$$\alpha_K = \frac{\mathrm{E}^{-1}_{\gamma_K}\left\{m_K \log_2\left(1 + \gamma_K \frac{\beta_K}{\alpha_K}\frac{S}{N}\right)\right\}}{\sum_{v=1}^{K} \mathrm{E}^{-1}_{\gamma_v}\left\{m_v \log_2\left(1 + \gamma_v \frac{\beta_v}{\alpha_v}\frac{S}{N}\right)\right\}} \tag{3.74}$$

which is equivalent to

$$\alpha_K = \frac{\prod_{w=1}^{K-1} \mathrm{E}_{\gamma_w}\left\{m_w \log_2\left(1 + \gamma_w \frac{\beta_w}{\alpha_w}\frac{S}{N}\right)\right\}}{\sum_{k=1}^{K} \prod_{w \neq k} \mathrm{E}_{\gamma_w}\left\{m_w \log_2\left(1 + \gamma_w \frac{\beta_w}{\alpha_w}\frac{S}{N}\right)\right\}} \tag{3.75}$$

This concludes the proof.

**Derivation II.** To prove that $\sum_{k=1}^{K} \frac{\beta_k}{\alpha_k} \approx K$, the capacity given by (3.12) is approximated utilising (2.97), which yields

$$C_v \approx \alpha_v \cdot \frac{\sqrt{\beta_v}}{\sqrt{\alpha_v}} \cdot \sqrt{\frac{S}{N}} \cdot \mathrm{E}_{\gamma_v}\left\{m_v \sqrt{\gamma_v / t_v}\right\} = \sqrt{\alpha_v} \cdot \sqrt{\beta_v} \cdot \sqrt{\frac{S}{N}} \cdot \mathrm{E}_{\gamma_v}\left\{m_v \sqrt{\gamma_v / t_v}\right\} \tag{3.76}$$

This suggests that the optimisation problem given by (3.11) is approximately symmetric to $\alpha_v$ and $\beta_v$. Therefore, $\alpha_v \approx \beta_v$ and $\frac{\beta_v}{\alpha_v} \approx 1$, from which (3.17) follows. The results presented throughout the chapter verify this approximation.

**Derivation III.** Equations (3.20)-(3.21) can be rewritten as

$$\sqrt[3]{\gamma_1 \cdot \Lambda^2(t_1, r_1)} \cdot \left[ K - \sum_{v=2}^{K} \frac{\beta_v}{\alpha_v} \right] = \sqrt[3]{\gamma_2 \cdot \Lambda^2(t_2, r_2)} \cdot \frac{\beta_2}{\alpha_2} \tag{3.77}$$

$$\vdots$$

$$\sqrt[3]{\gamma_1 \cdot \Lambda^2(t_1, r_1)} \cdot \left[ K - \sum_{v=2}^{K} \frac{\beta_v}{\alpha_v} \right] = \sqrt[3]{\gamma_K \cdot \Lambda^2(t_K, r_K)} \cdot \frac{\beta_K}{\alpha_K} \tag{3.78}$$

which can be rearranged to

$$\sqrt[3]{\gamma_1 \cdot \Lambda^2(t_1, r_1)} \cdot \left[ K - \sum_{v=2}^{K} \frac{\beta_v}{\alpha_v} \right] = \sqrt[3]{\gamma_K \cdot \Lambda^2(t_K, r_K)} \cdot \frac{\beta_K}{\alpha_K} \tag{3.79}$$

$$\sqrt[3]{\gamma_2 \cdot \Lambda^2(t_2, r_2)} \cdot \frac{\beta_2}{\alpha_2} = \sqrt[3]{\gamma_K \cdot \Lambda^2(t_K, r_K)} \cdot \frac{\beta_K}{\alpha_K} \tag{3.80}$$

$$\vdots$$

$$\sqrt[3]{\gamma_{K-1} \cdot \Lambda^2(t_{K-1}, r_{K-1})} \cdot \frac{\beta_{K-1}}{\alpha_{K-1}} = \sqrt[3]{\gamma_K \cdot \Lambda^2(t_K, r_K)} \cdot \frac{\beta_K}{\alpha_K} \tag{3.81}$$

Applying the same procedure as in Derivation I, finally yields (3.22).

**Derivation IV.** It is shown here that the throughput $\Theta$ relates to communication rate $\Phi$ and associated outage probability $P_{out}(\Phi)$ via

$$\Theta \propto \Phi \cdot \big(1 - P_{out}(\Phi)\big) \tag{3.82}$$

To this end, let $\Phi'$ be the amount of information in [bits] sent with reliability $1 - P_{out}$ over a bandwidth $W$ and time duration $T \to \infty$. Therefore, from the $\Phi'$ sent bits in average only $\Phi' \cdot (1 - P_{out})$ reach the receiver. The normalised throughput can hence be written as

$$\Theta \propto \lim_{T \to \infty} \frac{\Phi' \cdot \big(1 - P_{out}\big)}{WT} \tag{3.83}$$

The $\Phi' \cdot P_{out}$ bits which do not reach the receiver have to be re-sent, requiring an additional transmission time of $P_{out}$. With a single re-transmission, eq. (3.83) is expressed as

$$\Theta \propto \lim_{T \to \infty} \frac{\Phi' - \Phi' \cdot P_{out} + \Phi' \cdot P_{out} \cdot \big(1 - P_{out}\big)}{WT\,(1 + P_{out})} = \lim_{T \to \infty} \frac{\Phi'}{WT} \cdot \frac{1 - P_{out}^2}{1 + P_{out}} \tag{3.84}$$

Again, from the $\Phi' \cdot P_{out}$ re-sent bits, $\Phi' \cdot P_{out}^2$ do not reach the receiver and thus requiring re-transmission with an additional transmission time of $P_{out}^2$. This process is repeated $n$ times, where $n \to \infty$, which yields

$$\Theta \propto \lim_{n \to \infty} \lim_{T \to \infty} \frac{\Phi'}{WT} \cdot \frac{1 - (P_{out})^n}{1 + \sum_{i=1}^{n-1} (P_{out})^i} = \lim_{n \to \infty} \lim_{T \to \infty} \Phi \cdot \frac{1 - (P_{out})^n}{1 + \sum_{i=1}^{n-1} (P_{out})^i} \tag{3.85}$$

It is now straightforward to prove that

$$1 - (P_{out})^n = (1 - P_{out}) \cdot \left( 1 + \sum_{i=1}^{n-1} (P_{out})^i \right) \tag{3.86}$$

which concludes the proof.

**Derivation V.** It is conjectured here that the allocation $\epsilon_{v\in(1,K),i\in(1,t_v)}$, which maximises eq. (3.67) satisfying constraint (3.33), can be approximated by

$$\epsilon_{v,i} \approx \frac{\prod_{i'=1,i'\neq i}^{t_v}\left(\sum_{j=1}^{r_v}\gamma_{(i'-1)r_v+j}\right)^{-\{3,1/3\}}}{\sum_{k=1}^{t_v}\prod_{i'=1,i'\neq k}^{t_v}\left(\sum_{j=1}^{r_v}\gamma_{(i'-1)r_v+j}\right)^{-\{3,1/3\}}} \tag{3.87}$$

where the exponent is chosen from the set $\{3, 1/3\}$ such that the outage probability

$$P_{out}(\Phi_v) = \sum_{i=1}^{t_v}\sum_{j=1}^{r_v} K_{(i-1)r_v+j}\cdot\gamma\left(1, \frac{2^{\Phi_v/R_v}-1}{\frac{\epsilon_{v,i}\cdot\gamma_{v,(i-1)r_v+j}}{R_v}\frac{S}{N}}\right) \tag{3.88}$$

is minimised. The reason behind the two possible exponents lies in the non-linear behaviour of the outage probability rooted in Telatar's conjecture (c.f. Section 2.3.4). Recall that for a fixed communication rate, the number of antenna elements utilised for the actual transmission process changes in dependency of the available SNR. For the current analysis, the power in the sub-channels changes which triggers the optimum number of transmit antennas to change. This in turn may cause the change in exponent; however, more studies have to be conducted to draw a conclusive statement.

The performance of the conjectured transmit power distribution is assessed by means of Figures 3.35 and 3.36. Explicitly, Figure 3.35 depicts the outage probability at $\Phi = 2$ bits/s/Hz for a deployed Alamouti scheme with 2 transmit and 1 receive antenna versus the relative channel gain $\gamma_1$ in the first sub-channel, operating at various SNRs and $\gamma_2 = 2-\gamma_1$. Compared are three transmit power distribution algorithms: first, a numerically obtained optimum allocation; second, the conjectured allocation; and third, an equal transmit power allocation as suggested for approximately equal channel gains. It can be observed that optimum and conjectured allocation virtually yield the same outage probability over the entire range of $\gamma_1$. It can further be observed that at low outage probabilities, i.e. high SNR, the power distribution has marginal effect on the outage probability. A non-optimised transmit power only yields higher outage probabilities compared to the optimum case when the SNR is very low, and hence the optimum outage probability fairly high.

Figure 3.36 demonstrates the validity of the conjecture if more than one receive antenna is present. Here, the case of two transmit and two receive antennas is assumed, where the respective channel gains are (fairly arbitrary) determined as follows: $\gamma_2 = 1.5$, $\gamma_3 = 2-\gamma_1$, $\gamma_4 = 0.5$. It is further assumed that $\gamma_1$ and $\gamma_2$ are the gains of the sub-channels spanned from the first transmit antenna towards the two receive antennas; similarly, $\gamma_3$ and $\gamma_4$ are the gains from the second transmit antenna towards the two receive antennas. The same observations as above can be made.

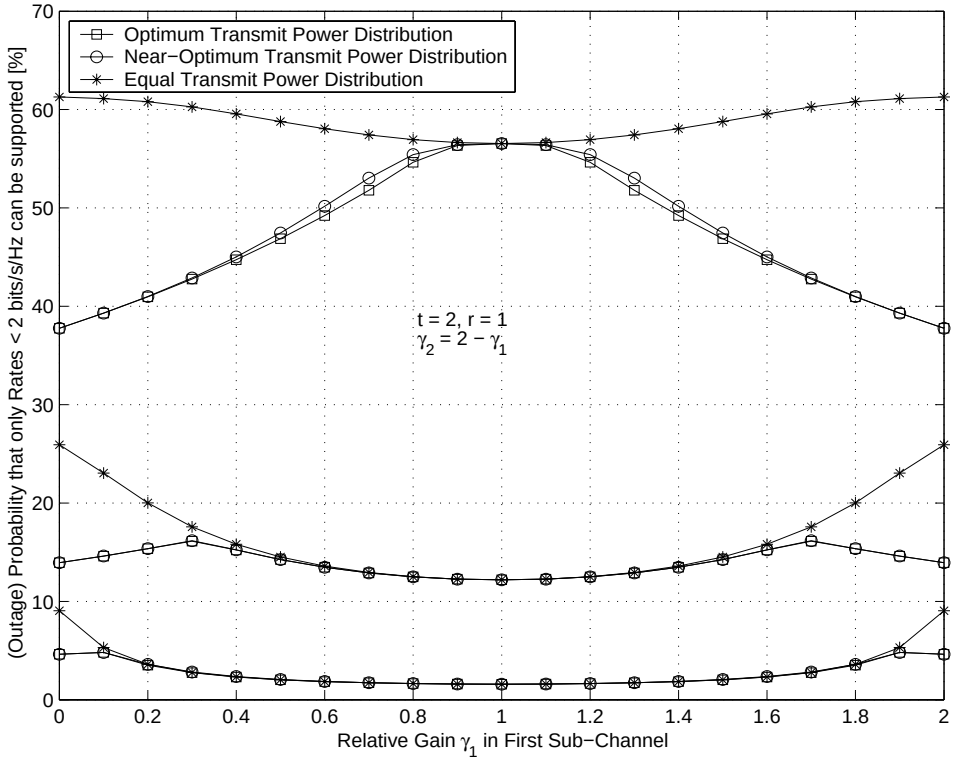


Figure 3.35: Outage probability for optimum, near-optimum and non-optimised transmit power distribution for deployed Alamouti scheme with one receive antenna.

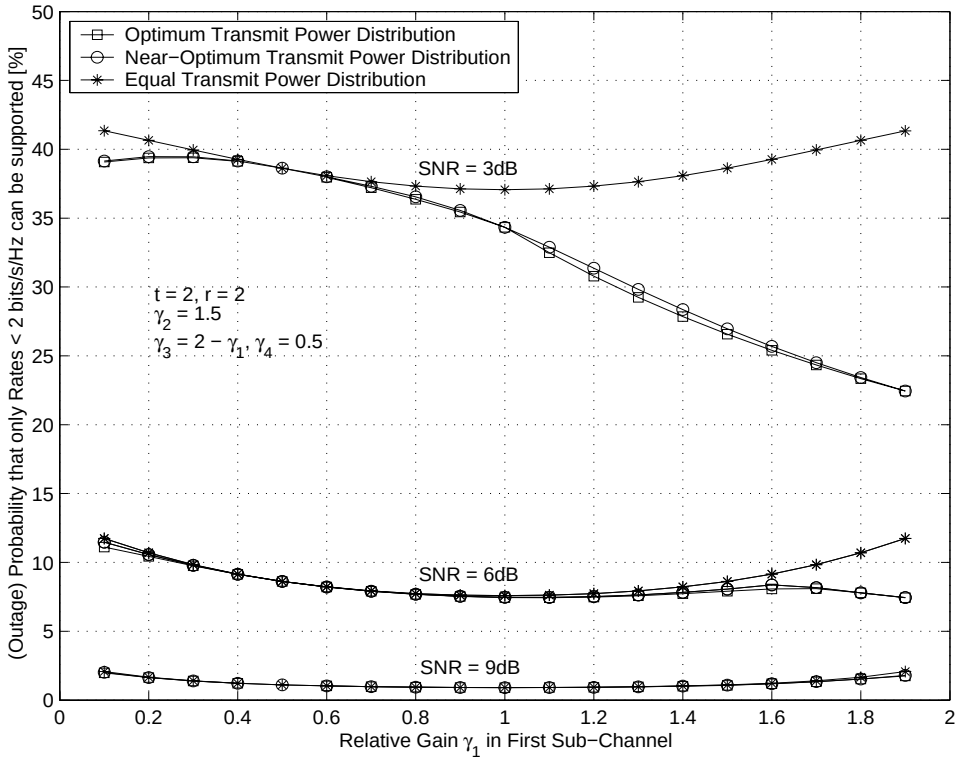


Figure 3.36: Outage probability for optimum, near-optimum and non-optimised transmit power distribution for deployed Alamouti scheme with two receive antennas.

# Chapter 4

# Link Level Performance

## 4.1 Introduction

The previous chapter dealt with the maximum achievable throughput over distributed-MIMO multi-stage communication networks taking into account certain communication conditions, e.g. whether the channel is ergodic or non-ergodic. In all the cases, however, the analysis was based on the notion of capacity which implied that transceivers of infinite complexity are available to the system designer.

The link level performance, on the other hand, assesses the behaviour of realistic transceivers in terms of error-rates versus the receiver signal-to-noise ratio (SNR). Error rates of interest are the bit-error-rate (BER), symbol-error-rate (SER) and frame-error-rate (FER). BER and SER are of importance when comparing various modulation or coding schemes, whereas modern packet based systems are gauged by the FER.

A simple communication system is a modulator/demodulator utilising binary phase-shift keying (BPSK), which operates over a wireless channel with a spectral efficiency of 1 bit/s/Hz. With reference to Figure 2.9 in Chapter 2, the SNR required to support such capacity over an ergodic Rayleigh fading channel amounts to 1dB.

To find an equivalent SNR at which communication is error-free for transceivers of finite complexity is not unique, as the error of such systems only decreases asymptotically with an increasing SNR. Therefore, to guarantee an error-free link, the SNR has to approach infinity (for the given additive Gaussian noise model). That has obviously little meaning for a system designer, which is the reason why finite complexity transceivers are said to yield a virtually error-free communication when the achieved error-rate falls below a certain threshold. For subsequent analysis, the BER threshold is assumed to be $10^{-5}$.

As will be shown in Section 4.3, the SNR required to allow for a virtually error-free communication with the above-defined threshold amounts to 44dB. The chosen low-complexity transceiver therefore operates 43dB away from the offered capacity limit. This large gap can be mitigated by introducing appropriate coding, which can only be met with an increase in transceiver complexity.

Various codes have been designed ever since Shannon published his famous monogram [1]. They range from low-complexity block codes, to trellis codes with an increase in decoding complexity [47]. For decades, none of the designed codes performed closer than 3dB to the theoretically predicted capacity limit. This gap could finally be closed with the introduction of turbo codes [36].

As for multiple-input-multiple-output (MIMO) channels, a first step towards the offered capacity was the introduction of space-time block codes (STBCs) with the concatenation of an outer code as described above [66]. This was followed by Tarokh's design guidelines to construct space-time trellis codes (STTCs) [17]. Space-time turbo codes are also available which allow one to approach the promised MIMO capacity bounds [4].

A thorough deployment analysis of the vast variety of available codes within the context of distributed-MIMO multi-stage relaying networks is certainly beyond the scope of this thesis. Therefore, subsequent analysis only concentrates on the deployment of STBCs. Other classes of codes are then a straightforward extension, where simply the union bound of the STBC needs to be replaced by the union bound of the specifically deployed code.

The aim here is to derive fractional resource allocation strategies tailored to finite complexity transceivers. The derivations are related to those already exposed in Chapter 3 for transceivers of infinite complexity. Of interest is the derivation of fractional frame duration, power and modulation order for each stage such as to achieve maximum end-to-end throughput.

It is also interesting to see whether the previously derived allocation strategies are applicable to finite complexity transceivers. It will be shown that the strategies are indeed applicable to the few analysed scenarios.

This chapter is organised as follows. In Section 4.2, the system model is introduced which includes a brief description of the transceiver and channel models. In this section, the developed simulation platform is also presented, which is then used throughout the chapter to verify various analytical results.

The derivation of error-rates, as well as some new twists relating to the analysis of distributed systems, are presented in Section 4.3. The analysis includes the derivation of BERs, SERs and FERs for space-time block encoded systems communicating over Rayleigh or Nakagami fading channels with different sub-channel gains.

Near-optimum allocation strategies are derived in Section 4.4, where it is assumed that a decision on an erroneously received packet is drawn at the t-MT. In Section 4.5, the analysis is then extended to the case where the decision on the correctness of a packet is drawn at each relaying stage. The derived fractional resource allocation strategies are then tested by means of a few case studies in Section 4.6. It is shown that relaying only yields performance gains until a given SNR threshold. Finally, conclusions are drawn in Section 4.7.

## 4.2 System Model

The general system model obeys the same topology as depicted in Figure 3.1, i.e. a source MT (s-MT) communicates with a target MT (t-MT) via a given number of relaying MTs (r-MTs). Spatially adjacent r-MTs are grouped into relaying Virtual Antenna Arrays (r-VAAs), the exact configuration of which has been thoroughly explained in Chapter 3. The system configurations described there-in are sufficiently precise for dealing with the capacity of such networks.

However, the deployment of realistic transceivers requires further explanations of how such system would work in reality. It is hence the aim of this section to provide this missing information. Of interest here are the transmitter and receiver used, as well as the prevailing communication channel.

### 4.2.1 Transceiver Model

The functional blocks of the transceivers forming the distributed-MIMO multi-stage relaying network are depicted in Figure 4.1. The top of Figure 4.1 relates to the source VAA containing the s-MT; the middle relates to an arbitrary relaying VAA tier; and the bottom relates to the target VAA containing the t-MT. In the figure, each VAA tier is shown to consist of three terminals; it is, however, understood that any reasonable number of terminals can be accommodated.

Specifically, the information source passes the information to a cooperative transceiver, which relays the data to spatially adjacent r-MTs belonging to the same VAA. Again, this is assumed to happen over an air interface distinct from the interface used for inter-stage communication or an air interface not requiring any optimisation, and is not considered further. It is also assumed that these cooperative links are error-free due to the short communication distances. Each of the terminals in the VAA perform distributed encoding of the information according to some prior specified rules. That information is then transmitted from the spatially distributed terminals after having been synchronised. Note that the problem related to synchronisation is beyond the scope of this thesis.

Any of the relaying VAA tiers functions as follows. First, each r-MT within that VAA receives the data which is optionally decoded before being passed onto the cooperative transceiver. Ideally, every terminal cooperates with every other terminal; however, any amount of cooperation is feasible. If no decoding is performed, then an unprocessed or a sampled version of the received signal is exchanged with the other r-MTs. Note that unprocessed relaying is equivalent to transparent relaying. After cooperation, appropriate decoding is performed. The obtained information is then re-encoded in a distributed manner, synchronised and re-transmitted to the following relaying VAA tier.

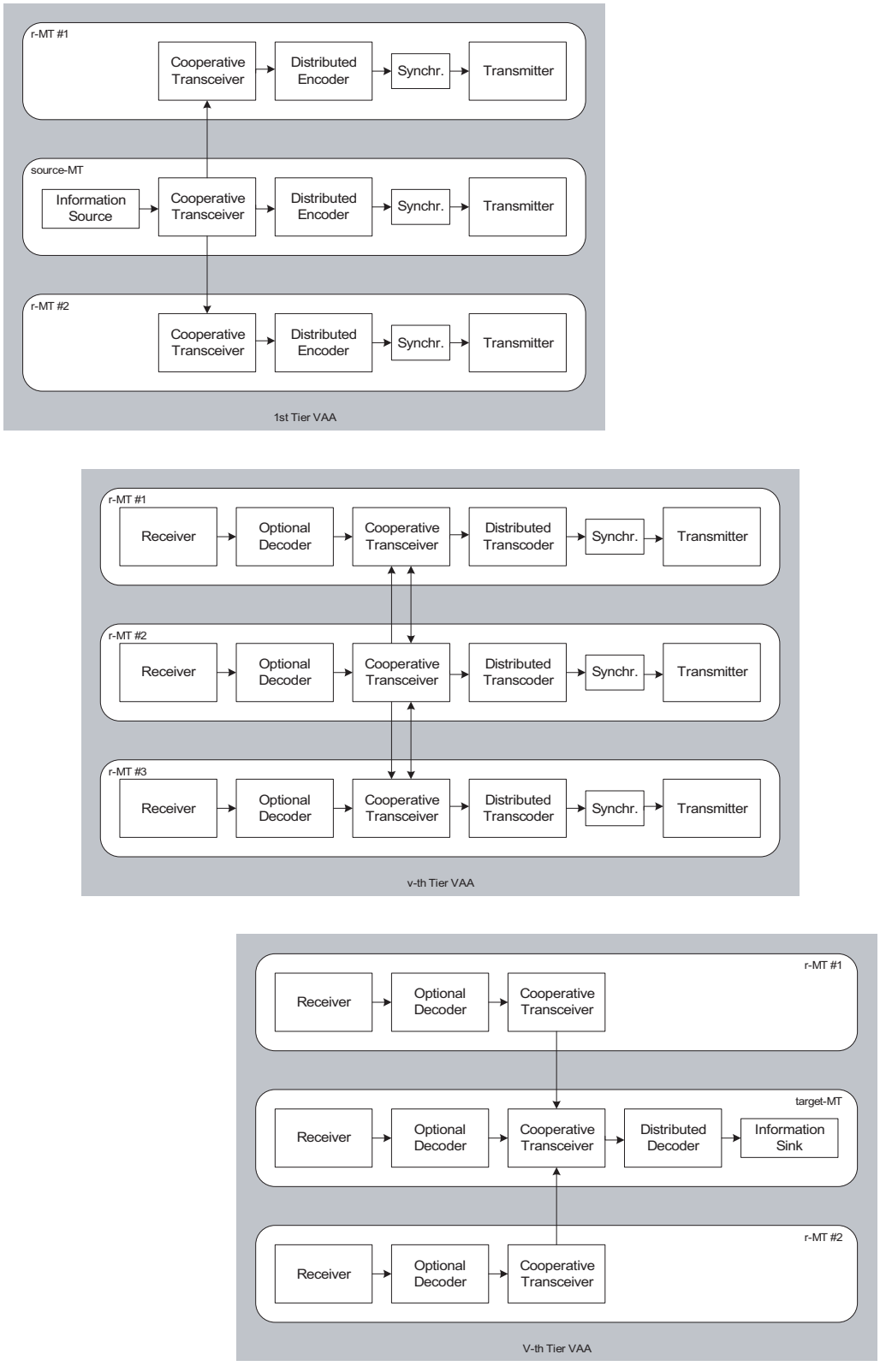


Figure 4.1: Functional blocks of the source VAA (top), the $v^{th}$ relaying VAA (middle) and the target VAA (bottom).

As for the target VAA, the functional blocks are exactly the opposite to the source VAA. All terminals receive the information, possibly decode it, then pass it onto the cooperative transceivers which relay the data to the target terminal. The data is processed and finally delivered to the information sink.

The functional blocks of the distributed transcoder, i.e. encoder and decoder, are now elaborated on in more detail. To this end, the encoder and decoder are shown in Figure 4.2.

Generally, the role of a channel encoder is to insert sufficient redundancy into the signal to mitigate the detrimental effects of noise and the fading channel. The insertion of redundancy decreases the data rate, where (with a good channel code) a decrease in rate comes along with an increase in coding gain. Together with the additional complexity, these need to be traded-off to yield optimum performance in terms of the BER versus $E_b/N_0$, where $E_b$ is the information bit energy and $N_0$ is the noise power spectral density.

The channel code is traditionally accomplished by means of a convolutional code, which 'convolutes' the redundancy into the original signal stream. Nowadays, it is considered to be a low complexity code and is often found to be available within communication chip-sets. Another class of codes are the block codes. These generate the redundant information from the original data stream, after which it is inserted into it. A more complex class of codes are turbo codes, which were shown to operate near the Shannon capacity. For a proper functioning and mathematical description of these codes, refer to [67].

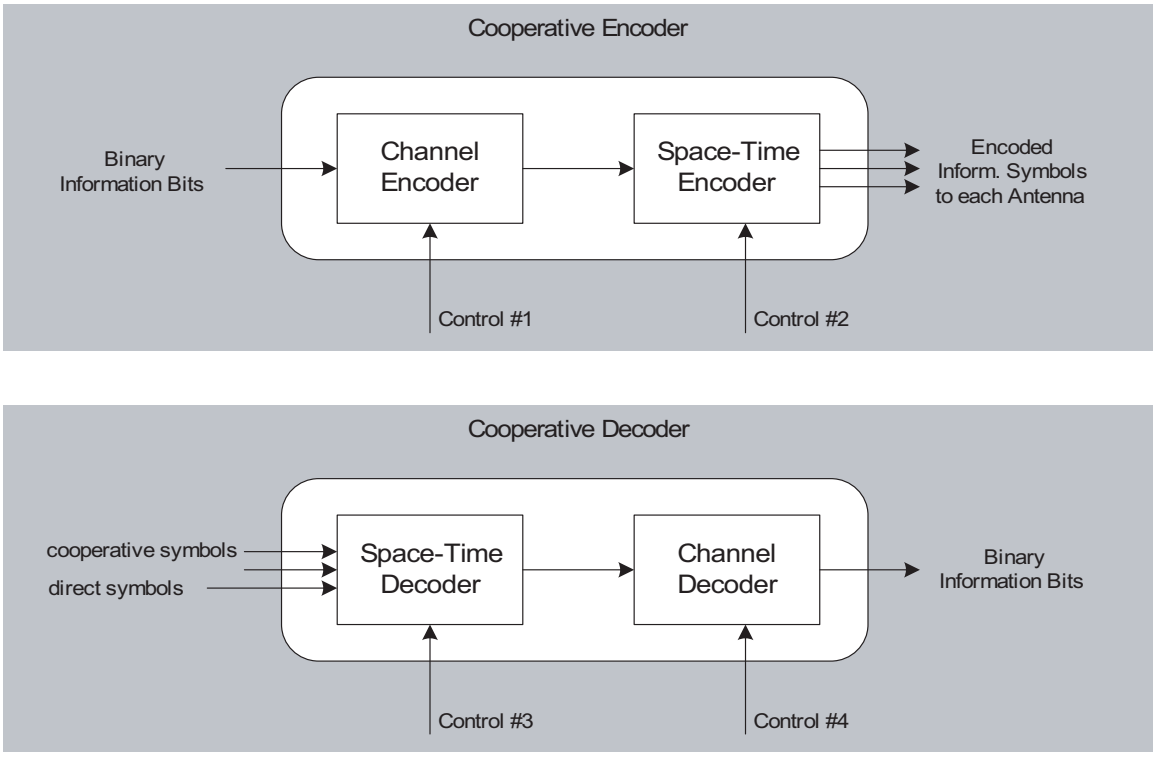


Figure 4.2: Distributed Encoder and Decoder.

The channel encoder may also consist of two or more concatenated codes, which are preferably connected by interleavers which break long error sequences. For example, trellis codes are known to produce a cluster of errors, which could then be corrected by appropriate block codes.

A channel encoder within a distributed encoder does not normally differ from a non-distributed encoder; however, it is generally possible to design channel codes which reflect the distributed nature of the encoding process. Example trellis codes are introduced in [31], where the encoder requires some form of control as to decide which code to employ.

The role of a space-time encoder is to utilise the additional spatial dimension created by sufficiently spaced antenna elements to increase the system performance. If each antenna element is used to transmit independent data streams, then such spatial multiplexing technique is referred to as BLAST [30]. Clearly, the data rate of such a system increases linearly with the number of transmit antennas; however, the lack of spatial redundancy makes it more susceptible to noise and interference when compared to coding techniques described below.

If, instead, the additional spatial domain is used to provide redundant information, then such a spatial encoding technique is referred to as space-time coding. The computationally simple space-time block codes (STBCs) have already been introduced in Chapter 2, where they were shown to orthogonalise the MIMO channel. More complex codes are space-time trellis codes (STTCs), or space-time turbo codes. Note that space-time codes (STCs) can also be concatenated with an outer channel code to yield additional performance gains as described above.

The functionality of distributed space-time codes (STCs) differs from a traditional deployment because only a fraction of the entire space-time codeword is transmitted from any of the spatially distributed terminals. The transmission across all terminals then yields the complete space-time codeword. Therefore, a control signal to each distributed space-time encoder is essential, as it tells each of them which fraction of the entire space-time codeword to pass onto the transmitting antenna(s). This is indicated as Control #2 in Figure 4.2. This control information is assumed to be available to the space-time encoder, and is thus not discussed further in this thesis.

The cooperative decoder can be realised as the inversion of all processes at the cooperative transmitter. Here, the space-time decoder is fed with the signals directly received from the available antenna(s), as well as the information received via the cooperative links from adjacent terminals. Again, a control signal is needed which specifies the type of information fed into the space-time decoder, to allow for optimum decoding. For example, the control signal could inform the decoder that the relayed signals are a one bit representation of the sampled soft information available at the respective cooperative relaying terminals.

After the space-time decoding process, the information is passed on to the channel decoder which performs the inverse process to the channel encoder. In a cooperative transcoder, the produced binary information output may then be fed into the cooperative encoder, to get relayed to the next VAA tier.

In subsequent analysis, a more realistic relaying access scheme based on TDMA is assumed. Therefore, the entire bandwidth $W$ is utilised by all relaying links, whereas only a fraction of the total frame duration $T$ is used by each stage to relay the information to the consecutive stage.

A brief overview of the potential application of VAAs with realistic encoding schemes has been presented. It is clear that neither an in-depth analysis to these codes can be exposed here nor can all possible code combinations be assessed. Further analysis and assessments therefore concentrate on a few examples, i.e. only the cases of no encoding and space-time block encoding. The performance of space-time trellis codes and the effect of an outer channel code has been left open for future research.

### 4.2.2 Channel Modelling

A signal travelling from a transmitter to a receiver via a wireless channel is known to be influenced by pathloss, shadowing and fading. Assuming a flat (narrow-band) fading channel, a transmitted complex symbol $\mathbf{s}_{\mathrm{Tx}}$ is received as

$$\mathbf{s}_{\mathrm{Rx}} = \gamma \cdot \varsigma \cdot \mathbf{f} \cdot \mathbf{s}_{\mathrm{Tx}} \tag{4.1}$$

where the scalar $\gamma$ is the pathloss, the scalar $\varsigma$ is the experienced shadowing, and $\mathbf{f}$ is the instantaneous fading which is generally complex.

#### Pathloss $\gamma$

Pathloss is a deterministic effect and is known to decay exponentially with distance $d$, where the decay factor is often referred to as the pathloss coefficient, and it is henceforth denoted as $n$. The pathloss can thus be related to distance and pathloss coefficient as

$$\gamma \propto d^{-n} \tag{4.2}$$

Friis transmission formula [37] shows that $n = 2$ for free-space propagation. The pathloss coefficient $n$ for environments other than free-space depends on the operational frequency, the environment, as well as the distance between transmitter and receiver. Various sophisticated models have been developed to account for these input dependencies [37]. For this thesis, it is assumed that $2 \leq n \leq 4$, where an increasing $n$ corresponds to an increasing clutter density around the transmitter and/or receiver. This effect can be attributed to shadowing, as explained below.

**Shadowing $\varsigma$**

Shadowing is a random effect and is therefore characterised by its probability density function (pdf) which is known to be lognormal, i.e. [37]

$$pdf_{\varsigma}(\varsigma) = \frac{10}{\log 10} \frac{1}{\sqrt{2\pi\sigma_{\varsigma}^2}} \frac{1}{\varsigma} e^{-\frac{(10\log_{10}(\varsigma)-\mu_{\varsigma})^2}{2\sigma_{\varsigma}^2}} \tag{4.3}$$

Here, $\mu_{\varsigma}$ and $\sigma_{\varsigma}^2$ are the mean and variance of the underlying Gaussian process, respectively. The lognormal pdf is attributed to the random nature of multiplicative reflections which, when expressed in [dB], yields a Gaussian distribution. Clearly, for an increasing distance $d$, the number of reflection increases, thereby causing $\sigma_{\varsigma}^2$ to increase and $\mu_{\varsigma}$ to decrease. The later is traditionally incorporated into the pathloss, which explains why highly cluttered environments yield a steeper pathloss curve. The variance is traditionally measured and it also depends on the operational frequency, the environment, and the distance between transmitter and receiver. Typical values range from $\sigma_{\varsigma}^2 = 3$dB for a lightly cluttered environment and/or short communication distances, to $\sigma_{\varsigma}^2 = 16$dB for a densely cluttered environment and/or large communication distances [68].

**Fading f**

The small-scale fading $\mathbf{f}$ can be categorised into four classes: (1) slow and flat fading; (2) fast and flat fading; (3) slow and frequency selective fading; and (4) fast and frequency-selective fading. With the narrowband assumption, only the first two cases are considered here. The characteristic of a slow fading channel is that the transmitter could potentially be provided with feedback from the receiver to allow for an optimum transmission. This is obviously only possible if the channel is sufficiently slow-fading, sometimes also referred to as quasi-static. In statistical terms, this means that the channel coherence time is larger than the feedback cycle.

A slow fading channel is simulated as being constant over a given frame length, where the channel realisations are independent from frame to frame. The channel realisations of a fast fading channel, on the other hand, are independent samples for each symbol transmitted. Both cases are somewhat ideal; however, they serve well to assess the performance within which a realistic channel would perform.

Flat fading, whether slow or fast, is characterised by the pdf of the envelope or power fading process. For outdoor communication scenarios with no line-of-sight (nLOS), the pdf was often found to obey a Rayleigh distribution (envelope)/central-$\chi^2$ distribution (power). For outdoor communication scenarios with line-of-sight (LOS), the pdf was often found to obey a Ricean distribution (envelope)/non-central-$\chi^2$ distribution (power). Finally, for indoor communication scenarios, the pdf was often found to obey a Nakagami distribution (envelope)/Gamma distribution (power).

### 4.2.3 Simulation Platform

A generic simulation platform has been written in C++ by the author, which is utilised to obtain error rates for various communication scenarios discussed in subsequent sections. The simulation platform has the functionalities listed below for transmitter, channel and receiver; most of these are self-explanatory and are thus not explained for the sake of brevity. Note that some of the listed features are not required for the described analysis; however, they may prove useful for any future link level analysis related to distributed networks.

**Transmitter**

- any number of bits per data packet
- any number of packets per transmission (jointly encoded)
- channel code: uncoded, half-rate convolutional code (constraint length 7)[1]
- time interleaver (block and random)[2]
- modulation: BPSK, QPSK, 16QAM, 64QAM, 256QAM
- SNR normalisation: $E_b/N_0$, $E_s/N_0$, $S/N$
- channel access: MC-CDMA (in frequency) + TDMA (in time)
- any number of sub-carriers, spreading factor
- frequency interleaver (block and random)
- space-time block encoder:

  - full-rate for real signal constellations ($R = 1$, $t = 1, \ldots, 8$),

  - half-rate for complex signal constellations ($R = 1/2$, $t = 1, \ldots, 8$),

  - sporadic 3/4-rate for complex signal constellations ($R = 3/4$, $t = 3, 4$)

- any number of cyclic prefix samples

MC-CDMA stands for Multi Carrier Code Division Multiple Acces, TDMA for time division multiple access. The flexibility of the platform allows one to simulate a pure TDMA system by setting the number of sub-carriers to one. An OFDMA system is obtained by choosing the number of sub-carriers greater than one and setting the spreading factor to one.

[1] The convolutional encoder and decoder have been obtained from Panos Fines.
[2] The time and frequency interleaver have been obtained from Dr. Fatin Said.

**Channel**

- Gaussian / fading
- any power delay profile (delay, power)
- normalisation: none, over power delay profile
- per tap: Rayleigh (Jakes), Ricean, Nakagami
- any Doppler shift
- any oversampling
- any correlation between adjacent Tx and/or Rx antennas

Jake's fading model assumes a scatter ring around the receiver, which does not always occur in reality [37]. In principle, it is possible to perform slight modifications to the platform such that each tap experiences a different angular power distribution.

**Receiver**

- perfect channel estimation
- imperfect channel estimation:
  - any pilot power
  - any number of pilots per estimate
  - Wiener filtering in frequency
- space-time block decoder for any number of antennas
- signal combiner: ORC, EGC, MRC, MMSEC
- hard and soft Viterbi decoding
- BER, SER, PER

The mentioned combining methods are orthogonality restoring combining (ORC), equal gain combining (EGC), maximum ratio combining (MRC) and minimum mean square error combining (MMSEC). Although not further used throughout the remainder of the thesis, it shall be noted that ORC (downlink only) and MMSEC (uplink and downlink) are applicable in a MC-CDMA system [69]. The EGC receiver requires only an estimate of the phase which makes it a low-complexity receiver for M-PSK modulation schemes. The MRC receiver is optimum for a single user scenario [47], and is therefore used within this thesis. The platform has undergone strict benchmarking against results in [47, 69, 70].

## 4.3 Error Rates for Distributed STBCs

The theory behind the performance analysis of various coding and modulation schemes is far too broad to be considered here in sufficient depth. The interested reader is referred to references [4, 39, 45, 46, 47].

Subsequent analysis relating to the error rates of STBC transceivers of finite complexity serves the purpose of this thesis, which is (1) the derivation of fractional resource allocation rules for finite complexity transceivers; and (2) how precisely the derived fractional resource allocation strategies perform when applied to realistic systems. Note that given a STBC encoded system, the performance of an uncoded SISO system is obtained by setting the number of transmit and receive elements to one.

### 4.3.1 Symbol Error Rates

The space-time encoder, as depicted in Figure 4.2, is realised by means of a STBC which has already been introduced in Chapters 2 and 3. In there, the STBC has been used to orthogonalise the MIMO channel, a property which will become apparent below.

A typical space-time encoded MIMO system with $t$ transmit and $r$ receive antennas is shown in Figure 4.3, which was referred to as an O-MIMO system in Chapters 2 and 3. Here, $b \cdot s$ information bits are fed into the modulator, which Gray-maps $b = \log_2 M$ consecutive bits onto an M-PSK or M-QAM signal constellation, thereby producing $s$ symbols, i.e. $x_1, x_2, \ldots, x_s$. To remind the reader, these are subsequently space-time encoded with an orthogonal space-time coding matrix $\mathcal{G}$ of size $d \times t$, where $d$ is the number of symbol durations required to transmit the space-time code word, and $t$ is the number of transmit elements. At each time instant $k = 1, \ldots, d$, the space-time encoded symbol $c_{k,i} \in \mathcal{G}$ is transmitted from the $i^{th}$ transmit element, where $i = 1, \ldots, t$. The reduction in transmission rate is $R = s/d$.

The space-time code generator matrix $\mathcal{G}$ therefore maps the symbols $x_1, x_2, \ldots, x_s$ onto a transmitted space-time matrix $\mathbf{X}$ of dimensions $t \times d$, i.e.

$$x_1, x_2, \ldots, x_s \overset{\mathcal{G}}{\longmapsto} \mathbf{X} \tag{4.4}$$

which is transmitted over a flat fading $r \times t$ space-time channel. The latter can be casted into a matrix $\mathbf{H}$ given by (2.13) in Chapter 2, which allows writing the received signal in

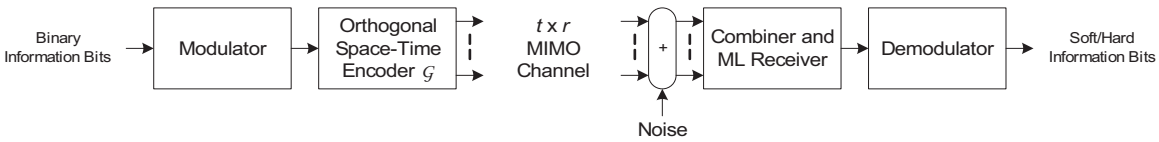


Figure 4.3: A space-time block encoded MIMO system (O-MIMO).

matrix form [39]

$$\mathbf{Y} = \mathbf{H}\mathbf{X} + \mathbf{N} \tag{4.5}$$

with $\mathbf{N}$ being the $r \times d$ receive noise matrix. The covariance matrix of the noise obeys $\mathrm{E}\left\{\mathbf{N}\mathbf{N}^{\mathrm{H}}\right\} = d \cdot N \cdot \mathbf{I}_{r\times r}$, where $N$ is the total noise power per sample in space and time. Under the condition of perfect CSI at the receiver, the problem of detecting $\mathbf{X}$ given $\mathbf{Y}$ is shown in [17] and [39] to be equal to minimising the maximum likelihood (ML) decision metric $\|\mathbf{Y} - \mathbf{H}\mathbf{X}\|$ over all possible symbols $x_1, x_2, \ldots, x_s$. The complexity therefore increases linearly with the total number of antennas $r \times t$ and exponentially with the modulation order $M$ and the codeword duration $d$.

In [39], however, it is proven that the orthogonality of the space-time code generator matrix $\mathcal{G}$ allows decomposing the ML problem into $s$ parallel ML decision metrics for each of the originally sent symbols $x_{l\in(1,s)}$. The optimum decision metrics can be found in [39, page 102]. The complexity therefore increases exponentially only with the modulation order $M$, which constitutes a great simplification to the detection process.

Using Theorem 7.3 in [39], it can been shown that the instantaneous SNR $\rho$ per symbol $x_{l\in(1,s)}$ at detection is given as

$$\rho = \frac{1}{R}\frac{\lambda}{t}\frac{S}{N} = \frac{\lambda}{t}\frac{E_s}{N_0} = \log_2(M)\frac{\lambda}{t}\frac{E_b}{N_0} \tag{4.6}$$

where $\lambda \triangleq \|\mathbf{H}\|^2$ (c.f. equations (2.62)), $S$ is the average transmitted signal power, $E_s$ is the average transmitted symbol energy, $E_b$ is the average transmitted bit energy, $N$ is the average receiver power, and $N_0$ is the average receiver noise power density. The instantaneous SNR $\rho$ is a random process due to the randomness of the power of the instantaneous channel realisations $\lambda$. Therefore, a given modulation scheme will yield a probability of error conditioned on $\rho$, i.e. $P(e|\rho)$. The average error probability $P(e)$ can then be obtained as

$$P(e) = \int_0^\infty P(e|\rho) \cdot pdf_\rho(\rho)\, d\rho \tag{4.7}$$

which is central to numerous problems relating to the BER or SER of communication systems. The conditioned error probability is often represented by intricate functions, such as the Marcum Q-function, which make it difficult to calculate the integral in (4.7). In [51], an alternative representation of (4.7) has been introduced which relies on the moment generating function (MGF) $\phi_\rho(s)$ of the instantaneous SNR $\rho$. With reference to (4.6), it is clear that

$$\phi_\rho(s) \equiv \phi_{\frac{1}{R}\frac{\lambda}{t}\frac{S}{N}}(s) \tag{4.8}$$

which proves useful, because the MGF $\phi_\lambda(\cdot)$ has already been exposed in Section 2.4.2 for Rayleigh and Nakagami fading channels with equal, unequal and generic channel gains.

The closed solution to (4.7) for generic M-PSK and M-QAM schemes is based on references [51] and [70]. From [51], one can obtain the average SER for coherent M-PSK to be

$$P_s(e) = \frac{1}{\pi}\int_0^{\pi\frac{M-1}{M}} \phi_\rho\left(\frac{g_{\text{PSK}}}{\sin^2\theta}\right) d\theta \tag{4.9}$$

where $g_{\text{PSK}} \triangleq \sin^2(\pi/M)$. Considering (4.8), this can be rewritten as

$$P_s(e) = \frac{1}{\pi}\int_0^{\pi\frac{M-1}{M}} \phi_{\frac{1}{R}\frac{\lambda}{t}\frac{S}{N}}\left(\frac{g_{\text{PSK}}}{\sin^2\theta}\right) d\theta \tag{4.10}$$

Similarly, the SER for coherent M-QAM is given as [51]

$$P_s(e) = \frac{4q}{\pi}\int_0^{\pi/2} \phi_{\frac{1}{R}\frac{\lambda}{t}\frac{S}{N}}\left(\frac{g_{\text{QAM}}}{\sin^2\theta}\right) d\theta - \frac{4q^2}{\pi}\int_0^{\pi/4} \phi_{\frac{1}{R}\frac{\lambda}{t}\frac{S}{N}}\left(\frac{g_{\text{QAM}}}{\sin^2\theta}\right) d\theta \tag{4.11}$$

where $g_{\text{QAM}} \triangleq 3/2/(M-1)$ and $q \triangleq 1-1/\sqrt{M}$. The SERs are now obtained in closed form for O-MIMO communication scenarios previously analysed in Chapter 2.

**Rayleigh Fading - Equal Sub-Channel Gains**

For equal sub-channel gains $\gamma_1 = \ldots = \gamma_u \triangleq \gamma$, the MGF of the instantaneously experienced SNR can be expressed as

$$\phi_{\frac{1}{R}\frac{\lambda}{t}\frac{S}{N}}(s) = \frac{1}{\left(1-\frac{1}{R}\frac{\gamma}{t}\frac{S}{N}\cdot s\right)^u} \tag{4.12}$$

where $u \triangleq t\cdot r$. The elegant analysis in [70] allows expressing the SER of M-PSK in closed form as

$$\begin{aligned} P_s(e) = \phi_{\frac{1}{R}\frac{\lambda}{t}\frac{S}{N}}\big(-g_{\text{PSK}}\big)\Bigg[&\frac{1}{2\sqrt{\pi}}\frac{\Gamma(u+1/2)}{\Gamma(u+1)}\,{}_2F_1\left(u,1/2;u+1;\left(1+\frac{g_{\text{PSK}}}{R}\frac{\gamma}{t}\frac{S}{N}\right)^{-1}\right) \\ &+\frac{\sqrt{1-g_{\text{PSK}}}}{\pi}\,F_1\left(1/2,u,1/2-u;3/2;\frac{1-g_{\text{PSK}}}{1+\frac{g_{\text{PSK}}}{R}\frac{\gamma}{t}\frac{S}{N}},1-g_{\text{PSK}}\right)\Bigg] \end{aligned} \tag{4.13}$$

where ${}_2F_1(a,b;c;x)$ is the generalised hypergeometric function with 2 parameters of type 1 and 1 parameter of type 2 [44] (§9.14.1); it is sometimes referred to as the Gauss hypergeometric function [44] (§9.14.2). The function $F_1(a,b,b';c;x,y)$ is a hypergeometric function of two variables [44] (§9.180.1); it is sometimes referred to as the Appell hypergeometric function. To simplify subsequent analysis, eq. (4.13) is denoted as $P_{\text{PSK}}(u,t,R,\gamma,S/N,M)$. Similarly, the SER of M-QAM is shown to be [70]

$$\begin{aligned} P_s(e) = \phi_{\frac{1}{R}\frac{\lambda}{t}\frac{S}{N}}\big(-g_{\text{QAM}}\big)&\frac{2q}{\sqrt{\pi}}\frac{\Gamma(u+1/2)}{\Gamma(u+1)}\,{}_2F_1\left(u,1/2;u+1;\left(1+\frac{g_{\text{QAM}}}{R}\frac{\gamma}{t}\frac{S}{N}\right)^{-1}\right) \\ -\phi_{\frac{1}{R}\frac{\lambda}{t}\frac{S}{N}}\big(-2g_{\text{QAM}}\big)&\frac{2q^2}{\pi(2u+1)}\,F_1\left(1,u,1;u+3/2;\frac{1+\frac{g_{\text{QAM}}}{R}\frac{\gamma}{t}\frac{S}{N}}{1+2\frac{g_{\text{QAM}}}{R}\frac{\gamma}{t}\frac{S}{N}},1/2\right) \end{aligned} \tag{4.14}$$

To simplify subsequent analysis, eq. (4.14) is denoted as $P_{\text{QAM}}(u,t,R,\gamma,S/N,M)$.

The M-QAM SERs are plotted for communication scenarios with different spectral efficiency throughout Figures 4.4−4.7. The Monte-Carlo simulations have been accomplished with the previously described C++ simulation platform, where the simple case of a single sub-carrier has been simulated.

The mathematical software used is Matlab which contains the Gauss hypergeometric function ${}_2F_1$. It is, however, very difficult to use; furthermore, it does not include the Appell hypergeometric function $F_1$. Both functions have hence been implemented by the author, where their series representations have been utilised, i.e. [44] (§9.14.1)

$$ {}_2F_1(a,b;c;x) = \sum_{n=1}^{\infty} \frac{\left(a\right)_n \left(b\right)_n}{\left(c\right)_n n!} x^n \tag{4.15} $$

and [44] (§9.180.1)

$$ F_1(a,b,b';c;x,y) = \sum_{n=1}^{\infty} \sum_{k=1}^{\infty} \frac{\left(a\right)_{n+k} \left(b\right)_n \left(b'\right)_k}{\left(c\right)_{n+k} n!k!} x^n y^k \tag{4.16} $$

where

$$ \left(a\right)_n \triangleq \frac{\Gamma(a+n)}{\Gamma(a)} \tag{4.17} $$

is the Pochhammer symbol [44] (page x1iii). All sums have been truncated after 11 terms, which was found to yield a high precision over the entire SNR range under consideration.

Figure 4.4 depicts the SER versus the SNR in [dB] labelled on the number of receive antennas for transmission schemes exhibiting a spectral efficiency of 2 bits/s/Hz. Here, the solid lines represent the analytically derived SER, whereas the markers correspond to specific points obtained by means of Monte-Carlo simulations. For all configurations, the simulations clearly corroborate the analytical results. Furthermore, increasing the number of receive antennas obviously enhances the performance of the transceiver.

The reader is reminded that STBCs do not provide any coding gain, but only diversity gain. From the analysis on O-MIMO channels (c.f. Chapter 2), the diversity gain is known to saturate with an increasing number of total antenna elements. This is once again corroborated by means of Figure 4.4. Having only one receive antenna, i.e. $r = 1$, the diversity gain provided by the half-rate STBC outweighs the loss in transmission rate. For example, to achieve a SER of $10^{-5}$, the full-rate QPSK scheme requires 30dB, whereas the half-rate 16-QAM scheme with 4 transmit antennas needs only 25dB, thereby saving 5dB transmission power. With four receive antennas, however, diversity is already saturated (fairly) independent of the number of transmit antennas. That explains why the full-rate scheme now outperforms the half-rate schemes. For example, to achieve a SER of $10^{-5}$, the full-rate QPSK scheme requires 10dB, whereas the half-rate 16-QAM scheme with 4 transmit antennas needs 2.5dB more transmission power.

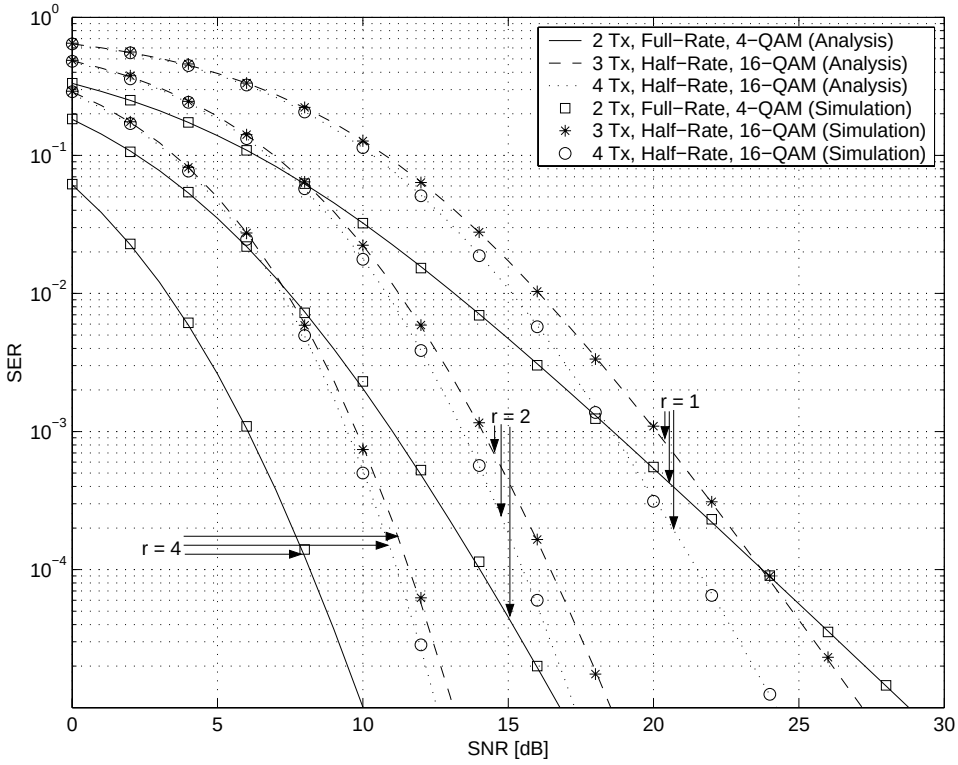


Figure 4.4: SER versus SNR labelled on the number of receive antennas for systems operating at 2 bits/s/Hz.

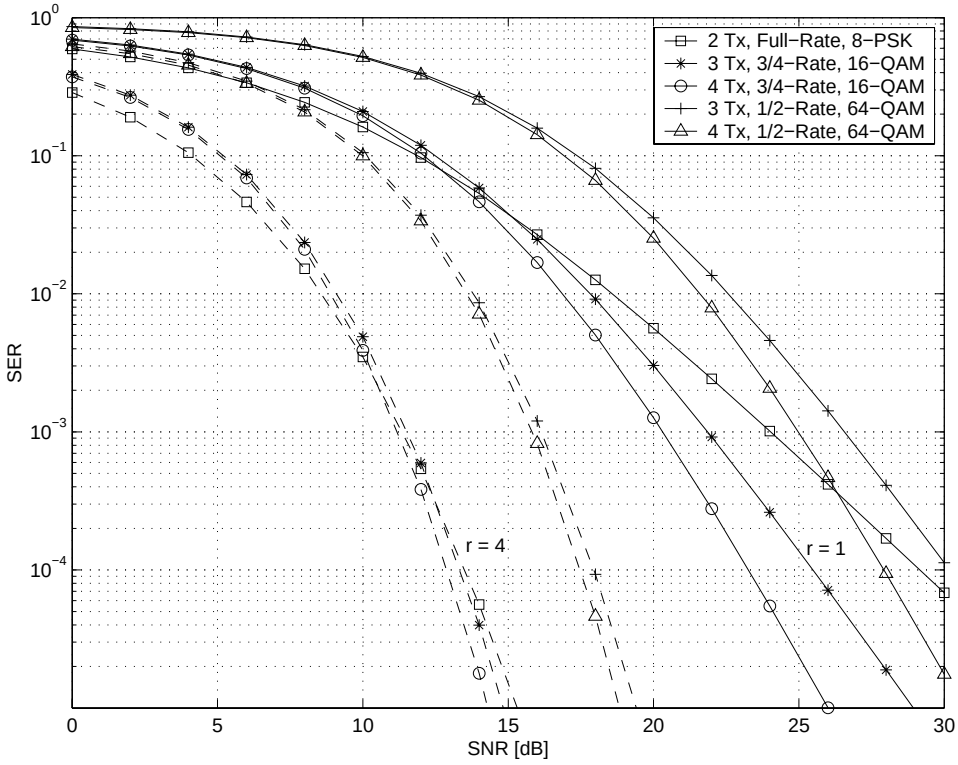


Figure 4.5: SER versus SNR labelled on the number of receive antennas for systems operating at 3 bits/s/Hz.

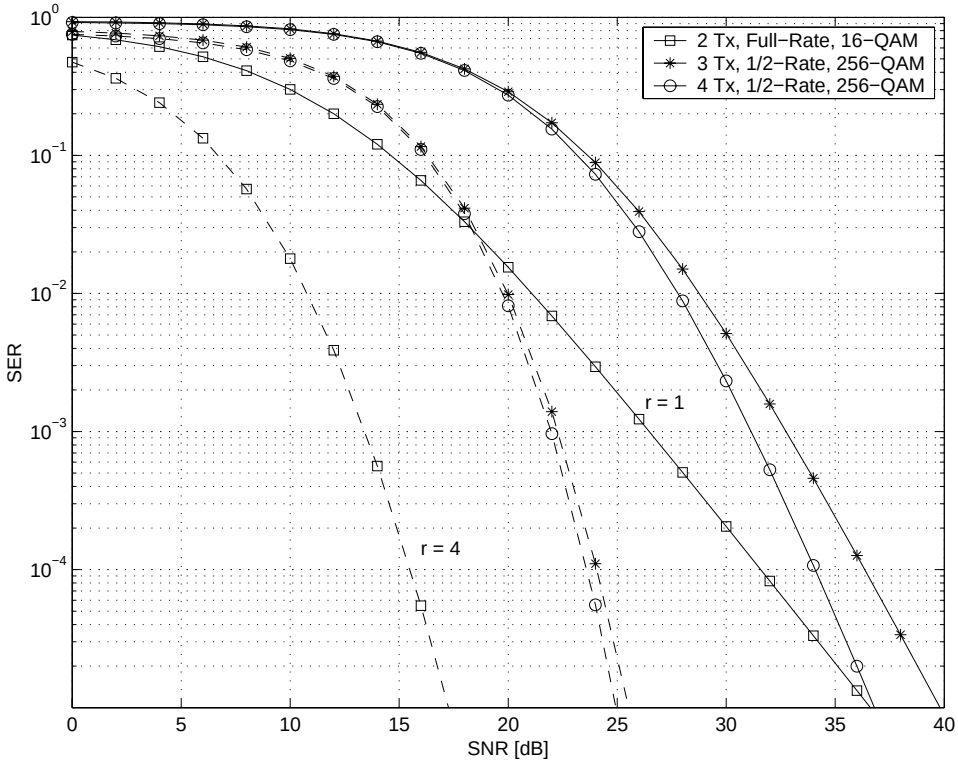


Figure 4.6: SER versus SNR labelled on the number of receive antennas for systems operating at 4 bits/s/Hz.

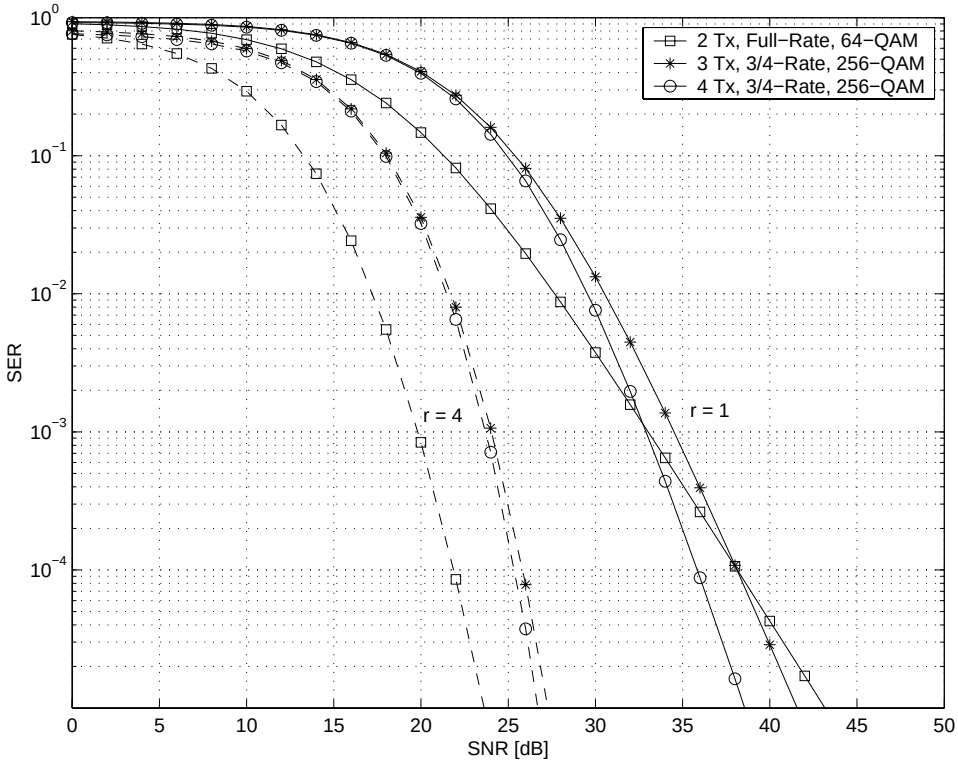


Figure 4.7: SER versus SNR labelled on the number of receive antennas for systems operating at 6 bits/s/Hz.

Figure 4.5 depicts the SER versus the SNR [dB] labelled on the number of receive antennas for transmission schemes exhibiting a spectral efficiency of 3 bits/s/Hz. Although not shown here, the Monte-Carlo simulations coincide again with the analytical results. The same explanations as above hold to explain the tendencies of the performance curves. Clearly, the 3/4-rate STBC outperforms any other code for a low number of receive antennas, whereas the full rate code performs almost as good as the 3/4-rate code.

Similar conclusions can be drawn for Figure 4.6 and Figure 4.7, which depict transmission schemes with a spectral efficiency of 4 bits/s/Hz and 6 bits/s/Hz, respectively.

**Rayleigh Fading - Unequal Sub-Channel Gains**

In Chapter 2, eq. (2.75), the MGF was shown to be

$$\phi_{\frac{1}{R}\frac{\lambda}{t}\frac{S}{N}}(s) = \sum_{i=1}^{u} K_i \cdot \phi_{\frac{1}{R}\frac{\lambda_i}{t}\frac{S}{N}}(s) \tag{4.18}$$

with constants $K_i$

$$K_i = \prod_{i'=1, i' \neq i}^{u} \frac{\gamma_i}{\gamma_i - \gamma_{i'}} \tag{4.19}$$

where $\gamma_i$ is the average channel gain of the $i^{th}$ path. This allows one to derive the closed form SER for distributed STBCs, where all the channel gains differ. With the simplified notation, the respective error rates can be expressed as

$$P_s(e) = \sum_{i=1}^{u} K_i \cdot P_{\text{PSK/QAM}}(1, t, R, \gamma_i, S/N, M) \tag{4.20}$$

These are illustrated in Figure 4.8 and Figure 4.9, the equivalent scenarios to which have already been dealt with in Section 2.4.2.

Explicitly, Figure 4.8 depicts the SER versus the SNR in [dB] for the distributed Alamouti scheme with one receive antenna only. As before, the power of the unequal channel coefficients is chosen such that $\gamma_1 + \gamma_2 \equiv 2$ and $\gamma_1 : \gamma_2 = 2 : 1$, i.e. $\gamma_1 = 4/3$ and $\gamma_2 = 2/3$. The cases are depicted where only the channel with power $\gamma_1$ is utilised, and where only the channel with power $\gamma_2$ is utilised, and where the distributed Alamouti STBC is utilised. The latter is corroborated by numerical simulations.

Clearly, the distributed scenario provides the diversity gain even for this case of unbalanced channel gains, whereas the single links exhibit a less steep error curve. The gain of the distributed case at a SER of $10^{-5}$ mounts to approximately 20dB. The large value is due to the fact that the current transceiver structure does not operate at the capacity limit. If it operated at capacity limit, then the gain would have been only 3dB over the weaker link, as predicted by Figure 2.14.

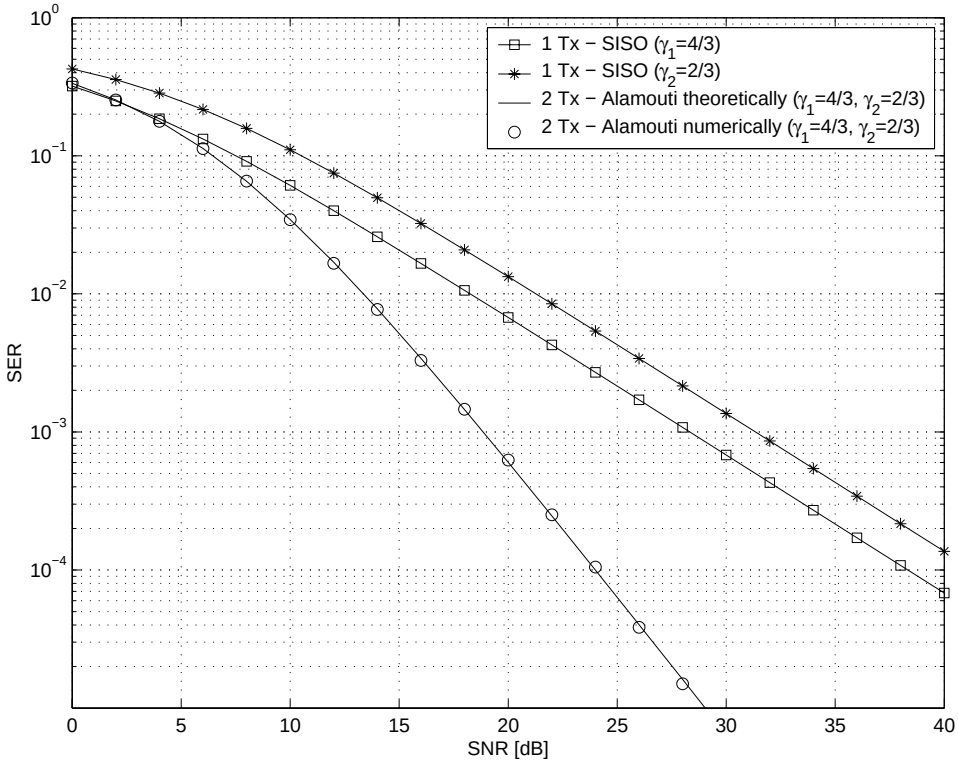


Figure 4.8: SER versus SNR for a distributed Alamouti system operating at 2 bits/s/Hz; $\gamma_1 + \gamma_2 \equiv 2$ and $\gamma_1 : \gamma_2 = 2 : 1$.

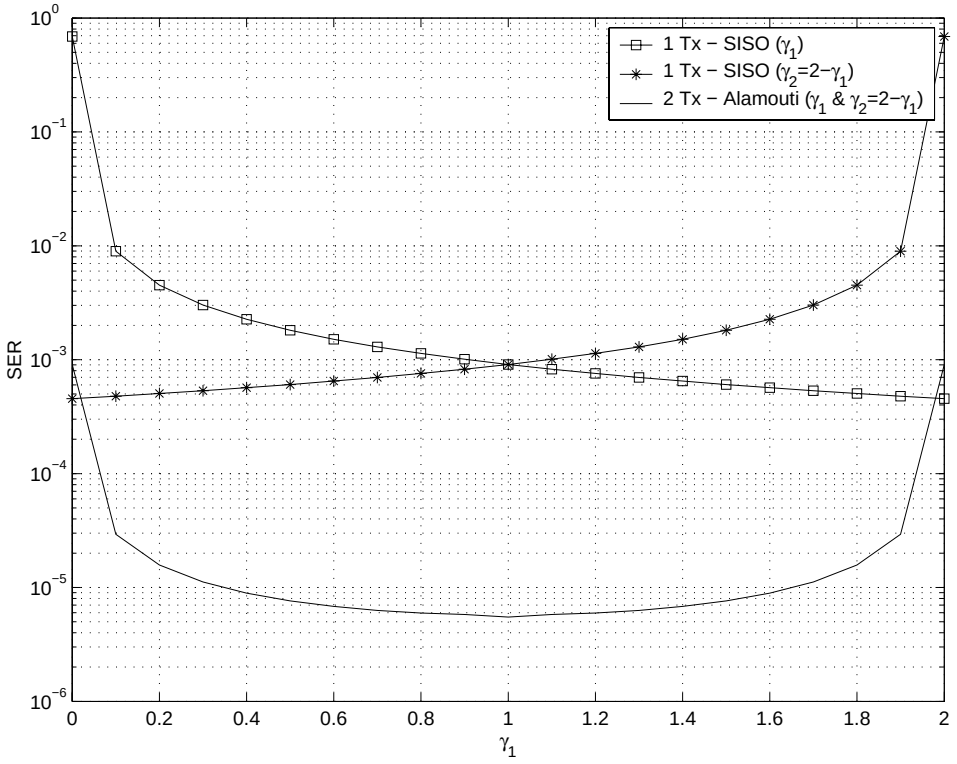


Figure 4.9: SER versus the normalised power $\gamma_1$ in the first link for a distributed Alamouti system operating at 2 bits/s/Hz; SNR=30dB and $\gamma_2 = 2 - \gamma_1$.

Figure 4.9 depicts the SER versus the normalised power $\gamma_1$ in the first link for the distributed Alamouti scheme with an SNR of 30dB. Furthermore, depicted are the cases where communication happens only over either of the single links, where $\gamma_2 = 2 - \gamma_1$. The SER of the distributed case are found to be two decades better than any of the single links, for most of the scenarios. Similar observations can be made for higher order STBCs. The simple example demonstrates the advantages of distributed communication networks operating with transceivers of finite complexity.

**Rayleigh Fading - Generic Sub-Channel Gains**

To remind the reader, in this case there are $g \leq u$ distinct sub-channel gains, which are were referred to as $\hat{\gamma}_{i\in(1,g)}$ with each of them being repeated $\nu_{i\in(1,g)}$ times. In this case, the MGF was shown to be

$$\phi_{\frac{1}{R}\frac{\lambda}{t}\frac{S}{N}}(s) = \sum_{i=1}^{g}\sum_{j=1}^{\nu_g} K_{i,j} \cdot \phi^j_{\frac{1}{R}\frac{\hat{\lambda}_i}{t}\frac{S}{N}}(s) \tag{4.21}$$

where the coefficients $K_{i,j}$ are given in (2.81). The respective error rates are hence expressed as

$$P_s(e) = \sum_{i=1}^{g}\sum_{j=1}^{\nu_g} K_{i,j} \cdot P_{\text{PSK/QAM}}(j, t, R, \hat{\gamma}_i, S/N, M) \tag{4.22}$$

which is not further illustrated.

**Nakagami Fading - Equal Sub-Channel Gains**

Given a Nakagami fading factor $f$, the respective error rates can be similarly derived as above with the MGF given through (2.87), which yields

$$P_s(e) = P_{\text{PSK/QAM}}(fu, ft, R, \gamma, S/N, M) \tag{4.23}$$

which is illustrated in Figure 4.10 and Figure 4.11.

Explicitly, Figure 4.10 depicts the performance of the scenario already discussed in Chapter 2 by means of Figure 2.18. The SER versus SNR in [dB] for various communication scenarios is shown utilising 4-QAM (QPSK) and two receive antennas. The cases with and without Alamouti transmit diversity are compared for $f = 1$ (Rayleigh) and $f = 10$ (strong LOS), as well as the performance over a Gaussian channel. Similar to the capacity, the Nakagami fading factor $f$ can be traded against the number of antenna elements involved. This is obvious as the STBC communication system only provides diversity gain, which is not required for strong LOS scenarios. For example, having one transmit antenna under strong LOS conditions ($f = 10$) yields a 5dB power gain over a scenario with two transmit and nLOS conditions ($f = 1$) at a SER of $10^{-5}$.

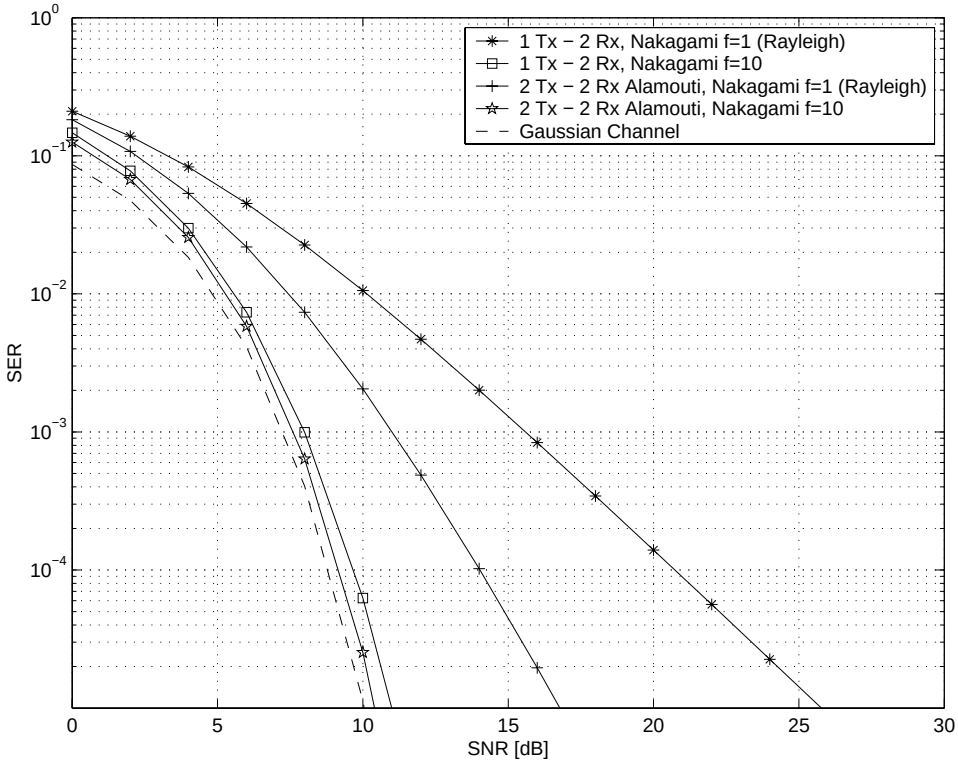


Figure 4.10: SER versus SNR for a distributed Alamouti system operating at 2 bits/s/Hz; $\gamma_1 + \gamma_2 \equiv 2$ and $\gamma_1 : \gamma_2 = 2 : 1$.

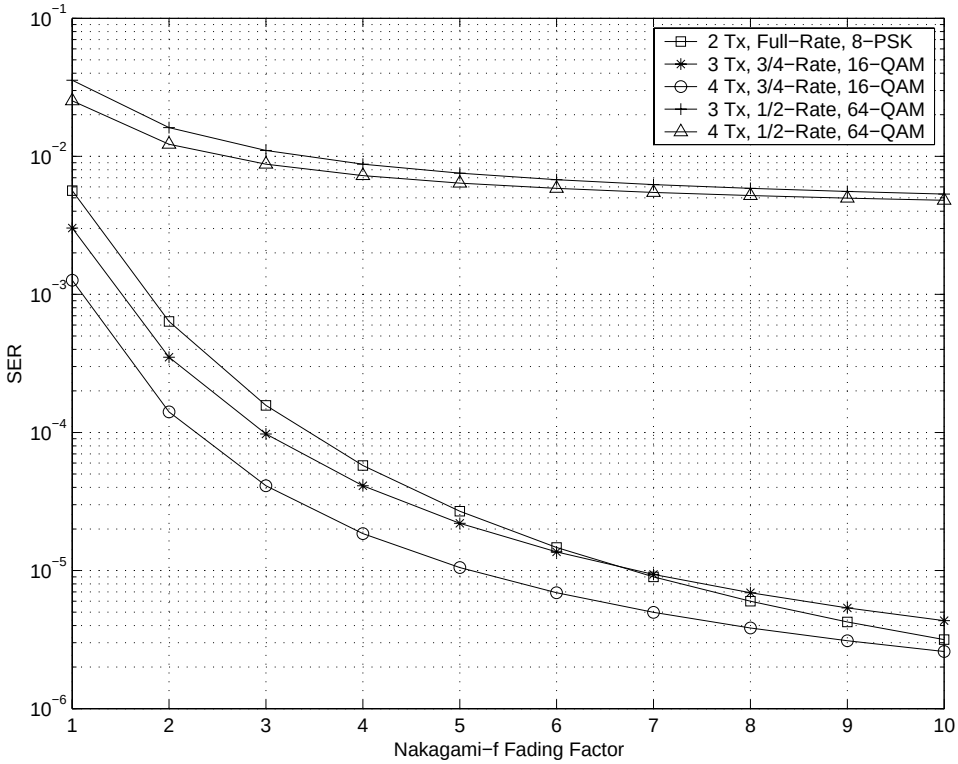


Figure 4.11: SER versus the Nakagami fading parameter $f$ for systems operating at 3 bits/s/Hz; SNR=20dB.

Figure 4.11 depicts the SER versus the Nakagami fading parameter $f$ for systems with one receive antenna operating at 3 bits/s/Hz and an SNR of 20dB. With reference to Figure 4.5, it is obvious that the diversity gain saturates very fast with increasing $f$, and the robustness offered by lower modulation schemes becomes more predominant. Therefore, the SERs of the half-rate 64-QAM schemes are inferior to the SERs of the 3/4-rate and full-rate schemes. It can also be observed that at a Nakagami fading factor $f = 7$ the performance of the 16-QAM 3/4-rate scheme with three transmit antennas equates the performance of the full-rate 8-PSK scheme, enforcing the above statement. It can be expected that for $f > 10$, the full-rate code outperforms any of the other STBCs.

**Nakagami Fading - Unequal Sub-Channel Gains**

Finally, the respective error rates for a Nakagami fading channel with different sub-channel gains $\gamma_{i\in(1,u)}$ and different fading factors $f_{i\in(1,u)}$ can be derived from (2.90) as

$$P_s(e) = \sum_{i=1}^{u} \sum_{j=1}^{f_i} K_{i,j} \cdot P_{\text{PSK/QAM}}(j, jt, R, \gamma_i, S/N, M) \tag{4.24}$$

where the coefficients $K_{i,j}$ are obtained by performing partial fractions on (2.90). This case is not further illustrated here.

**Nakagami Fading - Generic Sub-Channel Gains**

The respective SERs for the case of generic sub-channel coefficients is similarly obtained as for the Rayleigh channel with unequal sub-channel gains, and is thus also omitted here.

### 4.3.2 Bit Error Rates

The derived dependencies relate the average transmitted signal power to the SER. The exact BER of generic M-PSK and M-QAM schemes, however, is difficult to obtain. Analysis is greatly simplified if the bits are Gray-mapped onto the symbol, i.e. adjacent symbol constellation points differ only by one bit [47]. In that case, the BER $P_b(e)$ is easily related to the SER via [47]

$$P_b(e) \approx \frac{P_s(e)}{\log_2(M)} \tag{4.25}$$

at low BERs or SERs.

The performance of the numerically obtained exact BERs are compared with the approximate BERs given by (4.25) in Figure 4.12. Simulated is a system equivalent to Figure 4.4, i.e. with a spectral efficiency of 2 bits/s/Hz. The exact and approximate BERs clearly converge for an increasing SNR.

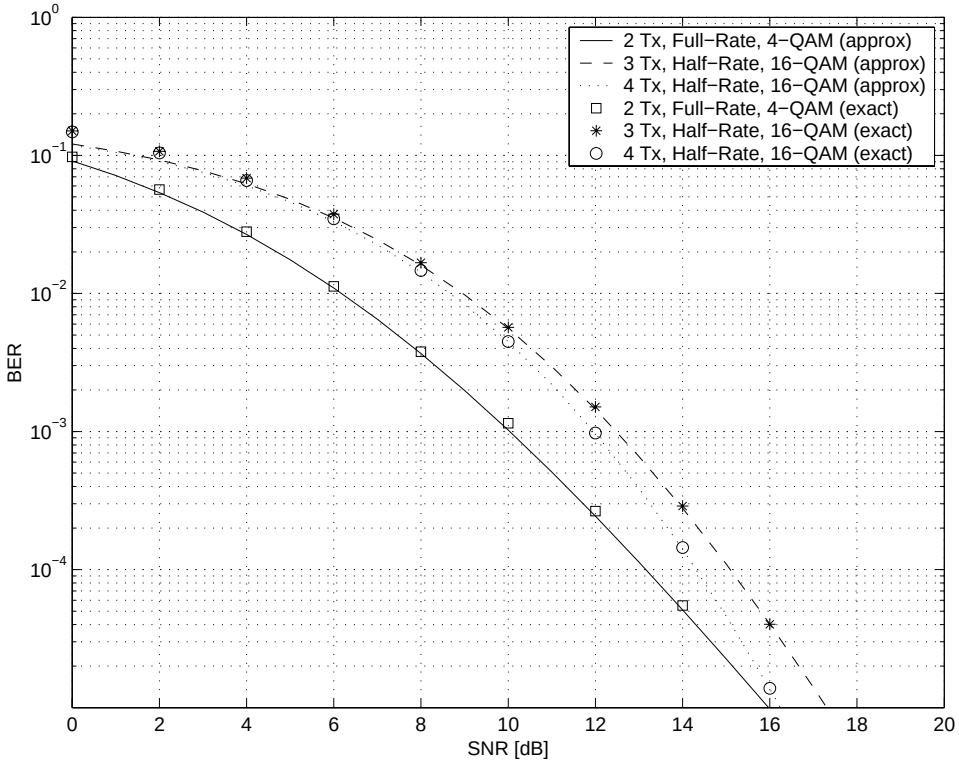


Figure 4.12: Exact and approximate BER versus SNR for systems with two receive antennas operating at 2 bits/s/Hz.

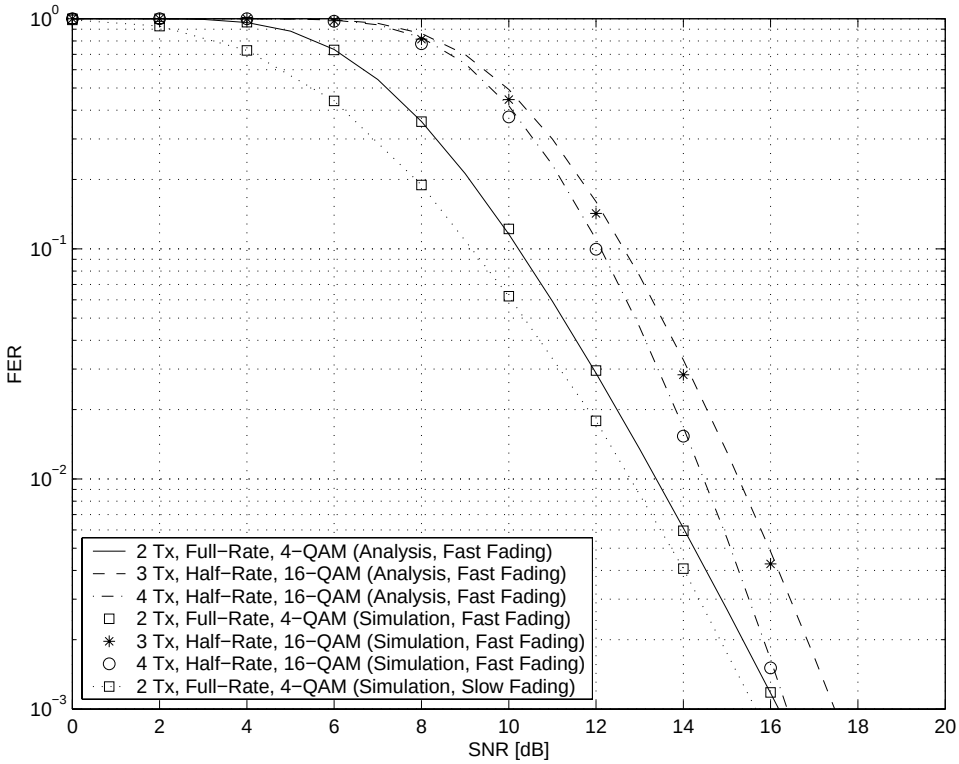


Figure 4.13: Exact (simulation) and approximate (analysis) FER versus SNR for systems with two receive antennas operating at 2 bits/s/Hz over fast-fading channels.

### 4.3.3 Frame Error Rates

A frame is assumed to consist of $B$ bits which, when transmitted, forms $D = B/\log_2(M)$ symbols. A frame error occurs if at least one of the $D$ symbols is in error. Since transmission happens over a wireless fading channel, the FER needs to be conditioned on the random channel realisations $\boldsymbol{\rho} \triangleq (\rho_1, \ldots, \rho_D)$ at each of the $D$ symbols. A $D$-dimensional integration with respect to the joint pdfs of $\rho_{i\in(1,D)}$ then yields the FER, i.e.

$$P_f(e) = \int_0^\infty P_f(e|\boldsymbol{\rho})\, pdf_{\boldsymbol{\rho}}(\boldsymbol{\rho})\, d\boldsymbol{\rho} \tag{4.26}$$

Due to the channel induced memory, a closed form of (4.26) is difficult to obtain. The memoryless space-time block encoding and the memoryless fading channel used here, however, allows one to assume that occurring symbol errors are independent, which yields for the FER

$$P_f(e) = 1 - \int \cdots \int_{\boldsymbol{\rho}} \prod_{i=1}^{D} \big(1 - P_s(e|\rho_i)\big) \cdot pdf_{\rho_1}(\rho_1) \ldots pdf_{\rho_D}(\rho_D)\, d\rho_1 \ldots d\rho_D \tag{4.27}$$

Performing the integrations finally results in $P_f(e) = 1 - \big(1 - P_s(e)\big)^D$. Note that the derived FER also holds for ergodic fading channels with memory for $D \to \infty$. The derived FER also holds approximately for fast fading channels with $D \cdot T_s \gg T_c$, where $T_s$ is the symbol duration and $T_c$ is the channel coherence time. It also holds for slow fading channels with time interleavers of sufficient depth, which may span over several frames. The role of the interleaver is to break the memory introduced by the slow fading channel, and therefore make it appear fast fading.

The FER is illustrated in Figure 4.13 versus the SNR for systems operating at 2 bits/s/Hz with two receive antennas over fast fading channels. The frame length has been chosen to be $B = 100$ bits; the QPSK modulated frame is therefore $D = 50$ symbols long, whereas the 16-QAM frame only $D = 25$ symbols. Clearly, the QPSK full-rate STBC matches the numerically obtained FER almost entirely. The 16-QAM half-rate STBCs, however, slightly deviate from the exact results, which is due to $D \cdot T_s$ not being sufficiently greater than $T_c$.

For completeness, one FER curve in Figure 4.13 corresponds to the quasi-static case (slow fading without interleaver) of an Alamouti transmitter with two receive antennas. Here, the channel was kept constant over the entire frame of $D = 50$ symbols. The quasi-static (slow) fading case clearly outperforms the ergodic (fast) fading case. To explain this, note that (4.26) can be written as $P_f(e) = \mathrm{E}_{\boldsymbol{\rho}}\{P_f(e|\boldsymbol{\rho})\} = \mathrm{E}_{\boldsymbol{\rho}}\{f(P_s(e|\boldsymbol{\rho}))\}$, where the function $f(\cdot)$ relating $P_f(e|\boldsymbol{\rho})$ with $P_s(e|\boldsymbol{\rho})$ can be shown to be a concave function in its argument. This allows Jensen's inequality [21] to be invoked to arrive at $P_f(e) = \mathrm{E}_{\boldsymbol{\rho}}\{f(P_s(e|\boldsymbol{\rho}))\} \leq f(\mathrm{E}_{\boldsymbol{\rho}}\{P_s(e|\boldsymbol{\rho})\}) = 1 - \big(1 - P_s(e)\big)^D$, which indicates that the FER of a memoryless signal over arbitrary channels is smaller than over an ergodic channel.

## 4.4 Maximum Throughput for End-to-End Transmission

The error rates obtained in the previous section are utilised here to derive fractional resource allocation rules assuming that a decision on the correctness of the received signal is done at the t-MT. This should not be confused with transparent relaying, where the information is simply amplified and forwarded. It is also in contrast to a stage-by-stage detection, where a decision on the correctness of the received signal is done at each stage; this case will be dealt with in Section 4.5.

If all r-MTs per stage cooperate and cooperation takes places at a sufficiently high SNR, then the signal samples from the previous stage are the same for all r-MTs. Therefore, if an error occurs in the signal from the previous stage, then that error is the same in all r-MTs belonging to the same stage. This applies not only for STBCs, but for any type of coding chosen.

Such a scenario provides a great simplification to analysis, since the errors in consecutive stages become independent. This is in contrast to a generic relaying process with partial cooperation (clustering), where one r-MT may have a more reliable estimate than another r-MT in the same relaying VAA, leading to error-dependencies between the stages.

Subsequently, the problem of maximising the end-to-end throughput is shown to be equivalent to the problem of minimising the end-to-end BER. The fractional resource allocation rules are then derived for the cases of full and partial cooperation.

### 4.4.1 Problem Simplification

It is assumed here that the source MT (s-MT) transmits $B$ bits per frame to the target MT (t-MT) via $K$ relaying stages. With reference to (3.38), the normalised end-to-end throughput can be expressed as

$$\Theta = \min_{v\in(1,K)} \left\{\alpha'_v R_v \log_2(M_v)\right\} \cdot \left(1 - P_{f,\mathrm{e2e}}(e)\right) \tag{4.28}$$

where $\alpha'_v$, $R_v$ and $M_v$ are the fractional frame duration, STBC rate and modulation index of the $v^{th}$ stage respectively, and $P_{f,\mathrm{e2e}}(e)$ is the end-to-end FER.

Eq. (4.28) has to be understood as follows. If there were no losses between a directly communicating s-MT and t-MT, then all of the $B$ bits reach the receiver; the throughput normalised by the total number of sent bits hence amounts to 1. The use of a modulation scheme with index $M$ and a STBC with rate $R$ during a fractional frame duration $\alpha'$ to accomplish such link results in a throughput, normalised by the utilised time and frequency, as $1 \cdot \alpha' \cdot R \cdot \log_2(M)$ [bits/s/Hz]. It is then diminished by the loss caused by the end-to-end FER $P_{f,\mathrm{e2e}}(e)$. For a communication system with $K$ relaying stages, the weakest link in the chain determines the throughput, hence $\min_{v\in(1,K)}\left\{\alpha'_v R_v \log_2(M_v)\right\}$. It is thus the aim to derive optimum resource allocation strategies, which maximise the end-to-end throughput.

To this end, note that $P_{f,\mathrm{e2e}}(e)$ is a function of $M_{v\in(1,K)}$ and $R_{v\in(1,K)}$ (hence also $\min_{v\in(1,K)}\{\alpha'_v R_v \log_2(M_v)\}$) and the fractional transmission power allocated to each stage. Optimising (4.28) w.r.t. these parameters is very complex, which is the reason why the optimisation process is performed in three stages.

First, the modulation indices $M_{v\in(1,K)}$ are fixed and the limiting case where SNR$\rightarrow\infty$ is considered. This reduces (4.28) to

$$\Theta = \min_{v\in(1,K)} \left\{\alpha'_v R_v \log_2(M_v)\right\} \tag{4.29}$$

where the fractional frame durations $\alpha'_v$ need to be chosen such as to maximise $\Theta$ under constraint $\sum_{v=1}^{K} \alpha'_v = 1$. This is clearly achieved by equating all $\alpha'_v R_v \log_2(M_v)$, which results in

$$\alpha'_v = \frac{\prod_{w=1,w\neq v}^{K} R_w \cdot \log_2(M_w)}{\sum_{k=1}^{K}\prod_{w=1,w\neq k}^{K} R_w \cdot \log_2(M_w)} \tag{4.30}$$

Second, it is shown now that under the current assumptions the throughput is maximised by minimising the end-to-end BER. To this end, the normalised throughput is expressed in terms of the end-to-end BER $P_{b,\mathrm{e2e}}(e)$ which, assuming independent bit errors, gives

$$\Theta = \min_{v\in(1,K)} \left\{\alpha'_v R_v \log_2(M_v)\right\} \cdot \left(1 - P_{b,\mathrm{e2e}}(e)\right)^B \tag{4.31}$$

Defining a non-decreasing (in $\Theta$) metric

$$\Theta' \triangleq \exp\left[\frac{\log\left(\Theta / \min_{v\in(1,K)}\left\{\alpha'_v R_v \log_2(M_v)\right\}\right)}{B}\right] - 1 \tag{4.32}$$

it can easily be shown that

$$\Theta' \approx -P_{b,\mathrm{e2e}}(e) \tag{4.33}$$

Therefore, to maximise the end-to-end throughput, one has to minimise the end-to-end bit error rate by optimally assigning fractional transmission power to each relaying stage. The BER at each stage is related with the occurring SER via (4.25), where for low error rates one symbol error causes one bit error.

Third, the optimum modulation order $M_{v\in(1,K)}$ has to be determined in dependency of the previously derived fractional resource allocations. This is easily done by permuting all possible modulation orders at each stage such as to maximise the end-to-end throughput. Since the number of modulation orders will be limited, such optimisation is feasible without consuming too much computational power.

Subsequently, the second step is performed assuming either total or partial (clustered) cooperation in each stage. The near-optimum fractional power allocation rules are first derived, then assessed in terms of their precision; finally, the maximum achievable throughput will be illustrated by means of a few examples.

### 4.4.2 Full Cooperation at each Stage

Under the assumption of full cooperation, each of the $K$ relaying stages experiences independent BERs $P_{b,v\in(1,K)}(e)$ caused by independent SERs $P_{s,v\in(1,K)}(e)$. A bit from the s-MT is received correctly at the t-MT only when at all stages the bit has been transmitted correctly[3]. The end-to-end BER can therefore be expressed as

$$P_{b,\mathrm{e2e}}(e) = 1 - \prod_{v=1}^{K}\big(1 - P_{b,v}(e)\big) \tag{4.34}$$

which, at low BERs at every stage, can be approximated as

$$\begin{aligned} P_{b,\mathrm{e2e}}(e) &\approx \sum_{v=1}^{K} P_{b,v}(e) && (4.35)\\ &\approx \sum_{v=1}^{K} \frac{P_{s,v}(e)}{\log_2(M_v)} && (4.36) \end{aligned}$$

where $M_v$ is the modulation order at the $v^{th}$ stage. Further analysis concentrates on the case of Rayleigh fading with equal channel gains per relaying stage; other cases are a straightforward extension to the exposed analysis. Assuming that each stage is allocated a fractional power $\beta'_v$, the above-given dependency can be expressed as

$$P_{b,\mathrm{e2e}}(e) \approx \sum_{v=1}^{K} \frac{P_{s,v}\big(u_v, t_v, R_v, \gamma_v, \beta'_v \cdot S/N, M_v\big)}{\log_2\big(M_v\big)} \tag{4.37}$$

where the SERs $P_{s,v}(\cdot) = P_{\mathrm{PSK/QAM}}(\cdot)$ are given through (4.13) and (4.14), respectively. Furthermore, $u_v \triangleq t_v \cdot r_v$, $t_v$ and $r_v$ are the number of transmit and receive antennas in the $v^{th}$ stage, $R_v$ is the rate of the STBC, $\gamma_v$ is the average attenuation experienced, $S$ is the total power given to deliver the information from source to sink, and $N$ is the noise power.

The optimisation process has only to be performed w.r.t. the fractional power allocation $\beta'_{v\in(1,K)}$. Even so, the optimisation process is very intricate. To simplify analysis further, an upper bound to the derived SERs for M-PSK and M-QAM is invoked. To this end, the integrant of (4.10) is upper-bounded by its largest argument, which occurs at $\theta = \pi/2$. The SER for M-PSK in the $v^{th}$ relaying stage is hence upper-bounded as

$$P_{s,v}(e) \leq \frac{\frac{M_v-1}{M_v}}{\left(1 + \beta'_v \frac{g_{\mathrm{PSK},v}}{R_v}\frac{\gamma_v}{t_v}\frac{S}{N}\right)^{u_v}} \tag{4.38}$$

where $g_{\mathrm{PSK},v} = \sin^2(\pi/M_v)$. The end-to-end BER for an M-PSK modulation scheme can finally be upper-bounded as

$$P_{b,\mathrm{e2e}}(e) \leq \sum_{v=1}^{K} \frac{M_v - 1}{M_v \log_2(M_v)} \left(1 + \beta'_v \frac{g_{\mathrm{PSK},v}}{R_v}\frac{\gamma_v}{t_v}\frac{S}{N}\right)^{-u_v} \tag{4.39}$$

[3]The cases where two or more wrong bits may result again in a correct bit is neglected here.

Following a similar approach, the upper bound for the end-to-end BER of an M-QAM modulation can be derived as

$$P_{b,\mathrm{e2e}}(e) \leq \sum_{v=1}^{K} \frac{2q_v}{\log_2(M_v)} \left[ \left(1 + \beta'_v \frac{g_{\mathrm{QAM},v}}{R_v} \frac{\gamma_v}{t_v} \frac{S}{N}\right)^{-u_v} + \frac{q_v}{2} \left(1 + 2\beta'_v \frac{g_{\mathrm{QAM},v}}{R_v} \frac{\gamma_v}{t_v} \frac{S}{N}\right)^{-u_v} \right] \tag{4.40}$$

$$\lessapprox \sum_{v=1}^{K} \frac{2q_v}{\log_2(M_v)} \left(1 + \beta'_v \frac{g_{\mathrm{QAM},v}}{R_v} \frac{\gamma_v}{t_v} \frac{S}{N}\right)^{-u_v} \tag{4.41}$$

where $g_{\mathrm{QAM},v} = 3/2/(M_v - 1)$ and $q_v = 1 - 1/\sqrt{M_v}$. Note that in (4.41) the second summand appearing in (4.40) was neglected due to $q_v/2 < 1$ and $(1+2x)^{-u_v}$ being much less than $(1+x)^{-u_v}$ for $x$ sufficiently large and $u_v \geq 1$. Either modulation scheme results in an upper bound unified below as

$$P_{b,\mathrm{e2e}}(e) \leq \sum_{v=1}^{K} A_v \left(1 + B_v \beta'_v\right)^{-u_v} \tag{4.42}$$

The constants $A_v$ and $B_v$ are obtained by comparing (4.42) with (4.39) or (4.41) to arrive at

$$A_v = \begin{cases} \frac{M_v - 1}{M_v \log_2(M_v)} & \text{for M-PSK} \\ \frac{2q_v}{\log_2(M_v)} & \text{for M-QAM} \end{cases} \tag{4.43}$$

and

$$B_v = \begin{cases} \frac{g_{\mathrm{PSK},v}}{R_v} \frac{\gamma_v}{t_v} \frac{S}{N} & \text{for M-PSK} \\ \frac{g_{\mathrm{QAM},v}}{R_v} \frac{\gamma_v}{t_v} \frac{S}{N} & \text{for M-QAM} \end{cases} \tag{4.44}$$

In Appendix 4.8 (Derivation I), it is shown that the fractional power allocations $\beta'_{v\in(1,K)}$ have to obey

$$\beta'_v \approx \left[ \sum_{w=1}^{K} \alpha'_w \left( \frac{u_v^{-1} A_v^{-1} B_v^{u_v}}{u_w^{-1} A_w^{-1} B_w^{u_w}} \right)^{\frac{1}{u_{\max}+1}} \right]^{-1} \tag{4.45}$$

where $u_{\max} = \arg\max(u_1, \ldots, u_K)$.

The performance of the developed algorithm is assessed by means of Figures 4.14−4.17 for M-QAM schemes only. Note that if reference is made to the non-optimised scenario, then only the fractional transmission power is meant not to be optimised since the frame duration is easily related to the modulation order.

Explicitly, Figure 4.14 depicts the end-to-end BER versus the SNR in the first link in [dB] for various 2-stage communication scenarios deploying the developed fractional power allocation strategy (4.45), which is also compared against a numerically obtained optimum and a non-optimum allocation.

The first scenario, where $t_{1,2} = r_{1,2} = 1$, $M_{1,2} = 4$ (QPSK) and $p = [0, 0]$dB, is entirely symmetric which leads to the same performance for all three allocation strategies. The second scenario is the same as the first, with the only difference that the channel in the second stage is now 10 times stronger than in the first stage, i.e. $p = [0, 10]$dB. The resulting non-symmetric scenario reveals a performance difference between the optimised (solid lines) and non-optimised (dashed line) power allocation.

It can be observed that the optimum and developed allocation strategy yield the same performance for any of the depicted configurations. Furthermore, the gain of an optimised system over a non-optimised system is highest for very asymmetric cases; here, for $t_1 = 2, r_1 = 2, t_2 = 2, r_2 = 1$, $M_1 = 256, M_2 = 64$ and $p = [0, 10]$dB. At a target end-to-end BER of $10^{-5}$, about 1dB in power can be saved.

Figure 4.15 is similar in its nature to Figure 4.14, with the only difference that a three-stage network is scrutinised. Similar observations can be made for these scenarios, where gains of almost 4dB can be observed. This corroborates the importance of the derived allocation strategy.

The throughput of a two-stage system is illustrated by means of Figure 4.16, which utilises the fractional resource allocation strategies (4.30) and (4.45). The system deployed has the number of bits fixed to $B = 100$; furthermore, for all configurations $M_{1,2} = 4$ (QPSK) and $p = [0, 10]$dB. It can be observed that in the region of low SNR, the developed allocation strategy performs worse than the optimum one. This is obvious, as the fractional frame durations have been derived assuming the SNR $\to \infty$.

For most of the transitional region from zero-throughput to maximum-throughput, however, the derived allocations yield near-optimum throughput. In contrast, no optimisation exhibits drastic losses in the transitional region. For example, given the scenario with $t_{1,2} = r_{1,2} = 2$ operating at an SNR in the first link of 6dB, around 0.4 bits/s/Hz are lost which mounts to approximately 40%.

Observe also that the cases of full-rate STBC in each stage yield the same maximum throughput, whereas the case with the 3/4-rate STBC has a lower maximum throughput, notwithstanding the fact that it has the strongest link with $(2 \times 4)/(4 \times 4)$. This is due to the limiting spectral efficiency of the STBC with a rate less than one. Clearly, the strength of the link determines the rate with which the system approaches the limiting throughput for the SNR $\to \infty$. This limit will be calculated in the consecutive section.

The precision of the fractional allocation algorithm for fixed modulation indexes allows a final numerical optimisation to be performed in each relaying stage over all possible modulation indexes. The low complexity of (4.30) and (4.45) guarantees that such optimisation comes at little additional computational power.

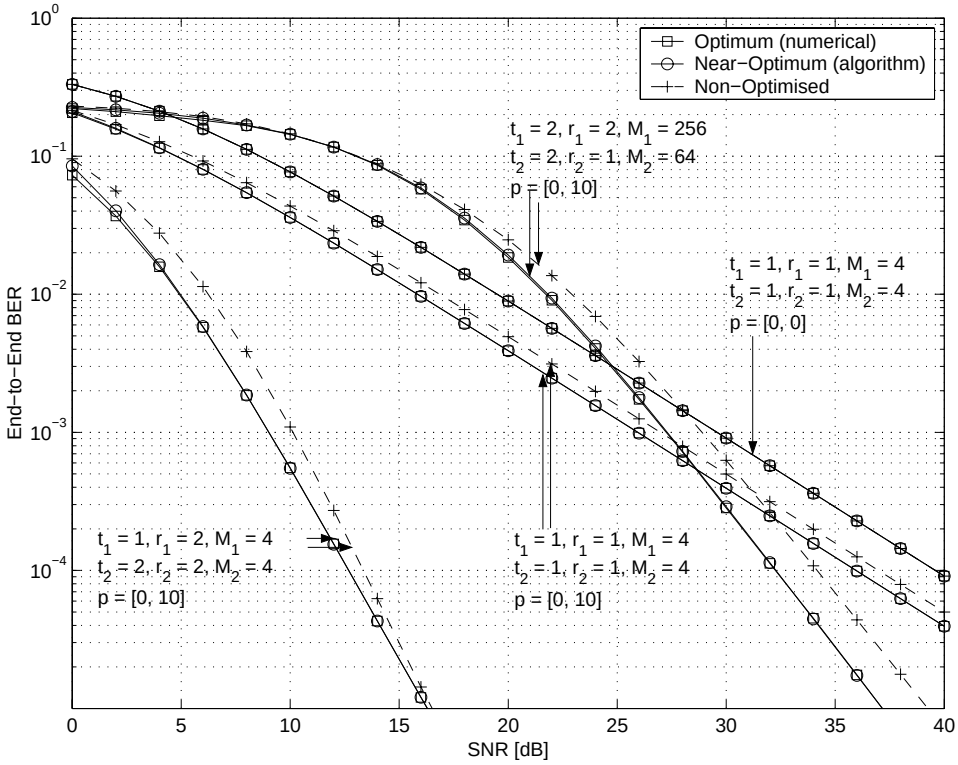


Figure 4.14: Comparison between optimum and near-optimum, as well as non-optimised end-to-end BER for various configurations of a two-stage relaying network.

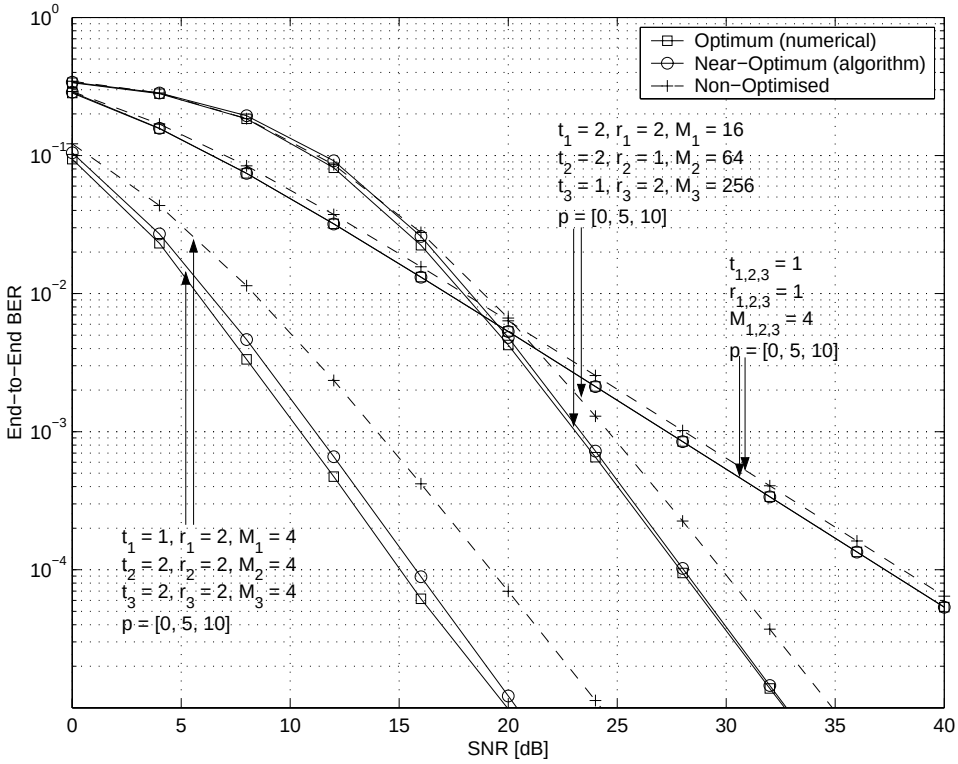


Figure 4.15: Comparison between optimum and near-optimum, as well as non-optimised end-to-end BER for various configurations of a three-stage relaying network.

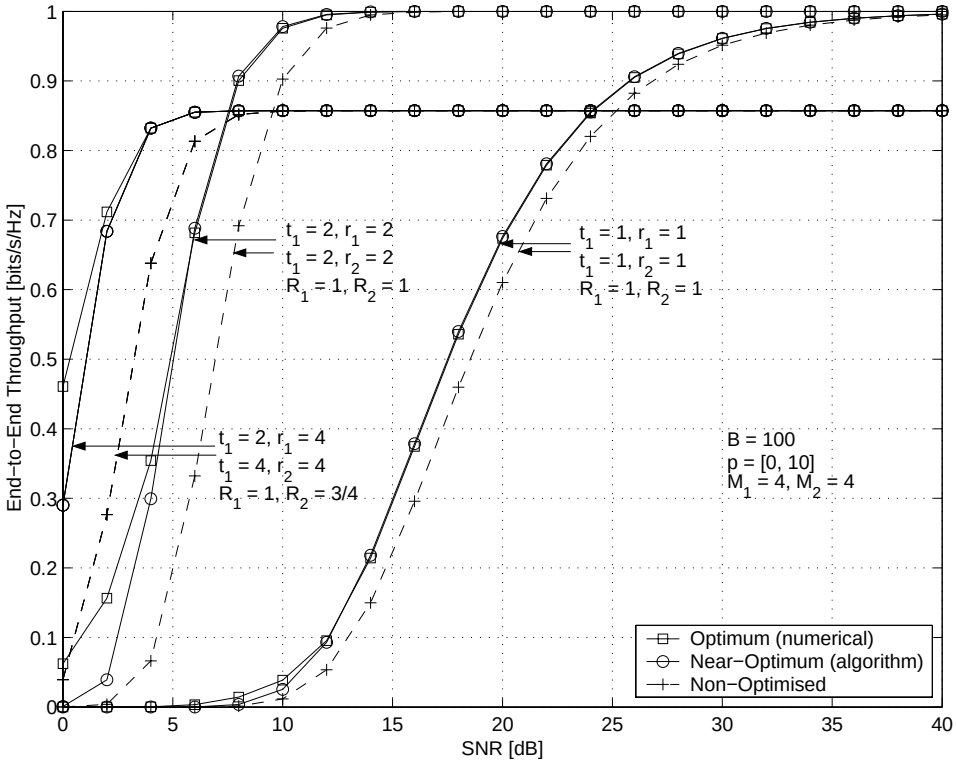


Figure 4.16: Comparison between optimum and near-optimum, as well as non-optimised end-to-end throughput for various configurations of a two-stage relaying network.

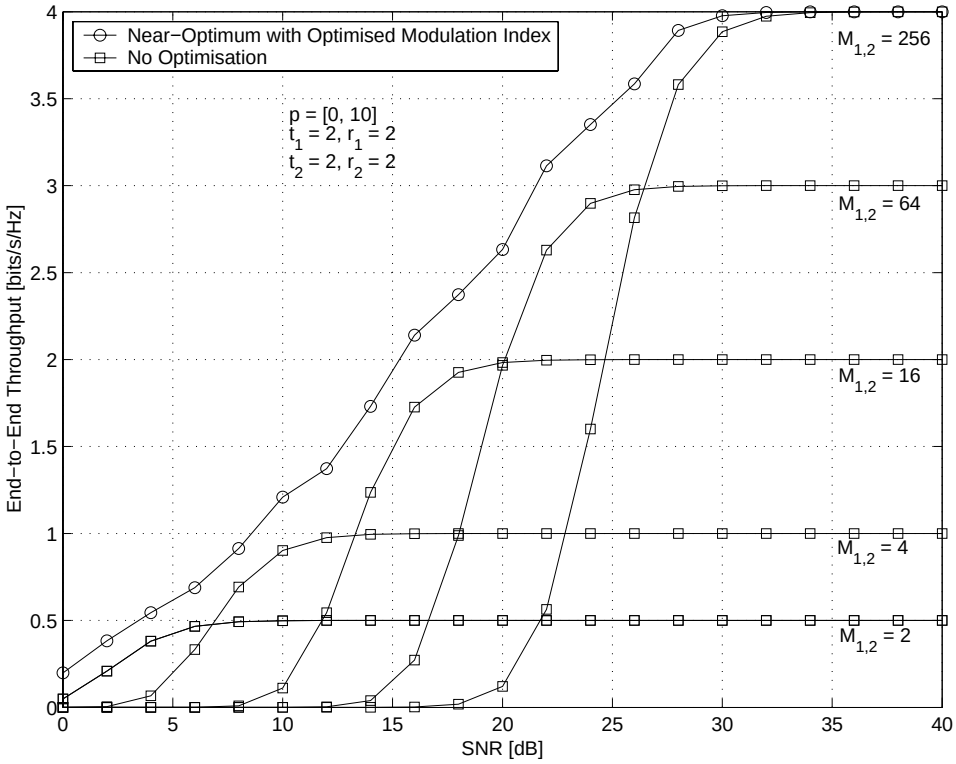


Figure 4.17: Numerically optimised modulation index where $M_{1,2} = (2, 4, 16, 64, 256)$ to yield near-optimum end-to-end throughput, compared to non-optimised systems.

Such numerical optimisation was performed for a 2-stage network with $p = [0, 10]$dB and $t_{1,2} = r_{1,2} = 2$. Each stage could choose a modulation index belonging to the set $M_{1,2} = (2, 4, 16, 64, 256)$; this leads to 25 possible combinations which are calculated in a fraction of a second. The performance gains in terms of increased throughput are clear from Figure 4.17, where the near-optimum adaptive modulation per stage is compared against various fixed combinations. At any SNR, the developed algorithm clearly outperforms any of the fixed configurations.

For example, if the system was to operate at an SNR in the first link of 20dB, then the best but fixed modulation index can only reach 2 bits/s/Hz; in this case either 16-QAM or 64-QAM in both stages. The optimum selection is 64-QAM with an optimised fractional power allocation, which yields a performance benefit of 30%.

### 4.4.3 Partial Cooperation at each Stage

Partial cooperation at each relaying stage results in parallel MIMO channels, all of possibly different strength. An example of such clustering process has been depicted in Figure 3.6 for a particular relaying stage. An analogous example to Figure 3.24 is depicted by means of Figure 4.18 with none of the involved r-MTs cooperating among each other.

Here, the first stage spans two independent SISO channels with average attenuation $\gamma_{1,1}$ and $\gamma_{1,2}$, respectively. Each of these channels causes independent BERs, denoted as $P_{1,1}$ and $P_{1,2}$, respectively. Similarly, the second stage spans two independent MISO channels, where the first MISO channel consists of channels with average attenuations $\gamma_{2,1}$ and $\gamma_{2,3}$, and the second MISO channel consists of channels with average attenuations $\gamma_{2,2}$ and $\gamma_{2,4}$. Furthermore, assuming an error free input into the second VAA relaying tier, the BERs at the output of the MISO channels are $P_{2,1}$ and $P_{2,2}$. Finally, the third stage spans a single MISO channel with a BER $P_{3,1}$.

Note that the r-MTs belonging to the same stage need to communicate at the same rate; furthermore, they obviously need to know which part of the space-time block code to transmit. Although already previously stated, it is assumed that synchronisation among all terminals is perfect.

To obtain the exact end-to-end BER is not trivial, as an error in the first stage may propagate to the t-MT; however, it may also be corrected at the next stage. Referring to Figure 4.18, for example, it is assumed that the same information bit is erroneously received over the link denoted as $(1, 1)$ and correctly for $(1, 2)$. Then, the STBC formed by (2,1) and (2,3) has as its input one erroneous and one correct information bit. Assuming that $\gamma_{2,3} \gg \gamma_{2,1}$, then the error does not further propagate since it will be outweighed by the correct bit. Alternatively, if $\gamma_{2,3} \ll \gamma_{2,1}$, then there is a large likelihood that the error propagates.

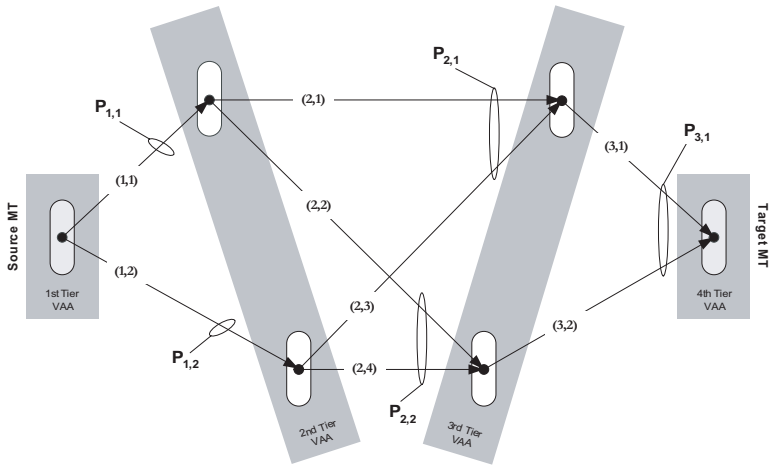


Figure 4.18: 3-stage distributed O-MIMO communication system without cooperation.

This creates dependencies between the error events at each stage in dependency of the modulation scheme used, the prevailing channel statistics, the average channel attenuations, as well as the STBC chosen. The fairly complex interdependencies call for suitable simplifications, which are exposed and justified below.

Generally, it is desirable to develop an approximation which decouples the error events at the respective stages. To this end, it is assumed that the system operates at low error rates which causes only one error event at a time in the entire network. Let us assume that an error occurs in link (1,1); however, (1,2) is error free. Then the probability that the error propagates further is related to the strengths of channels (2,1) and (2,3). It is intuitive and hence conjectured here that the probability that such error propagates is proportional to the strength of the STBC branch it departs from, here (2,1) for one of two MISO channels, and (2,2) for the other one.

Therefore, the probability that an error which occurred in link (1,1) with probability $P_{1,1}$ propagates through the O-MISO channel spanned by (2,1) and (2,3) is approximated as $P_{1,1} \cdot \gamma_{2,1}/(\gamma_{2,1} + \gamma_{2,3})$, where the strength of the erroneous channel (2,1) is normalised by the total strength of both sub-channels. To capture the probability that such an error propagates until the t-MT, all possible paths in the network have to be found and the original probability of error weighed with the ratios between the respective path gains.

Taking the above-said into account and assuming that at high SNRs only one such error will occur at any link, the end-to-end BER for the network depicted in Figure 4.18 can be expressed as

$$\begin{aligned} P_{b,\mathrm{e2e}}(e) \approx & \left[P_{1,1}(e)\left(\frac{\gamma_{2,1}}{\gamma_{2,1}+\gamma_{2,3}}\frac{\gamma_{3,1}}{\gamma_{3,1}+\gamma_{3,2}} + \frac{\gamma_{2,2}}{\gamma_{2,2}+\gamma_{2,4}}\frac{\gamma_{3,2}}{\gamma_{3,1}+\gamma_{3,2}}\right) + \right. \\ & \left. P_{1,2}(e)\left(\frac{\gamma_{2,4}}{\gamma_{2,2}+\gamma_{2,4}}\frac{\gamma_{3,2}}{\gamma_{3,1}+\gamma_{3,2}} + \frac{\gamma_{2,3}}{\gamma_{2,1}+\gamma_{2,3}}\frac{\gamma_{3,1}}{\gamma_{3,1}+\gamma_{3,2}}\right)\right] + \\ & \left[P_{2,1}(e)\left(\frac{\gamma_{3,1}}{\gamma_{3,1}+\gamma_{3,2}}\right) + P_{2,2}(e)\left(\frac{\gamma_{3,2}}{\gamma_{3,1}+\gamma_{3,2}}\right)\right] + \left[P_{3,1}(e)\right] \end{aligned} \tag{4.46}$$

This can be simplified to

$$P_{b,\mathrm{e2e}}(e) \approx \Big[\xi_{1,1}P_{1,1}(e)+\xi_{1,2}P_{1,2}(e)\Big]+\Big[\xi_{2,1}P_{2,1}(e)+\xi_{2,2}P_{2,2}(e)\Big]+\Big[\xi_{3,1}P_{3,1}(e)\Big] \tag{4.47}$$

where $\xi_{v,i}$ is the probability that an error occurring in link $(v,i)$ will propagate to the t-MT. This result is easily generalised to networks of any size and any form of partial cooperation. To this end, remember that there are $Q_{v\in(1,K)}$ cooperative clusters at the $v^{th}$ stage, each of which will yield an error probability of $P_{v\in(1,K),i\in(1,Q_v)}$. The end-to-end BER is hence approximated as

$$P_{b,\mathrm{e2e}}(e) \approx \sum_{v=1}^{K}\sum_{i=1}^{Q_v}\xi_{v,i}P_{v,i}(e) \tag{4.48}$$

where the probabilities $\xi_{v,i}$ are easily found from the specific network topology. The BERs $P_{v,i}(e)$ can be found from (4.25) and any of the previously derived SERs with an appropriate number of transmit and receive antennas per cluster, as well as prevailing channel conditions. The applicability of the derived end-to-end BER is assessed by means of Figures 4.19 and 4.20.

Explicitly, Figure 4.19 compares the numerically obtained and derived end-to-end BER versus the SNR in the first link for a two-stage network as depicted in Figure 4.18 without the second stage. For all simulations, QPSK has been used. The graphs are labelled on the respectively utilised channel gains. It can be observed that the derived BER differs from the exact one for low SNRs; however, for an increasing SNR, both curves converge.

Figure 4.20 compares the numerically obtained and derived end-to-end BER versus the SNR in the first link for a three-stage network as depicted in Figure 4.18. The curves are again labelled on the channel gains. From Figure 4.20 it is clear that the derived end-to-end BER holds with high precision for a variety of different scenarios.

The derived end-to-end BERs in form of (4.48) allow one to assign optimum fractional powers $\beta'_{v\in(1,K)}$ such that, together with the fractional frame durations $\alpha'_{v\in(1,K)}$, near-optimum end-to-end throughput is achieved. The fractional frame durations are clearly independent of the channel statistics or the degree of cooperation in the high SNR mode; therefore, eq. (4.30) holds for $\alpha'_{v\in(1,K)}$. The fractional power allocations are derived as follows.

Without loss of generality, let us assume that all links obey Rayleigh fading and have a different channel gain. The error rates are then governed by (4.20), where $u$ has to be replaced by the number of sub-channels created in each of the $Q_v$ clusters. The fractional power allocations are derived in Appendix 4.8 (Derivation II) as

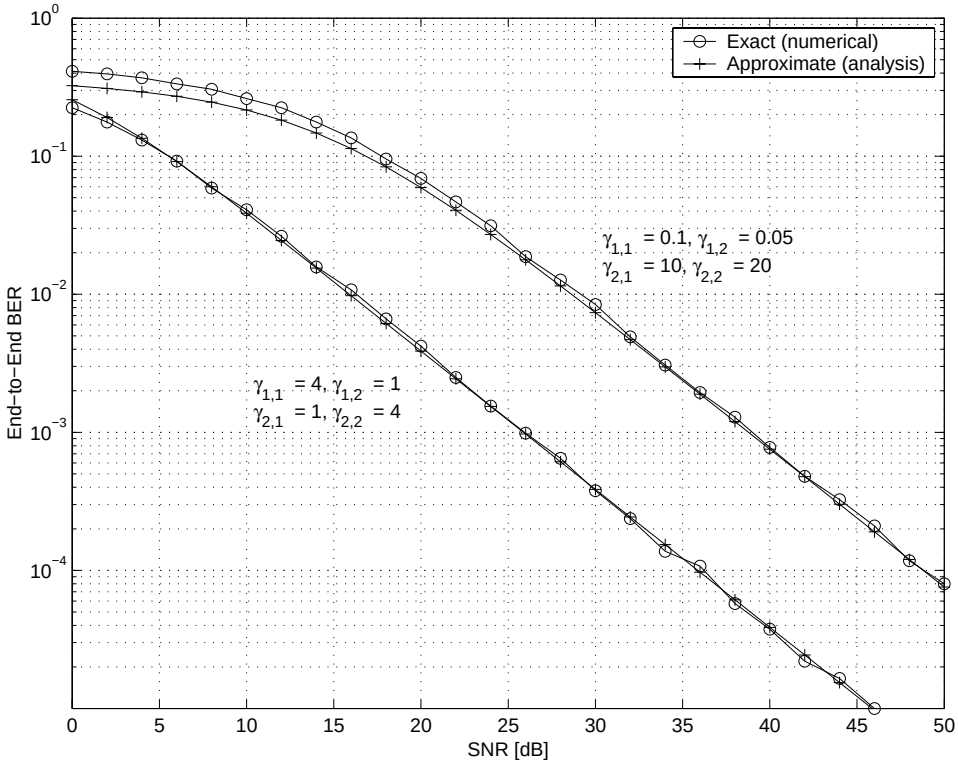


Figure 4.19: Numerically obtained and derived end-to-end BER versus the SNR in the first link for a two-stage network without cooperation.

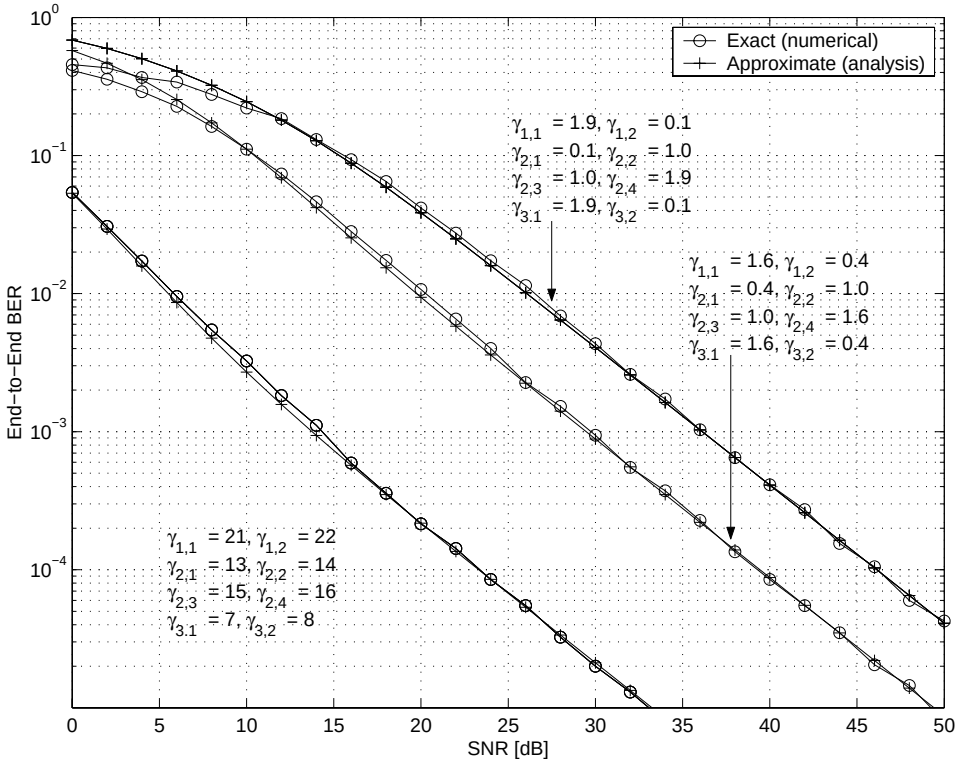


Figure 4.20: Numerically obtained and derived end-to-end BER versus the SNR in the first link for a three-stage network without cooperation.

$$\beta'_v \approx \left[ \sum_{w=1}^{K} \alpha'_w \sqrt{\frac{\sum_{i=1}^{Q_v} \sum_{j \in i} \xi_{v,i}^{-1} K_{v,i,j}^{-1} A_v^{-1} B_{v,i,j}}{\sum_{i=1}^{Q_w} \sum_{j \in i} \xi_{w,i}^{-1} K_{w,i,j}^{-1} A_w^{-1} B_{w,i,j}}} \right]^{-1} \tag{4.49}$$

where the notation $j \in i$ represents the $j^{th}$ sub-channel belonging to the $i^{th}$ cluster. The partial expansion coefficients $K_{v,i,j}$ in the $v^{th}$ stage for the $i^{th}$ cluster can be written as

$$K_{v,i,j} = \prod_{j' \in i, j' \neq j} \frac{\gamma_{v,j}}{\gamma_{v,j} - \gamma_{v,j'}} \tag{4.50}$$

which has $u_{v,i}$ multiplicative terms. The constant $A_v$ is given by (4.43), whereas

$$B_{v,i,j} = \begin{cases} \frac{g_{\mathrm{PSK},v}}{R_v} \frac{\gamma_{v,j \in i}}{t_v} \frac{S}{N} & \text{for M-PSK} \\ \frac{g_{\mathrm{QAM},v}}{R_v} \frac{\gamma_{v,j \in i}}{t_v} \frac{S}{N} & \text{for M-QAM} \end{cases} \tag{4.51}$$

This case is not further illustrated.

Note that no waterfilling has been deployed prior to the above optimisation; however, numerically obtained simulation results indicate that waterfilling for the transmit power at each stage does not yield notable performance gains, which is the reason why it has been omitted for the above analysis.

## 4.5 Maximum Throughput for Stage-by-Stage Detection

In contrast to the previous section, the decision on the correctness of a received symbol or frame of symbols is accomplished at every relaying stage. This approach is a step closer to the capacitive approach taken in Chapter 3, where throughput was maximised assuming decoding and re-encoding at each stage.

Subsequently, the fractional resource allocation rules assuming full cooperation at each relaying stage are derived assuming a frame-by-frame detection. The case of partial cooperation is then a straightforward extension, and thus not considered further. Finally, the allocation strategies derived in Chapter 3 for transceivers of infinite complexity are mapped onto allocation strategies for finite transceivers.

### 4.5.1 Full Cooperation at each Stage

It is assumed here that a decision on the correctness of the received signal is accomplished at frame level, which is easily realised by adding a cyclic redundancy check (CRC) of negligible overhead to each transmitted frame. Therefore, the $v^{th}$ relaying stage receives a frame of duration $D_v$ containing symbols of modulation order $M_v$, which are STBC encoded with a rate $R_v$. Not to cause any congestion, the average throughput at each stage has to be the same, while the average end-to-end throughput ought to be maximum.

It is therefore again the aim to find fractional resource allocation rules such as to maximise the end-to-end throughput; however, now tailored to a stage-by-stage detection. With reference to (4.28) and the above-said, the normalised throughput at the $v^{th}$ stage can be expressed as

$$\Theta_v = \alpha'_v R_v \log_2(M_v) \cdot \big(1 - P_{s,v}(e)\big)^{D_v} \tag{4.52}$$

$$\approx \alpha'_v R_v \log_2(M_v) \cdot \big(1 - D_v P_{s,v}(e)\big) \tag{4.53}$$

where $\alpha'_v$ is the fractional frame duration, $R_v$ is the rate of the STBC, $M_v$ is the modulation order, $P_{s,v}(e)$ is the SER, and $D_v \in \mathbb{N}$ is the frame duration in symbols used in the $v^{th}$ stage. Defining $D$ to be the total length of the frame used for communication from s-MT to t-MT, $D_v$ can be related to the fractional frame duration $\alpha'_v$ as $D_v = \alpha'_v D$.

Note that with an increasing fractional frame length $D_{v\in(1,K)}$, the normalised throughput clearly decreases which is due to the increased probability of error. However, the signalling overhead inherent to each transmitted frame also decreases, and so does the strength of a potential outer channel code. The system designer should hence determine an optimum (according to certain constraints) frame length, after which the exposed resource allocation algorithms are applied. An optimum choice of such frame duration is clearly beyond the scope of this thesis.

Adapting similar arguments as in Chapter 3 and the previous section, the resource allocation strategies have to guarantee that the throughput is the same at each of the $K$ relaying stages, i.e. $\Theta_1 = \ldots = \Theta_K \triangleq \Theta$. Further analysis concentrates on the case of Rayleigh fading with equal channel gains per relaying stage; other cases are a straightforward extension to the exposed analysis.

Under these assumptions, the throughput in each stage can be upper-bounded by

$$\Theta_v \lessapprox \alpha'_v R_v \log_2(M_v) \cdot \left(1 - \frac{\alpha'_v A_v D}{(1 + B_v \beta'_v)^{u_v}}\right) \tag{4.54}$$

where $A_v$ differs from the $A_v$ in (4.43) by $\log_2(M_v)$ due to the SER (and not the BER), i.e.

$$A_v = \begin{cases} \frac{M_v - 1}{M_v} & \text{for M-PSK} \\ 2q_v & \text{for M-QAM} \end{cases} \tag{4.55}$$

and $B_v$ is given by (4.44). Following the same approach as before, the fractional frame durations are obtained as

$$\alpha'_v = \frac{\prod_{w=1, w\neq v}^{K} R_w \cdot \log_2(M_w)}{\sum_{k=1}^{K} \prod_{w=1, w\neq k}^{K} R_w \cdot \log_2(M_w)} \tag{4.56}$$

and the fractional power allocations are derived in Appendix 4.8 (Derivation III)

$$\beta'_v \approx \left[\sum_{w=1}^{K} \alpha'_v \left(\frac{{\alpha'_v}^{-1}}{{\alpha'_w}^{-1}} \frac{A_v^{-1} B_v^{u_v}}{A_w^{-1} B_w^{u_w}}\right)^{\frac{1}{u_{\max}}}\right]^{-1} \tag{4.57}$$

where $u_{\max} = \arg\max(u_1, \ldots, u_K)$.

The performance of the developed algorithm is assessed by means of Figures 4.21−4.23 for M-QAM schemes only. M-PSK has been omitted here to limit the number of simulation results; however, they were found to exhibit the same performance trends as the M-QAM schemes. Note further that, unless otherwise stated, the number of bits sent by the s-MT in one frame has been fixed to $B = 100$.

Explicitly, Figure 4.21 depicts the normalised end-to-end throughput in [bits/s/Hz] versus the SNR which occurs in the first link in [dB]. Not to simulate an entirely symmetric scenario, the strength of the channel in the second stage is 10 times stronger than the first one, i.e. $p = [0, 10]$dB. Furthermore, the modulation scheme has been fixed to QPSK in either stage. The performance of the numerically obtained optimum throughput is compared against the throughput obtained by means of the allocation rules (4.56) and (4.57) for a varying number of transmit and receive antennas in each stage. The algorithms clearly perform near-optimum.

It can also be observed that the throughput saturates, which can be attributed to the limiting spectral efficiency of a QPSK scheme. For a high SNR, the SER at each stage is negligible; the limiting throughput $\Theta_\infty$ can hence be obtained from (4.56) and (4.54) as

$$\Theta_\infty \triangleq \Theta(\text{SNR} \to \infty) = \frac{\prod_{w=1}^{K} R_w \cdot \log_2(M_w)}{\sum_{k=1}^{K} \prod_{w=1, w\neq k}^{K} R_w \cdot \log_2(M_w)} \tag{4.58}$$

which, when applied to the full-rate examples in Figure 4.21, yields

$$\Theta_\infty = \frac{1 \cdot \log_2(4) \cdot 1 \cdot \log_2(4)}{1 \cdot \log_2(4) + 1 \cdot \log_2(4)} = 1 \text{ bit/s/Hz} \tag{4.59}$$

and which, when applied to the 3/4-rate example, yields

$$\Theta_\infty = \frac{1 \cdot \log_2(4) \cdot 3/4 \cdot \log_2(4)}{1 \cdot \log_2(4) + 3/4 \cdot \log_2(4)} = 0.86 \text{ bits/s/Hz} \tag{4.60}$$

Both results are confirmed by Figure 4.21. Furthermore, $\Theta_\infty = 1$ bit/s/Hz is approached faster by the $(1 \times 2)/(2 \times 1)$ configuration when compared to $(1 \times 1)/(1 \times 1)$. This is clearly attributed to the faster decay in the SER probability for increasing SNR.

Comparing Figure 4.21 with its equivalent for the end-to-end transmission, i.e. Figure 4.16, the throughput of the stage-by-stage transmission and detection is higher in the transitional region. This is due to the fact that a stage-by-stage transmission does not re-transmit erroneous frames.

Figure 4.22 depicts the throughput of a $(2 \times 2)/(2 \times 2)$ full-rate configuration with a varying modulation index in each stage, where $p = [0, 10]$dB. Explicitly, compared are the cases where the first (weaker) stage uses QPSK, whereas the second (stronger) stage varies its modulation from QPSK to 256-QAM. Also, depicted is the case where the first (weaker) stage uses 64-QAM and the second (stronger) stage 256-QAM.

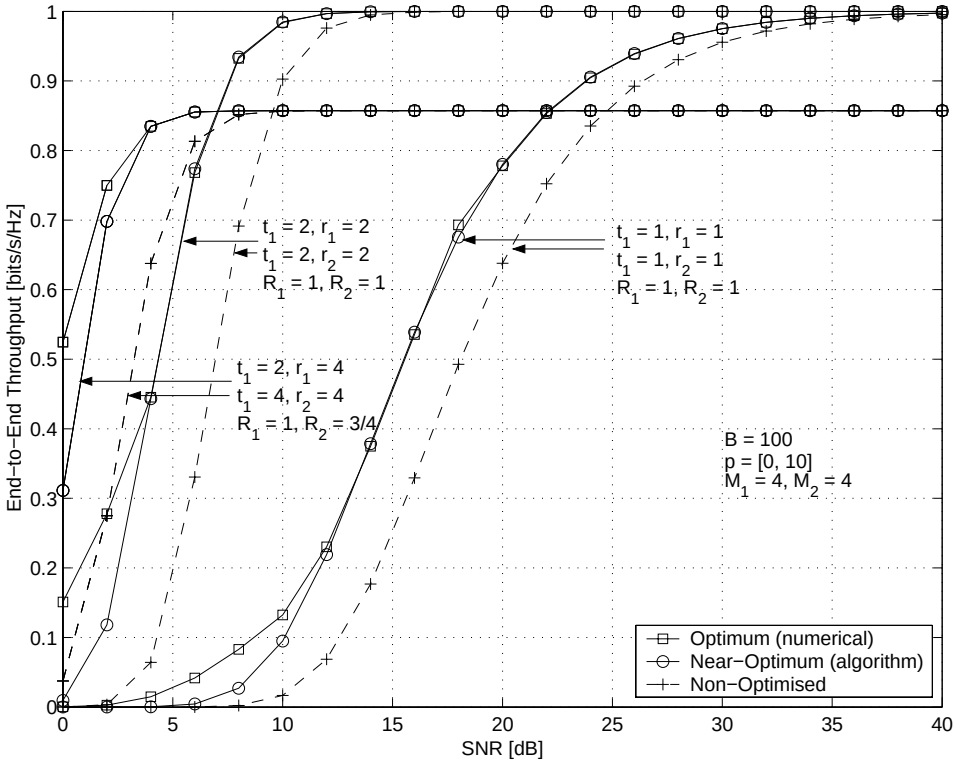


Figure 4.21: Comparison between optimum, near-optimum and non-optimised end-to-end throughput of a two-stage relaying network, assuming stage-by-stage detection.

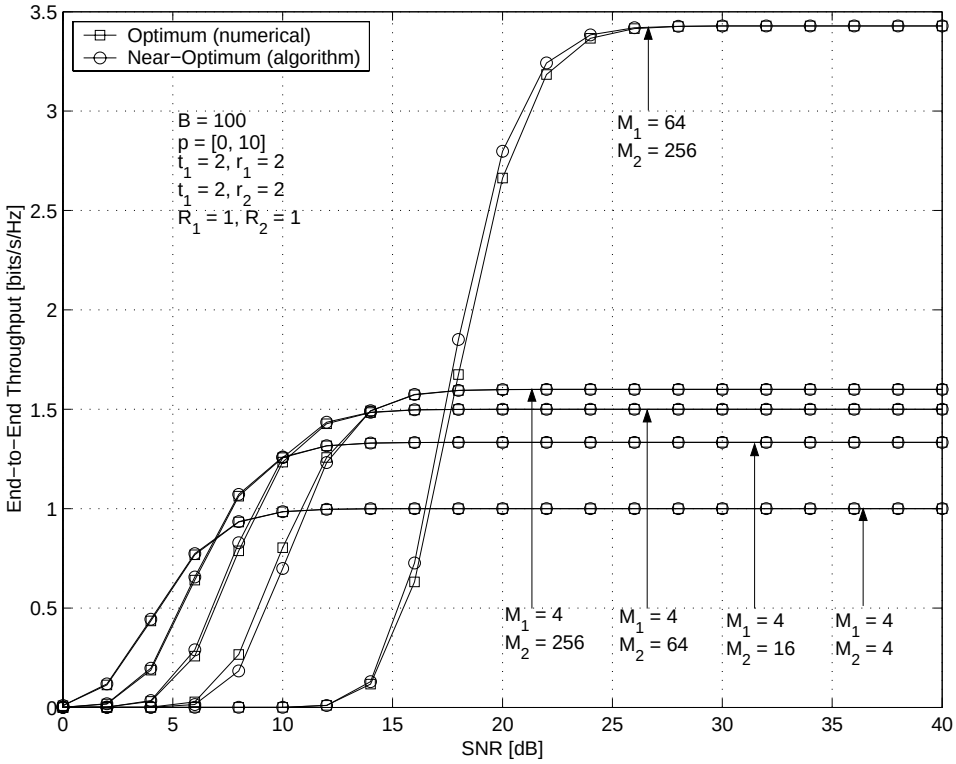


Figure 4.22: Optimum, near-optimum and non-optimised end-to-end throughput for a two-stage relaying network with fixed modulation index.

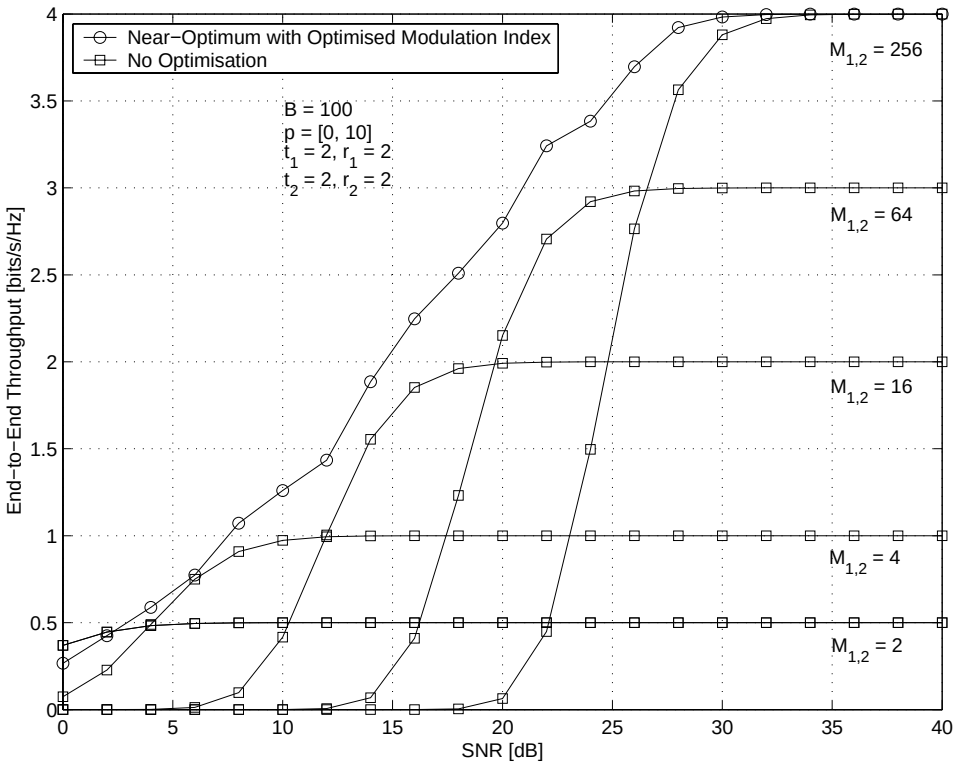


Figure 4.23: Numerically optimised modulation index where $M_{1,2} = (2, 4, 16, 64, 256)$ to yield near-optimum end-to-end throughput, compared to non-optimised systems.

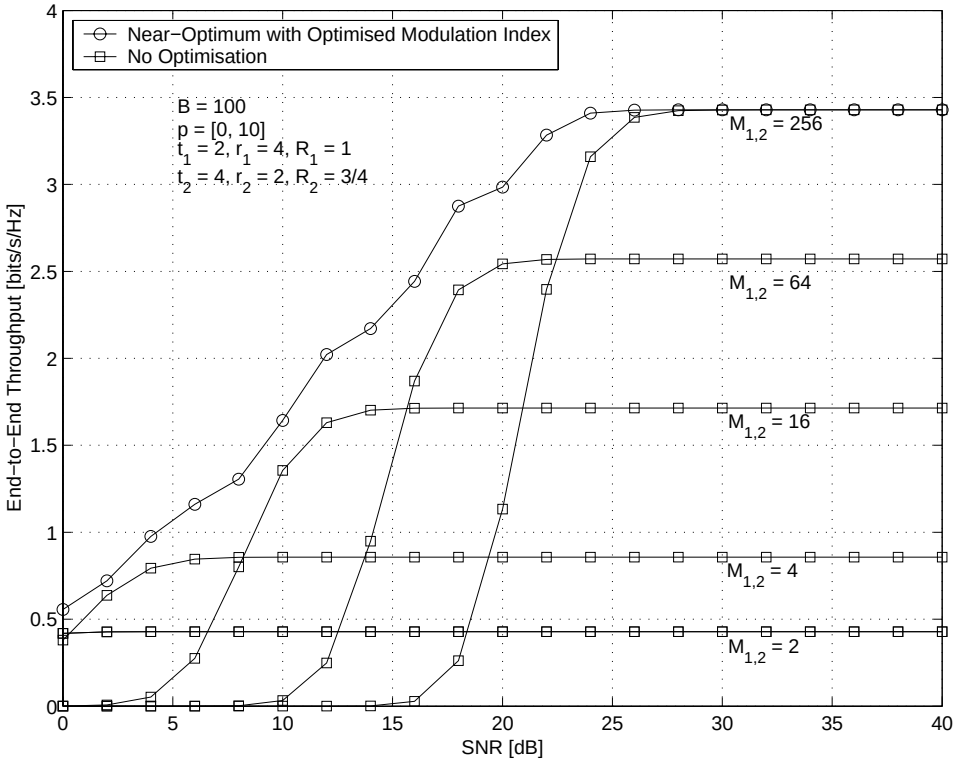


Figure 4.24: Numerically optimised modulation index where $M_{1,2} = (2, 4, 16, 64, 256)$ to yield near-optimum end-to-end throughput, compared to non-optimised systems; $R_2 = 3/4$.

In the limiting cases, the respective $\Theta_\infty$ are clearly reached, which means that the (64-QAM)/(256-QAM) scheme yields highest throughput and the (4-QAM)/(4-QAM) scheme the lowest throughput. Of interest, however, is the zone where the throughputs cross, i.e. SNR<15dB. This zone is due to the trade-off between throughput, i.e. preferably a high modulation index, and susceptibility to errors, i.e. preferably a low modulation index. Furthermore, the large difference in throughput between (64-QAM)/(256-QAM) and (4-QAM)/(256-QAM) indicates that the spectral efficiency is really the limiting factor for SNR $\rightarrow \infty$. Therefore, if there is a distributed-MIMO multi-stage network operating at a high SNR, and there is one stage which is using a modulation index lower than any other stage in the network, then it may make sense not to incorporate that stage into the relaying process. The derivations of the conditions under which such stage should be excluded is beyond the scope of this thesis.

The precision of the fractional allocation algorithm for fixed modulation indexes allows performing a final numerical optimisation in each relaying stage over all possible modulation indexes. The low complexity of (4.56) and (4.57) guarantees that such optimisation comes at little additional computational power.

Such numerical optimisation was performed for a 2-stage network with $p = [0, 10]$dB and $t_{1,2} = r_{1,2} = 2$. Each stage could choose a modulation index belonging to the set $M_{1,2} = (2, 4, 16, 64, 256)$; this leads to 25 possible combinations which are calculated in a fraction of a second. The performance gains in terms of increased throughput are clear from Figure 4.23, where the near-optimum adaptive modulation per stage is compared against various fixed combinations.

Figure 4.24 is equivalent to Figure 4.23 with the only difference that $t_1 = 2, r_1 = 4, R_1 = 1$ and $t_2 = 4, r_2 = 2, R_2 = 3/4$. Although the limiting throughput is lower in comparison to the previous case due to the loss in rate, the limiting throughput is reached for a lower SNR. For example, if a system required a normalised throughput of 2 bits/s/Hz, then the current scenario would require an SNR of 12dB, whereas the previous scenario almost 15dB.

### 4.5.2 Mapping of $(\alpha_v, \beta_v)$ to $(\alpha'_v, \beta'_v, M_v)$

The circle is now closed by mapping the previously derived fractional resource allocation rules for transceivers operating at capacity limit, to system operating with transceivers of finite complexity, i.e.

$$(\alpha_v, \beta_v) \longmapsto (\alpha'_v, \beta'_v, M_v) \tag{4.61}$$

A successful mapping would allow utilising the fractional resource allocation rules derived for Shannon transceivers operating over MIMO or O-MIMO relaying with or without resource reuse for the same systems with limited complexity. Two different mappings are suggested.

First, it is assumed that the modulation index $M_{v\in(1,K)}$ is fixed at all stages. With reference to the previous section, the determination of the fractional frame duration $\alpha'_{v\in(1,K)}$ is hence trivial and assumed to be given in form of (4.56). Of importance here is to allocate the fractional power $\beta'_{v\in(1,K)}$ utilising the theory developed in Section 3.3.1, where $\beta'_v \approx \beta_v/\alpha'_v$ and $\beta_v$ is the fractional power determined for an FDMA-based relaying system with the same parameters as the current TDMA-based relaying system. Such successful mapping is shown in Figure 4.25, which is the equivalent to Figure 4.21. The performance clearly differs; however, it outperforms the cases without any transmit power optimisation.

Second, it is assumed that the throughput-maximising modulation index $M_{v\in(1,K)}$ needs to be determined in each stage. Remember that previously all possible $M_v$ needed to be permutated to determine the maximum throughput. Although not a serious burden for systems with, e.g., 5 different modulation orders, i.e. $O = 5$, and 2-3 stages, i.e. $K = 2, 3$; however, it may be a serious limit for systems with more than 3 stages, as the number of combinations increases with $O^K$. Also, despite the simplicity of the previously introduced algorithms, it is always an aim of the system designer to simplify these even further.

To this end, an allocation is suggested which increases only linearly in $O$. Without loss of generality, it is assumed that $R_{v\in(1,K)} = 1$. Then, according to (4.56), the fractional frame allocation and modulation order for all stages relate as follows

$$\alpha'_v \log_2(M_v) = \text{constant} \tag{4.62}$$

Therefore, a small $\alpha'_v$ requires a large $M_v$. To proceed, it is suggested to sort all $\alpha'_v$ in descending order which, without loss of generality, yields $\alpha'_1 \geq \ldots \geq \alpha'_K$. Further, the $K^{th}$ stage is allocated the highest possible modulation order $M_{\max}$, e.g. $M_K = M_{\max} = 256$. All the other stages then allocate their modulation orders according to (4.62), which obviously requires some rounding. The throughput is determined, after which the $K^{th}$ stage is allocated the next smallest modulation order, e.g. $M_K = 64$. Again, the remaining modulation orders obeying (4.62) and the achieved throughput are determined. This process is repeated for all $O$ modulation orders. Finally, the one with the highest throughput is chosen. Clearly, such proceeding requires only $O$ combinations, instead of $O^K$ as before.

The achieved end-to-end throughput of such proceeding is depicted in Figure 4.26, which is the equivalent configuration already described by means of Figure 4.23. The achieved throughputs deviate, with the throughput optimised for a realistic transceiver generally being larger than for a Shannon transceiver. Nonetheless, results are satisfactory close.

These examples demonstrate that the error behaviour of finite complexity transceivers scales approximately the same way as the capacity limit of transceivers of infinite complexity. This is a remarkable, however not obvious result. More research, however, has to be undertaken before a conclusive statement can be made. This is left open for future research.

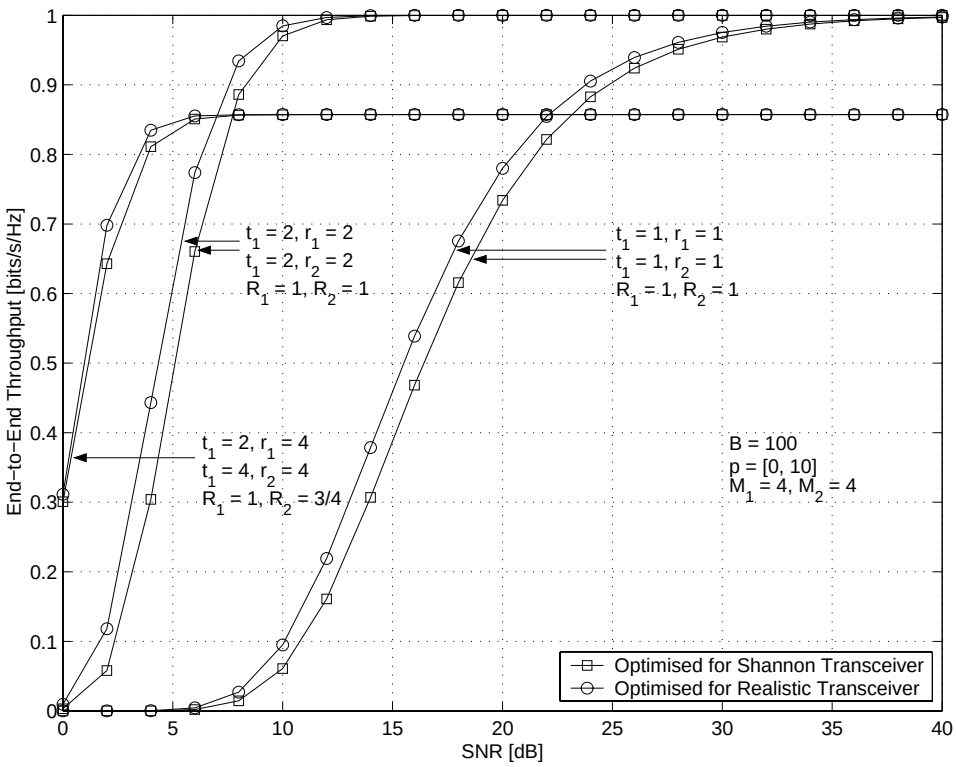


Figure 4.25: Comparison between achieved throughput utilising fractional resource allocations derived for realistic and Shannon transceivers (power only).

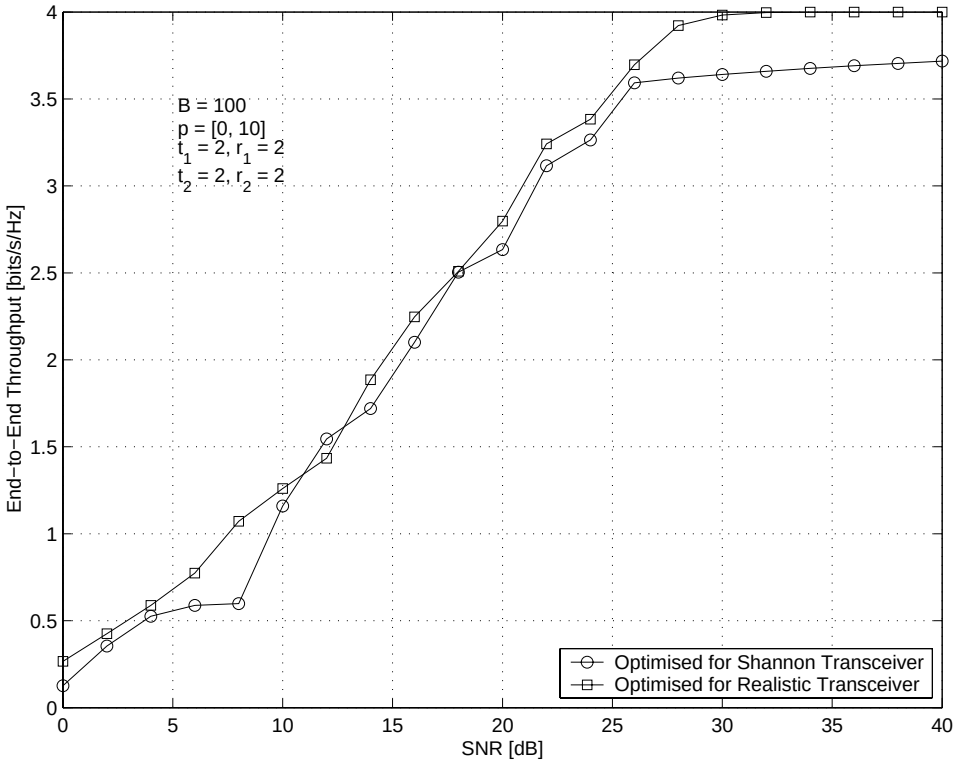


Figure 4.26: Comparison between achieved throughput utilising fractional resource allocations derived for realistic and Shannon transceivers for $M_{1,2} = (2, 4, 16, 64, 256)$.

## 4.6 Case Studies

The resource allocation rules derived throughout this chapter are now applied to certain specific scenarios. For these, the conditions under which relaying yields performance gains over direct communication is assessed. It will also be demonstrated that further performance benefits are obtained when utilising the given algorithms.

This thesis has so far dealt with the performance of systems experiencing instantaneous attenuations due to fading, where the average power of such a fading channel was associated with the channel gain or pathloss as defined in (4.2). The occurring fades indicate that there is some form of mobility present in the communication network, which will prompt the channel gains to change over time. It is assumed here that the mobility of the introduced distributed-MIMO multi-stage communication network is limited such that an update of the experienced average channel gains is feasible within each of the involved MT. To derive an upper bound on such mobility is not straightforward as it depends on many system assumptions; it is hence left for future research.

The channel in most realistic communication scenarios also undergoes shadowing as introduced in Section 4.2.2. Shadowing, as pathloss, changes in the spatial domain. Again, it is assumed that the mobility of the network is restricted so that an update of the average channel gains caused by pathloss and shadowing is feasible. Since shadowing is a random process, a rigorous approach needs to incorporate its pdf into the capacity and error rate analysis. The complexity of the lognormal shadowing process, however, makes such an analysis very difficult (particularly for distributed-MIMO systems) which is the reason why a numerical approach has been opted for here. Further case studies relate to scenarios with and without shadowing. Prior to that, however, the SNR gains due to relaying are derived, and shown to be dependent on the pathloss coefficient $n$.

### 4.6.1 SNR Relaying Gains

The normalised throughput of systems operating with realistic transceivers is subsequently analysed. Networks of different configurations are compared, i.e. number of antennas per VAA relaying tier, position of the relaying tiers with respect to the t-MT and s-MT, etc.

To allow for a fair comparison between various relaying schemes, the SNR at each relaying stage is obtained with reference to the SNR a direct communication system would experience. Furthermore, the total energy $E$ to deliver information from source to sink is assumed to be the same for all analysed configurations. Under this condition, remember that an FDMA-based relaying system requires each r-MT to allocate a fractional transmission power of $\beta_{v\in(1,K)}$, whereas a TDMA-based system allocates to each r-MT a fractional transmission power of $\beta_{v\in(1,K)}/\alpha_{v\in(1,K)}$, c.f. Section 3.2.3.

Under these assumptions, the directly received power $S_{\mathrm{Rx}}$ at the t-MT assuming a transmission power $S_{\mathrm{Tx}}$ at the s-MT, can be expressed as

$$S_{\mathrm{Rx}} \propto S_{\mathrm{Tx}} \cdot d_0^{-n} \tag{4.63}$$

where $d_0$ is the distance between s-MT and t-MT and $n$ is the pathloss coefficient. Similarly, the received power at the $v^{th}$ relaying stage can be expressed as

$$S_{\mathrm{Rx},v} \propto S_{\mathrm{Tx},v} \cdot d_v^{-n} \tag{4.64}$$

where $d_v$ is the distance spanning the $v^{th}$ relaying stage, and the pathloss coefficient is assumed to be the same for all relaying stages. Since a fractional power $\beta_v$ of the total power $S_{\mathrm{Tx}}$ is assigned to the $v^{th}$ stage assuming FDMA-based relaying, the respective received power is given as

$$S_{\mathrm{Rx},v} \propto \beta_v \cdot S_{\mathrm{Tx}} \cdot d_v^{-n} \tag{4.65}$$

which, with reference to (4.63), yields

$$S_{\mathrm{Rx},v} = \beta_v \cdot S_{\mathrm{Rx}} \cdot \left(\frac{d_0}{d_v}\right)^n \tag{4.66}$$

To arrive at the SNR for the $v^{th}$ relaying stage, eq. (4.66) is divided by the noise power $\alpha_v N$, which finally yields

$$\mathrm{SNR}_v = \frac{\beta_v}{\alpha_v} \cdot \left(\frac{d_0}{d_v}\right)^n \cdot \frac{S}{N} \tag{4.67}$$

where $S/N$ is the SNR experienced at the t-MT if direct communication took place. Exactly the same relation is derived for a TDMA-based relaying system. Since $\alpha_v \approx \beta_v$, the SNR gain is hence mainly dictated by the ratio between the respective distances and the pathloss coefficient.

### 4.6.2 Scenarios without Shadowing

The achieved end-to-end throughput of a direct communication system is compared against the achieved throughput of a two-stage relaying system by means of Figures 4.27−4.34.

Explicitly, Figure 4.27 investigates the achieved throughput versus the SNR in the direct link in dependency of the pathloss index $n = 2, 3, 4$. The packet size is $B = 100$ bits, the modulation order in all links is $M_{0,1,2} = 4$, $d_{1,2} = 0.5\, d_0$ and $t_{0,1,2} = r_{0,1,2} = 1$. Here, the subscript 0 relates to the direct communication scenario.

It can be observed that the normalised throughput for SNR $\rightarrow \infty$ reaches 2 bits/s/Hz for the direct communication scenario, and only 1 bit/s/Hz for the relaying case. This is obvious since resources have to be shared for the relaying system, whereas the direct link can utilise the full bandwidth and frame duration.

Nonetheless, a threshold SNR can be observed until which the relaying system outperforms the direct system. This is in the region where the error term $1 - D_0 P_{s,0}(e)$ in (4.52) dominates over the normalised throughput term $R_0 \log_2(M_0)$. In this region, however, the relaying links perform already nearly error-free due to the SNR advantage derived in (4.59).

The threshold SNR is easily calculated where, without loss of generality, only full-rate STBCs are assumed. With reference to (4.54), the equated throughputs are expressed as

$$\frac{\log_2(M_1)\log_2(M_2)}{\log_2(M_1)+\log_2(M_2)}\left(1-\frac{A_1 D_1}{(1+B_1\beta_1')^{u_1}}\right) = \log_2(M_0)\left(1-\frac{A_0 D_0}{(1+g_{\mathrm{QAM},0}/t_0\cdot \mathrm{SNR}_{\mathrm{th}})^{u_0}}\right) \quad (4.68)$$

which can easily be resolved in favour of the threshold SNR. In the limiting case that the relaying stages already perform error free, i.e. $\frac{A_1 D_1}{\left(1+B_1\beta_1'\right)^{u_1}} \to 0$, this can be approximated as

$$\mathrm{SNR}_{\mathrm{th}} \approx \frac{t_0}{g_{\mathrm{QAM},0}}\left[\sqrt[u_0]{\frac{D_1 A_1}{1-\frac{1}{\log_2(M_0)}\frac{\log_2(M_1)\log_2(M_2)}{\log_2(M_1)+\log_2(M_2)}}}-1\right] \quad (4.69)$$

For the scenario depicted in Figure 4.27, the approximate threshold SNR is calculated as 20dB which deviates from the exact crossover by 2dB.

Figure 4.28 compares the achieved throughput for a direct communication system with $M_0 = 4$, $t_0 = r_0 = 1$ and $B = 100$. Various relaying configurations are shown for comparison, where first the number of antenna elements in the relaying stage is increased to $r_1 = t_2 = 2$, and then the modulation order in the second stage is increased from QPSK to 16QAM and 64QAM. All scenarios are assumed to have a pathloss coefficient of $n = 4$ [68].

It can be observed that strengthening the relaying links by introducing a second antenna element in the relaying terminal causes the throughput to level off faster than for the single antenna case; however, it does not shift the threshold SNR significantly. In contrast, increasing the modulation order in the second link allows increasing the achieved throughput, as well as shifting the threshold SNR towards higher SNRs.

Figure 4.29 depicts the achieved throughput versus the distance in the first link normalised by the total distance in [%], i.e. $d_1/d_0 \cdot 100\%$. The following scenario is assumed: $t_0 = 1, r_0 = 1$, $M_0 = 4$; $t_1 = 1, r_1 = 2$, $M_1 = 4$; $t_2 = 2, r_2 = 1$, $M_2 = 16$; $B = 100$ and $n = 4$.

For a low direct link SNR of 10dB, the direct link clearly achieves a close to zero throughput. The relaying system, on the other hand, yields significant gains over the direct case which depend on the exact location of the relaying stage. The end-to-end throughput is non-symmetric because the links are asymmetric in O-MIMO gains and modulation order. For a higher direct SNR of 20dB, the gains achieved due to relaying are clearly diminished.

Figure 4.30 exhibits a similar performance, where the same scenario as above has been simulated with the modulation orders in each stage reversed, i.e. $M_{0,1} = 16$ and $M_2 = 4$.

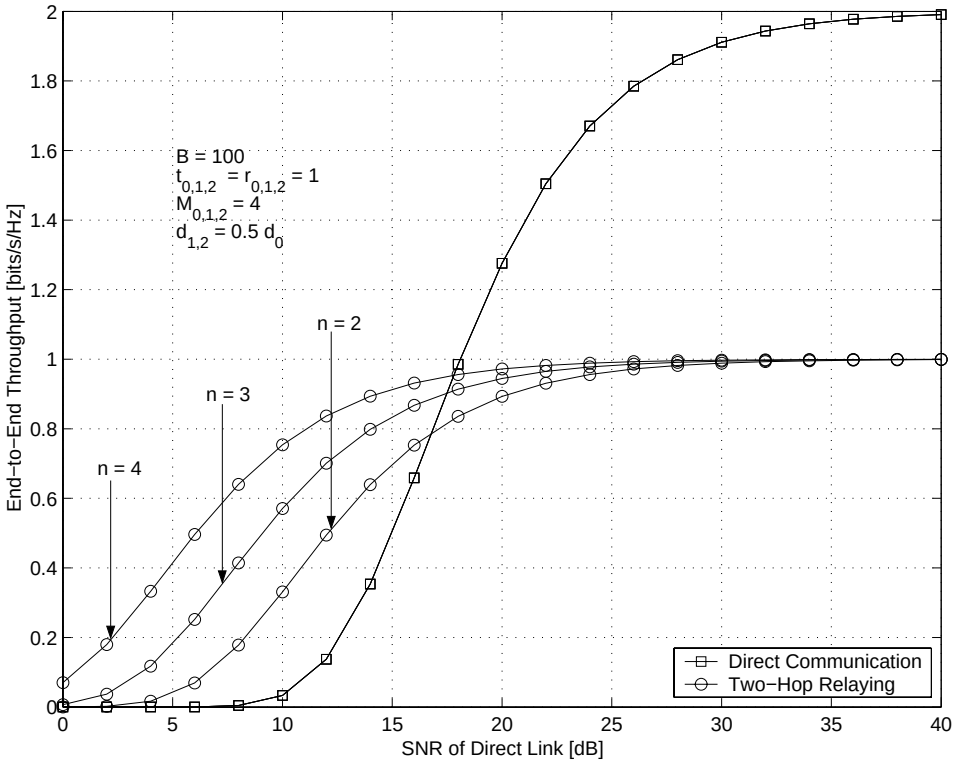


Figure 4.27: End-to-end throughput for a direct communication link and two-stage relaying links with varying pathloss coefficient.

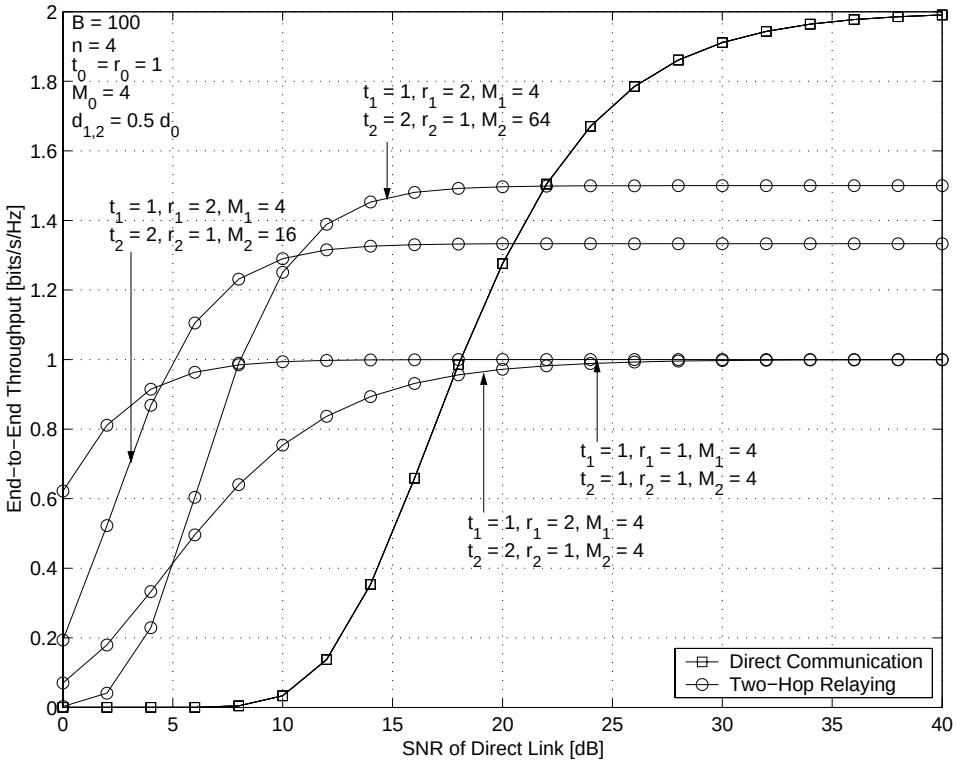


Figure 4.28: End-to-end throughput for a direct communication link and two-stage relaying links with a varying relaying scenario.

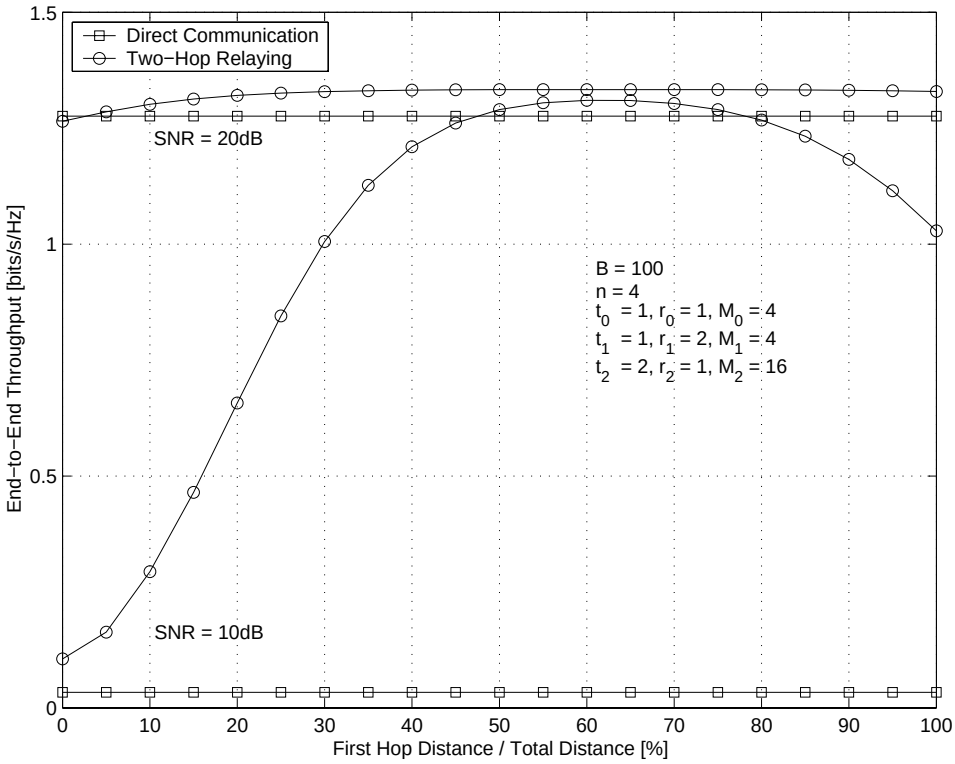


Figure 4.29: End-to-end throughput versus distance of first direct link normalised by the total distance at different direct link SNRs.

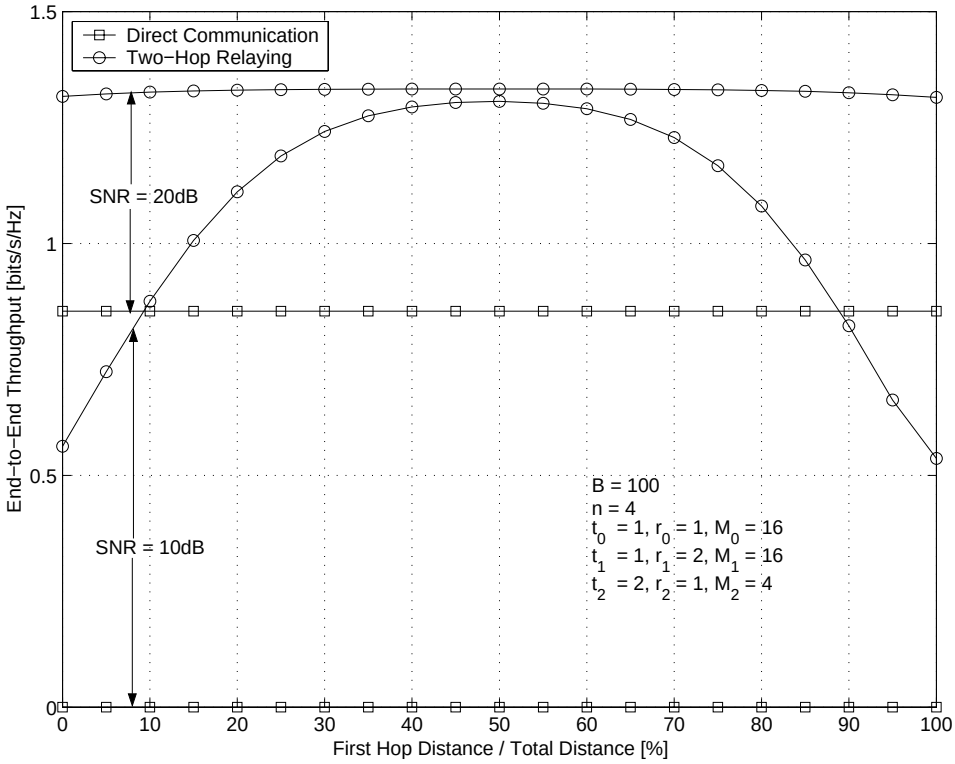


Figure 4.30: End-to-end throughput versus distance of first direct link normalised by the total distance at different direct link SNRs.

The remaining simulations relate to the communication scenario depicted in Figure 4.31. Here, the MTs are placed randomly in the shaded area of size $a \times b$ which are placed at distance $c$ from each other, thereby realising a two-stage distributed-MIMO communication system. Direct communication happens without the relaying stage, here the second relaying VAA tier. Relaying is accomplished by means of one or two cooperating r-MTs. It is assumed that the two cooperating r-MTs are spatially close together, thereby experiencing approximately the same pathloss from the s-MT and towards the t-MT.

All simulations use a packet length of $B = 100$ and a pathloss coefficient of $n = 4$; the dimensions of the shaded areas are (fairly arbitrary) set to $a = b = 50$ with a mutual distance of $c = 100$. The terminal placement within these areas obey a uniform distribution. Furthermore, for all simulations, the optimum combination of modulation orders is obtained for every SNR by trying all possible combinations out of $M = (4, 16, 64, 256)$.

Figure 4.32 depicts the achieved end-to-end throughput versus the SNR in the direct link in [dB] for a scenario as depicted in Figure 4.31 with only one r-MT and one antenna per stage, i.e. $t_{0,1,2} = r_{0,1,2} = 1$. Compared are the cases of direct communication, relaying with optimised frame duration and power, relaying with optimised frame duration only, and the cases of non-optimised fixed modulation indices.

As expected, a threshold SNR is observed above which relaying does not achieve any gains, here $\text{SNR}_{\text{th}} = 29\text{dB}$. Below that SNR, the throughput with optimised frame duration and power is highest, closely followed by the case of optimised frame duration only. This is expected because the links are fairly symmetric with $t_{0,1,2} = r_{0,1,2}$ and $a, b < c$. Furthermore, the fixed modulation schemes are outperformed by any of the optimised schemes.

In dependency of the region of operation, the gains achieved by optimisation can be significant. For instance, if one wished to maintain a normalised throughput of 2 bits/s/Hz, then direct communication would require an SNR of 24dB. An equivalent relaying system, however, would require only 20dB.

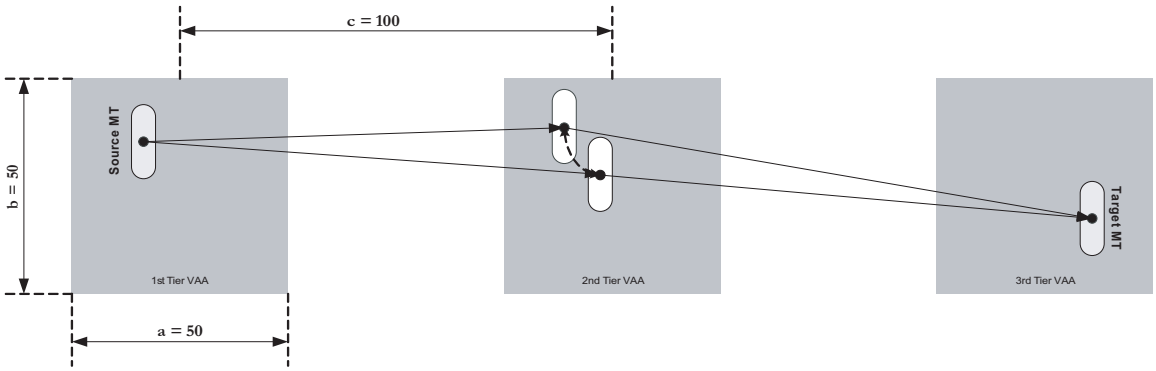


Figure 4.31: Possible terminal positions for a 2-stage distributed O-MIMO communication system with two cooperating r-MTs.

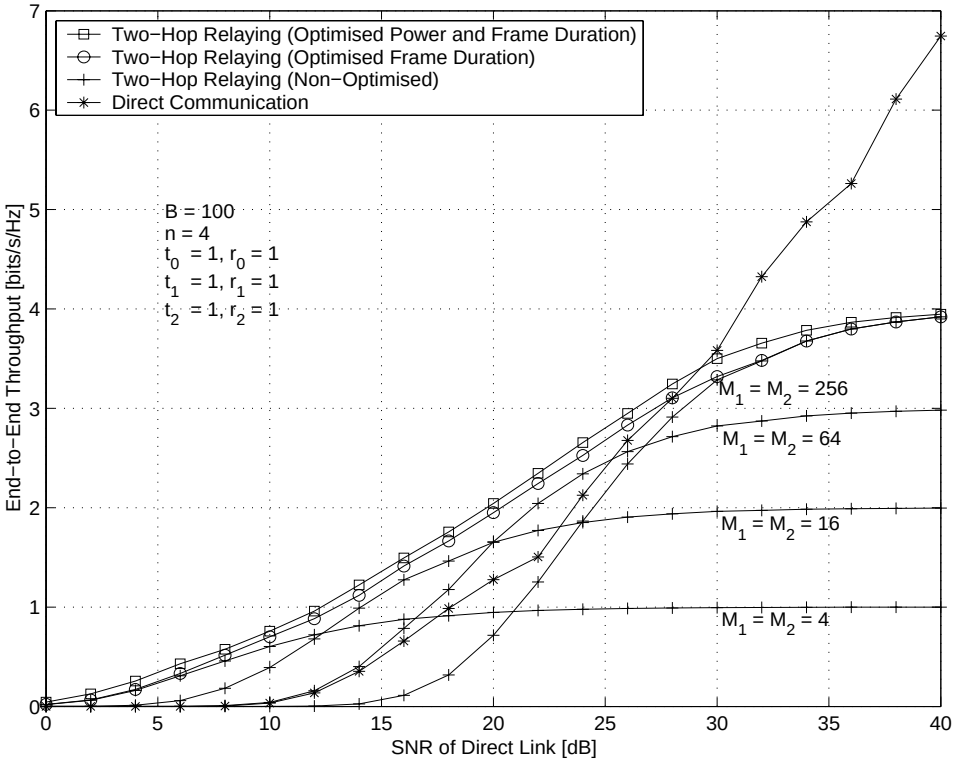


Figure 4.32: End-to-end throughput for a scenario as depicted in Figure 4.31 with only one r-MT and one antenna per stage.

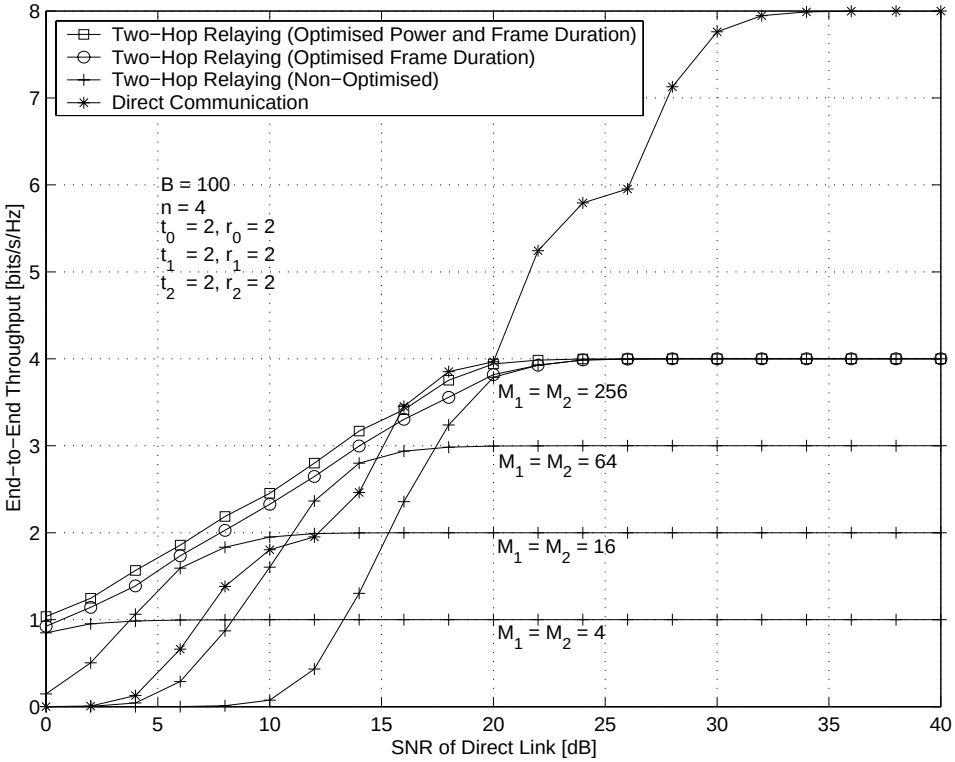


Figure 4.33: End-to-end throughput for a scenario as depicted in Figure 4.31 with two r-MTs and two antennas in s-MT and t-MT.

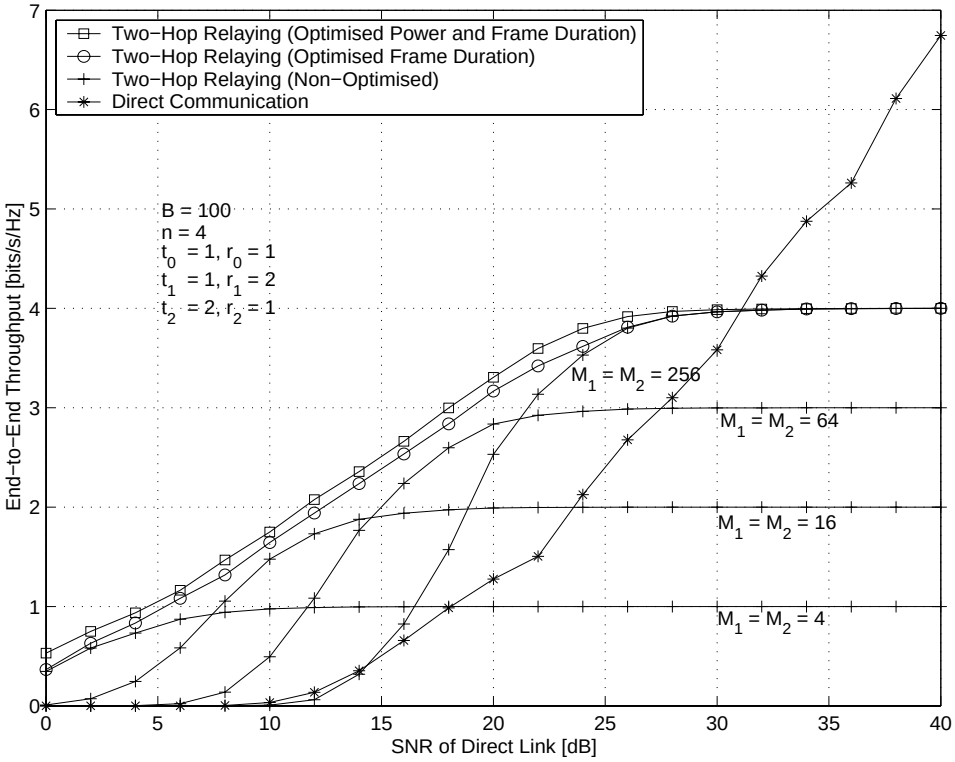


Figure 4.34: End-to-end throughput for a scenario as depicted in Figure 4.31 with two r-MTs and one antenna in s-MT and t-MT.

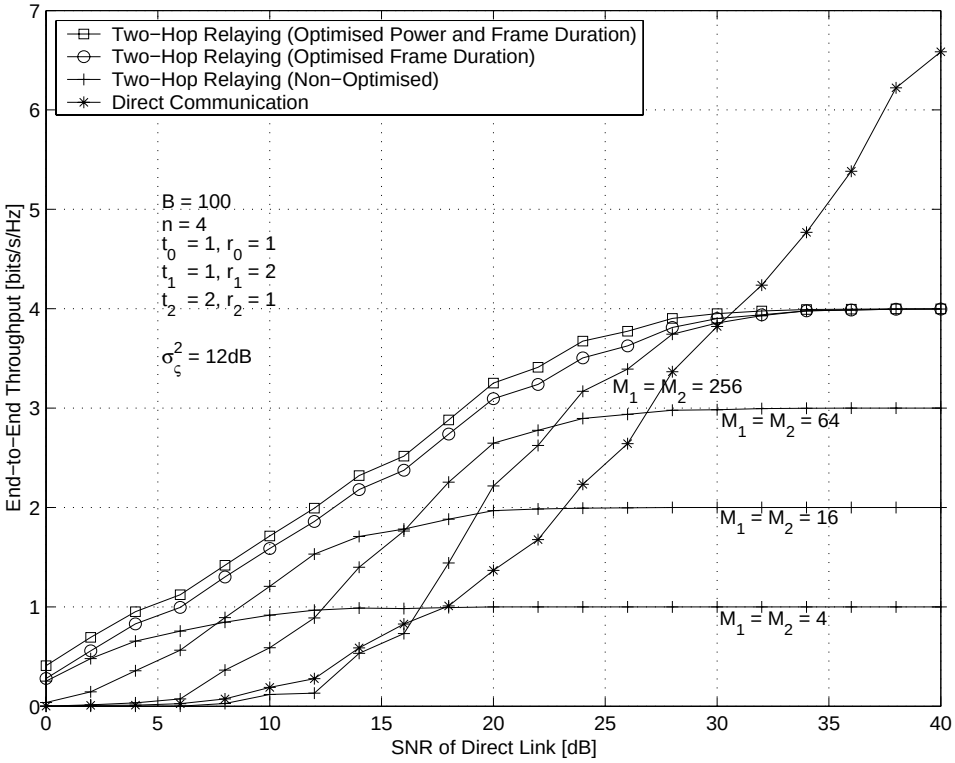


Figure 4.35: End-to-end throughput for a scenario with shadowing as depicted in Figure 4.31 with two r-MTs and one antenna in s-MT and t-MT.

Or, if a direct communication scenario operated at 20dB, then it would be able to achieve approximately 1.2 bits/s/Hz; an equivalent relaying system, however, achieves 2 bits/s/Hz. This clearly demonstrates the benefit of the developed optimisation algorithms.

Figure 4.33 is equivalent to Figure 4.32 with the only difference that now the s-MT and t-MT are in possession of two antenna elements, and there are two cooperating r-MT in the relaying stage. The threshold SNR clearly decreased, here to approximately 16dB. This can be directly observed from (4.68), where $u_0$ is increased from $u_0 = 1$ to $u_0 = 2$. It is also intuitively clear, because the stronger direct communication link now reaches its limiting throughput faster.

Nonetheless, high gains can be observed when operating below the threshold SNR. For instance, if the direct link operated at and SNR of 5dB, then the achieved throughput is only 0.3 bits/s/Hz. An equivalent relaying scenario, however, achieves around 1.6 bits/s/Hz.

From the above it is clear that relaying yields more gains when the relaying stages are stronger compared to the direct link, i.e. there are more antenna elements available in the relaying link than for the direct link. The performance of such configuration is depicted in Figure 4.34, where the s-MT and t-MT posses only one antenna element, whereas the relaying stage contains two cooperating r-MTs.

The threshold SNR does not change much in comparison to Figure 4.32 since the relaying scenario operates almost at the limiting throughput in both cases. Nonetheless, a shift of almost 2dB can be observed. Also, the case depicted here achieves the limiting throughput for a lower SNR. Therefore, compared to the scenario assessed in Figure 4.32, the gains due to an optimised relaying system are higher as long as the system operates below the threshold SNR.

For instance, if one wished to maintain a normalised throughput of 2 bits/s/Hz, then direct communication would require an SNR of 24dB. An equivalent relaying system now requires only 12dB (in contrast to the 20dB before). A saving of 12dB is hence achieved.

### 4.6.3 Scenario with Shadowing

Finally, the case of shadowed links is considered here. It was assumed that the shadowing variance of all links is 12dB. This corresponds to an indoor communication scenario at frequencies of around 2 GHz [68].

The achieved end-to-end throughput is depicted in Figure 4.35, which is the equivalent to Figure 4.34 with added shadowing. It can be observed that shadowing does not significantly change the throughput. This is attributed to the fact that the shadowing experienced at both r-MTs is the same due to the close spatial proximity. It is certainly an interesting topic of future research to evaluate the influence of shadowing when the terminals are sufficiently apart such as to experience uncorrelated (or slightly decorrelated) shadowing.

## 4.7 Conclusions

### 4.7.1 Summary

This chapter finalised the analysis of distributed-MIMO multi-stage communication networks, where the emphasis has been on transceivers utilising space-time block coding only. The error-rates of such transceivers have been derived, which were then shown to be vital in determining fractional resource allocation rules such as to maximise the normalised end-to-end throughput in dependency of the communication scenario. These strategies have then been tested by means of a few selected communication scenarios.

In Section 4.1, the topic of optimising fractional resources for transceivers of finite complexity has been introduced. The differences to Shannon transceivers have been highlighted, with the main difference being that transceiver complexity can be traded against performance. It was also shown that the concept of error-free transmission does not apply to finite complexity transceivers with the given additive noise models. For that reason a threshold error rate needs to be defined, below which the system is assumed to operate error-free.

The content of Section 4.2 can be viewed as preliminaries, where the transceiver model used has been introduced in Section 4.2.1, the channel models used in Section 4.2.3 and the simulation platform in Section 4.2.3. As for the transceiver model, it has been assumed that detection, decoding and re-encoding takes place at each stage, whereas a decision on an erroneously received signal can be done at each stage or at the target receiver. It was further assumed that the signalling, controlling the distributed encoding and decoding process, functions perfectly, and so do all synchronisation algorithms.

The narrowband channel model was assumed to consist of a pathloss (or channel gain) coefficient, a shadowing coefficient, as well as a fading coefficient. Although most of the analysis in this thesis has neglected the random effects of shadowing, it has been included in a few numerical studies at the end of the chapter. Also, the features of the simulation platform have been listed, the generality of which allows testing of the link level performance of a variety of distributed-MIMO multi-stage communication scenarios.

Section 4.3 has been dedicated to the derivation of error rates for distributed O-MIMO scenarios. Closed form expressions of SERs for M-PSK and M-QAM over Rayleigh and Nakagami fading channels with unequal channel gains have been derived, where analysis was based on the closed form expressions for equal channel gains found in literature. The SERs have been derived by means of the moment generating functions already derived and utilised in Chapter 2. Finally, the relationship between the SER, BER and FER has been exposed. It has been demonstrated that a closed form expression of the FER is difficult to obtain under generic fading conditions; however, the expressions simplify greatly for an ergodic fading channel. A fast fading channel for large frame length, as well as a slow fading

channel with sufficient interleaver depth, can be approximated as an ergodic channel which simplified consecutive analysis.

In Section 4.4, it was assumed that a source MT (s-MT) transmits a packet of $B$ bits to the target MT (t-MT) via a given number of relaying VAAs (r-VAAs). Since the modulation order may vary from stage to stage, the effective frame length may also be different. It has been assumed that each relaying stage detects and space-time re-encodes the packet, where a final decision on the correctness of the $B$ bits is performed at the t-MT.

The previously derived error rates have been utilised to derive fractional resource allocation algorithms such as to maximise the end-to-end throughput. It has been shown that the rigorous optimisation process is fairly intricate, which was the reason why the process was split into three stages. First, the modulation order in each stage has been fixed, after which the fractional frame durations have been determined. In a second step, the fractional power allocations have been determined. Finally, all available modulation orders in each stage have been permutated to yield the maximum end-to-end throughput.

The second step has been shown to be equivalent to minimising the end-to-end BER, which has been performed for the scenarios of full and partial cooperation at each relaying stage. The case of full cooperation could be reduced to a similar problem as already encountered for the capacitive maximisation of Chapter 3, which yielded the fractional power allocations. The scenario with partial cooperation (or clustering) at each stage was shown to cause error dependencies between the stages; a suitable simplification has hence been suggested, which was sufficiently justified and assessed by means of various communication scenarios. This allowed finally to derive the throughput-maximising fractional power allocations for the case of partial cooperation. Simulation results for selected communication scenarios have confirmed the applicability and precision of the developed algorithms where, in dependency of the communication scenario, significant gains can be achieved compared to the case of no optimisation.

In contrast to Section 4.4, it has been assumed in Section 4.5 that the decision on the correctness of a received frame is accomplished at each stage. Such deployment is in-line with the relaying process introduced in Chapter 3, where transceivers of infinite complexity had been assumed at each stage. The case of full cooperation has been dealt with only, where the analysis on the derivation of fractional power and frame duration was shown to be similar to the case of end-to-end transmission.

As mentioned before, the only difference to the analysis exposed in Chapter 3 has been the complexity of the transceivers utilised. It was hence tested whether the fractional resource allocation rules derived for transceivers of infinite complexity were applicable to such simple transceivers as the one utilised in this section. To this end, two mapping strategies have been investigated in Section 4.5.2. The first one mapped the fractional power derived

for a Shannon transceiver onto the fractional power of a STBC transceiver assuming the modulation order (and hence fractional frame duration) given. The second one, however, mapped the fractional resources of a Shannon transceiver onto the modulation index, fractional frame duration and transmission power. Since the mapping from two parameters on three parameters is not unique, a linear search over the modulation order has to be performed. The achieved throughput has been shown to coincide with sufficient precision, indicating that the fractional resource allocation rules scale proportionally, thereby being fairly independent on the complexity of the transceiver.

Finally, some case studies with the previously derived allocation strategies have been performed in Section 4.6. To this end, the SNR gains due to relaying have been derived first. This was then applied to studying the achieved throughput for systems operating on a stage-by-stage basis. It could be observed that relaying only yields benefits until a certain threshold SNR, which was also derived and assessed. The crossover in the throughput curves is explained with the limited normalised throughput of relaying systems due to the required resource sharing, which is not needed for direct communication.

The throughput has also been studied for a system which experiences shadowing. Although not analysed before, numerical results could confirm that relaying yields even greater performance gains in the presence of shadowing.

### 4.7.2 Contributions

The contributions by the author to the research community can be summarised as follows:

1. Closed form expressions for the symbol error rate of space-time block encoded systems operating over Rayleigh and Nakagami fading channels with different channel gains have been derived.

2. Given a distributed-MIMO multi-stage communication system with full cooperation at each relaying stage, where the decision on erroneously received data is performed at the target MT, a three-step strategy for obtaining optimised fractional resources in terms of modulation order, frame duration and transmission power has been exposed.

3. The above allocation strategy has been extended to the case of partial cooperation, where the exact end-to-end bit error rate has been simplified such as to allow an analytical formulation of the optimisation problem.

4. Given a relaying system where the decision on erroneously received data is performed at each relaying stage, again a three-step strategy for obtaining optimised fractional resources in terms of modulation order, frame duration and transmission power has been exposed.

5. Mapping rules have been established which map the fractional resource allocation rules derived in Chapter 3 for transceivers of infinite complexity to allocation rules appropriate for transceivers of finite complexity. This mapping yields further simplifications of the above-mentioned three-step algorithm.

6. Relaying does only yield throughput gains until a certain threshold SNR, which depends on the actual communication scenario. This threshold SNR has been calculated for a specific scenario, which can be obtained in total analogy for any communication scenario.

### 4.7.3 Future Research

To the belief of the author, this chapter really only touched the tip of the iceberg. The theory outlined here can be used to find fractional allocation rules for any type of transceiver, any form of cooperation, any channel, etc. A non-exhaustive list of future research topics can be found below.

1. General Coding. The outlined derivations can be extended to any form of coding, i.e. potentially concatenated trellis and block codes, space-time block and trellis codes, as well as their differential realisations.

2. Local Channel Knowledge. Again, it might be important to find optimum allocation strategies if not all channel gains are known to the allocation algorithm.

3. Multi-User. Also, the extension to the multi-user scenario is desirable which would allow one or more r-MTs to be used by more than one relaying chain.

4. Error Dependency. The susceptibility of the derived allocation strategies to channel gain estimation errors is also an important topic. Such errors could be caused by erroneous measurements, by a corrupted feedback channel which reports all channel gains to all MTs, or by high mobility which renders the channel estimates outdated.

5. Mobility. The latter is an important topic on its own. Here, it is interesting to quantify the maximum terminal mobility in the network without compromising the allocation strategies.

6. Terminal Selection Process. So far, it has been assumed that a given topology is given to which the allocation strategies have been applied. It is also vital to study the conditions under which the network benefits if a given terminal is included into the network.

7. Waterfilling. Finally, it may also prove useful in deriving the optimum transmit power allocation for STBCs operating over channels with different gains.

## 4.8 Appendix

**Derivation I.** To prove (4.45), eq. (4.42) is rearranged as follows

$$P_{b,\mathrm{e2e}}(e) \leq \frac{A_1}{(1+B_1\beta_1')^{u_1}} + \sum_{v=2}^{K} \frac{A_v}{(1+B_v\beta_v')^{u_v}} \tag{4.70}$$

$$= \frac{A_1}{\left(1+{\alpha_1'}^{-1}B_1\alpha_1'\beta_1'\right)^{u_1}} + \sum_{v=2}^{K} \frac{A_v}{(1+B_v\beta_v')^{u_v}} \tag{4.71}$$

$$= \frac{A_1}{\left(1+{\alpha_1'}^{-1}B_1\left(1-\sum_{v=2}^{K}\alpha_v'\beta_v'\right)\right)^{u_1}} + \sum_{v=2}^{K} \frac{A_v}{\left(1+B_v\beta_v'\right)^{u_v}} \tag{4.72}$$

where the constraints $\sum_{v=1}^{K}\alpha_v'\beta_v' = 1$ for a TDMA-based relaying system have been used, c.f. Section 3.2.3, below equation (3.4). The above-given representation allows one to proceed as already outlined in the appendix of Chapter 3. Without loss of generality, the fractional power allocation $\beta_K'$ for the last relaying stage will be derived. To obtain the optimum fractional power allocations which yield a minimum end-to-end BER, eq. (4.72) is differentiated $K-1$ times along $\beta_{v\in(2,K)}$. The obtained $K-1$ equations are equated to zero to arrive at

$$\frac{u_1A_1{\alpha_1'}^{-1}B_1}{\left(1+{\alpha_1'}^{-1}B_1\left(1-\sum_{v=2}^{K}\alpha_v'\beta_v'\right)\right)^{u_1+1}} = \frac{u_2A_2B_2}{\left(1+B_2\beta_2'\right)^{u_2+1}} \tag{4.73}$$

$$\vdots$$

$$= \frac{u_KA_KB_K}{\left(1+B_K\beta_K'\right)^{u_K+1}} \tag{4.74}$$

For low target SERs, $B_v\beta_v' \gg 1$ for any $v \in (1,K)$, which allows rearranging the above equations to

$$\frac{{\alpha_1'}^{-u_1}B_1^{u_1}}{u_1A_1}\left(1-\sum_{v=2}^{K}\alpha_v'\beta_v'\right)^{u_1+1} = \frac{B_K^{u_K}}{u_KA_K}\left(\beta_K'\right)^{u_K+1} \tag{4.75}$$

$$\frac{B_2^{u_2}}{u_2A_2}\left(\beta_2'\right)^{u_2+1} = \frac{B_K^{u_K}}{u_KA_K}\left(\beta_K'\right)^{u_K+1} \tag{4.76}$$

$$\vdots$$

$$\frac{B_{K-1}^{u_{K-1}}}{u_{K-1}A_{K-1}}\left(\beta_{K-1}'\right)^{u_{K-1}+1} = \frac{B_K^{u_K}}{u_KA_K}\left(\beta_K'\right)^{u_K+1} \tag{4.77}$$

The above set of equations is difficult to resolve in closed form in favour of any $\beta_{v\in(1,K)}'$. To this end, the $(u_{\max}+1)$-st square root is taken of eqs. (4.75)$-$(4.77), where $u_{\max} = \arg\max(u_1,\ldots,u_K)$. The choice of $u_{\max}$ is motivated by the fact that the error in approximating $(\beta_v')^y$ by $\beta_v'$ for $0<\beta_v'<1$ and $y \leq 1$ is smaller compared to the case when $y>1$. Since such approximation is vital in further steps, it has to be made sure that the

approximation error for the above equations is minimised. This justifies the choice of $u_{\max}$, as it guarantees that $y = (u_v + 1)/(u_{\max} + 1) \leq 1$ for any $v \in (1, K)$. Eqs. (4.75)−(4.77) can hence be recast into

$$\begin{aligned}
\alpha_1'^{-1} \left(\frac{B_1^{u_1}}{u_1 A_1}\right)^{\frac{1}{u_{\max}+1}} \left(1 - \sum_{v=2}^{K} \alpha_v' \beta_v'\right) &\approx \left(\frac{B_K^{u_K}}{u_K A_K}\right)^{\frac{1}{u_{\max}+1}} (\beta_K') && (4.78)\\
\left(\frac{B_2^{u_2}}{u_2 A_2}\right)^{\frac{1}{u_{\max}+1}} (\beta_2') &\approx \left(\frac{B_K^{u_K}}{u_K A_K}\right)^{\frac{1}{u_{\max}+1}} (\beta_K') && (4.79)\\
&\vdots \\
\left(\frac{B_{K-1}^{u_{K-1}}}{u_{K-1} A_{K-1}}\right)^{\frac{1}{u_{\max}+1}} (\beta_{K-1}') &\approx \left(\frac{B_K^{u_K}}{u_K A_K}\right)^{\frac{1}{u_{\max}+1}} (\beta_K') && (4.80)
\end{aligned}$$

Eqs. (4.79)−(4.80) are now easily resolved in favour of $\beta_2', \ldots, \beta_K'$,

$$\begin{aligned}
\beta_2' &\approx \beta_K' \left(\frac{u_K^{-1} A_K^{-1} B_K^{u_K}}{u_2^{-1} A_2^{-1} B_2^{u_2}}\right)^{\frac{1}{u_{\max}+1}} && (4.81)\\
&\vdots \\
\beta_{K-1}' &\approx \beta_{K-1}' \left(\frac{u_K^{-1} A_K^{-1} B_K^{u_K}}{u_{K-1}^{-1} A_{K-1}^{-1} B_{K-1}^{u_{K-1}}}\right)^{\frac{1}{u_{\max}+1}} && (4.82)
\end{aligned}$$

which, when inserted into (4.78), yield

$$\beta_K' \cdot \sum_{v=1}^{K} \alpha_v' \left(\frac{u_K^{-1} A_K^{-1} B_K^{u_K}}{u_v^{-1} A_v^{-1} B_v^{u_v}}\right)^{\frac{1}{u_{\max}+1}} = 1 \qquad (4.83)$$

where $\beta_K'$ is now obtained and shown to be equivalent to (4.45) for $v = K$. Other coefficients are similarly obtained. This concludes the proof.

**Derivation II.** To prove (4.49), recall that the end-to-end BER is approximated as

$$P_{b,\mathrm{e2e}}(e) \approx \sum_{v=1}^{K} \sum_{i=1}^{Q_v} \xi_{v,i} P_{v,i}(e) \qquad (4.84)$$

where the weights $\xi_{v,i}$ are derived in dependency of the network topology. With reference to (4.20), the BER of the $i^{th}$ cluster in the $v^{th}$ stage can be expressed as

$$P_{v,i}(e) = \sum_{j \in i} K_{v,i,j} \cdot P_{\mathrm{PSK/QAM}}(1, t_v, R_v, \gamma_{v,j}, S/N, M_v) \qquad (4.85)$$

where the expansion coefficients are given in (4.50). With reference to the analysis exposed in Section 4.4.2, it can be upper-bounded as

$$P_{v,i}(e) \leq \sum_{j \in i} \frac{K_{v,i,j} A_v}{1 + B_{v,i,j} \beta_v'} \qquad (4.86)$$

where the coefficients $A_v$ are given by (4.43) and $B_{v,i,j}$ by (4.51). Inserting (4.86) into (4.84) yields

$$P_{b,\mathrm{e2e}}(e) \leq \sum_{v=1}^{K} \sum_{i=1}^{Q_v} \sum_{j \in i} \frac{\xi_{v,i} K_{v,i,j} A_v}{1 + B_{v,i,j} \beta'_v} \tag{4.87}$$

The same procedure is now followed as already outlined in Derivation I, where (4.70) is extended by the additional sums; furthermore, $A_v$ is replaced by $\xi_{v,i} K_{v,i,j} A_v$ and $u_v$ by 1, which finally yields (4.49).

**Derivation III.** To prove (4.57), the throughputs (4.54) are equated to yield

$$\begin{aligned} \alpha'_1 R_1 \log_2(M_1) \left(1 - \frac{\alpha'_1 A_1 D}{(1 + B_1 \beta'_1)^{u_1}}\right) &= \\ &\vdots \\ &= \alpha'_K R_K \log_2(M_K) \left(1 - \frac{\alpha'_K A_K D}{\left(1 + B_K \beta'_K\right)^{u_K}}\right) \end{aligned} \tag{4.88}$$

which, when inserting the fractional frame durations $\alpha'_v$ given by (4.56), is equivalent to

$$\begin{aligned} \frac{\alpha'_1 A_1 D}{(1 + B_1 \beta'_1)^{u_1}} &= \\ &\vdots \\ &= \frac{\alpha'_K A_K D}{\left(1 + B_K \beta'_K\right)^{u_K}} \end{aligned} \tag{4.89}$$

For a fairly high SNR, the above-given equations can be approximated by

$$\begin{aligned} \frac{\alpha'_1 A_1 D}{(B_1 \beta'_1)^{u_1}} &= \\ &\vdots \\ &= \frac{\alpha'_K A_K D}{\left(B_K \beta'_K\right)^{u_K}} \end{aligned} \tag{4.90}$$

Using the same arguments as for Derivation I, the $(u_{\max})^{th}$-root is taken of (4.90) to arrive at

$$\begin{aligned} \beta'_1 \left({\alpha'_1}^{-1} A_1^{-1} B_1^{u_1}\right)^{\frac{1}{u_{\max}}} &\approx \\ &\vdots \\ &\approx \beta'_K \left({\alpha'_K}^{-1} A_K^{-1} B_K^{u_K}\right)^{\frac{1}{u_{\max}}} \end{aligned} \tag{4.91}$$

which, under constraint $\sum_{v=1}^{K} \alpha'_v \beta'_v = 1$, yields (4.57).

# Chapter 5

# Concluding Remarks

It was the aim of this thesis to pose and answer many unsolved questions relating to the understanding of relaying communication systems. As with any scientific work, it has brought up more questions than is has solved, some of which are illuminated below. Before that, however, the contributions of the thesis are glued together to give a better picture of the choice of the research conducted.

In this thesis, the concept of Virtual Antenna Arrays has been introduced which was then applied to relaying networks, thereby introducing distributed-MIMO multi-stage communication networks. It has been demonstrated that such a deployment yields significant gains in data throughput independent of the complexity of the available transceivers. A prerequisite for achieving a higher data throughput is the deployment of suitable communication protocols. These have been derived in form of fractional resource allocation strategies for a wide variety of communication scenarios.

An understanding of the Shannon capacity offered by each relaying stage played a central role in deriving the allocation strategies, which was the sole purpose of Chapter 2. It has been reiterated that the appropriate capacity measure for ergodic channels is the Shannon capacity, whereas for non-ergodic channels the outage probability for a given communication rate is appropriate. Consecutive analysis throughout the thesis therefore distinguished between these two types of channels.

Although the topic of MIMO capacity has been the research focus for nearly a decade, novel results on the general MIMO capacity over ergodic flat Rayleigh fading channels have been obtained in Chapter 2. This is attributed to the solution of the capacity integral, which allowed expressing the MIMO capacity in closed form. The same integral was then utilised to derive closed form expressions for the capacity of space-time block encoded MIMO channels obeying Rayleigh or Nakagami fading with arbitrary channel gains. The later case was referred to as orthogonalised MIMO (O-MIMO) channel, because space-time block codes are known to orthogonalise the MIMO detection problem into parallel SISO detection problems.

In a similar manner, the outage probabilities for O-MIMO channels obeying Rayleigh and Nakagami fading with arbitrary channel gains have been obtained. Finally, at the end of Chapter 2 suitable approximations to the MIMO and O-MIMO capacities and outage probabilities have been introduced. These proved vital in a later stage to derive the fractional allocation rules, because the approximations allowed to decouple the intricate expressions attributed to the MIMO gain from the fractional power, bandwidth and frame duration.

The analysis has then been extended to the multi-stage communication scenario in Chapter 3. The aim was to develop communication protocols which maximised the end-to-end data throughput for a given network topology. Further analysis was then split into ergodic and non-ergodic channels. As for the ergodic channel realisations, it has been shown that maximising the end-to-end throughput is equivalent to maximising the end-to-end capacity for the weakest links in the network. The previously exposed exact and approximate expressions of the MIMO capacity allowed to derive fractional power, bandwidth and frame duration allocation strategies which guaranteed near-optimum end-to-end throughput. Not only were the cases of MIMO and O-MIMO relaying considered, but also the possibility to reuse resources in form of bandwidth or frame duration after a given number of relaying stages.

The theory behind non-ergodic channel realisations turned out to be slightly more involved. It was first shown that the end-to-end throughput is related to the communication rate in each stage as well as its associated outage probability. The previously exposed approximation of the outage probability, however, allowed simplifying the problem to the cases encountered for ergodic channels. This enabled the derivation of fractional resource allocation rules for the same scenarios as described above.

The merits of the derived allocation strategies are their simplicity and precision, thereby rendering a numerical optimisation within each relaying mobile terminal superfluous. The strategies were assessed by means of numerous communication scenarios, all of which confirmed that significant gains in terms of throughput are achieved when comparing to non-optimised relaying systems.

In contrast to previous analysis, Chapter 4 was dedicated to relaying systems consisting of finite complexity transceivers. In the introduction to the chapter, it has been shown that such systems are usually quantified by means of error rates versus the signal-to-noise ratio at the detection instant. The different performance measure was the reason why different allocation strategies were expected to achieve optimum end-to-end throughput with such systems. It was also expected that for an increasing complexity of channel and space-time codes, the allocation strategies derived for infinite and finite-complexity transceivers converge. An investigation into different classes of codes was beyond the scope of the thesis.

Instead, this thesis has dealt with distributed-MIMO multi-stage space-time block encoded communication systems only. The derived fractional resource allocation rules relied on upper bounds of the occurring error rates, which allows one to extend the analysis to any form of coding as long as the respective upper bounds are given.

The upper bounds required to derive the allocation rules were obtained from closed form expressions of the symbol error rate for space-time block encoded systems operating over Rayleigh and Nakagami fading channels with arbitrary channel gains. These have been derived using analysis exposed in the open literature, as well as in Chapter 2.

Consecutively, resource allocation rules in terms of modulation order, fractional power and fractional frame duration were derived assuming a packet based transmission from source to sink. Distinction was then made between relaying systems, where erroneous packets are discarded at the target terminal only or on a stage-by-stage basis. To simplify the derivation of the allocation strategies, only ergodic channels have been assumed which can observed for large block lengths and fast fading channels (or, slow fading channels with appropriate interleavers).

The derived algorithms were then assessed by means of a few selected communication scenarios. For these scenarios, it could be shown that considerably higher throughputs are achieved when compared to non-optimised systems. Finally, two mapping strategies were investigated which perform a suitable mapping of the fractional resources derived in Chapter 3 onto the resources derived in Chapter 4. It was found that the mapping yields almost equivalent results in terms of throughput, indicating that capacity and error rates scale in a similar fashion.

From this summary it is clear that research on distributed-MIMO multi-stage communication systems is far from complete. This is mainly due to the fact that the here investigated PHY layer performs only a fraction of the functionalities needed to accomplishes a modern relaying communication system. The analysed single-link scenarios therefore need to be extended to the multi-link case, where more than one source terminal communicates with more than one target terminal over common relaying terminals. Control mechanisms above the PHY layer hence need to be invoked, which are traditionally accomplished by means of two fairly decoupled entities, i.e. the radio resource management (RRM) and the medium access control (MAC).

The RRM is mainly responsible for assigning radio resources to each user (or traffic flow) in dependency of the users' traffic characteristics, also taking into account the scheduling conditions reported by the MAC and the channel conditions reported by the PHY. The MAC, on the other hand, simply schedules the data of all users onto the same physical medium such that interference is minimised and the throughput is still (near-)optimum for all users.

Clearly, the herein derived fractional resource allocation strategies are the basis for any further work on suitable throughput maximising and interference minimising MAC protocols. They can also be utilised to design PHY and MAC assisted routing protocols, where the capacity offered at the PHY and MAC layers is taken into account to influence the packet routing path from the information source towards the information sink.

In a further step, the allocation strategies should not only reflect the channel conditions at each relaying stage, but also the statistical nature of the transmitted data traffic. Conversely, one could also think of the possibility that the allocation strategies influence the packet length and statistics at the source to match the PHY characteristics of the relaying network, and thereby achieving further throughput benefits.

Of imminent practical interest is additionally the derivation of resource allocation strategies for networks with mutual interference. From an information theoretical point of view, this clearly leads to layered architectures where the interference is cancelled iteratively [27, 30]. Realistic networks, however, have rarely the opportunity to use such complex transceivers, which is the reason why simple and explicit resource allocation strategies would be of great benefit.

Finally, appropriate distributed coding schemes need to be investigated which allow approaching the capacity bounds promised by the allocation protocols of Chapter 3. Some steps in this direction have already been paced by the work reported in [31]; however, much more effort is needed to design robust and low-complexity coding schemes.

A final word on the potential applications of the derived communication protocols. In a cellular deployment, one can think of deploying multi-stage VAAs to enhance the high data rate coverage area of a BS. The algorithms could also be used to relay data from hot-spots to less congested areas, e.g. during or after a football match where everybody in the stadium wishes to communicate with a friend somewhere outside. Furthermore, with the ever increasing amount of wireless local area networks (W-LANs), the algorithms can be utilised to accomplish a highly efficient provision of data services to users out of direct access point range.

Finally, with emerging personal area networks (PANs) these algorithms may also find their application. Assume, for instance, a lecture theatre full with students each of which possesses a PAN. The total data throughput of such a scenario, where any PAN may wish to communicate with any other PAN in the network, can drastically be increased if referring to the developed algorithms or extensions thereof.

In conclusion, the ultimate purpose of this thesis was to positively contribute to scientific knowledge, clarify several aspects relating to distributed-MIMO multi-stage relaying networks, and hopefully, to pose many questions that may catch the imagination of future researchers.

# Appendix A

# Related Publications

## A.1 Journals and Letters

[10] **Near-Optimum Resource Allocation Strategies for Distributed Ad-Hoc Networks**

**M. Dohler**, A. Gkelias, H. Aghvami, IEEE J-SAC on Ad-Hoc Networks, October 2003, submitted.

[9] **Closed Form Capacity Expressions of Orthogonalised Correlated MIMO Channels**

L. Musavian, **M. Dohler**, R. Nakhai, H. Aghvami, IEEE Communications Letter, September 2003, submitted.

[8] **Relay-based Deployment Concepts for Wireless and Mobile Broadband Cellular Radio**

R. Pabst, **M. Dohler**, H. Aghvami, et. al., IEEE Communications Magazine, September 2003, submitted.

[7] **On the Approximation of MIMO Capacity**

**M. Dohler**, H. Aghvami, IEEE Letter Wireless Communications, July 2003, submitted.

[6] **Resource Allocation for FDMA-based Regenerative Multi-Hop Links**

**M. Dohler**, A. Gkelias, H. Aghvami, IEEE Letter Wireless Communications, accepted in Oct 2003.

[5] **The Capacity of Distributed PHY-Layer Sensor Networks**

**M. Dohler**, A. Gkelias, H. Aghvami, IEEE J-SAC on Sensor Networks, July 2003, submitted.

[4] **Capacity Allocation Strategy for Orthogonal Regenerative Multi-Hop Links**

**M. Dohler**, A. Gkelias, H. Aghvami, IEEE Trans. on Vehicular Technology, June 2003, submitted.

[3] **A Resource Allocation Strategy for Distributed MIMO Multi-Hop Communication Systems**

**M. Dohler**, A. Gkelias, H. Aghvami, IEEE Communications Letter, accepted in September 2003.

[2] **2-Hop Distributed MIMO Communication System**

**M. Dohler**, A. Gkelias, H. Aghvami, IEE Electronics Letters, vol. 39, no. 18, Sept. 2003, pp.1350-1351.

[1] **A Closed Form Expression of MIMO Capacity over Ergodic Narrowband Channels**

**M. Dohler**, H. Aghvami, IEEE Correspondence Information Theory, May 2003, submitted.

## A.2 Refereed Conference Papers

[8] **Distributed PHY-Layer Mesh Networks**

**M. Dohler**, H. Aghvami, PIMRC, Beijing, China, Sept 2003, Conference CD-ROM.

[7] **Performance Evaluation of STTCs for Virtual Antenna Arrays**

**M. Dohler**, B. Rassool, H. Aghvami, VTC Spring, Jeju, Korea, April 2003, Conference CD-ROM.

[6] **Influence of Channel Characteristics on the Performance of VAA with deployed STBCs**

A. Kastrisios, **M. Dohler**, H. Aghvami, VTC Spring, Jeju, Korea, April 2003, Conference CD-ROM.

[5] **Higher Order Space-Time Block Codes for Virtual Antenna Arrays**

**M. Dohler**, F. Said, H. Aghvami, ICT2003, Tahiti, French Pol., Febr 2003, Conference CD-ROM.

[4] **Space-Time Block Codes for Virtual Antenna Arrays**

**M. Dohler**, E. Lefranc, H. Aghvami, PIMRC, Lisbon, Portugal, Sept 2002, Conference CD-ROM.

[3] **Link Capacity Analysis of Virtual Antenna Arrays**

**M. Dohler**, J. Dominguez, H. Aghvami, VTC Fall, Vancouver, Canada, Sept 2002, Conference CD-ROM.

[2] **Virtual Antenna Arrays for Future Wireless Mobile Communication Systems**

**M. Dohler**, E. Lefranc, H. Aghvami, ICT2002, Beijing, China, June 2002, Conference CD-ROM.

[1] **System Performance of a W-CDMA based Network with deployed VAA**

Z. Zeng, **M. Dohler**, H. Aghvami, ICT2002, Beijing, China, June 2002, Conference CD-ROM.

## A.3 Patents

[3] **Frequency Relaying** Filed 28th June 2001. UK Patent Application 0115-807.0.

[2] **Forced Synchronisation** Filed 28th June 2001. UK Patent Application 0115-804.7.

[1] **Virtual Antenna Arrays** Filed 28th June 2001. UK Patent Application 0115-799.9.

# Bibliography


[1] C.E. Shannon, "A mathematical theory of communication," *Bell Syst. Tech. J.*, vol. 27, pp. 379-423, 623-656, July-Oct. 1948.

[2] E. Telatar, "Capacity of multi-antenna Gaussian channels," *European Trans. on Telecomm.*, vol. 10, no. 6, pp. 585-595, Nov./Dec. 1999.

[3] G.J. Foschini and M.J. Gans, "On limits of wireless communications in a fading environment when using multiple antennas", *Wireless Personal Communications*, vol. 6, pp. 311-335, 1998.

[4] B. Vucetic, J. Yuan, *Space-Time Coding*, John Wiley & Sons, Inc., 2003.

[5] C. Balanis, *Antenna Theory*, John Wiley & Sons, Inc., 1997.

[6] M. Dohler, et al., "VAA for hot-spots with applied STC", *M-VCE*, Internal Reports I, II, III and IV, 1999-2002.

[7] H. Holma, A. Toskala, *W-CDMA for UMTS: Radio Access for Third Generation Mobile Communications*, John Wiley & Sons, Ltd., 2000.

[8] R. Morrow, *Bluetooth Operation and Use,* McGraw-Hill, 2002.

[9] H. Aghvami, *Digital Communications*, Lecture Notes, 2000.

[10] M. Dohler, F. Said, A. Ghorashi, H. Aghvami, "Improvements in or Relating to Electronic Data Communication Systems", Publication No. WO 03/003672, priority date 28 June 2001.

[11] M. Dohler, A. Gkelias, H. Aghvami, "Near-Optimum Resource Allocation Strategies for Distributed Ad-Hoc Networks," *IEEE J-SAC on Ad-Hoc Networks*, October 2003, submitted.

[12] M. Dohler, A. Gkelias, H. Aghvami, "The Capacity of Distributed PHY-Layer Sensor Networks," *IEEE J-SAC on Sensor Networks*, July 2003, submitted.

[13] 3G TR 25.924 V1.0.0 (1999-12) *3rd Generation Partnership Project,* Technical Specification Group Radio Access Network; Opportunity Driven Multiple Access.

[14] T. J. Harrold, A. R. Nix, "Capacity Enhancement Using Intelligent Relaying For Future Personal Communications System", *Proceedings of VTC-2000 Fall*, pp. 2115-2120.

[15] S. M. Alamouti, "A simple transmit diversity technique for wireless communications," *IEEE J-SAC*, vol. 16, No. 8, Oct. 1998.

[16] V. Tarokh, H. Jafarkhani, A. Calderbank, "Space-Time Block Codes from Orthogonal Design," *IEEE Trans. Inform. Theory*, vol 45, no. 5, pp. 1456-1466, July 1999.

[17] V. Tarokh, N. Seshadri, A. Calderbank, "Space Time Codes for high data rate wireless communication: performance criterion and code construction," *IEEE Trans. Inform. Theory*, vol 44, no. 2, pp. 744-765, March 1998.

[18] E. van der Meulen, "Three-terminal communication channels," *Adv. Appl. Prob.,* vol. 3, pp. 120-154, 1971.

[19] H. Sato, "Information transmission through a channel with relay," The Aloha System, University of Hawaii, Honolulu, Tech. Rep. B76-7, March 1976.

[20] T. Cover, A. el Gamal, "Capacity Theorems for the Relay Channel," *IEEE Trans. on Inform. Theory,* vol. IT-25, no. 5, pp.572-584, September 1979.

[21] T. Cover, J.A. Thomas, *Elements of Information Theory*, John Wiley & Sons, Inc., 1991.

[22] A. Sendonaris, E. Erkip, B. Aazhang, "Increasing Uplink Capacity via User Cooperation Diversity," *Proc. IEEE ISIT*, p. 196, August 1998.

[23] A. Sendonaris, E. Erkip, B. Aazhang, "User Cooperation Diversity - Part I: System Description," *IEEE Transactions on Communications*, vol. 51, no. 11, November 2003, pp. 1927-1938.

[24] A. Sendonaris, E. Erkip, B. Aazhang, "User Cooperation Diversity - Part II: Implementation Aspects and Performance Analysis," *IEEE Transactions on Communications*, vol. 51, no. 11, November 2003, pp. 1939-1948.

[25] J.N. Laneman, G.W. Wornell, "Energy-efficient antenna sharing and relaying for wireless networks," *IEEE WCNC*, September 2000, Conference CD-ROM.

[26] J.N. Laneman, *Cooperative Diversity in Wireless Networks: Algorithms and Architectures,* PhD Disseration, MIT September 2002.

[27] P. Gupta, P.R. Kumar, "The Capacity of Wireless Networks," *IEEE Trans. on Inform. Theory,* vol. 46, no. 2, pp. 388-404, March 2000.

[28] P. Gupta, P.R. Kumar, "Towards an Information Theory of Large Networks: An Achievable Rate Region," *IEEE Trans. on Inform. Theory,* vol. 49, pp. 1877-1894, August 2003.

[29] M. Grossglauser, D. Tse, "Mobility Increases the Capacity of Ad Hoc Wireless Networks," *IEEE ACM Trans. on Networking,* vol 10, no 4, August 2002.

[30] G.J. Foschini, "Layered Space-Time Architecture for Wireless Communication in a Fading Environment When Using Multi-Element Antennas," *Bell Labs Technical Journal*, vol. 1, no. 2, pp 41-59, Autumn 1996.

[31] A. Stefanov, E. Erkip, "Cooperative Space-Time Coding for Wireless Networks," *Proc. IEEE ITW*, pp. 50-53, April 2003.

[32] S. Verdu, "Fifty Years of Shannon Theory," *IEEE Trans. on Inform. Theory*, vol. 44, no. 6, pp. 2057-2078, Oct. 1998.

[33] H. Nyquist, "Certain topics in telegraph transmission theory," *Bell Syst. Tech. J.*, vol. 3, pp. 324-352, Apr. 1924.

[34] R.V.L. Hartley, "Transmission of information," *Bell Syst. Tech. J.*, vol. 7, pp. 535-563, July 1928.

[35] S.O. Rice, "Mathematical analysis of random noise," *Bell Syst. Tech. J.*, vol. 23-24, pp. 282-332 and 146-156, July 1944 and Jan. 1945.

[36] C. Berrou, A. Glavieux, P. Thitimajshima, "Near Shannon Limit Error-Correcting Coding and Decoding: Turbo Codes," *ICC*, pp. 1064-1070, 1993.

[37] R. Vaughan, J.B. Andersen, *Channels, Propagation and antennas for mobile communications*, IEE Electromagnetic Wave Series, 2003.

[38] R.G. Gallager, *Information Theory and Reliable Communications*, John Wiley & Sons, Inc., 1968.

[39] E.G. Larsson, P. Stoica, *Space-Time Block Coding for Wireless Communications*, Cambridge University Press, 2003.

[40] A. Paulraj, R. Nabar, D. Gore, *Introduction to Space-Time Wireless Communications*, Cambridge University Press, 2003.

[41] A. Edelman, *Eigenvalues and Condition Numbers of Random Matrices*, PhD thesis, Department of Mathematics, MIT, Cambridge, MA, 1989.

[42] M. Kang, M.S. Alouini, "On the Capacity of MIMO Rician Channels," *40th Allerton Conference on Communication, Control, and Computing*, Illinois, October 2002, pp. 936-945.

[43] H. Shin, J.H. Lee, "Closed-form Formulas for Ergodic Capacity of MIMO Rayleigh Fading Channels," *IEEE ICC,* May 2003, pp. 2996-3000.

[44] I.S. Gradshteyn, I.M. Ryshik, *Table of Integrals, Series, and Products*, Academia Press, sixth edition, 2000.

[45] R. U. Nabar, H. Bölcskei, and A. J. Paulraj, "Outage performance of space-time block codes for generalized MIMO channels," *IEEE Trans. Information Theory*, Mar. 2002, submitted.

[46] M.K. Simon, M-S. Alouini, *Digital Communication over Fading Channels*, John Wiley & Sons, Inc., Wiley Series in Telecommunications and Signal Processing, 2000.

[47] J. Proakis, *Digital communications*, McGraw Hill, Third edition, 1995.

[48] Q.T. Zhang, D.P. Liu, "A Simple Capacity Formula for Correlated Diversity Ricean Fading Channels," *IEEE Comm. Letters*, vol. 6, no. 11, pp. 481-483, Nov. 2002.

[49] M. Dohler, H. Aghvami, "On the Approximation of MIMO Capacity," *IEEE Letters in Wireless Communications*, July 2003, submitted.

[50] J.W. Nilsson, S.A. Ridel, *Electric Circuits*, Prentice-Hall International, Inc., sixth edition, 2000.

[51] M.O. Hasna, M-S. Alouini, "Performance Analysis of Two-Hop Relayed Transmissions over Rayleigh Fading Channels", *IEEE VTC-Fall 2002*, Vancouver, Canada, 2002, Conference CD-ROM.

[52] L. Tassiulas and A. Ephremides, "Jointly optimal routing and scheduling in packet radio networks", *IEEE Transactions on Information Theory*, vol. 38, no. 1, pp. 165-168, January 1992.

[53] T.E. Batt and A. Ephremides, "Joint Scheduling and Power Control for Wireless Adhoc Networks", *IEEE INFOCOM*, June 2002, Conference CD-ROM.

[54] B. Radunovic and J-Y.L. Boudec, "Joint Scheduling, Power Control and Routing in Symmetric, One-dimensional, Multi-hop Wireless Networks", WiOpt'03, March 2003, Conference CD-ROM.

[55] S. Toumpis, A.J. Goldsmith, "Capacity Regions for Wireless Ad Hoc Networks", *Submitted to the IEEE Transactions on Wireless Communications*, Sept. 2001.

[56] N. Jindal, A.J. Goldsmith, "Capacity and Optimal Power Allocation for Fading Broadcast Channels with Minimum Rates", *Submitted to IEEE Transactions on Information Theory*, Sept. 2001.

[57] L. Li, A.J. Goldsmith, "Capacity and Optimal Resource Allocation for Fading Broadcast Channels - Part I: Ergodic Capacity", *IEEE Transactions on Information Theory*, vol. 47, no. 3, pp. 1083-1102, March 2001.

[58] L. Li, A.J. Goldsmith, "Capacity and Optimal Resource Allocation for Fading Broadcast Channels -Part II: Outage Capacity", *IEEE Transactions on Information Theory*, vol. 47, no. 3, pp. 1103-1127, March 2001.

[59] A. J. Goldsmith, "The capacity of downlink fading channels with variable rate and power", *IEEE Transactions on Vehicular Technology*, vol. 46, no.3, pp. 569 -580, August 1997.

[60] A. Ben-Tal, A. Nemirovski, *Lectures on Modern Convex Optimization,* SIAM, Philadelphia, 2001.

[61] S. Saunders, *Antennas and Propagation for Wireless Communicaton Systems*, John Wiley & Sons, Ltd., 1999.

[62] K. Liu, V. Raghavan, A.M. Sayeed, "Capacity Scaling and Spectral Efficiency in Wideband Correlated MIMO Channels", *IEEE Transactions on Inormation Theory*, submitted October 2002, revised June 2003.

[63] R. Prasad, *CDMA for Wireless Personal Communications*, Artech House Mobile Communications Series, 1996.

[64] S. Ulukus, R.D. Yates, "Iterative Construction of Optimum Signature Sequence Sets in Synchronous CDMA systems," *IEEE Transactions on Information Theory*, vol. 47, pp. 1989-1998, 2001.

[65] L. Hanzo, M. Muenster, B.J. Choi, T. Keller, *OFDM and MC-CDMA for Broadband Multi-User Communications, WLANs and Broadcasting*, John Wiley & Sons, 2003.

[66] T.H. Liew, L. Hanzo, "SpaceTime Codes and Concatenated Channel Codes for Wireless Communications", *Proceedings of the IEEE*, vol. 90, no. 2, February 2002.

[67] B. Vucetic, J. Yuan, *Turbo Codes: Principles and Applications,* Kluwer Academic Publishers, Boston, June 2000.

[68] T.S. Rappaport, *Wireless Communications,* Prentice Hall, 2000.

[69] S. Hara, R. Prasad, "Design and Performance of Multicarrier CDMA System in Frequency-Selective Rayleigh Fading Channels", *IEEE Trans. on Vehicular Techn.*, vol. 48, no. 5, Sept. 1999.

[70] H. Shin and J.H. Lee, "Exact symbol error probability of orthogonal space-time block codes," *Proc. of the IEEE Globecom*, Taipei, Taiwan, Nov. 17-21, pp.1547-1552, 2002.